Protection of Double-Stranded RNA for Delivery through Complexation with Block Copolymers: Optimising Polymer Architecture for *Drosophila suzukii*-specific Control

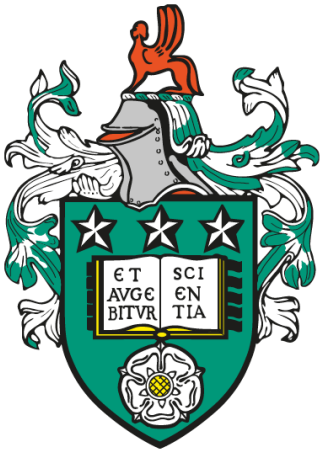

Charlotte Eloise Pugsley

The University of Leeds

School of Chemical and Process Engineering & School of Biological Sciences

Submitted in accordance with the requirements for the degree of *Doctor of Philosophy*

December 2022

Declaration of Intellectual Property

The candidate confirms that the work submitted is their own, except work, which has formed part of jointly authored publications that has also been included. The contribution of the candidate and the other authors to this work has been explicitly indicated below. The candidate confirms that appropriate credit has been given within the thesis where reference has been made to the work of others.

List of Refereed Journal Articles and Book Chapters:

1. Chapter 1: Pugsley, C. E.; Isaac, R. E.; Warren, N. J.; Cayre, O. J. Recent Advances in Engineered Nanoparticles for RNAi-Mediated Crop Protection Against Insect Pests. Front. Agron. **2021**, 3. https://doi.org/10.3389/fagro.2021.652981.

2. Chapter 3: Pugsley, C. E.; Isaac, R. E.; Warren, N. J.; Behra, J. S.; Cappelle, K.; Dominguez-Espinosa, R.; Cayre, O. J. Protection of Double-Stranded RNA via Complexation with Double Hydrophilic Block Copolymers: Influence of Neutral Block Length in Biologically Relevant Environments. *Biomacromolecules* **2022**. https://doi.org/10.1021/acs.biomac.2c00136.

3. Pugsley, C. E.; Yow, H. N.; Biggs, S.; Cayre, O. J. Chapter 5: Applications of Stimuli-Responsive Functional Colloids. In *Chemoresponsive Materials*; 2022; pp 129–169. https://doi.org/10.1039/9781839166136-00129.

4. Chapter 4: Pugsley, C. E.; Isaac, R. E.; Warren, N. J.; Cayre, O. J. Linear ABC amphiphilic triblock copolymers for complexation and protection of dsRNA, *Polymer Chemistry*, **2022**. https://doi.org/10.1039/D2PY00914E.

5. Chapter 5: Pugsley, C. E.; Isaac, R. E.; Warren, N. J.; Stacey, M.; Cappelle, K.; Dominguez-Espinosa, R.; Cayre, O. J. Effective delivery and selective insecticidal activity of double-stranded RNA *via* complexation with diblock copolymers varies with polymer block composition *(Under review)*, https://doi.org/10.21203/rs.3.rs-2272882/v1.

The research in this thesis was carried out solely by C. E. Pugsley with the following exceptions:

Chapter 3 & 4: High resolution (400 MHz) ^{1}H NMR spectra were obtained by Dr. Yasmeen Jhons, Eleanor Hilton and Samuel Turvey.

Chapter 5: Cell viability by MTS assay with Sf9 cells and luciferase protein assay with transformed Sf9 cells were performed with assistance from Dr. Julia Y. Rho (University of Warwick).

Acknowledgements

I saved writing these acknowledgements until last, as summarising 4 years' worth of support from colleagues, friends and family is not an easy task. Over the years I have had one or two successes, but mainly *many* challenges, and I have grown and changed along the way. But most importantly, I could not have survived this PhD without the support and encouragement of the people mentioned here.

Firstly, I would like to acknowledge my three supervisors: *Elwyn Isaac*, *Nicholas Warren* and *Olivier Cayre*. Thank you for your ongoing support throughout my project. Thank you to *Elwyn*, for your endless ideas and for keeping the *Drosophila* alive throughout the entire pandemic! Thank you to *Nick*, for pushing me to write papers and for letting me switch your GPC to an aqueous eluent! And my biggest thank you has to go to *Olivier*, for always building me up when I was down. You are one of the most encouraging and supportive people that I have ever had the pleasure of meeting, and I know that I would not have finished my PhD without you!

Sam P, thank you for kicking off my project by showing me the ropes of RAFT polymerisation, and *Juliette*, thank you for giving me the run-down of all things light scattering. Getting started on my PhD would have been a lot more challenging without both of you there to guide me. Thank you to *Calum*, for endlessly letting me re-produce your drawing of a *Drosophila*.

Elpi, thank you for teaching me the ways of biology, your enthusiasm for well-conducted experiments set me up for the rest of my PhD! *Dan* and *Johan*, thank you for letting me use your light scattering instrument, *Dan* thank you for attempting to show me how to code! *Martin*, thank you for helping me to understand a small part of the world of cell culture. I hope that one day I can convince you that chemistry *can* be sexy!

Thank you to Diamond/ISIS, for letting me attend your small angle scattering courses, thank you to *Sam B* for collecting SAXS data for me and to *Michael*, *Gerome*, *Arwen* and *Matthew* for helping to interpret it (even though it didn't make it into my thesis!).

Sébastien, thank you for hosting my visit to your labs at the University of Warwick, and *Julia*, thank you so much for helping me to conduct experiments with the Sf9 cells. Thank you for the hours of conversation and discussion about our projects and *not* about our projects, especially when we were in Ghent together! Your confidence and enthusiasm helped encourage some of my own self-belief toward the end of my PhD.

Thank you to *Kaat*, *Olivier*, *Rosa*, *Marta*, *Lien*, *Matt*, *Annette* and everyone else on the team at Syngenta, for your guidance and funding, and for hosting me on a fantastic trip to Ghent (where on the Saturday after my week at Syngenta, I got engaged!).

To the Cayre group, *Ben*, *Daniel*, *Cheng*, *Oisin*, *Amna*, and *James*, thank you for the lunches and coffee breaks, and many interesting in-lab and out-of-lab discussions.
To the Warren group, *Jonny*, *Clarissa*, *Yaz*, *Eleanor*, *Pete*, *Adan*, *Bart*, *Larissa*, *Ste*, *Kude*, and *Toby*, thank you for the bowling sessions, bringing coffee and cake to our meetings, and for listening to me talk about biology rather than polymers.

Laurin, my *Drosophila* friend! Thank you for bringing lots of great conversation about flies and life in general to the Isaac lab during the last few months of my experiments. Perhaps one day when you are back from Korea we can reunite and finally get the FlyPad up and running!

To my office mates, *Sebastian*, *Prashant*, *Chris*, *Abdul*, *Kieran*, *Mustafa*, and *Cheng*, thank you for offering me plenty of biscuits and other snacks, and a special thank you to *Prashant* for helping me to plan my post-PhD trip to India with my cousin! To the rest of CPEG, thank you for suffering my pestering and agreeing to present at our group meetings (sometimes).

To the Leeds SOFI Cohort 5 group, *Adele*, *Kate*, *Merin*, *Kalila*, and *Jordan*, thank you for your friendship and our shared commiserations and celebrations over these last 4 years. I am glad we all got through it together in the end! Thank you *Adele* for your incredible cakes, *Kate* for graciously listening to my constant complaining, and thank you *Merin* for talking to me about Kerala and helping me to plan my trip there. *Kalila*, thank you for surviving living with me for 2 years! Thank you for introducing me to cycling, for baking lots of sourdough bread, and for the TV-binging evenings. And thank you *Jordan* for occasionally checking the Facebook chat and coming to dinner with all of us!

Thank you to my wonderful friends outside of the academic world, *Lizzie, Bella, Abbie, Laura W, Emily, Becca, Maryann, Mili, Soph PC, Alice, Soph L, Phoebe, Rachel, Bethan, Laura P,* and *Rowan*. All of whom listened attentively to my many PhD woes and offered time and space for joy and frivolity, to remind me that there is more to life than the lab and my experiments.

Finally, thank you to *Sam* and *Mum*, *Dad* and *Eddy*, for supporting and loving me over the years. Thank you for listening to my fears and anxieties about my PhD, whether rational or irrational, and for encouraging me to keep going throughout the entire process. I owe everything to you, and I love you all very much. Thank you.

Extenuating Circumstances

Research on this PhD thesis began in May 2019. In March 2020, after 10 months of research (much of which was initial training), the Covid-19 pandemic hit and the UK went into a national lockdown. We were out of the laboratory for 8 months, until October 2020, when research resumed once again. During this time, I was able to successfully research, write and publish a literature review, which is included as part of the introductory chapter of this thesis.

Upon our return to research facilities, training opportunities were reduced and there were increased restrictions on laboratory occupancy and equipment use. The movement of the Physics department (that houses the light scattering instrument used in this thesis) from the E C Stoner to the new Bragg building, caused further disruption to my research for a large part of 2021. In January 2022 after the winter break, I personally contracted Covid-19, causing further delays to my return to the laboratory and research.

Fortunately, I was kindly awarded a 3-month extension for this PhD thesis by the University of Leeds, and I am very grateful for this allowance. However, I ask that the examiners of this PhD thesis take into account the large-scale disruption that the Covid-19 pandemic has caused to research at the University of Leeds.

Thank you for your consideration.

Abstract

Chemical insecticides are a typical tool used by growers to control pest insect species, such as the invasive fruit fly *Drosophila suzukii*. However, the rise of resistance to common chemical pesticides and widespread concerns of eco-toxicity has led to an increasing demand for biological alternatives with new modes-of-action and improved biosafety profiles.

RNA interference, discovered in 1998 by Fire and Mello *et al.*, can be exploited as a species-specific method of pest control. The application of exogenous double-stranded RNA to cells can induce the degradation of pre-determined mRNA transcripts, which can result in enhanced mortality of an insect pest if specific transcripts are targeted.

Induction of systemic RNAi can be generated in select insect species through oral administration of dsRNA. However, many insect species such as dipterans or lepidopterans are recalcitrant to RNAi through oral feeding of dsRNA. This is due to degradation of the orally delivered dsRNA by RNases in the haemolymph, saliva and intestines of the insect, or within the environment prior to ingestion. *Drosophila* in particular show low cellular uptake of dsRNA, due to the lack the SID-1-like transporter protein that ordinarily provides a faster cellular uptake pathway in comparison to endocytosis.

Polymeric delivery vehicles can therefore be developed to protect dsRNA against enzymatic degradation, and to enhance cellular uptake to induce insect mortality and thus pest management through RNAi-based control. This thesis describes the design, synthesis, characterisation, and *ex vivo*, *in vitro* and *in vivo* biological assessment of novel block copolymers, to act as protective vehicles for dsRNA for species-specific bio-insecticidal activity in *Drosophila suzukii*.

Table of Contents

Table of Figures

Table of Tables

Abbreviations

ACVA	4,4’-Azobis(4-cyanovaleric acid)
ATP	Adenosine 5′-triphosphate
ATRP	Atom transfer radical polymerisation
***t*BAA**	*tert*-butyl acrylamide
BSA	Bovine serum albumin
CCCP	4-((((2-Carboxyethyl)thio)carbonothioyl)thio)-4-cyano-pentanoic acid
CpC	*Drosophila* copper cell
CPP	Cell-penetrating peptides
CRP	Controlled radical polymerisation
CTA	Chain transfer agent
DAPI	4′,6-Diamidino-2-phenylindole
DCM	Dichloromethane
DHBC	Double hydrophilic block copolymer
DLS	Dynamic light scattering
DMEM	Dulbecco's Modified Eagle's Medium
DNA	Deoxyribonucleic acid
DP	Degree of polymerisation
dsRNA	Double-stranded RNA
EB	Ethidium bromide
EDTA	Ethylenediaminetetraacetic acid
FBS	Fetal bovine serum
GFP	Green fluorescent protein
GPC	Gel permeation chromatography
HCl	Hydrochloric acid
IAC	Intensity auto-correlation
IPEC	Interpolyelectrolyte complexes
IPM	Integrated pest management
IVT	In vitro transcription
LAM	Less activated monomers
LCST	Lower critical solution temperature
LS	Light scattering
MAM	More activated monomers
MHPB	Monohydroxybenzoic acid

MPC	2-Methacryloyloxyethyl phosphorylcholine
mRNA	Messenger RNA
MW	Molecular weight
MWCO	Molecular weight cut off
NMP	Nitroxide-mediated polymerisation
NMR	Nuclear magnetic resonance
PBS	Phosphate-buffered saline
PDMAm	Poly(*N*,*N*-dimethylacrylamide)
PDMAEMA	Poly(2-(dimethylamino)ethyl methacrylate)
pDNA	Plasmid DNA
PEG	Poly(ethylene glycol)
PEGMA	Poly(ethylene glycol) methacrylate
PEI	Poly(ethylene imine)
PLL	Poly(L-lysine)
PQDMAEMA	Quaternised poly(2-(dimethylamino)ethyl methacrylate
QDMAEMA	[2-(Methacryloyloxy)ethyl] trimethylammonium chloride
QELS	Quasi-elastic light scattering
RAFT	Reversible addition-fragmentation transfer
RDRP	Reversible deactivation radical polymerisation
RISC	RNA-induced silencing complex
RNA	Ribonucleic acid
RNAi	RNA interference
siRNA	Short-interfering RNA
SLS	Static light scattering
TAE	Tris base, acetic acid and EDTA
TEM	Transmission electron microscopy

Chapter 1. Introduction and review of recent literature

The chapter is partly based on the review published in *Frontiers in Agronomy* under the title, 'Recent Advances in Engineered Nanoparticles for RNAi-Mediated Crop Protection Against Insect Pests', 10.3389/fagro.2021.652981.

This first chapter introduces the background of the pest insect species of focus, the current insect control landscape and the need for novel insecticides, the RNA interference mechanism and barriers to delivery, a review of the recent literature on engineered nanoparticles for RNAi-mediated crop protection (in which target insects other than *Drosophila suzukii* will be considered) and the motivation behind the research in this thesis.

1.1 *Drosophila suzukii:* Pest insect species

The Asian vinegar fly, spotted-wing *Drosophila* (also known as *Drosophila suzukii*, first described by Matsumura in 1931[1]), is an invasive pest species that is native to South-East Asia. *D. suzukii* can be easily identified from their close relative *Drosophila melanogaster* by the distinctive dark spots on the wings of the males and the large, serrated ovipositor of the females (see Figure 1.1).

Figure 1.1. Light microscopy image of two male *Drosophila suzukii* adults (top), with the distinctive dark spots on the leading edge of their wings shown by dark blue circles. Two female *D. suzukii* adults are in the bottom half of the image, with their unique serrated ovipositors highlighted by light blue circles. The right-hand *D. suzukii* female has an egg attached to her ovipositor.

1.1.1 **Biology and ecology**

Drosophila suzukii are part of the *melanogaster* species group of the subgenus *Sophophora*, and of the Drosophilidae family of the order Diptera.[2,3] Female *D. suzukii* can lay up to 21 eggs per day, with each female laying approximately 200 eggs throughout her lifetime.[4,5] *D. suzukii* eggs will hatch after 1 – 3 days and go through three larval instar stages over the next 3 – 13 days. The larvae then pupate, undergo metamorphosis and eclose as adult flies to live for around 60 days, Figure 1.2.[2,6]

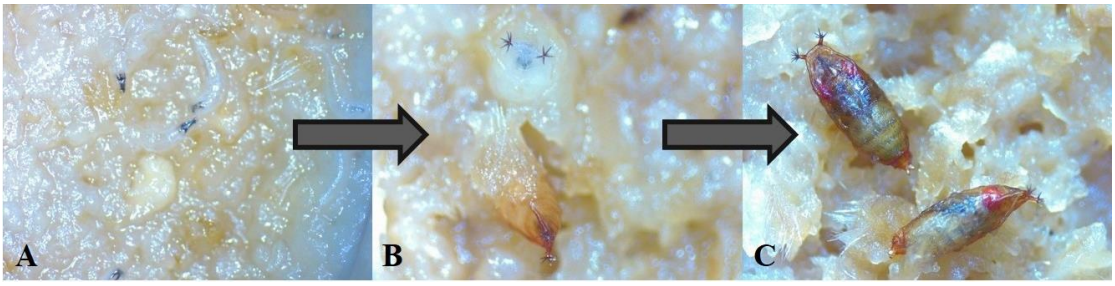

Figure 1.2. Light microscopy images of *D. suzukii* 3rd instar larvae (A) feeding on the standard diet as used in this research, *D. suzukii* pupae in their early stages, whilst forming the sclerotized pupal case (B) and *D. suzukii* pupae in a late stage, prior to adult eclosion (C).

D. suzukii are extremely sensitive to temperature, and their oviposition, mating and longevity are affected by the temperature of the surrounding environment. For example, Tochen *et al.* found that the development of *D. suzukii* from eggs through to adults could range from ~ 29 days at 14 °C, to ~ 11 days at 26 °C.[5]

The closely related species, *Drosophila melanogaster*, oviposit their eggs in overripe, fermenting fruit, and as such, are not characterised as a pest species.[7] In contrast, *D. suzukii* oviposit in ripening and fully ripe soft and stone fruits. They favour oviposition in fruits such as cherries, blueberries, blackberries, raspberries and other soft and stone fruits, at their peak ripeness or just prior. Their serrated ovipositors (as highlighted in Figure 1.1) are able to pierce the skin of these soft fruits, laying their eggs within the internal fruit tissues. As the larvae develop through each instar, their feeding causes the collapse of the fruit tissue and severe damage to the crop. Third instar larvae make their way to the surface of the fruit, typically pupating outside of the skin.

The impact of *D. suzukii* on crop fruits is therefore two-fold. Directly, the internal oviposition and larval feeding cause fruit tissue collapse. Following oviposition, there is the indirect impact of exposing the fruit to attack from external pathogens and other drosophilid species through the damage made by the ovipositor of the female *D. suzukii*.[4]

1.1.2 Economic impact

The two-fold crop damage caused by *D. suzukii* is a huge cause for concern for growers in areas where the pest insect is prevalent. *D. suzukii*, over the last couple of decades, has become a global economic pest, causing significant crop damage leading to large revenue losses for growers.

The first reports of *D. suzukii* date back to 1931 in Japan, followed by a spread to China in 1949. The flies can now be found in at least 22 of China's provinces. In Japan and China, *D. suzukii* target sweet cherries, blueberries and wax myrtle fruits. The rapid global spread of *D. suzukii* began in earnest after the fruit flies were detected in California in 2008. Goodhue *et al.* have estimated the revenue losses in California, due to the infestation as 37 and 20% for raspberries and strawberries, respectively.[8] As *D. suzukii* spread across North America, crops of blueberries, raspberries, blackberries and cherries, were affected. The reported total revenue loss in the states of California, Oregon and Washington combined (due to crop losses of strawberries, blueberries, raspberries, blackberries and cherries in 2008) was $2.6 billion.[9,10]

Following the spread across North America, Europe followed suit with an invasion of *D. suzukii* that began initially in the south of Europe, detected in Spain and Italy in 2008. From 2008 to 2014, *D. suzukii* spread to France, then the UK, Poland and across the rest of Eastern Europe. An assessment by De Ros *et al.* of the economic impact of *D. suzukii* on Trentino in Italy, suggested a total revenue loss of over €3 million in 2011.[11,12]

1.2 Chemical, biological and management controls

To mitigate against the mass infestation of *D. suzukii* and subsequent destruction of crops, a variety of different control measures have been trialled. These include physical crop management, biological controls and chemical insecticides.

Growers of susceptible crops need to employ a variety of management strategies as part of an integrated pest management (IPM) framework. For example, the use of high tunnels (tunnels covered with plastic or netting) to cover berries has been shown to significantly reduce the infestation of *D. suzukii*. Berries covered by a plastic high tunnel, untreated with insecticide, incurred a mean infestation of just 2%, in comparison to the open plots, treated and untreated by insecticide, that had 60% and 81% infested berries, respectively.[13] Other important

strategies include the prompt removal of infested and overripe fruit, and careful control of harvest intervals to reduce the amount of infestation. Growers are requested to monitor *D. suzukii* populations with traps set with apple cider vinegar, fruit purees, or yeast/sugar solutions, to keep track of the spread of the pest insects.

Biological control, exploiting the use of natural predators, is another method of pest insect management that can be utilised to control populations as part of an IPM strategy. Hymenopteran parasitoid wasps are known to be able to regulate *Drosophila* populations. The parasitic wasps attack *Drosophila* at either the larval or pupal stage, by delivering their eggs into the larvae (or through the pupal case) *via* their needle-like ovipositor.[14] The wasp larvae then develop within the larvae/pupae, at the expense of the *Drosophila.* However, *Drosophila* have developed their own methods to resist parasitoids, by encapsulating the parasitic eggs and preventing their further development. In turn, some parasitoid wasp species have evolved a strategy to produce virus-like particles to prevent encapsulation by the *Drosophila*.[14,15] When selecting a biological predator, it is important for the predator be specific to the host, and be efficacious in their population control of the host species. Recent work by Häussling *et al.* has found a significant preference of the parasitoid species *Trichopria drosophilae* for *D. suzukii* pupae specifically, indicating that it could be a promising candidate for controlling *D. suzukii* within a wider IPM framework.[16]

In terms of chemical control, there are a selection of insecticides that are effective and commonly used to manage populations of *D. suzukii*. These include organophosphates, neonicotinoids, spinosyns and pyrethroids.[4,6,10] However, the high reproduction rate of *D. suzukii* means that the species is able to quickly develop resistance to insecticides. This is particularly problematic for organic growers, who are already limited to a smaller pool of chemical control options. Spinosad (a naturally occurring substance made by soil bacterium) is a well-known organic bio-insecticide, but some resistance has already been shown by *D. suzukii*.[17] It therefore remains critical for growers to operate a rotation of control chemicals to

prolong their effectiveness. Additionally, it is important for growers to carefully consider the timing of insecticide spraying. This is particularly relevant for growers of bee-pollinated crops, as they need to ensure that bees are removed before insecticide application so that they will not be harmed, whilst they must spray crops early enough in order to protect them from infestation of *D. suzukii* that will attack the ripening fruit.[10]

The need for bio-insecticides with novel modes-of-action is clear, due to the susceptibility of *D. suzukii* to developing resistance to chemical insecticides, and the off-target effects of these insecticides on beneficial species such as pollinators.[18]

1.3 The urgent need for pesticides with novel modes-of-action

The world population is increasing rapidly, and food supply must equally rise to meet demand. It has been estimated, however, that ~18% of total crop production is destroyed by insect pests, with wheat and cotton hit the hardest with losses of up to 50 and 80%, respectively. This induces a financial penalty, with the global crop loss due to insect pests valued at an estimated US$470 billion.[19–22] As described in the previous section, the effectiveness of synthetic chemical pesticides introduced since the 1940s is continually being undermined by the appearance of resistant insect populations. Indeed, incidences of resistance to one or more synthetic pesticide has been reported for over 586 arthropod species, with the Arthropod Pesticide Resistance Database[23] actively growing at an alarming rate.[24–26] Consequently, growers are increasingly relying on IPM programmes in order to prolong the effectiveness of their arsenal of chemical pesticides.[21] Moreover, the lack of specificity of pesticides is a critical issue, with increasing reports of the detrimental impacts of these chemicals on beneficial pollinator species, predators, and other animals, occurring through bioaccumulation or leaching into the environment.[27–29] Thus, a variety of biological-based insecticides, such as the bacterial toxins of *Bacillus thuringiensis* (*Bt*) and *Saccharopolyspora spinosa*, have been developed as alternatives to synthetic chemical pesticides. These have modes-of-action quite

distinct from the traditional synthetic chemicals, and whilst this minimises the risk of cross-resistance, field resistance has been widely reported for both biologicals.[21,30–34] Thus, RNA interference offers a promising, alternative solution.

Since the discovery of RNA interference (RNAi) in the nematode worm *Caenorhabditis elegans* in 1998 by Fire and Mello *et al.*, strides have been made in exploiting RNAi for therapeutic applications, and more recently, for highly selective insect pest control. The mechanism of RNAi is described in the following section. Although triggering mRNA degradation in insects through RNAi offers significant opportunities in crop protection, the application of exogenous dsRNA is often ineffective in eliciting an RNAi response that results in pest lethality. The evolution of resistance of pest insect species to RNAi-based formulations also needs to be considered appropriately when developing delivery vectors (vehicles that are capable of carrying and protecting dsRNA). Introducing a large selection pressure could lead to mutations causing changes to core RNAi machinery.[35–38] For example, a population of western corn rootworm, *Diabrotica virgifera virgifera*, with resistance to DvSnf7 dsRNA showed cross-resistance to other dsRNAs.[39] Future research must focus on specific management strategies to slow the development of this resistance, particularly in species that are already refractory to RNAi.

In this context, RNAi offers a promising solution capable of generating biological insecticides with high selectivity toward target pest species. Triggering RNAi is a well-controlled approach that can target pest-specific transcripts and prevent specific protein production with low risk of off-target toxicity.[40,41]

1.4 RNA interference

RNAi was first discovered in animals by Fire and Mello *et al.* in 1998 and has since been widely adopted in the post-genomic era for functional gene analysis.[42] RNAi (Figure 1.3) is induced when exogenous double-stranded RNA (dsRNA) is internalised by cells and is cleaved by cytoplasmic ribonuclease III enzyme (Dicer-2) into 21–25 nucleotide-long duplexes called short-interfering RNA (siRNA), which bind to the RNA-induced silencing complex (RISC). Proteins of the complex unwind the loaded duplex into its sense (passenger) and antisense (guide) strands. The passenger strand is degraded, whilst the guide is used to locate the complimentary messenger-RNA (mRNA) sequence. Upon recognition, the mRNA is cleaved by the RISC, leaving the fragments to be subsequently degraded by cytoplasmic nucleases. The degradation of the mRNA and failure to translate to protein thus results in sequence-specific effects. Within the field of insect control, exogenously supplied dsRNA can result in insect mortality if the target protein has an essential function. The likelihood of mortality is significantly increased if the RNAi response is systemic *via* the transportation of the RNAi signal throughout the insect's body. However, not all insect species generate systemic RNAi

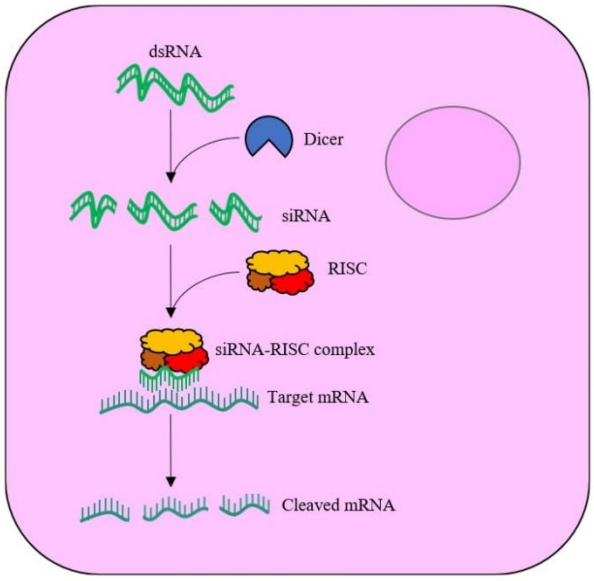

Figure 1.3. Schematic of the RNA interference (RNAi) mechanism within a cell. The exogenously supplied double-stranded RNA (dsRNA) enters the cell cytoplasm, where the enzyme, Dicer-2, cleaves the dsRNA into short–interfering RNA (siRNA) duplexes. The siRNA binds to the RNA-induced silencing complex (RISC), with the antisense (guide) strand maintained. The guide strand is used to locate complimentary messenger-RNA (mRNA), which is cleaved by RISC upon recognition.

responses to exogenously applied dsRNA. The reason for species differences in the spreading of RNAi between insect tissues is not fully understood.[41–47]

The exploitation of RNAi for crop pest control requires efficient uptake of exogenously supplied dsRNA by the target insect. Various strategies have been employed in research environments to administer the nucleic acid to crop pest insects, ranging from direct microinjection to the *in planta* expression of dsRNA. The microinjection or soaking of the insect in a solution of dsRNA have often been shown to be more effective in comparison to topical application and oral administration.[35,48–50] However, there are some examples of the successful application of exogenous dsRNA by topical or oral administration in certain insect species.[48,51–55] Use of dsRNA as an insecticide for crop protection requires deposition by foliar or soil spraying, followed by uptake either by contact with the insect's cuticle or by ingestion by the feeding insect.[45,56,57]

1.5 Barriers to RNA-mediated pest control

The failure to elicit a strong RNAi response by feeding or topical application of naked dsRNA in some insect species, despite success when administered by microinjection, highlights limitations in developing dsRNA as a general pest control solution.[48,58] The ineffective induction of RNAi by environmental, naked dsRNA is often due to its degradation.[59–66] There are several possible barriers to an effective insect response, as summarised in Figure 1.4.

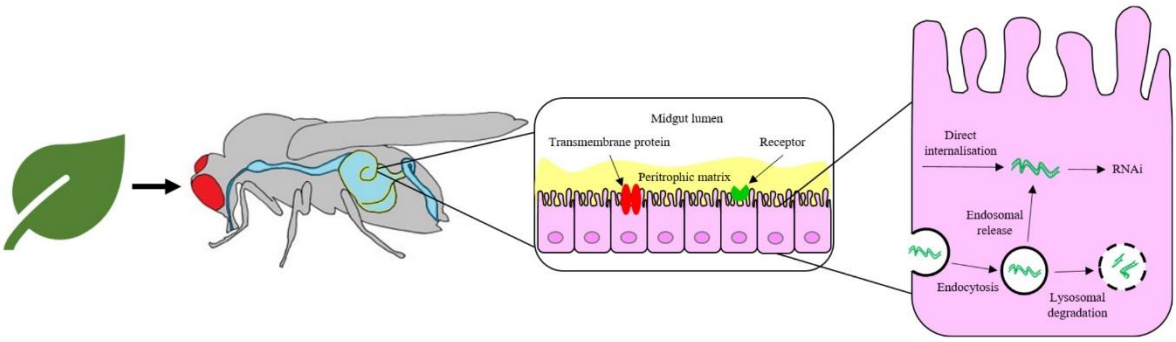

Figure 1.4. Pathway for the delivery of exogenous, naked RNA to insect gut cells *via* foliar or soil application and oral feeding of the insect. The barriers to efficient delivery include metabolic instability in the gut lumen, inefficient uptake by gut epithelial cells and poor release of dsRNA from endosomes.

The most likely option for delivery of a formulated dsRNA-based insecticide is through sprayed deposition onto the crop followed by ingestion by the insect pest. Thus, it is paramount to take into account the requirements of the method of application in designing a delivery solution for the dsRNA, in particular, the following considerations for successful pest control:

i. Prior to application, the insecticide must be designed as a dispersion with a homogenous distribution of dsRNA. Thus, dsRNA vectors (or carriers) must retain their colloidal stability throughout the various stages of the application, from the storage in the formulated pesticide, the dilution in water upon application, the spraying in the field, the deposition and drying on the crop and finally, during transport through the digestive tract of the insect and cellular uptake. In addition, the vectors should have low off-target toxicity.

ii. Upon application of the formulation, the nucleic acid must survive deposition onto leaves or soil by withstanding harsh physical conditions and environmental biodegradation. Exogenously applied dsRNA can be fully degraded in soil and aquatic environments in less than 3 days by microbial-produced RNases.[60,64,67,68] In particular, RNA, due to the additional hydroxyl group in the 2’ position of the pentose ring, is more susceptible to degradation by hydrolysis than DNA.[69]

iii. Following ingestion by the insect, the dsRNA must survive attack by enzymatic nucleases and pH changes within the intestinal gut lumen before cellular

internalisation by first traversing the inert peritrophic matrix that lines the gut and then the midgut epithelial cell membrane. The means of cellular uptake from the gut lumen appear to vary between species and might involve one or more mechanism, such as passive transport *via* a transmembrane protein, pinocytosis or receptor-mediated endocytosis.[65,66] It has been reported that the size limit for non-specific uptake into cells is 150 nm, thus size is critical for efficient transfection.[69]

iv. If internalised by endocytosis, the dsRNA must escape the endosomal compartment prior to lysosomal degradation[70,71] before dsRNA may at last take part in the RNAi mechanism.

1.6 Variability in RNAi efficiency of exogenous dsRNA

The species variability in the efficacy of exogenous dsRNA to elicit RNAi is well-documented.[65,66,72,73] Insects of the order Coleoptera, e.g., the red flour beetle *Tribolium castaneum*, respond efficiently to both microinjection and oral feeding of dsRNA. In contrast, many lepidopteran and dipteran species only respond to naked dsRNA through microinjection.[48,51,72,74] The life stage of the insect and the experimental protocol used have also been observed to influence RNAi efficiency. Why there are these differences between species and during different stages of the life-cycle is not fully understood, but some contributing factors have been identified.[36,37,45,47,59,59,62,65,75–78]

The degradation of dsRNA by RNases within the intestinal gut lumen, saliva or haemolymph of the insect species will reduce RNAi efficiency. Increased RNase activity at a particular life stage or differences in the chemical environment (e.g. gut pH) can explain some of the variability seen in the RNAi responses of insects. Lepidopterans, in particular, can be refractory to RNAi *via* both microinjection and feeding with recent research by Singh *et al.* showing the reduced processing of dsRNA to siRNA within this insect order.[61,62] The *up56* gene, encoding for an additional RNAi efficiency-related nuclease (REase), could be

responsible for the decrease in RNAi efficiency.[79] In addition, ineffective endosomal escape within cells has also been suggested to contribute to lower RNAi efficiency in Lepidoptera.[61,79,80]

An in-depth discussion of the factors that contribute to varying RNAi efficiency in different insect species can be found in several recent review articles (Cooper *et al.*, Scott *et al.*, Terenius *et al.* and Liu *et al.*) that also recommend strategies, such as the use of nanocarriers for the delivery and uptake of dsRNA, to improve the RNAi response for insect pest control.[35,47,65,72,81,82]

1.7 Novel methods of delivery

The exciting potential of exogenous dsRNA to provide a new generation of highly selective insect control agents has focused attention in the last 10 years on the development of delivery systems to counter the physical and metabolic instability of the nucleic acid in the field, which can result in the complete degradation of dsRNA within days.[60,64] In the last decade, many novel nanoparticle delivery vehicles (also known as vectors or carriers) for dsRNA have been developed, including self-assembled block and branched copolymer nanoparticles, dendrimers, inorganic nanoparticles, and natural product-based nanoparticles, see Figure 1.5.

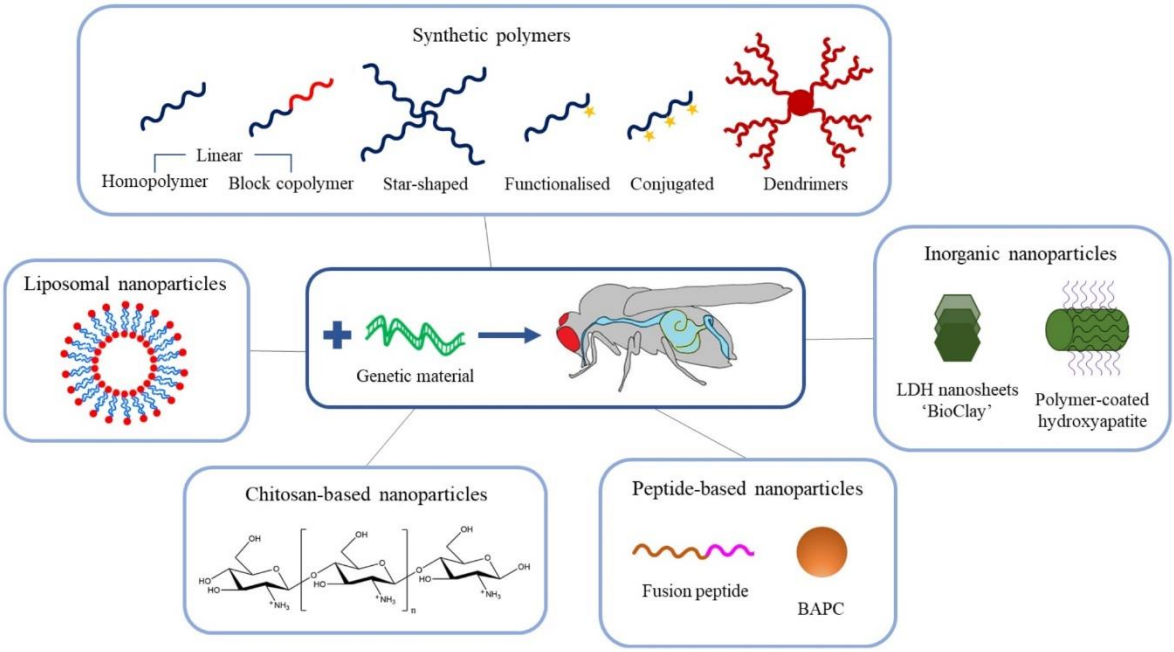

Figure 1.5. Schematic overview of the recent advances in engineered nanoparticles for RNA-mediated crop protection strategies.

The majority of dsRNA delivery solutions utilise the electrostatic interaction between the anionic phosphate backbone of dsRNA and some cationic character expressed on the nanoparticle vector to assemble a system capable of protecting and transporting the dsRNA. Further details of these systems are discussed in the following sections.

1.7.1 **Synthetic polymeric delivery vectors**

Synthetic polymeric delivery vectors often require well-defined polymer chains with precise molecular weight, narrow molar mass dispersity (*Đ*) and defined (co)polymer architecture (e.g., homo, block, star, or graft polymers). They are also tolerant to chemical functionalities, enabling the polymerisation of functional monomers without the need for protecting groups.[83] These highly desirable credentials have enabled not only the precise engineering of functional polymeric vectors, but also the ability to conduct highly systematic studies of the influence of the polymer construct on delivery efficiency. Hence, polymeric delivery vehicles have been designed, synthesised and investigated in this thesis.

1.7.1.1 Linear homopolymers

The simplest polymeric architectures used for the delivery of dsRNA are linear homopolymers, such as poly(2-(dimethylamino)ethyl methacrylate) (PDMAEMA), poly(ethylene imine) (PEI), and poly(L-lysine) (PLL).[84–89] These polymers only comprise of one monomer, which incorporates amine groups within the polymer chain backbone or on pendant groups which are positively charged below their pKa (e.g., 7.4–7.8 for PDMAEMA[90], 8.2 – 9.5 for PEI[91,92] and 9 – 11 for PLL[93]). This cationic character facilitates complexation with the anionic dsRNA phosphate backbone, through electrostatic attraction of the two macromolecules, a process that is entropically favourable due to the release of counterions.[84–86] The resulting complexes are often referred to as polyplexes.

PDMAEMA and PEI have often been selected as gene transfection agents due to their 'proton sponge' capabilities for endosomal escape. Bus *et al.* describe the different strategies of endosomal escape for polycation/nucleic acid polyplexes in detail.[94] In brief, there are three current theories of endosomal escape:

→ **'Proton sponge' effect.** The effect by which buffering polycations, such as PEI or PDMAEMA, become protonated within the acidifying late endosomes (pH ~ 5). This leads to an influx of chloride ions and thus an osmotic imbalance, inducing the influx of water into the endosome. The endosome swells, causing membrane tension and eventually rupture, releasing the polyplex cargo. Whilst there is evidence to suggest that the proton sponge effect plays a significant role in endosomal escape, other experimental evidence is contradictory and thus the debate is still open as to what role it plays in the gene delivery process.[94–98]

→ **Polyplex-mediated membrane disruption.** This theory suggests that rather than full endosomal membrane rupture, a minor membrane disruption occurs instead. This is

mediated by a positive overall charge of the polyplexes, causing membrane disruption (which can also lead to cell lysis and death). The nanoscale holes formed in the membrane allows the release of polyplexes into the cytoplasm.[94,99–102]

→ **Polymer-mediated membrane disruption.** The third theory is similar to the above polyplex-mediated theory, in that the endosome membrane remains mainly intact throughout the process of escape. However, this theory suggests that free polymer (decomplexed from the nucleic acid) is able to intercalate within the membrane, inducing membrane permeability (or nano-hole formation) to allow the nucleic acid and/or polyplex to escape. This strategy relies on the ability of the polymer to freely complex and decomplex from the nucleic acid in order to intercalate into the membrane.[94,101,103–106]

PEI and PDMAEMA homopolymer delivery vehicles are often found to have low cellular internalisation efficiency and can be highly toxic to mammalian and insect cells.[95,107] This cytotoxicity is likely a result of polymer interaction with the cell membrane, leading to pore formation and cell death.[108–111] These factors mean that linear homopolymers are not the most effective vehicle for the delivery of dsRNA, which is unfortunate given their low cost. Thus, to address these issues, many other, more complex polymeric architectures and functional groups have been designed to enhance dsRNA stability and efficiency of cellular uptake, whilst reducing cytotoxicity. For example, chain extension with additional monomers to form diblock or triblock copolymers, or a change of architecture to form star-shaped polymers, have been investigated to synthesise novel vehicles for more efficient delivery of dsRNA to a variety of insect species.[64,112–116]

Variation in molecular weight, charge density, pKa, and ionic strength, which can be achieved by simply altering the chemistry of the polymeric vectors, have also been considered in order to overcome the aforementioned issues, with varying degrees of success.[108,117–121] For example,

whilst higher molecular weight homopolymers complexed with dsRNA (or DNA) exhibit greater transfection efficiency, the cytotoxicity of the polyplexes increases with the increase in molecular weight.[121] In the next sections, recent advances in the development and application of these various architectures are described, as summarised in Table 1.1.

Table 1.1. Polymeric delivery vehicles for RNA-mediated crop protection from the last 10 years that conducted *in vitro* or *in vivo* assay with the resulting polyplexes.

Nanoparticle type	**Target transcripts**	**Insect/plant species or cell type**	**RNAi efficiency**	**Ref.**
Guanidinium-functionalised polymers	*SfV-ATPase*	*Spodoptera frugiperda*	>80 % knockdown	114
	AgCHSB	*Spodoptera exigua*	53 % mortality	115
CPNs	*NtCesA-1*	Tobacco BY-2 protoplasts	>76 % transcript reduction	112
PAMAM dendrimer	*TCTP*	*Bombyx mori* cells	Knockdown at higher PAMAM concentrations	122
PAMAM dendrimer with fluorescent PDI core	*Hemocytin*	*Drosophila* S2 cells	95.4 % transcript reduction	123
	Decapentaplegic	*Drosophila*	Larvae body length reduced by 35 %	124
	Serpin-3	*Ostrinia furnacalis*	mRNA level reduced by 51 %	125
	STM and *WER*	*Arabidopsis thaliana*	*STM* and *WER* mRNA level reduced by 84 % and 87 %	126
	CHT10	*O. furnacalis*	Reduced body weight, size of larvae and CHT10 mRNA level	127
PAMAM-CNT	*Mtpol* and *α-tub*	*T. castaneum*	*Mtpol* and *α-tub* expression levels reduced by 89 % and 99.5 %, respectively, 72 h after microinjection	128

1.7.1.2 Branched polymers

More complex polymer architectures, such as branched polymers, have been investigated with the aim of improving transfection and RNAi efficiency, whilst reducing cytotoxicity levels.

Synatschke *et al.* used atom transfer radical polymerisation (ATRP) to highlight the difference between linear PDMAEMA and 3- and 5-arm PDMAEMA star-shaped equivalents in terms of their cytotoxicity and transfection efficiency in mammalian cells. Linear, 3- and 5-arm polymers were prepared with dispersity (*Đ*) ranging from 1.09 to 1.80. In this study, it was evident that as the complexity of branching increased (i.e. number of arms), the cytotoxicity decreased as a result of the majority of the complexing nitrogen atoms being contained within the dense core of the star-shaped polymer. Consequently, interaction of the more branched polymers with membrane phospholipids, and thus destabilisation of cell membranes, is reduced. Transfection efficiency was comparable between the linear and star-shaped polymers, however a higher amount of polymer was required to fully stabilise the DNA in the case of the 3- and 5-arm polymers, as fewer nitrogen complexing moieties were available.[111]

Whitfield *et al.* also compared linear and star-shaped polymers, instead using poly(2-(dimethylamino)ethyl acrylate) (PDMAEA) to investigate the protection afforded to dsRNA. The aim of their work was to mitigate environmental biodegradation of dsRNA in soil.[60] For this purpose, linear and 4-arm star-shaped PDMAEA were synthesised by ATRP with *Đ*-values of 1.18 and 1.14, respectively.[64] The complexed dsRNA was more persistent in living soil, delaying metabolic degradation by an additional 7 and 14 days with linear and star-shaped PDMAEA, respectively. Molecular dynamics simulations indicated a stronger binding between star-shaped PDMAEA and DNA, with more compact polyplexes formed due to the efficient bending around the DNA. The reduced surface area of the more compact star-shaped PDMAEA polyplexes limits contact of the nucleic acid with degrading nucleases, hence enhanced protection and slower release of dsRNA. In a different study, linear and 4-arm star-shaped PDMAEA were synthesised by reversible addition-fragmentation transfer (RAFT)

polymerisation, with *Đ* of 1.14–1.15 for the linear and 1.35–1.38 for the star-shaped polymers.[129] These polymers were complexed with DNA and used to transfect mouse 3T3 fibroblast cells. The 4-arm star-shaped PDMAEA formed more compact DNA polyplexes, with less polymer required for equivalent stable binding in comparison to polyplexes made with the linear polymer.[64,129]

It is important to note that PDMAEA, in contrast to PDMAEMA, is prone to self-catalysed hydrolysis, see Figure 1.6 and Figure 1.7[90,130,131], resulting from a phenomenon that is explained by Ros *et al.*[132]

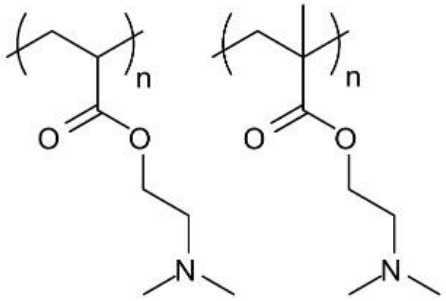

Figure 1.6. Structures of PDMAEA (left), used by Whitfield *et al.*[64] in comparison to PDMAEMA (right) used by Synatschke *et al.*[111] The additional methyl group on the PDMAEMA polymer backbone leads to a significant lowering of the polymer hydrolysis rate resulting in less biodegradability.

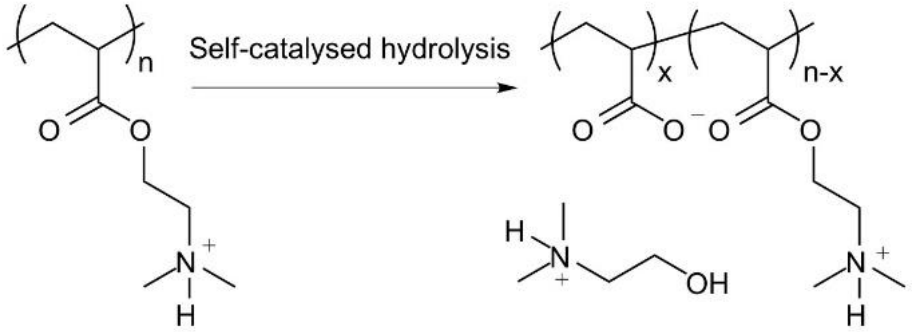

Figure 1.7. Outcome of the self-catalysed hydrolysis of PDMAEA to polyacrylic acid and 2-dimethylaminoethanol.

This hydrolysis has been linked to more efficient release of complexed dsRNA for incorporation into the RNAi machinery, thus inducing RNAi more easily.[65,116] However, a potential drawback of incorporating self-catalysed hydrolysis mechanisms into polymers, is

that the complexes may be prone to premature release of dsRNA prior to reaching the cells where RNAi occurs.

1.7.1.3 Guanidinium-modified polymers

The recognised potential of RNAi in therapeutics has provided much of the impetus in the design and development of functionalised polymers as vectors for dsRNA. For example, recent developments in this field have included pH-responsive polymers that undergo a pH-dependent conformational change to release dsRNA in the acidic environment of the endosome compartment of the cell, over the physiological to endosomal pH transition.[133–138] However, this targeted pH transition range may not be applicable for insect control strategies. Lepidopteran pests, such as *Spodoptera* (armyworm) species, have an intestinal gut lumen pH of 10 to 11, which can increase dsRNA instability in the insect gut. The development of polymers designed to protect dsRNA in this highly alkaline environment requires special consideration of the effect of pH on polymer complexation.

Guanidinium-based polymers have been designed for the protection of dsRNA over the alkaline pH range found in the gut of lepidopteran pests. These polymers bear similarity to arginine-rich cell-penetrating peptides (CPPs) that aid endocytic passage through cell membranes, as well as the escape of RNA from endosomes.[139–142] The cationic homopolymer poly(N-(3-guanidinopropyl)methacrylamine) (PGPMA), prepared by RAFT polymerisation, has a pKa of 12.5 to ensure protonation of the guanidinium functional groups even in the alkaline gut. Complexation of PGPMA with dsRNA was shown to occur at pH 10, forming more compact polyplexes than those formed at pH 7.4, see Figure 1.8.

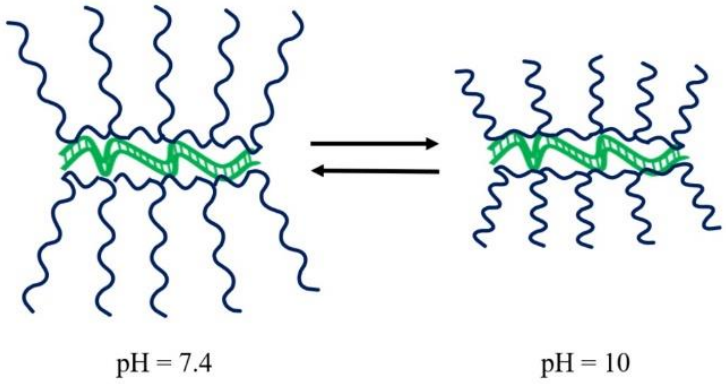

Figure 1.8. Schematic of the impact of pH on PGPMA polymers whilst complexed to dsRNA. Upon increasing pH, the polyplexes become more compact. Modified from work by Parsons *et al.*[114]

PGPMA/dsRNA complexes induced suppression of the *CDC27* transcript in Sf9 cells after 48 h incubation, with ~ 90% reduction in *CDC27* mRNA. Feeding second and third instar larvae of the fall armyworm, *Spodoptera frugiperda*, on PGMA/*CDC27*-dsRNA polyplex-supplemented diet for 7 days, resulted in 80% transcript reduction, with ~ 30% larval/pupal mortality after 29 days.[114]

Christiaens *et al.* synthesised a series of homopolymers and copolymers of poly(*N*-(2-aminoethyl) methacrylate) (PAEMA) and PDMAEMA *via* free radical polymerisation, which were further functionalised by reacting some of the primary amine moieties of the PAEMA block with 1*H*-pyrazole-1-carboxamidine hydrochloride (HPC) to yield copolymers with guanidine (GUMA) (*Đ* of the copolymer ranged between 1.41 and 2.86).[115] The copolymer (poly(AEMA-*co*-GUMA)) with the highest proportion of guanidine content protected dsRNA to a greater extent than the other polyplexes, when incubated with the midgut contents of *Spodoptera exigua* larvae, buffered at both pH 7.5 and 11. A low molecular weight poly(AEMA-*co*-GUMA) polymer complexed with dsRNA of the vital *chitin synthase B* (*ChSB*) gene, stabilised the dsRNA for at least 30 h in *S. exigua* gut juice at pH 11. Oral presentation of 50 µg of poly(AEMA-*co*-GUMA)/*ChSB* dsRNA to *S. exigua* larvae on cabbage leaves inhibited larval development and resulted in over a three-fold increase in mortality after 13 days when compared to feeding naked dsRNA. Confocal microscopy of

cultured CF302 midgut cells incubated with Cy3-labelled dsRNA complexed with FITC-labelled poly(AEMA-*co*-GUMA) indicated greater cellular internalisation of polyplexes compared to naked dsRNA.[115]

These studies indicate that the incorporation of guanidine functional groups within the polymer structure provides enhanced protection for dsRNA in the alkaline pH conditions found in the gut of *Spodoptera*. They also show that the guanidine-functionalised copolymers can greatly improve the *in vivo* efficacy of RNAi as an insect growth regulator and biocide. However, other pest insect species (such as the *D. suzukii* targeted in this thesis), unlike *Spodoptera,* may have midgut sections that are highly acidic. For example, Ferguson *et al*. determined that the central section of the midgut of *D. suzukii* displays pH < 3.[143] Therefore, varying pH conditions (rather than only alkaline environments) must be considered for *D. suzukii*-focused applications.

1.7.1.4 Conjugated polymer nanoparticles

Conjugated polymer nanoparticles (CPNs) are composed of polymers with a backbone of alternating single and double bonds that create a conjugated system of π-electrons, for example polyacetylene. This induces a variety of useful properties such as conductivity and fluorescence.[144]

CPNs have been introduced for delivery of siRNA to HeLa cells.[145] These nanoparticles comprised an amine-containing poly(phenylene ethynylene) (PPE) polymer, with a hydrophobic backbone to facilitate cellular internalisation and endosomal escape. These CPNs appear to form loosely aggregated particles, allowing effective complexation with siRNA due to their large, exposed surface area. A 94% knockdown of *actin B* expression was found when CPN/siRNA complexes were transfected into HeLa cells.

A similar PPE polymer was synthesised to form CPNs for use in plant protection against viral challenges and for the oral delivery of siRNA to insects. *NtCes1-A* siRNA, a cellulose synthase gene, was complexed with the CPNs and incubated with protoplasts. A calcofluor white M2R staining assay revealed that following a 72 h incubation with the CPN-siRNA, protoplasts displayed 33 – 38% regeneration of their cell walls, in comparison to 51 – 54% in protoplasts that were either untreated or treated with naked siRNA or CPNs alone. Additionally, the transcription levels for *NtCes1-A* in CPN-siRNA treated protoplasts after a 48 h incubation were reduced by over 76%, compared to a 17% *NtCes1-A* mRNA reduction with CPN treatment alone. Internalisation of nucleic acids by protoplasts has traditionally been achieved with poly(ethylene glycol) (PEG) or by electroporation, which enhances the cell membrane permeability through short, high-intensity electrical pulses.[146,147] However, with use of both PEG and electroporation, there was a detrimental impact on protoplast viability.[112,146,148] In comparison, delivery of siRNA to plant protoplasts with CPNs significantly reduced cytotoxicity.[112]

It is worth mentioning here, a recent development of conjugated polymer/siRNA nanoparticle complexes for application in therapeutics that may also hold promise for delivery of dsRNA for crop protection. Indeed, the recent design of conjugated polymer-dots that are formed by nanoprecipitation could be adapted to developing systems for delivery of dsRNA in other areas. These polymer-dots combine a core of conjugated polymer with a functional corona copolymer and a cationic lipid for complexation with siRNA. The resulting conjugated polymer dot/siRNA complexes have shown comparable efficiency and lower cytotoxicity than the industry-standard, Lipofectamine 2000®.[149]

1.7.1.5 Dendritic nanocarriers

Dendrimers are highly branched polymer architectures defined by a central core, a branched interior structure of defined dimensions and a surface that contains functional groups. They

can be used as delivery vehicles by retaining active species within the pores created by the branched structure and/or on their surface. So-called 'Starburst' dendrimers were reported for gene transfection in 1993[150] and such macromolecular species are now commonplace for therapeutic gene delivery within commercial DNA transfection kits such as SuperFect®.[151] However, the use of dendritic nanocarriers for delivery of dsRNA to insect species was not realised until 2013 by He *et al.*, and the first report of the successful use of generation 5 (G5, referring to 5 cycles of repeated branching during the dendrimer synthesis) poly(amido amine) (PAMAM) dendrimers for dsRNA delivery to insect cells was reported in 2019.[122,127,152]

Dendrimers for the delivery of dsRNA are most commonly formed from PAMAM. They have well-defined nano-scale structures with a cationic surface charge that enables electrostatic capture of dsRNA. Lu *et al.* report the use of a G5 PAMAM dendrimers for the delivery of both dsRNA and plasmid DNA (pDNA) to two types of cultured cells from the lepidopteran insect, *Bombyx mori* (silkworm). G5-PAMAM/dsRNA dendriplexes were effective at interfering with the expression of the translationally controlled tumour protein (*TCTP*) and the fluorescent red-ubiquitin (*Ub*) genes in BmE and BmN cell cultures.[122]

Fluorescently labelled PAMAM dendrimers have been synthesised with a perylenediimide (PDI) fluorophore core, see Figure 1.9, to aid visualisation of delivery *via* fluorescence microscopy.

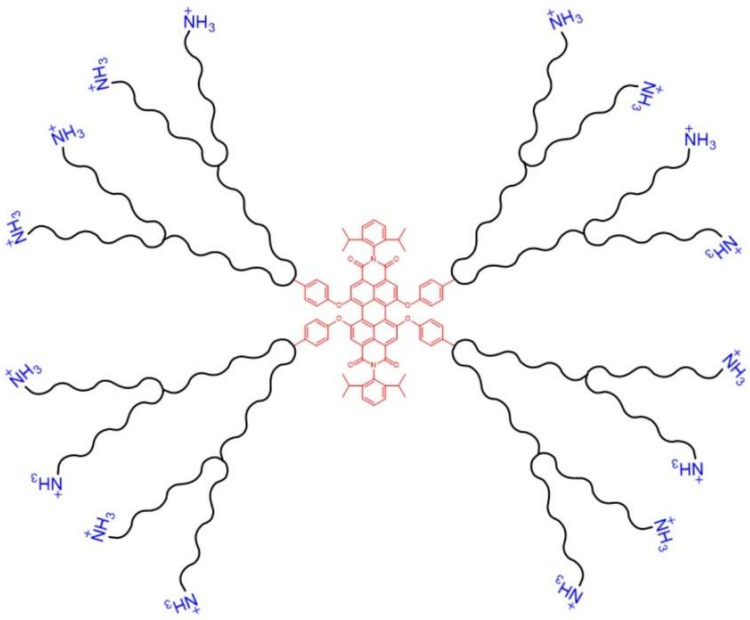

Figure 1.9. Schematic of a dendritic nanocarrier, with a PDI core (shown in red, centre) and NH_3 groups for complexation with dsRNA (shown in blue, outer layer).

On topical application of the PDI-G2-PAMAM/dsRNA complexes, targeting the *haemocytin* transcript, to 4th instar *Aphis glycines* (soybean aphids), fluorescence from the PDI core was observed within 1 h in the circulating haemolymph and various internal tissues, demonstrating the systemic delivery of the dendriplexes. *Haemocytin* expression was reduced by 95% and a population density decrease of 81% was achieved by 5 days post treatment.[123]

A similar water-soluble PDI-G3-PAMAM nanocarrier, with extended dendritic arms (a higher generation dendrimer) was synthesised by Xu *et al.*, and provided steric stability to the dendriplexes, preventing aggregation in aqueous solution due to the water insoluble PDI core. The nanocarrier was complexed with DNA and used to transfect *Drosophila* S2 cells. Fluorescence from the PDI core was seen in cultured cells 1 h post-incubation, with > 90% cell viability. The same dendriplexes, targeting the developmental *decapentaplegic* transcript, fed to *Drosophila melanogaster* larvae, reduced the body length of 3rd instar larvae by 35%. This growth deficiency shows the potential of PDI-PAMAM as a dsRNA delivery vehicle.

The high transfection capability of dendriplexes is in part due to the globular structure of the nanocarrier.[124]

A dendritic nanocarrier with a PDI core has also been employed to deliver *serpin-3* dsRNA by feeding to newly hatched larvae of the Asian corn borer, *Ostrinia furnacalis*. The cationic dendrimer was efficiently taken up by the midgut and fat body cells of the feeding larvae. When fed larvae were challenged with the bacterium *Micrococus luteus*, the transcript of *serpin-3* (a critical immune-response gene) was reduced by 51% overall and more strikingly yet, serpin-3 protein was undetectable in the haemolymph. Similar fluorescent nanoparticle dendriplexes have been used for oral delivery of dsRNA targeting a vital chitinase-like transcript (*CHT10*) of *O. furnacalis*. Feeding 1st instar larvae with the nanoparticles stunted growth and after 5 days resulted in failure to moult and insect death.[125,127]

The use of dendrimer-coated carbon nanotubes (PAMAM-CNTs) to deliver α–tubulin (*α-tub*) and mitochondrial RNA polymerase (*mtpol*) dsRNA to *T. castaneum* has recently been demonstrated. In both targets, 4th instar larvae injected with PAMAM-CNT-dsRNAs showed significantly greater reduction in gene expression after 72 h, in comparison to the naked dsRNA controls.[128]

Thus, several studies have shown that dendrimers based on PAMAM are effective polymeric vectors for dsRNA-mediated RNAi. These dendriplexes typically have high transfection efficiencies, low cytotoxicity and high water solubility, and show efficient RNAi induction in insect tissues through oral feeding. Further research on the effectiveness of these nanoparticle formulations to trigger RNAi in pest species from different orders is required to establish dendrimer/dsRNA formulations as a generic insect control solution, but the studies discussed above have demonstrated the potential of such systems for specific insects.

1.7.2 **Inorganic nanoparticles**

1.7.2.1 Clay nanosheets

A novel vector consisting of layered double hydroxide clay nanosheets (LDH), for delivery of virus-specific dsRNA, has been developed to protect plants against viral infections.[153] The non-toxic LDH forms a positively charged layered lamellar structure with dsRNA (tested within the range of 300 to 1800 base pairs (bp)) which either adsorbs to the surface, or sandwiches between multiple particles, to create what has been called 'BioClay' formulations. The LDH material degrades in an atmosphere of CO_2 and moisture due to the formation of carbonic acid, with around 25% degradation after 7 days at 5% CO_2 and 95% relative humidity (RH). Importantly, the BioClay formulation protects dsRNA from leaf surface run-off and from metabolic breakdown for up to 30 days. The formulation provides sustained release of dsRNA on the leaf, which in turn results in long-term systemic protection against the targeted viral infection.

These properties are critical to overcoming the barriers of foliar sprayed application to crops, such as run-off and enzymatic degradation prior to ingestion by insect species that must be reduced for efficient RNAi delivery and action. In particular, these recent studies demonstrated that *Vigna unguiculate* and *Nicotiana tabacum* plants were protected against viral challenges from Cucumber mosaic virus (CMV) and Pepper mild mottle virus (PMMoV), respectively, by the sprayed application of *CMV2b* and *PMMoVIR54*-specific BioClay formulations. A systemic RNAi response was observed in *N. tabacum* plants. Subsequently it was reported that bean common mosaic virus coat protein (BCMVCP) dsRNA incorporated within LDH BioClay nanosheets also protected *Nicotiana benthamiana* against virus transmission by the peach-potato aphid, *Myzus persicae*.[154] This recent work provides early evidence that BioClay has the potential to protect plants against viral challengers transmitted by pest insect species *via* a long-lasting integrated RNAi strategy.[153]

1.7.2.2 Polymer-coated inorganic nanoparticles

Studies are specifically highlighted here, where inorganic nanoparticles are used as a template of known properties, particularly size and size distribution, to build hybrid polymer structures designed for efficient interaction with, and retention of, dsRNA. Indeed, the use of particles (or a well-known template particle) onto which appropriate chosen/designed polymers are coated allows for control of the carrier properties.

Biocompatible calcium phosphate (CaP) nanoparticles have been used in therapeutic applications for drug or gene delivery. CaP nanoparticles carrying dsRNA have been shown to enter cells *via* endocytosis and release their cargo within the endosome.[155] In therapeutic applications, the process of cellular internalisation and *in vivo* RNAi can be made more efficient by using polymeric coatings such as PEG and PEI to modify the nanoparticle surface.[155,156]

In recent research by Elhaj Baddar *et al.*, a hydroxyapatite (HA) inorganic nanocarrier with a polymer coating was used to induce RNAi in insect Sf9 cells. The HA nanoparticle template was coated in poly(acrylic acid) (PAA) through layer-by-layer electrostatic assembly. The addition of cationic amine groups is known to improve binding, therefore a layer of poly(arginine) (PLR10) was added to the nanoparticles to electrostatically interact with dsRNA.[157,158] When targeting the *luciferase* transcript in Sf9 cells, a 35% transcript reduction was achieved at a mass ratio of PLR_{10}+PAA-coated HA nanoparticle to dsRNA of 5:1. In comparison, both naked dsRNA (25 ng/100 μL) and the PAA-coated HA nanoparticle/dsRNA system did not lead to significant mRNA degradation.

Moreover, the same arginine-containing polymer (PLR_{10}-PAA-HA) was complexed with dsRNA possessing a fluorescent probe, CypHer5E, that fluoresces specifically at the pH of late endosomes (pH 5), to test the endosomal escape of dsRNA following delivery to cells. It was found that, upon delivery of the complex, a significant reduction in the fluorescence

within the acidic bodies of Sf9 cells occurred. In contrast, delivery of naked CypHer5E-dsRNA had a strong fluorescence in endosomal compartments. The enhanced RNAi response due to dsRNA complexation with PLR_{10}-PAA-HA nanoparticles is thought to be a result of enhanced endosomal escape.[159]

Gold (Au) is another inorganic nanoparticle that has been employed as a template for dsRNA delivery, due to its tuneable surface and low toxicity.[160] In a recent report, a PLR_{10} polymer was covalently attached to the surface of Au nanoparticles (AuNPs) with hydroxysuccinimide (NHS) surface groups to which a bovine serum albumin (BSA) ligand was also attached to achieve a mixed surface layer of the polymer and BSA.[161] The BSA ligand, an amphiphilic peptide, is suggested to improve endosomal escape in a similar mechanism to cell-penetrating peptides (CPPs). The PLR_{10}-Au-BSA/siRNA nanoparticles induced a 31% reduction of the *luciferase* transcript in Sf9 cells, but, in comparison, PLR_{10}/siRNA polyplexes elicited an efficiency of 58%, with the strong binding of PLR_{10} to the AuNPs hypothesised as the cause of the lower transfection efficiency. However, the binding of PLR_{10} to citrate-stabilised gold nanoparticles through electrostatic layer-by-layer coating of PLR_{10}, rather than covalent binding with NHS, led to less successful attachment of PLR_{10} and thus resulted in aggregation of the nanoparticles.[161]

These studies demonstrate important steps towards using polymer-coated inorganic nanoparticles for dsRNA delivery, as surface functional groups could improve cell-targeting and thus enhance dsRNA uptake and endosomal escape.[161] Table 1.2 summarises the recent reports in this area.

Table 1.2. Novel inorganic nanoparticles for RNA-mediated crop protection from the last 10 years that conducted *in vitro* or *in vivo* assay with the nanoparticle complexes.

Nanoparticle Type	Target transcripts	Insect/Plant Species or Cell Type	RNAi Efficiency	Ref.
Layered double hydroxide clay nanosheets	*CMV2b* and *PMMoVIR54*	*Vigna unguiculate* and *Nicotiana tabacum*	Reduction in lesions after CMV viral challenge on *V. unguiculate* and after PMMoV challenge on *N. tabacum*	153
Polymer-coated calcium phosphate	*Luciferase*	Luciferase expressing *S. frugiperda* cells	35 % transcript knockdown	159
Polymer-coated gold	*Luciferase*	Luciferase expressing *S. frugiperda* cells	31 % transcript knockdown	161

1.7.3 Peptide-based nanoparticles

There has been a drive to use natural product-based formulations in the design of nanoparticle vectors for dsRNA delivery, for example peptide-based systems, as they are generally non-toxic and more biodegradable in comparison to synthetic polymeric materials, and therefore more environmentally friendly.[162] Table 1.3 summarises the recent advances on this topic and the paragraphs below describe the main two systems developed.

Table 1.3. Peptide-based nanoparticles for RNA-mediated crop protection from the last 10 years that conducted *in vitro* or *in vivo* assay with the polyplexes.

Nanoparticle Type	**Target transcripts**	**Insect/Plant Species or Cell Type**	**RNAi Efficiency**	**Ref.**
Branched amphiphilic nano-capsules	*BiP* *Armet* and *BiP*	*A. pisum* and *T. castaneum*	Premature death 75 % mortality rate	163
Cell penetrating peptides	*YFP* and *CHS*	*A. thaliana* and *Populus tremula*	YFP reduced by 80 % in *A. thaliana*	164
	Renilla luciferase and *GFP*	*N. benthamiana* and *A. thaliana*	Increased transfection efficiency	165
	AgCHS2	*Anthonomus grandis*	80 % transcript reduction	142

1.7.3.1 Branched amphiphilic peptide capsules

In the past 10 years a new peptide-based nanoparticle (branched amphiphilic peptide capsule, BAPC) has been developed for the delivery of nucleic acids. These systems have a similar structure to liposomes but with much greater stability, self-assembling into bilayer delimited supramolecular nano-vesicle structures. BAPCs have cationic lysine surface groups that form nanoparticle complexes with nucleic acids of ~80 – 200 nm in size.[166–169] BAPCs are biodegradable by a common soil fungus *Aspergillus nidulans*, lessening the potential impact of these nanoparticles on the environment.[162] Avila *et al.* reported the first use of BAPCs for the oral delivery of dsRNA to the pea aphid *Acyrthosiphon pisum* and the red flour beetle *T. castaneum.*[163]

In their report, feeding BAPC/*BiP*-dsRNA complexes to adult *A. pisum* resulted in mortality 6 – 9 days earlier, compared to aphids fed naked dsRNA alone. Two different *T. castenaum*

transcripts, *BiP* and *Armet*, were targeted by feeding dsRNA to early instar *T. castaneum* larvae, with mortality reaching 75% when BAPC/dsRNA complexes for both targets were fed simultaneously.

The potential for orally administered BAPC/dsRNA to generate RNAi effects in pest species other than aphids and beetles now needs to be demonstrated.[62,163]

1.7.3.2 Cell-penetrating peptides

There are many naturally occurring proteins (pore/channel-forming proteins, fusion proteins, and cell-penetrating peptides (CPPs)) that facilitate the movement of molecules across cell membranes. These proteins can be exploited to enhance dsRNA uptake by cells and to assist endosomal escape within the cell.[170]

The discovery of the membrane traversing properties of the Tat protein (Trans-Activator of Transcription) from both the HIV-1 virus and the *D. melanogaster* Antennapedia homeodomain, led to the development of CPPs.[171–173] The Tat peptide is an arginine-rich peptide, with a cationic guanidinium-based functionality that can interact with the anionic cell surface, provoking endocytic cellular uptake.[139,140,170]

The combination of a CPP covalently bound to a polycationic peptide forms a fusion peptide that can serve as a delivery vector for dsRNA or pDNA.[164,165,174] A copolymer of histidine and lysine, $(KH)_9$, combined with the CPP Bp100, is an example of a fusion peptide that complexes with dsRNA.[164] The $(KH)_9$-Bp100/*yellow fluorescent protein* (*YFP*)-dsRNA complex, at a molar ratio of 2:1, targeted the transcript of *YFP* and the chalcone synthase genes in *A. thaliana* leaves. The exogenous and endogenous transcripts were both successfully impacted < 12 h post-application and the effect was sustained for at least a further 24 h. Similar fusion peptides: nonarginine (R9)-Bp100, $(KH)_9$-Bp100 and R9-Tat_2 have been complexed with

plasmid DNA. Rapid transfection was measured within the first 12 h of incubation of these fusion peptides complexed with *Renilla luciferase* pDNA with both *N. benthamiana* and *A. thaliana* leaves. Transfection efficiency then decreased for the remaining measurement time of 144 h.[164,165]

A significant issue with the use of peptides for the delivery of dsRNA or pDNA is the susceptibility of peptides to intracellular proteolysis, which can attenuate the RNAi effect. The use of proteins/peptides (e.g. silk proteins) that are more resistant to metabolic degradation might provide a mechanism for the sustained release of dsRNA.[164,165,175]

An example of a fusion peptide/dsRNA nanoparticle for an insect-specific application was recently reported.[142] In this work, a chimeric protein of a CPP fused to a DRBD (dsRNA binding domain) was synthesised, with the CPP including the fusogenic peptide haemagglutinin that aids the endosomal escape of the complex following endocytosis into the cell by destabilising the endosomal membrane. The CPP-DRBD/dsRNA complexes (or ribonucleoprotein particles (RNPs)) enhanced both the protection of dsRNA at pH 5.5 and the cellular uptake of Cy3-labeled dsRNA into Sf21 cells. Oral delivery of CPP-DRBD/*chitin synthase II* (*Ag-ChSII*) dsRNA RNPs to the cotton boll weevil (*Anthonomus grandis*), reduced *Ag-ChSII* transcript by 80%, in comparison to delivery of *Ag-ChSII* dsRNA alone that resulted in a reduction of only 30%. No significant mortality, however, was seen.[142]

1.7.4 **Chitosan nanoparticles**

Chitosan, the polysaccharide derived from crustacean shells, is a naturally derived polymer that has been used for complexation with dsRNA to improve delivery for insect control. It is of particular interest to researchers due to its inherent biocompatibility and non-toxic nature.[176] Chitosan contains cationic groups along its polymer chain that electrostatically interact with dsRNA.[177] Table 1.4 summarises the recent advances in the use of chitosan/dsRNA nanoparticles for crop protection.

Table 1.4. Chitosan nanoparticles for RNA-mediated crop protection from the last 10 years that conducted *in vitro* or *in vivo* assay with the chitosan/dsRNA complexes.

Target transcripts	**Insect/Plant Species or Cell Type**	**RNAi Efficiency**	**Ref.**
IAP	*S. frugiperda* larvae	47 % mortality	178
AgCHS1 and *AgCHS2*	*Anopheles gambiae*	62.8 % reduction of transcripts	177
Sema1a	*Aedes aegypti*	32 % reduction of transcripts	179
YHV	*S. frugiperda* cells	50 % reduction in YHV infection	180
SNF7 and *SRC*	*A. aeqypti*	46.7 % and 26.7 % mortality with *SNF7* and *SRC* targeting	157
Vg	*A. aeqypti*	30 % mortality	181
IAP	*A. aeqypti*	>65 % mortality	182

Complexation of chitosan with dsRNA results in nanoparticles that can aid the endosomal escape of dsRNA and consequently increase the RNAi efficiency. This has been illustrated in *EGFP::Rab7* expressing Sf9 cells, with 60% reduction in the accumulation of CypHer-5E-labelled green fluorescent protein (GFP) dsRNA (dsGFP) in endosomal compartments when complexed with chitosan, in comparison to naked dsGFP. Upon oral feeding of chitosan/dsIAP nanoparticles to 3rd instar *S. frugiperda* larvae, a mortality rate of 47% was measured, in comparison to 25% mortality when larvae were fed naked dsIAP alone.[178]

Chitosan/dsRNA complexes have been used to target the aquatic larval stages of mosquito pest species such as *Anopheles gambiae* and *Aedes aegypti*, with varying degrees of success. For example, chitosan/dsRNA nanoparticles targeting two different *chitin synthase* transcripts in *A. gambiae* reduced mRNA by 63% in comparison to the control. However, the levels of chitin produced were only reduced by 34% and no insect mortality was observed as desired.[177,179] The targeting of the *A. aegypti vestigial* (*vg*) transcript through delivery of chitosan/dsRNA complexes also did not significantly increase larval mortality (30% insect

mortality compared to 20% mortality in the control group).[181] In a comparative study, chitosan/*SNF7*-dsRNA nanoparticles outperformed *SNF7*-dsRNA complexed with amine-functionalised silica nanoparticles (ASNP) in killing *A. aegypti* larvae and in knockdown of the *A. aegypti SNF7* transcript. However, carbon quantum dot (CQD)/dsRNA complexes reduced mRNA levels for two different gene targets (*SRC* and *SNF7*), whereas chitosan/dsRNA complexes only produced a significant RNAi response with *SNF7*-dsRNA.[157]

Chitosan-based dsRNA nanoparticles are insoluble at neutral and alkaline pH regimes, affecting their performance as effective delivery vectors of dsRNA.[157,176] Consequently, recent developments have sought to improve chitosan-based nanoparticles by increasing the positive charge of chitosan through chemical modification (e.g. quaternisation).[180] The greater charge density of the quaternised chitosan (QCH) increases the polymer solubility and also improves stability of its complexes with dsRNA within cells. Typically, complexation of chitosan/dsRNA is achieved at a weight ratio of 1.5:1, with complexes ~ 350 – 650 nm in size. In comparison, QCH/dsRNA achieves full complexation at 0.24:1 weight ratio, with smaller sizes measured of the complexes, ~ 150 – 350 nm (measurements made with a Zetasizer Nano ZS). The more compact complexes formed with QCH are due to a stronger electrostatic interaction with dsRNA, thus enhanced binding. The cytotoxicity of both complexes is lower than that of the commercial liposomal transfection agent, Cellfectin®, and both chitosan and QCH-based complexes with *YHV*-dsRNA were successful in reducing the viral infection of YHV (yellow head virus) in Sf9 cells by at least 50%, 24 h post-viral challenge. Whilst QCH binds more strongly to dsRNA, due to the increased cationic charge, the difference in cell viability and RNAi efficiency was negligible.[180]

The addition of sodium tripolyphosphate (TPP) to chitosan as an ionic cross-linking agent, prior to complexation with dsRNA (CS-TPP-dsRNA), has also been investigated to improve the stability of chitosan/dsRNA nanoparticles. The introduction of cross-links to the polyplexes induced an increase in the mortality rate in *A. aegypti* larvae of 65%, when

targeting the *IAP* transcript, which was significantly more than the 35% mortality observed upon feeding chitosan/dsIAP nanoparticles without TPP.[182]

The improved properties of chitosan-based dsRNA nanoparticles, by cross-linking or increased charge density, coupled with their low general toxicity, adds to the attractiveness of this class of natural polymers for the delivery of dsRNA to insects. When chitosan/siRNA nanoparticles have been used for therapeutic applications, the solubility and colloidal stability of complexes were improved by using PEG-modified chitosan or by combining chitosan with PEI and carboxymethyl dextran.[183–186] Enhanced cellular internalisation and endosomal escape were also achieved through grafting a CPP (e.g. Tat or nonarginine peptides) to chitosan.[176,187–189] Such chitosan-based materials for dsRNA complexation and delivery may also be of value for crop protection applications.

1.7.5 **Liposomes**

Liposomes are spherical vesicles formed from a phospholipid bilayer (resembling that of cell membranes) and are commonly used to encapsulate materials for drug delivery, with the first reported publication in literature in 1987 by Felgner *et al.* and Malone *et al.*[190,191] Since then liposomes have been developed as non-viral vectors for dsRNA delivery, and mass-produced in commercial kits, such as Lipofectamine 2000® or Cellfectin®.[192,193] Upon complexation of a cationic liposome with negatively charged dsRNA by electrostatic interaction, a lipoplex can be formed. It is thought that lipoplexes traverse the cell membrane *via* adsorptive endocytosis[45,88,194–196], which exemplifies their appeal for delivery of dsRNA to cells.[197]

Liposome encapsulated dsRNA has often been used to introduce nucleic acids to insect species that do not display systemic RNAi responses, such as *Drosophila suzukii*. For example, Taning *et al.* demonstrated that feeding *rps13* and *vha26* dsRNA, encapsulated in Lipofectamine 2000®, to *D. suzukii* larvae and adults resulted in significant mortality after feeding, whereas

naked dsRNA did not result in mortality.[58] The lack of a SID-1-like transporter protein in *Drosophila* species means that the pathway for cellular uptake occurs *via* endocytosis[48,198,199], considered to be a slower uptake pathway in comparison to SID-1-like systems. The use of a liposome-based transfection agent improves cellular uptake and delivery of dsRNA in these recalcitrant species.[45,48]

Liposomes have also recently been shown to aid the release of dsRNA from endosomal compartments in *S. frugiperda*. Visualisation of CypHer-dsGFP dsRNA complexed to Cellfectin II® transfection reagent showed an 80% reduction in accumulation in the late endosomes, in comparison to the naked CypHer-dsGFP.[71]

1.7.5.1 Lipoplex delivery in a variety of arthropod species

Liposomal encapsulation of dsRNA has been shown to be an effective method of delivery in the tick species *Rhipicephalus haemaphysaloides*, the German cockroach *Blattella germanica* and the Neotropical stink bug *Euschistus heros.*[200–203]

In the case of *R. haemaphysaloides*, the Cy3-labelled dsRNA was encapsulated in three different commercial liposomal uptake facilitators (Lipofectamine 2000®, DMRIE-C® and Cellfectin®) and the formulation was delivered *via* soaking of larvae, nymphs and adults. All three lipoplexes induced more efficient RNAi than the dsRNA formulated in water alone.[202] The soaking of arthropods has been shown to be more effective than oral feeding, thus *in vivo* assay with feeding would provide greater insight, in particular as a *SID-1* gene has not been discovered in ticks.[35,48–50,204,205]

B. germanica are refractory to orally fed dsRNA due to enzymatic degradation by midgut nucleases, whereas microinjection can induce an efficient RNAi response.[200] The problem of metabolic instability in the cockroach midgut was overcome through encapsulation of the dsRNA in liposomes, which resulted in 60% mortality over 40 days. Mortality rates from

continuous oral feeding of lipoplexes increased from 8 days of feeding to 16 days of feeding, suggesting that modifications to liposomal nanoparticles could be introduced to shorten the time required for effective RNAi.[200,201]

1.7.5.2 Modifications to liposomal transfection agents

The efficacy of liposome-encapsulated dsRNA to elicit RNAi has been improved by the addition of a chelating agent to the formulation and through modification of the lipid component. For example, in the stinkbug *E. heros*, metal-dependent nuclease activity within the insect saliva is a limiting factor for the oral delivery of lipoplexes. A chelating-agent, ethylenediaminetetraacetic acid (EDTA), which can isolate metal ions and prevent them from interacting with the liposomes, has been shown to improve mortality rate in these insects when added in combination with lipoplexes.[203]

Modifications to lipids for the encapsulation of dsRNA have been reported for therapeutic applications of RNAi. The 1,2-dioleoyl-3-dimethylammonium-propane (DAP) lipid was modified by anchoring PDMAEMA-*b*-PEG block copolymers, to act as a pH-tuneable surface, see Figure 1.10.

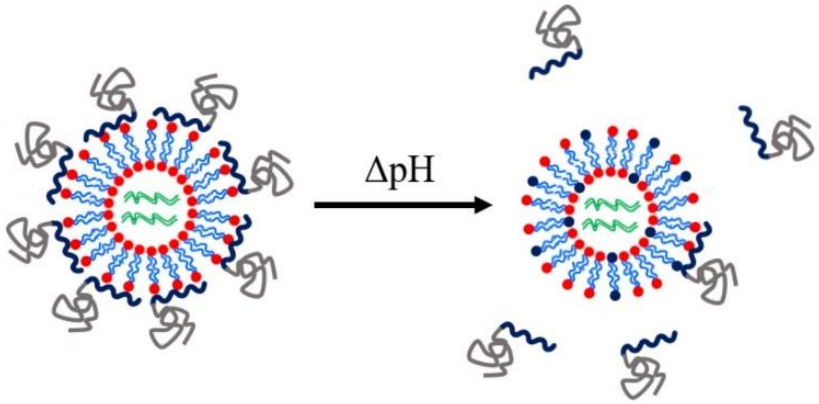

Figure 1.10. Schematic of a pH-tuneable liposome with adsorbed block copolymers that allow endosomal release upon decrease of pH. Modified from work by Auguste *et al.*[133]

This polymer-coated liposomal nanoparticle was shown to improve the protection of siRNA and enhance endosomal escape. More efficient targeting of GFP in GFP-expressing HeLa cells

was found with the polymer-coated lipoplexes in comparison to the oligofectamine/siRNA control.[133,206] A similar modification has yet to be reported for RNAi triggering in either insects or plants. Table 1.5 summarises the recent reports of lipoplex nanoparticles for RNA-mediated crop protection.

Table 1.5. Liposomal nanoparticles for RNA-mediated crop protection from the last 10 years that conducted *in vitro* or *in vivo* assay with the lipoplexes.

Target transcripts	**Insect/Plant Species or Cell Type**	**RNAi Efficiency**	**Ref.**
IAP	*S. frugiperda*	60 % mRNA reduction with 55 % mortality	71
Alpha-COP, *rp113* and *vha26*	*D. suzukii*	32 – 42 % transcript reduction with 22 – 42 % mortality	58
P0	*Rhipicephalus haemaphysaloides*	20 % and 84 % reduction in engorgement and oviposition rate, respectively	202
Tub	*Blattella germanica*	60% transcript reduction	201
Tub	*B. germanica*	60 % mRNA reduction after 16 days continuous ingestion	200
V-ATPase A and *muscle actin*	*Euschistus heros*	45% and 42% mortality, respectively	203

1.8 Future directions

It is clear that there is a direct comparison to be drawn between engineered nanoparticles for therapeutic triggering of RNAi, and novel strategies for agricultural applications. Indeed, it has often been the case that strides in the field of therapeutics are swiftly followed by exploitation of these new routes in the area of crop protection. For example, Howard *et al.* reported the use of chitosan/siRNA nanoparticles in 2006, Eguchi *et al.* used CPP-DRBD/siRNA complexes in 2009 and Treat *et al.* synthesised guanidine-containing copolymers in 2012[207–209], all for induction of RNAi in therapeutic applications, prior to

reports of similar RNAi-based crop protection strategies. It is anticipated that further insights and technological achievements in the clinical field will continue to be valuable for developing improvements in the formulation of dsRNA for crop protection.

There has been significant progress in the design of responsive nanoparticle vectors for dsRNA delivery for application within therapeutics, due to the in-depth knowledge of physiological temperature and pH. Whilst temperature-responsive nanoparticles may remain impractical for RNA-mediated insect control, pH-responsive nanoparticles have been the focus of recent developments. In reports by Parsons *et al.* and Christiaens *et al.,* the insect midgut pH was characterised and exploited for a pH-tuneable delivery vehicle.[114,115] An example of this strategy within the field of lipid-based uptake facilitators has also been reported by Auguste *et al.* with pH-tuneable liposome nanoparticles.[133]

Due to the revolutionary introduction of CRISPR/Cas9 as a gene editing biotechnology, there has been increasing interest in genetic material delivery. Thus, tailored polymer architectures have been synthesised to enable the improved efficacy of RNA cellular internalisation. Tan *et al.,* for example, devised a triblock copolymer of PDMAEMA, hydrophobic poly(*N*-butyl methacrylate) (P*n*BMA), and poly(ethylene oxide) (PEO) as a hydrophilic corona, capable of forming micelleplexes with sgRNA (single guide RNA) and Cas9 proteins for delivery to the cell nucleus.[210] Recent advances in therapeutic applications of RNA delivery have also included reports of conjugated siRNA to nanoparticles, often with a brush-like polymer architecture. The use of cleavable disulphide linkages to the siRNA allows for a steady release mechanism within the cells.[211,212] It is expected that formulations with similar technologies will soon be developed within the field of RNA-mediated crop protection.

The complexity of the pathway and barriers to induce RNAi, including enzymatic degradation, traversal of the cell membrane and subsequent endosomal escape, requires tailored (and often complex) nanoparticle designs to ensure that both the protection and delivery of dsRNA can

be achieved. The recent developments discussed in this chapter clearly demonstrate that more complex polymer architectures and nanoparticle modifications are possible and should provide future directions for enhancing efficacy of the use of dsRNA for crop protection. Additionally, it is evident that developing such polymer architectures will also need to take into account the more practical aspects of delivering the biopesticides to insects in a crop field. For example, a novel method of delivery through a non-invasive application has been developed to reduce the degradation of dsRNA. This high-throughput method integrates the dsRNA-nanoparticle complexes into aerosols, which could be a useful application tool for future pesticide formulation developments.[213,214] Furthermore, any delivery system carried forward in the future will also need to show robustness when integrated within pesticide formulations (which vary depending on, for example, location and type of crop) and when sprayed and dried onto crop leaves. Sustainability issues will also have to be taken into account, as the polymer particles should fully degrade in the environment to avoid long-term persistence. Additional concerns for the real-world application of dsRNA-based formulations include regulation of these products to ensure bio-safety, as well as the cost of large-scale production.[35,215–217] These additional requirements will bring about significant challenges to overcome.

1.9 Research aims

The overarching aim of the research described in this thesis was to develop polymeric vehicles to deliver species-specific dsRNA to the fruit pest insect *Drosophila suzukii*, in order to achieve gene knockdown and subsequent insect mortality.

As described, the development of suitable polymeric delivery vehicles could address some of the key issues associated with current pest insect control methods, such as off-target toxicity and the rise of resistance to common chemical insecticides with typical modes-of-action. The barriers to efficient induction of RNAi need to be considered and, by carefully designing block

copolymers with desired functionality, overcome. In order to achieve the overall aim of this research in the long-term, the work in this thesis has been broken down into stages to investigate the impact of different block copolymer properties on the protection and delivery of dsRNA. The aim of each stage is summarised below.

1.9.1 Development of water-soluble diblock copolymers for delivery of dsRNA

Homopolymer delivery vehicles (such as PDMAEMA, PEI or PLL) have been used for gene delivery ubiquitously. However, they can cause high levels of cytotoxicity, and the combination of a polycation and polyanion (e.g. dsRNA) can lead to aggregation and precipitation in the case of electro-neutralisation when close to the isoelectric point. Thus, an excess of polycation is required to stabilise complexes, which in turn induces greater cytotoxicity. Therefore, this research aims to develop water-soluble diblock copolymers that contain a neutral, non-interacting polymer block to reduce cytotoxicity, enhance formulation stability and improve the protection of dsRNA. In developing these diblock copolymers, we aim to fully characterise the resulting polyplexes in terms of size, surface charge, binding capability and stability in the presence of salt with respect to neutral block length. As different mRNA transcripts can be targeted to achieve RNAi, the impact of the length of dsRNA will also be considered with respect to the size and stability of the polyplexes.

1.9.2 Development of self-assembled triblock copolymers for delivery of dsRNA

In much of the literature surrounding the delivery of DNA/RNA, for both therapeutic and agrochemical applications, the complexes are prepared in ‘ideal’ environments, negating to consider the impact of competing ions or other molecules present in the formulation or application environment. In agrochemical applications, adjuvants will be added to aid, for example, the wetting of the formulation for foliar application. In the second research chapter, we aim to develop triblock copolymers that self-assemble in solution, without the addition of

dsRNA, in order to improve the stability of the resulting polyplexes in the presence of an increasing salt concentration. The systems will be fully characterised, prior to and after complexation with dsRNA, in terms of size, surface charge, binding capability and salt stability, with respect to the hydrophobicity/hydrophilicity of the polymers. The impact of the length of dsRNA will also be considered with respect to the size and stability of the triblock copolymer-based polyplexes.

1.9.3 *Ex vivo* protection of dsRNA and *in vitro* and *in vivo* delivery

Following the synthesis and in-depth characterisation of diblock copolymers and triblock copolymers and the polyplexes that they form through electrostatic interaction with dsRNA, we aim to test the formulations on a biological level. The *ex vivo* protection of dsRNA against degradation by enzymes will be investigated, in particular, the protection against enzymes specific to the gut of *D. suzukii* adult and late stage larvae. *In vitro* study of the interaction and/or uptake of dsRNA to cells will be investigated, identifying whether the polymers aid delivery of the dsRNA through the plasma membrane, and subsequently, whether effective mRNA degradation is induced through the release of dsRNA. Finally, *in vivo* assay will determine whether the oral feeding of species-specific *vha26* dsRNA to *D. suzukii*, through polymer complexation, induces significantly enhanced insect mortality and whether there is off-target toxicity to the closely related species, *Drosophila melanogaster*.

Chapter 2. Relevant techniques and associated theory

In this chapter the theory behind the techniques used throughout the research in this thesis is described. Such techniques include controlled radical polymerisation, dynamic light scattering (and other physical characterisation methods), and the primary biological assays.

2.1 Polymer synthesis and theory

2.1.1 Controlled radical polymerisation

There are a variety of controlled radical polymerisation (CRP) techniques that are commonly used to synthesise polymers and are particularly popular for vectors of DNA/RNA delivery. CRP is a facile approach for making well-defined complex polymer architectures. Atom transfer radical polymerisation (ATRP), nitroxide-mediated polymerisation (NMP) and reversible addition-fragmentation transfer polymerisation (RAFT) are all CRP processes, and are defined as ‘pseudo-living’. Prior to the discovery of ‘living’ polymerisations, step-growth and chain-growth were the common methods for polymer synthesis. Figure 2.1 highlights the differences between these polymerisation methods in terms of how molecular weight (MW) changes with conversion.

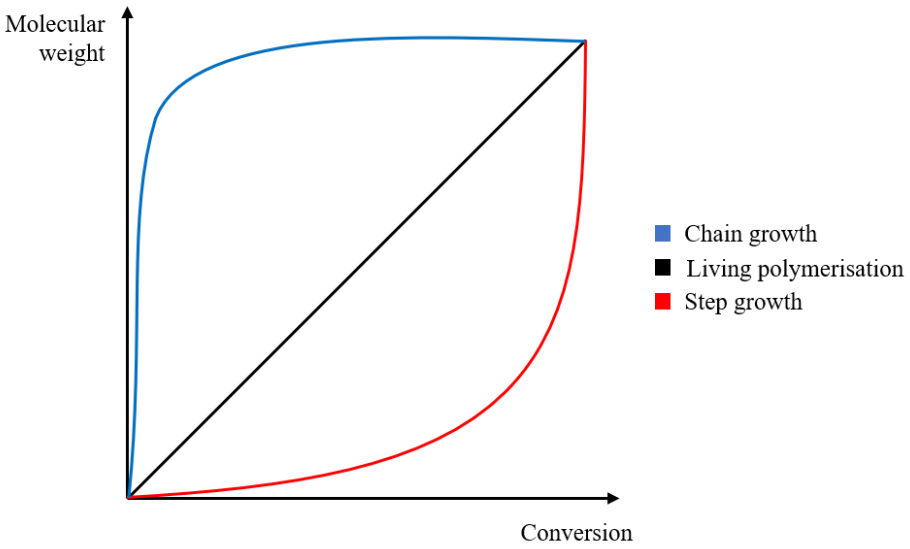

Figure 2.1. Schematic graph to illustrate the difference between step-growth, chain-growth and living polymerisations, showing how molecular weight changes as conversion increases.

Step-growth polymerisation, such as a polycondensation, occurs by the reaction of any two unlike monomers. This causes the rapid formation of many small chain polymers as monomer is consumed quickly, leading to high MW polymers only at high conversion and a final product with chains of many different lengths. Chain-growth polymerisation, however, involves a single reactive centre and one monomer unit at a time adding to the polymer chain. The MW, therefore, remains fairly stable throughout the polymerisation, constant at most conversion levels after an initial rapid increase. Termination and chain transfer are significant issues associated with chain-growth polymerisation, unlike step-growth polymerisation where no termination step is possible. 'Living' polymerisations, first developed by Michael Szwarc in 1956, are similar to chain-growth mechanisms except that the termination and chain transfer steps are eliminated.[218] MW therefore linearly increases with conversion. The rate of propagation $\left(\ln\frac{[M_0]}{[M_t]}\right)$ *vs.* time should also reveal a linear relationship and the resulting polymers will possess narrow dispersity (*Đ*), even at high levels of conversion. These linear relationships confirm the absence of chain transfer and termination steps, with the MW controlled only by the ratio of monomer to initiator concentration. In addition, living polymerisations benefit from the maintenance of chain end functionality, which provides the

opportunity to create more complex polymer architectures such as block copolymers, star polymers or graft/brush polymers.[219–221]

CRPs are a form of 'pseudo-living' polymerisation, allowing the precise control of molecular weight, dispersity and polymer architecture.

2.1.2 **RAFT polymerisation**

Of the three types of CRPs (ATRP, NMP and RAFT), RAFT is the most versatile technique and is commonly used to synthesise polymers for biological applications. RAFT is particularly suitable for the polymerisation of acrylates, acrylamides (and their methylated equivalents), vinyl monomers and styrenes, due to its tolerance to different functional groups. RAFT is a facile and inexpensive process and can be performed under aqueous or organic conditions. Similar to chain-growth polymerisation, CRPs involve initiation and propagation steps, however in the case of RAFT polymerisation, multiple chains are able to grow simultaneously at a consistent rate until monomer is depleted or the reaction is quenched. In both ATRP and NMP polymerisations there is a reversible termination step that slows the termination of the polymerisation and formation of dead chains. This is not the case with RAFT as it is a *degenerative* chain transfer process, with the active chains spending the majority of time in a 'dormant' state. Figure 2.2 demonstrates the mechanism of a RAFT polymerisation.[219–221]

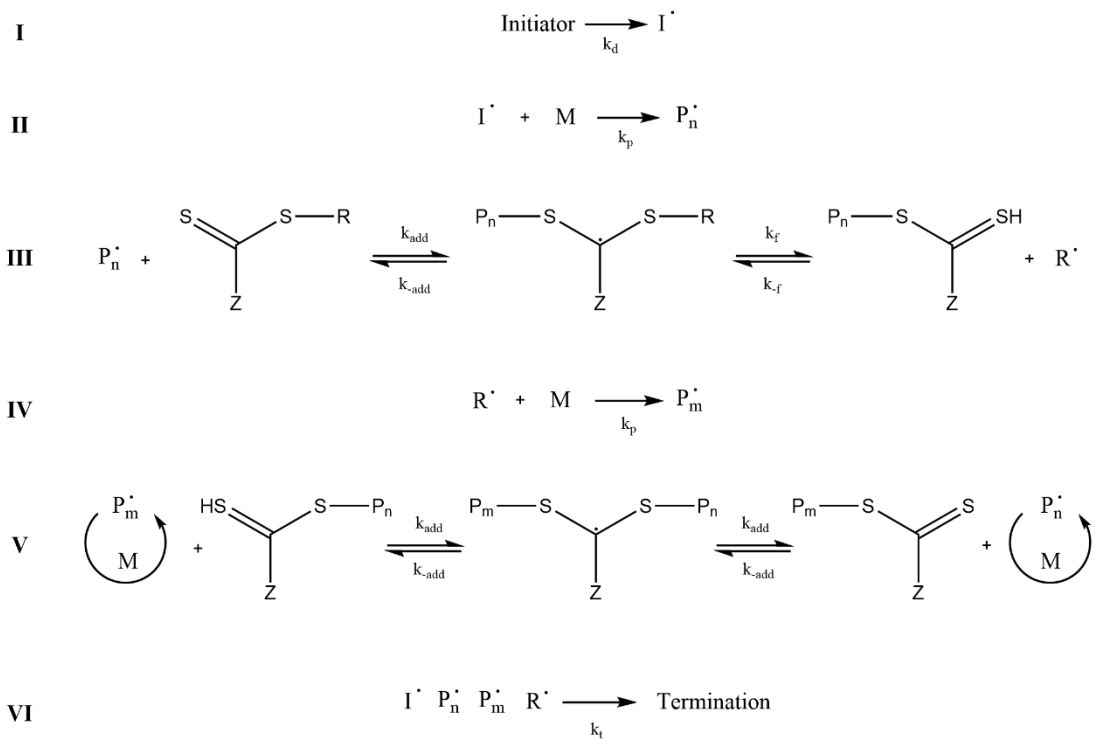

Figure 2.2. Reversible addition-fragmentation transfer mechanism. Initiator-derived chains are formed (I and II), followed by a pre-equilibrium stage (III). Re-initiation causes the formation of R-derived chains (IV) before the reaction reaches an equilibrium between dormant and active species (V). The combination of radicals will leave to termination (VI). Figure created in ChemDraw Prime 17.0.

An external source of radicals must be incorporated to initiate the RAFT polymerisation, as shown in step I. Following the formation of initiator-derived chains (P_n, steps I and II), addition-fragmentation occurs in a pre-equilibrium with a chain transfer agent (CTA, commonly a thiocarbonylthio (ZC(=S)S-) species, step III) to form a new set of $R^{\cdot}$ radicals. This leads to formation of R-derived chains (P_m, step IV) in a re-initiation step, and the polymerisation continues in an equilibrium between dormant and active species (step V). It is essential that the majority of the reaction time is spent with the polymer chains in the dormant state, attached to either end of the CTA with $k_{addP} >>> k_p$. Each 'cycle' will add a minimal amount of monomer to the end of each polymer chain, allowing the simultaneous and equal growth of all polymer chains throughout the polymerisation. The rate of propagation therefore linearly increases with time, and MW linearly increases with conversion. In the case of RAFT polymerisation, termination is not suppressed, and so the combination of radicals (step VI)

results in the formation of dead polymer chains (hence RAFT is classed as 'pseudo-living'). At the end of the polymerisation, the polymer chains (largely) retain their thiocarbonylthio (ZC(=S)S-) functionality, which can then be used for chain extension or further end-group functionalisation.[219–221] The precise control of RAFT polymerisation allows determination of the degree of polymerisation (DP) and theoretical molar mass (M_n(*theo.*)) (assuming a well-controlled RAFT polymerisation in which the number of initiator-derived chains is low) through the following equations, Eq. 2.1 and Eq. 2.2.

$$DP = \frac{[M_0]}{[CTA_0]} \qquad \text{Eq. 2.1}$$

$$M_n(theo.) \approx \frac{([M_0] - [M_t])}{[CTA_0]} \times M_m + M_{CTA} \qquad \text{Eq. 2.2}$$

Where $[M]_0$ is the initial monomer concentration, $[M]_t$ is the monomer concentration at *time = t*, $[CTA]_0$ is the initial CTA concentration, M_m is the molar mass of the monomer and M_{CTA} is the molar mass of the CTA.[221]

There are several critical variables that must be considered prior to conducting RAFT polymerisation; in particular, the choice of CTA needs to be carefully considered to control the polymerisation and ensure low molar mass dispersity. The R and Z groups of the CTA are alterable components, whose effectiveness is dependent on the specific monomer that is being polymerised. Monomers can be categorised into two groups: more activated monomers (MAMs), which are more stable and therefore less reactive as 'macro-radicals', and less activated monomers (LAMs) that are more reactive propagating radicals. Examples of MAMs include methacrylamides and methacrylates, and examples of LAMs include vinyl acetates and *N*-vinylpyrrolidones.

The Z group is critical for controlling the reactivity of the CTA, defined by the chain transfer coefficient (C_{tr}), which is the ratio between the rates of chain transfer ($k_{tr} = \phi k_{add}$) with respect to propagation. Typically, CTAs with a higher C_{tr} are preferred for use with MAMs,

and vice versa for LAMs. The suitable Z groups for different monomer polymerisations are summarised in Figure 2.3.

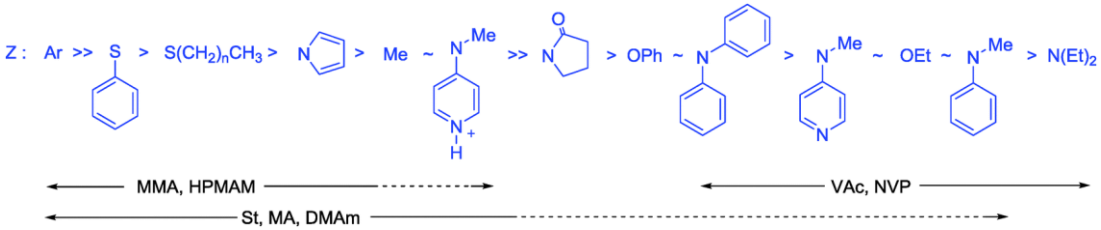

Figure 2.3. Examples of Z groups that achieve good control over polymer synthesis for certain monomers. For example, trithiocarbonates are good Z group choices for methyl methacrylate monomers. Abbreviations: MMA – methyl methacrylate, HPMAM – *N*-(2-hydroxypropyl) methacrylamide, St – styrene, DMAm – *N*,*N*-dimethylacrylamide, VAc – vinyl acetate, NVP – *N*-vinylpyrrolidone. Reproduced from Ref. 221, with permission from the Royal Society of Chemistry.

The R group is also very important for controlling RAFT polymerisation. The R group must be a good homolytic leaving group, and needs to be able to reinitiate the polymerisation of the second monomer. MAMs are typically better homolytic leaving groups, as the tertiary propagating radicals ensure resonance and steric stabilisation, and thus the corresponding R group must be carefully selected for its homolytic leaving group ability (see Figure 2.4).

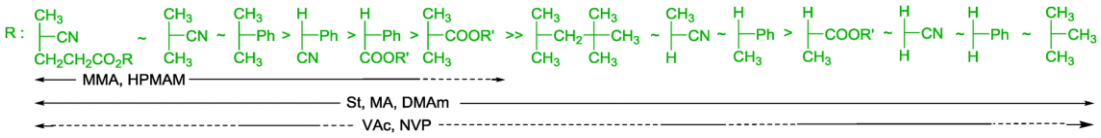

Figure 2.4. Examples of R groups that achieve good control over polymer synthesis for certain monomers. For example, methyl methacrylates are good leaving groups, requiring an R group that is more polymeric and therefore a better homolytic leaving group due to steric factors. Abbreviations: MMA – methyl methacrylate, HPMAM – *N*-(2-hydroxypropyl) methacrylamide, St – styrene, DMAm – *N*,*N*-dimethylacrylamide, VAc – vinyl acetate, NVP – *N*-vinylpyrrolidone. Reproduced from Ref. 221, with permission from the Royal Society of Chemistry.

This is to ensure that the partition coefficient (ϕ), described in Eq. 2.3, is ≥ 0.5. A high ϕ ensures that the pre-equilibrium stage (step III in Figure 2.2) will occur rapidly, leading to low dispersity.

$$\phi = \frac{k_f}{k_{-add} + k_f} \qquad \text{Eq. 2.3}$$

Block copolymers can be synthesised by sequential RAFT polymerisation. As the majority of polymer chains made by RAFT polymerisation will retain their thiocarbonylthio group, they can be chain extended through addition of monomer and fresh initiator, with the polymer chains now acting as macro-chain transfer agents (macro-CTAs). The sequence of addition of polymer blocks must be carefully chosen, as the previously polymerised block will become the R group for the next polymerisation. Figure 2.5, re-produced from Keddie[221], describes the order of polymer block addition for block copolymer synthesis. For example, methacrylates should be polymerised as the first block, forming the macro-CTA, to effectively polymerise a second polymer block, such as of an acrylate.

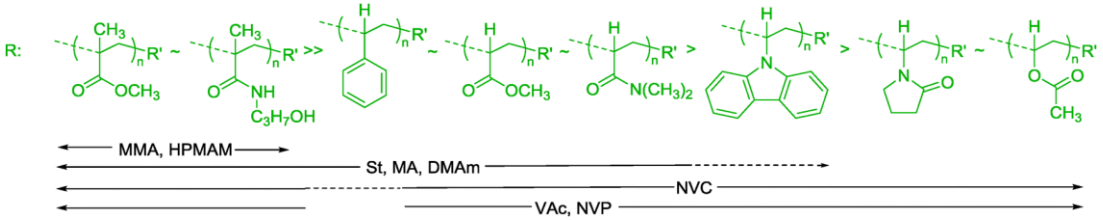

Figure 2.5. Examples of macro-R groups for block copolymer synthesis. The polymer blocks on the left hand side have better homolytic leaving group ability. For example, a methyl methacrylate should be polymerised before a vinyl ester polymer block. Abbreviations: MMA – methyl methacrylate, HPMAM – *N*-(2-hydroxypropyl) methacrylamide, St – styrene, DMAm – *N*,*N*-dimethylacrylamide, NVC – *N*-vinylcarbazole, VAc – vinyl acetate, NVP – *N*-vinylpyrrolidone. Reproduced from Ref. 221, with permission from the Royal Society of Chemistry.

Aside from the CTA, initiator needs to be considered when planning a RAFT polymerisation for block copolymer synthesis. Due to the termination processes in RAFT polymerisation, a number of unwanted defects can occur alongside the desired product. These include initiator-derived homopolymer and block copolymer, and dead homopolymer and copolymer chains. Initiator choice and concentration can reduce the quantity of defects. For example, a suitable concentration must be chosen to generate an optimal polymerisation rate, without producing

a large number of dead chains. The overall solution concentration will also influence the rate of polymerisation and the control over the RAFT mechanism. More details on the RAFT polymerisation mechanism, and initiator and CTA choice, can be found in published work by Keddie and Perrier.[220,221]

2.1.3 **Block copolymers**

Block copolymers, as described above, are macromolecules made up of covalently linked polymer blocks. These can be diblock copolymers (two different polymer blocks), triblock copolymers (three polymer blocks), or multi-block copolymers (more than three polymer blocks).[222] Block copolymers differ from random copolymers in that they possess distinct regions (blocks) that only contain one type of monomer unit, rather than a statistical distribution of different monomer units. This property can be exploited by incorporating separate functionalities into each polymer block to tailor the block copolymer for its specific application.

2.1.3.1 Amphiphilic block copolymers

Block copolymers containing at least one hydrophilic (water 'loving') polymer block and one hydrophobic (water 'hating') polymer block are known as *amphiphilic* block copolymers, from the Greek word '*amphi'* meaning '*on both sides*'. The presence of contrasting polymer blocks that either 'love' or 'hate' water means that amphiphilic block copolymers will exhibit self-assembling behaviour, forming structures such as micelles, vesicles (or polymersomes), worms, or rods, depending on the polymer characteristics and solvent environment. The formation of these different structures is determined by the packing parameter, $p = \frac{v}{a_0 l_c}$ (where v are l_c are the volume and length of the hydrophobic chain, respectively, and a_0 is the area of the hydrophilic 'head group'). The self-assembly of amphiphilic block copolymers is useful for many applications. The formation of micelles, for example, with a hydrophobic core and a hydrophilic corona, can aid the delivery of drugs that are typically synthesised to be

hydrophobic, but need to be delivered to a *hydrophilic* therapeutic environment. These block copolymers designed for drug delivery also require a biocompatible and non-toxic interface. For this reason, poly(ethylene glycol) (PEG) (also known as poly(ethylene oxide) (PEO) when prepared at higher molecular weights) is commonly chosen as the hydrophilic polymer block.[223]

2.1.3.2 Double hydrophilic block copolymers (DHBCs)

Double hydrophilic block copolymers (DHBCs, referred to as hydrophilic diblock copolymers in this thesis) are made up of two water-soluble (hydrophilic) polymer blocks with different chemical make-up. The first synthesis of a DHBC was described in 1972 by Kamachi *et al*.[224] Whilst amphiphilic block copolymers will self-assemble in aqueous solution, hydrophilic diblock copolymers require an external stimulus to induce self-assembly. Typically, DHBCs consist of one block that is non-ionic (uncharged) and non-interacting, and therefore acts as a sterically stabilising influence. The other polymer block is usually ionic (charged), able to interact with a substrate, and is often pH, temperature or otherwise responsive. Research over the last two decades has focussed on DHBCs due to their ability to reversibly self-assemble with an external trigger. In dilute aqueous solution, the hydrophilic chains are fully solvated, acting as randomly coiled polymers. The external stimuli used to induce self-assembly ranges from pH, temperature, or ionic strength, to the introduction of an oppositely charged molecule (often a macromolecule). Introducing an oppositely charged molecule causes the charge neutralisation of the polyelectrolyte (ionic) block of the hydrophilic diblock copolymer, triggering a transition from hydrophilicity to hydrophobicity. This amphiphilicity will thus induce self-assembly in aqueous solution. These self-assembled structures are often known as polyion complexes (PICs), block ionomer complexes (BICs), or interpolyelectrolyte complexes (IPECs), and polyplexes, when the oppositely-charged macromolecule is DNA or RNA.[222,225,226]

2.2 Physical characterisation

When preparing complexes between RNA (or DNA) and polycationic macromolecules (for example, homopolymers, diblock copolymers or triblock copolymers), the N/P ratio is usually used to characterise the relative proportions of charged units. The N/P ratio will be used throughout this thesis, in both physical characterisation methods and biological assays. The N/P ratio expresses the ratio between the number of ammonium groups present as part of the polycation and the number of phosphate groups present in the phosphodiester backbone of DNA or RNA, as described in Eq. 2.4.

$$N/P\ ratio\ = \frac{Number\ of\ tertiary\ amine\ groups}{Number\ of\ phosphate\ groups} \qquad \text{Eq. 2.4}$$

The *vha26* dsRNA that is primarily used in this thesis contains 222 bp, a total of 444 nucleotides. Therefore, at an N/P ratio = 1, there will be approximately 4 polymer chains (as each polymer contains ~ 110 amino groups) to every 1 dsRNA molecule.

2.2.1 Light scattering

2.2.1.1 Dynamic light scattering theory

Dynamic light scattering (DLS) measures the temporal fluctuations in scattered light and can provide information about the size and structure of particles in solution. Otherwise known as photo-correlation spectroscopy (PCS) or quasi-elastic light scattering (QELS), DLS measures the fluctuations in the intensity of scattered light over time. When the scattered light is collected by the detector, a 'speckle' pattern is observed, which fluctuates with the Brownian motion of the scattering particles. The change in the intensity of the light (due to destructive or constructive interference) is measured over time by the detector, which produces a count trace. The product of the scattering intensity between time intervals separated by a delay in time (t and ($t + \tau$)) is computed by the correlator, which produces an intensity auto-correlation (IAC) function. Eq. 2.5 shows this approximated correlation function.

$$\langle I(t)I(t+\tau)\rangle \approx \frac{1}{N}\sum_{i}^{\infty} I(t_i)I(t_i+\tau)\,dt \qquad \text{Eq. 2.5}$$

This can be understood qualitatively, as over a short time interval there is a stronger likelihood that the intensities of the signals will be correlated, whereas after a longer period of time the intensities will no longer be correlated. In the same way, smaller particles will have an IAC function that decays more quickly than larger particles, as they move more rapidly and therefore become uncorrelated faster. A normalised IAC function is usually used, Eq. 2.6.

$$g_2(\tau) = \frac{\langle I(t)I(t+\tau)\rangle}{\langle I(t)\rangle^2} \qquad \text{Eq. 2.6}$$

Importantly, $g_2(\tau)$ is ascertained from experiments, however it is information about the scattered electric field $g_1(\tau)$ that is required, Eq. 2.7. Fortunately, these are closely related by the Siegert relationship, Eq. 2.8.

$$g_1(\tau) = \frac{\langle E(t)E^*(t+\tau)\rangle}{\langle E(t)E^*(t)\rangle} \qquad \text{Eq. 2.7}$$

$$g_2(\tau) = 1 + \sigma[g_1(\tau)]^2 \qquad \text{Eq. 2.8}$$

In Eq. 2.8, σ is the coherence factor. It is usually close to one if a single speckle is used by the LS instrument for measurements (multiple speckle measurements will have $\sigma < 1$). The coherence factor is calculated as the intercept of the following equation: $\ln(g_2(\tau) - 1) = \ln\sigma - \frac{2t}{\tau}$ as illustrated in Figure 2.6.

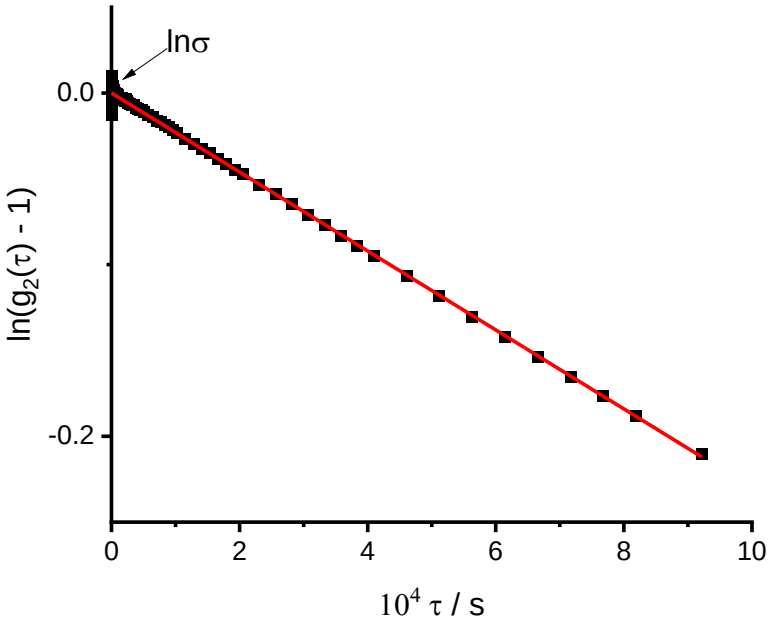

Figure 2.6. An example of the determination of the coherence factor, from the intercept when plotting $ln(g_2(\tau)-1)$ against τ.

In monodisperse samples, the intensity auto-correlation curve will consist of a single exponential, decaying rapidly after the relaxation time, Eq. 2.9.

$$g_1(\tau) = e^{-\frac{\tau}{\tau_R}} \qquad \text{Eq. 2.9}$$

Polydisperse samples, however, are identified by a broader IAC curve, and can be described by Eq. 2.10 using the sum of multiple exponentials (where *i* is the number of relaxation modes and *A* as the relative amplitude of each mode).

$$\frac{g_2(\tau)-1}{\sigma} = \sum_i \left[A_i exp\left(-\frac{\tau}{\tau_{R,i}}\right)\right]^2 \qquad \text{Eq. 2.10}$$

After determination of relaxation time (τ_R), the decay rate (Γ) is obtained through Eq. 2.11, relating to the diffusion coefficient (D) by the scattering vector, q. The magnitude of the scattering vector, q, is defined by Eq. 2.12.

$$\Gamma = \frac{1}{\tau_R} = Dq^2 \qquad \text{Eq. 2.11}$$

$$q = \frac{4\pi n}{\lambda}\sin\frac{\theta}{2} \qquad \text{Eq. 2.12}$$

Where n is the refractive index of the medium, λ is the wavelength of light in a vacuum and θ is the scattering angle.

If Γ is proportional to q^2, this is indicative of diffusive motion. The dynamic modes are diffusive in most polymer-based systems, as well as polymer particulate and self-assembled systems. The diffusion coefficient (D) can be related to the hydrodynamic radius, R_H, of the particles, assuming a spherical shape, through the Stokes-Einstein equation, Eq. 2.13.

$$R_H = \frac{kT}{6\pi\eta D} \qquad \text{Eq. 2.13}$$

The *hydrodynamic* radius is calculated, as polymers in solution are affected by hydrodynamic coupling. The coupled mobility of a polymer chain and its surrounding solvent molecules causes a larger, hydrated radius to be measured.

2.2.1.2 Data analysis

There are several methods that are commonly used to interpret and analyse DLS data. In this thesis, multi-exponential analysis was chosen as the principal method of analysis, with cumulant analysis used for determination of polydispersity. The cumulant method is the most basic method of analysis, using a Taylor expansion of the logarithm of the IAC function (see Eq. 2.14 and Figure 2.7).[227,228] This method relies on the linearity of $\ln[g_1(\tau)]$ with τ, relying on monodisperse samples with narrow Gaussian-like distribution.

$$\ln[g_1(\tau)] = \sum_{m=1}^{\infty}\frac{k_m}{m!}(-\tau)^m = -\Gamma\tau + \frac{k_2}{2!}\tau^2 - \frac{k_3}{3!}\tau^3 \ldots \qquad \text{Eq. 2.14}$$

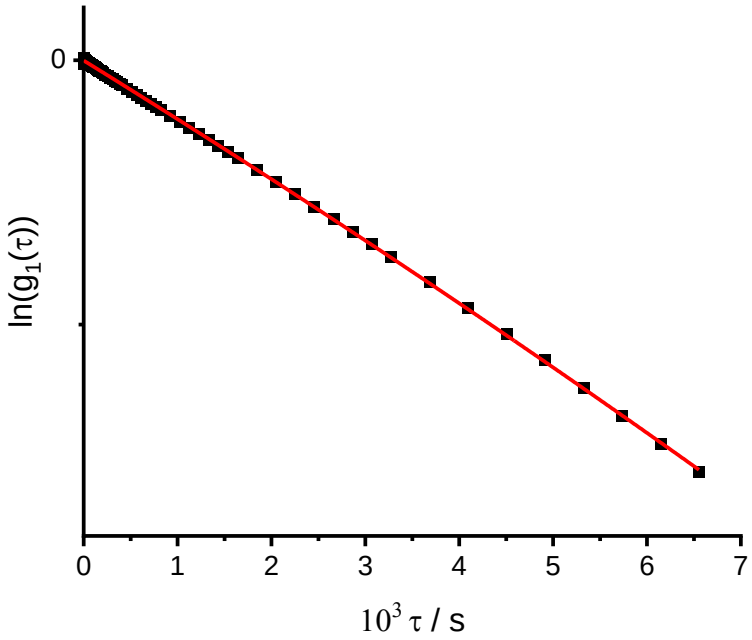

Figure 2.7. Example of polynomial fitting of the logarithm of intensity auto-correlation function data for cumulant analysis.

The first term, k_1 (i.e. Γ), is the mean decay rate, the second term, k_2, is the variance and k_3, is the skew of the function. Polydispersity is calculated through the following relationship: $\frac{k_2}{\Gamma^2}$.

Multi-exponential analysis, in this thesis, was performed using the Levenberg-Marquardt algorithm, which adjusts the parameters: A_i and $\tau_{R,i}$, to the best fit of Eq. 2.15 for the measured IAC data.

$$\frac{g_2(\tau)-1}{\sigma} = \left[A_1 exp\left(-\frac{\tau}{\tau_{R,1}}\right) + A_2 exp\left(-\frac{\tau}{\tau_{R,2}}\right) + A_3 exp\left(-\frac{\tau}{\tau_{R,3}}\right)\right]^2 \qquad \text{Eq. 2.15}$$

A_2 and A_3 are set to zero when the suspension is relatively monodisperse, with the option to fit these parameters if multiple exponentials are required.

2.2.1.3 Static light scattering theory

Static light scattering (SLS), as opposed to DLS, relies on the time-averaged scattered light intensity. The intensity of the scattered light is measured with respect to either change in concentration or change in scattering angle. In this work, the scattering angle is varied. From

SLS data, one can derive information about particle size in the form of the radius of gyration (R_g, the root mean-square distance of the particle segments from the centre of mass), and particle shape.

In scattering experiments, the form factor, *P(q)* (defined in Eq. 2.16), describes the particle shape. Particles with a distinct symmetry (spheres or cylinders, for example), will scatter light less efficiently as *q* increases (scattering angle decreases).

$$P(q) = \frac{\ln I_s(q)}{\ln I_0(q)} \qquad \text{Eq. 2.16}$$

Where $I_s(q)$ is the intensity of scattered light at scattering vector, q (related to the scattering angle), $I_s(0)$ is the intensity of scattered light at a scattering angle of 0°, which is not experimentally determined but can be ascertained by extrapolation.

The Guinier approximation, at low-*q* values (so that *qR* is sufficiently small), can be used to calculate the radius of gyration by plotting the logarithm of the time-averaged scatter light intensity ($I_s(q)$) against q^2, Eq. 2.17.[229]

$$\ln I_s(q) = \ln I_s(0) - \frac{q^2 R_g}{3} \qquad \text{Eq. 2.17}$$

At low scattering angles a linear relationship will fit the data, and thus gradient and R_g may be calculated. Information about the shape of particles can be gathered by determination of the size ratio between R_g and R_H (hydrodynamic radius), Eq. 2.18.

$$\rho = \frac{R_g}{R_H} \qquad \text{Eq. 2.18}$$

Typically, as ρ tends towards unity, more spherical morphologies can be assumed. As ρ increases above one, this is indicative of rod-like shapes.[230]

2.2.1.1 Cleaning

For both dynamic and static light scattering experiments, it is crucial to ensure that all glassware and preparation materials are free from dust. Dust scatters light heavily, and can skew DLS/SLS measurements entirely. To prevent dust contamination upon sample preparation in this work, all glass vials, lids and stirrer bars were washed 3× with filtered ultrapure Milli-Q water (filtered through two 0.2 µm pore-size nylon membrane non-sterile Fisherbrand® filters mounted in series) and filtered isopropanol (IPA) (filtered through two 0.2 µm pore-size polytetrafluoroethylene (PTFE) membrane non-sterile Fisherbrand® filters mounted in series) before drying at ~50 °C in a dust-free environment. Prior to measurements, samples were, on occasion, filtered through a 0.8 µm pore-size surfactant-free cellulose acetate membrane (Sartorius™) into the pre-washed (as described above) glass light scattering (LS) tubes (rimless Pyrex® culture tubes 75 × 10 mm), to remove dust contamination.

2.2.1.2 Instrumentation

Experiments were most often performed using a 3D LS spectrometer (LS instruments, Switzerland) using the '2D mode'. The spectrometer is fitted with a diode-pumped solid-state (DPSS) laser operating at 660 nm with a maximum power of 105 mW (Cobolt FlamencoTM, Cobalt). Laser attenuation was automated, two avalanche photodiode detectors were used, and the light was vertically polarized. All experiments were performed at a temperature of 25 ± 0.5 °C controlled by a water bath. A pseudo-cross correlation mode was used. The angle of measurement was altered from 30 – 130°.

2.2.2 **Electrophoretic mobility**

2.2.2.1 Theory

Particles with a net charge will attract a layer of strongly bound counterions to their surface, known as the Stern layer. Beyond the Stern layer, co-ions will be attracted, as well as additional counterions that are attracted to the co-ions, forming a diffuse electrical double

layer. When the particle migrates, a certain proportion of ions will move along with it, whilst some will remain where they are. This boundary of ions is known as the slipping plane, or the boundary of hydrodynamic shear, and the potential at this boundary is defined as the zeta (ζ) potential. Zeta potential is directly proportional to electrophoretic mobility, and therefore electrophoretic mobility can be considered as relative to the surface charge of the measured particles.

2.2.2.1 Instrumentation

The self-assembled structures prepared in this thesis can be considered as charged particles. A zeta potential analyser (Zetasizer Nano-ZS, Malvern) was thus used for the determination of their electrophoretic mobility. This instrument uses electrophoretic (phase analysis) light scattering (ELS), and measurements were taken measured at 25 ± 0.5 °C. The folded capillary cell (DTS1070, Malvern) contains two electrodes, between which an oscillating electrical field is applied. The movement of particles at a particular velocity to either electrode is measured as their electrophoretic mobility. This can then be converted to zeta potential, if required, by using the Henry equation with a Smoluchowski approximation. Data were collected in triplicate with the average taken over three runs.

2.2.3 **Transmission electron microscopy**

Transmission electron microscopy (TEM) can be used to image nano-scale particles. However, this technique can prove challenging for polymeric samples due to their organic nature and lack of 'heavy' components. Hence, negative staining with uranyl acetate was required for all samples imaged in this thesis. For polyplexes, samples were prepared similarly to a protocol used by Lam *et al.*, through the addition of dsRNA (25 μL, 0.1 mg mL^{-1}) to polymer solution (0.1 mg mL^{-1}) with the volume of polymer solution varied to maintain an N/P ratio = 2. Solutions were diluted to a 250 μL total volume, with an overall complex concentration of ~ 30 μg mL^{-1}.[231] For imaging of self-assembled triblock copolymers (in

aqueous solution without the presence of dsRNA), the samples were formulated by directly mixing triblock copolymers in Milli-Q water to a concentration of 10 mg mL^{-1}.

TEM grids were 400-mesh carbon-coated copper, prepared through the addition of 5 μL of sample before washing with Milli-Q water and staining with 1% uranyl acetate. Images were captured using an FEI Tecnai G^2-Spirit microscope, with a Gatan Ultrascan 4000 CCD camera, operated at 120 keV with a tungsten filament.

2.3 Biological assays and sample preparation

2.3.1 *Drosophila suzukii*-specific *vha26* dsRNA

The primary dsRNA used in this thesis targets the gene *vha26*. Vacuolar H^+-ATPase 26 kDa subunit (*vha26*) encodes for a subunit within V-ATPase, a plasma membrane proton pump. V-ATPase pumps are particularly ubiquitous in the apical membrane of *Drosophila* 'copper cells' (CpCs) (a type of columnar cell, which are the main cells in the insect gut and are responsible for nutrient absorption and digestive enzyme production and secretion). Reports from Overend *et al.* describe how the acidic section of the midgut of *Drosophila* (pH ~ 2 – 4) is maintained through the proton transport by V-ATPases in CpCs.[232–235] In addition, V-ATPases are needed to allow the formation of the correct morphology of *Drosophila* tracheal cells. The *vha26* dsRNA used in this work is specific to *Drosophila suzukii*, and the vital role of this gene means that its silencing leads to insect lethality.[236,237] The *vha26* dsRNA was synthesised by Genolution AgroRNA, with 222 base pairs (bp) and at a stock concentration of 4.68 μg $μL^{-1}$ in distilled water. The *vha26* dsRNA has the following nucleotide sequence:

ACGTGGCCACTCAGCATTGTTGCCCGCCGAAACACCGAAATGGTCCCAAAAAAC
CAATTTCGCTGCTTCGAGGGCAACGGACACGTGTGCAGCTGCCACTGGCCCATC
AAAAGCCCCGAAAGTCATCAATGTCTGTTGTTGAGTTAGCGAAAGTAACGAATA

CACACTATTAAGCACGCAACATTTACTCTCCATAATTCACCGCACCCAAGACGA
AGAAGT

2.3.2 **IVT dsRNA purification**

In vitro transcription (IVT) dsRNA was also prepared and provided by Syngenta for this work. Syngenta supplied long and short GFP dsRNA and long and short 'active target' dsRNA. The 'active target' dsRNA is named as such as to protect the IP rights of Syngenta. The IVT dsRNA was provided in an un-purified form, thus ethanol purification was performed as follows.

Equal volumes of dsRNA and 8M LiCl solution were mixed and left to precipitate for 24 h at -20 °C. Samples were then centrifuged at 13,000 RPM for 20 min at 4 °C. Supernatant was discarded and the dsRNA pellet was washed by adding ice-cold 70% ethanol (83 μL) and centrifuging at 8,000 RPM for 3 min at 4 °C. The supernatant was discarded and the wash step (with ice-cold 70% ethanol) was repeated twice more. The dsRNA pellet was then suspended in RNase- and DNase-free water. Concentration of the resulting dsRNA solutions were measured using a NanoDrop 2000 (260/280 nm).

2.3.3 **Agarose gel retardation**

Agarose gel electrophoresis assays were used to confirm the complexation of polymers with dsRNA through their retardation in an agarose gel. These were also used to assess the levels of degradation by synthetic and naturally derived enzymes. Ordinarily, dsRNA inserted into the formed well (by the comb) at the top of the agarose gel will migrate to a specific location driven by the electric current. 'Naked' dsRNA is able to migrate freely in the agarose gel toward the anode, arriving at a specific location that is relative to the length (number of base pairs (bp)) of the dsRNA. The dsRNA that was primarily used in this thesis is 222 bp long, and runs slightly above the 200 bp band when comparing to a 100 bp DNA ladder. Thus, if

complexation by a polymer is unsuccessful, the dsRNA will remain free and will migrate through the gel lane. If complexation is only partial, the complexed dsRNA will be retained in the loading well, and the free un-complexed dsRNA will migrate towards the anode, resulting in a 'smear' effect caused by the different degrees of interaction with the polycation. If complexation of the polymer with dsRNA is complete, dsRNA migration will be entirely prevented and the dsRNA will be retarded in the loading well.

It is well documented that ethidium bromide (EB) fluorescence is quenched upon the strong binding of a polycation with dsRNA.[238–245] Therefore, as polycation concentration is increased (i.e. N/P ratio is increased) the resulting fluorescence of the EB will be reduced as it is displaced from the dsRNA. As such, the degradation of dsRNA assessed through agarose gel electrophoresis was compared to a control sample, comparing the fluorescence intensity of the dsRNA when enzyme was added with respect to when enzyme was absent.

Agarose gel retardation assays were performed using the following method, unless otherwise stated. Aliquots of polymer were added to 1 μg dsRNA, in quantities to vary the N/P ratio, with solutions left to incubate at RT for 1.5 h to allow for complexation. 6X blue/orange loading dye (2 μL) was added to samples, and each solution (~17 μL) was loaded onto a 2% (w/w) agarose gel containing EB (3.5 μL), prepared with 1X TAE (Tris base, acetic acid and EDTA) buffer. Assays were run for 25 min at 90 V. A 100 bp DNA ladder (1 μL), alongside 6X purple non-sodium dodecyl sulphate (SDS) dye (1 μL) and nuclease-free water (4 μL), was run for comparison. The gels were imaged under a UV transilluminator set at 365 nm. When RNase A (0.5 μL, 5 mg mL^{-1}) was added to the solutions, the samples were incubated at 37 °C for 30 min prior to analysis. When *D. suzukii*-extracted enzymes were added to the formulations, incubation was varied depending on the length of time required for complete degradation of naked dsRNA, and samples were kept at 26 °C.

2.3.4 **Fluorescence spectroscopy**

Ethidium bromide (EB) was used as a nucleic acid-intercalating fluorophore. EB fluoresces strongly when intercalated between the base pairs of DNA or dsRNA, and fluoresces weakly in aqueous solution. As mentioned above, EB fluorescence can be quenched through its displacement by a polycation. Fluorescence quenching can therefore be used as a proxy for the strength of binding of a polycation to DNA/dsRNA.[238–245]

Fluorescence intensity was detected in EB exclusion assays and RNase A degradation profiles using an Omega FLUOstar® (BMG LABTECH GmbH) multi-mode micro-plate reader, with λ_{ex} set at 320 nm and λ_{em} set at 594 nm. EB solution was stored in an opaque container at 4 °C prior to use. Samples were measured in a Corning® Costar 96-well opaque microplate. Gain was set at 1600 – 1900.

For equilibrated 'static' samples, endpoint measurements were taken with ten flashes per well. The volume of each well was made up to 200 µL with nuclease-free water. For all samples, dsRNA (8 µL, 0.468 mg mL^{-1}) was added to each well alongside EB (2.9 µL, 0.4 mg mL^{-1}) to provide sufficient fluorescence intensity at the ratio [EB]:[P] = 0.12 (molar concentration of EB in relation to molar concentration of dsRNA phosphate groups, approximately one molecule of intercalated EB per four pairs of dsRNA bases). The dsRNA-EB solutions were left to incubate for at least 10 min prior to analysis, to allow for full intercalation of EB. In EB exclusion assays, an equilibration time was incorporated after each polymer addition prior to endpoint measurement.

Fluorescence intensity (F_I) was normalised using Eq. 2.19, with respect to the fluorescence intensity of dsRNA-EB alone (F_0), subtracting the weak fluorescence intensity of EB in water (F_{EB}):

$$\frac{I}{I_0} = \frac{F_I - F_{EB}}{F_0 - F_{EB}} \qquad \text{Eq. 2.19}$$

For time-resolved studies, two flashes were used for each sample in the 6 – 8 s measurement cycle. Aliquots of polymer solution (1 mg mL^{-1}) were added to dsRNA (8 µL, 1 mg mL^{-1}) to achieve the desired N/P ratio, with 1.5 h complexation time prior to measurement. The volume of each well was made up to 200 µL with nuclease-free water. EB (1 µL, 0.4 mg mL^{-1}) and RNase A (1 µL, 5 mg mL^{-1}) were added immediately prior to analysis if required. The incubator was set to 37 °C and the data were normalised with respect to fluorescence intensity at *t = 0*.

For fluorimetric NaCl titration assays, fluorescence intensity was detected using a FluoroMax® (Horiba Scientific) spectrofluorometer, with λ_{ex} set at 320 nm, and λ_{em} measured over a 335 – 800 nm window. Polyplex samples were prepared prior to analysis through the addition of polymer to dsRNA (120 µL, 1 mg mL^{-1}) to achieve an N/P ratio = 5. After incubation at RT for 1.5 h, nuclease-free water was added to reach *ca.* 3 mL and EB (91.5 µL) was added to [EB]:[P] = 0.25 (approximately one molecule of intercalated EB per two pairs of dsRNA bases). An equilibration time of 5 min was incorporated after each NaCl addition and prior to measurement.

Chapter 3. Influence of neutral block length on the complexation and protection of dsRNA by hydrophilic diblock copolymers

A portion of the contents of this chapter has been published in *Biomacromolecules* under the title, 'Protection of Double-Stranded RNA via Complexation with Double Hydrophilic Block Copolymers: Influence of Neutral Block Length in Biologically Relevant Environments.', 10.1021/acs.biomac.2c00136.

3.1 Abstract

The interaction between the anionic phosphodiester backbone of DNA/RNA and polycations is electrostatic in nature. The complexation of a nucleic acid and a polymer-based delivery vehicle, yielding 'polyplexes', can be exploited as a means of delivering genetic material for therapeutic and agrochemical applications, as described in Section 1.7.1. In this chapter, the synthesis of quaternised poly(2-(dimethylamino)ethylmethacrylate)-*block*-poly(*N*,*N*-dimethylacrylamide) (PQDMAEMA-*b*-PDMAm, Q-*b*-D) diblock copolymers *via* reversible addition-fragmentation chain transfer (RAFT) polymerisation is described, to be used as non-viral delivery vehicles for double-stranded RNA (dsRNA). The assembly of the diblock copolymers with dsRNA formed distinct polyplexes that were thoroughly characterised to establish a relationship between the length of the charge-neutral polymer block and the polyplex size, complexation efficiency and colloidal stability. Dynamic light scattering revealed the formation of smaller polyplexes when formed with diblock copolymer of increasing neutral polymer block length and *Drosophila suzukii*-specific *vha26* dsRNA, while

agarose gel electrophoresis confirmed that these polyplexes require a higher N/P ratio for full complexation. The diblock copolymer-based polyplexes exhibited enhanced stability in low ionic strength environments in comparison to homopolymer-based polyplexes. *Ex vivo* enzymatic degradation assays demonstrated that both the homopolymer and diblock copolymers efficiently protect dsRNA against degradation by the synthetic RNase A enzyme. In addition, the impact of dsRNA length (number of base pairs) was investigated, corroborating that more consistent polyplex stability is provided by the diblock copolymer with a longer neutral polymer block.

3.2 Introduction

Typically, polycations such as polyethylenimine (PEI) or poly(2-(dimethylamino)ethyl methacrylate) (PDMAEMA) have been employed for gene delivery.[85,86,88,89,107,119] PEI and PDMAEMA contain amine groups capable of protonation at physiological pH and have, as a result, favourable electrostatic interaction with DNA/RNA phosphate groups driving efficient complexation. However, cationic homopolymers can exhibit high levels of cytotoxicity, and the polyplexes they form with DNA/RNA can be unstable, with the likeliness of electro-neutralisation upon complexation leading to increased aggregation.[88,107,119,120,246–248] Thus, tailored polymer architectures including branched,[64,116,249] dendritic[152] or block copolymers[113,250–252] have recently been evaluated for improving the stabilisation of polyplexes for the protection and targeted release of genetic material (see Section 1.7.1).

In this chapter, attention is focused on hydrophilic diblock copolymers (also referred to as double hydrophilic block copolymers, DHBCs) for the stabilisation and protection of dsRNA upon complexation. Novel diblock copolymers have been synthesised *via* aqueous RAFT polymerisation, containing quaternised poly(2-(dimethylamino)ethyl methacrylate) (PQDMAEMA, Q) and poly(*N*,*N*-dimethylacrylamide) (PDMAm, D) polymer blocks.

There are swathes of literature devoted to the study of amphiphilic diblock copolymers that self-assemble into micelles (or other aggregated structures such as vesicles or worms) due to phase separation of the separate polymer blocks.[210,253–261] However, mixtures of oppositely charged polyelectrolytes (for example, dsRNA and polycation) can also self-assemble into micellar aggregates based on phase separation.[222,225,262]

The interaction of oppositely charged polyelectrolytes was first reported in 1949 by Fuoss *et al.*, and the resulting complexes have garnered attention under a plethora of names, such as polyplexes (usually associated with complexes formed with DNA or RNA), interpolyelectrolyte complexes (IPECs), block ionomer complexes (BICs) or polyion complexes (PICs). The charged polymers alone in aqueous solution do not self-assemble by themselves. They are surrounded by oppositely charged small counterions, which are released upon complexation with an oppositely charged polyelectrolyte, inducing an entropic gain that provides the driving force behind the complexation. Figure 3.1 shows a coarse-grained simulation of the complexation between a polycation and polyanion, performed by Zhan *et al*.[263] The interaction of two oppositely charged polyelectrolyte chains forms a hydrophobic complex, which can be more readily dispersed by incorporation of a hydrophilic, neutral block onto one of the polyelectrolyte chains.

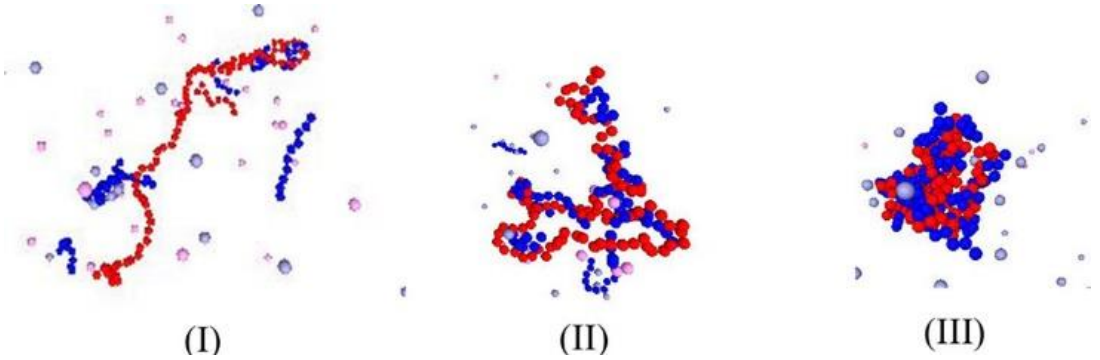

Figure 3.1. Snapshots of the complexation of a polycation (blue) and polyanion (red), in the presence of small counterions, as coarse-grained simulated by Zhan *et al.* Reprinted with permission from B. Zhan, K. Shi, Z. Dong, W. Lv, S. Zhao, X. Han, H. Wang and H. Liu, Coarse-Grained Simulation of Polycation/DNA-Like Complexes: Role of Neutral Block, *Mol. Pharmaceutics*, 2015, **12**, 2834–2844. Copyright 2022 American Chemical Society.

In designing the diblock copolymer constructs in this thesis, we hypothesised that condensation of the polyanion, dsRNA, by the 'strong' (positive charge is maintained regardless of pH[264]) polyelectrolyte, PQDMAEMA (Q), will form the interpolyelectrolyte core of the polyplex. The hydrophilic, non-ionic polymer block, PDMAm (D), covalently attached to Q, will thus form a corona to provide steric stabilisation, preventing aggregation between the formed polyplexes.[265] This hypothesis is corroborated in coarse-grained simulations by Zhan *et al*, Figure 3.2, which shows an entangled core of oppositely charged polyelectrolyte chains (blue and red) surrounded by hydrophilic, neutral chains that extend out into the solvent (shown in pink).[263]

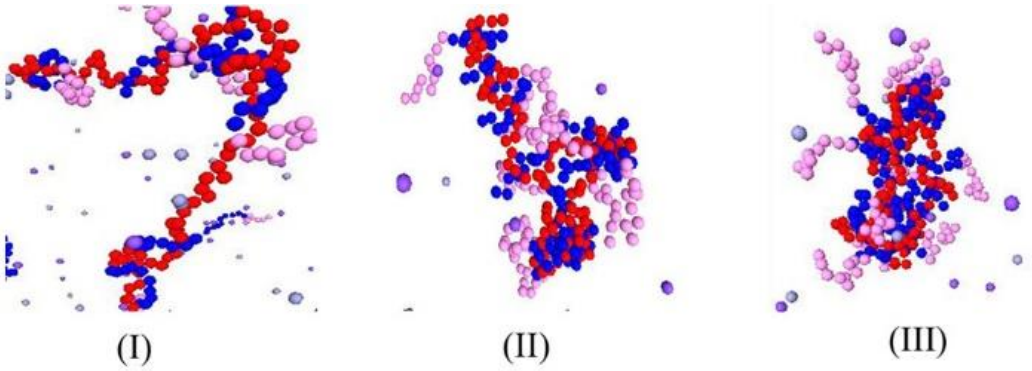

Figure 3.2. Snapshots of the complexation of positively charged diblock copolymers (blue is the cationic block and pink is the hydrophilic, neutral block) and a polyanion (blue), as coarse-grained simulated by Zhan *et al*. Reprinted with permission from B. Zhan, K. Shi, Z. Dong, W. Lv, S. Zhao, X. Han, H. Wang and H. Liu, Coarse-Grained Simulation of Polycation/DNA-Like Complexes: Role of Neutral Block, *Mol. Pharmaceutics*, 2015, **12**, 2834–2844. Copyright 2022 American Chemical Society.

Prior experimental studies, as well as coarse-grained simulation, have indicated that hydrophilic, neutral blocks incorporated alongside a cationic polymer block can significantly impact polyplex morphology, stability and transfection efficiency.[43,263,266–268] Typically, a poly(ethylene glycol) (PEG) chain has been used as the stabilising polymer block.[248,269–271] However, some studies suggest that PEG reduces the cellular uptake of siRNA/DNA.[272–274] Ensuring the use of cationic and neutral polymer blocks that are both hydrophilic in nature enhances the biocompatibility and dispersibility of the resulting polyplexes.[262,268] Therefore, PDMAm (D) was chosen as an alternative polymer block to PEG due to its uncharged, hydrophilic and biocompatible nature.[275]

Aqueous RAFT polymerisation enables facile control over the degree of polymerisation (DP), allowing tailored variation of block length, as discussed in Section 2.1.2. Therefore, the D polymer block length was varied and a systematic comparison of the physicochemical properties was conducted, including investigating the impact of neutral block length on morphology and stability of the resulting polyplexes with dsRNA. In both therapeutic and agrochemical applications, the influence of environmental conditions such as electrolyte

concentration (driving competitive adsorption/desorption of counterions) and the presence of nuclease enzymes (e.g. RNases) should be taken into account to create an effective formulation of dsRNA-based polyplexes. Therefore, the polyplexes are tested under varying conditions to determine their potential stability in the challenging environments found in pesticide formulations and upon their application.

In this chapter, polyplex size, stability and efficiency of dsRNA protection are specifically probed as a function of the diblock copolymer characteristics, using dynamic light scattering (DLS), fluorescence spectroscopy, electrophoretic mobility assays and agarose gel electrophoresis. The complexation of homopolymer/diblock copolymers with alternative *in vitro* transcription (IVT) dsRNAs is also investigated, using DLS to explore the impact of dsRNA length on polyplex size and stability.

3.3 Materials and methods

3.3.1 **Materials**

[2-(Methacryloyloxy)ethyl] trimethylammonium chloride solution (QDMAEMA, 80 wt% in H_2O), *N*,*N*-dimethylacrylamide (DMAm, 99%), sodium chloride (NaCl, 99.5%), D_2O (99.9%) and hydrochloric acid (HCl, 12 M) were purchased from Sigma Aldrich. 4-((((2-carboxyethyl)thio)carbonothioyl)thio)-4-cyano-pentanoic acid (CCCP, 95%) was purchased from Boron Molecular. 4,4'-Azobis(4-cyanovaleric acid) (ACVA, 97%) was purchased from Acros Organics. V-ATPase 222 bp dsRNA was synthesised by Genolution AgroRNA (4.68 μg μL^{-1}), sequence specific to the pest insect, *Drosophila suzukii*. Ethidium bromide (EB, 10 mg mL^{-1}) and regenerated cellulose dialysis (membrane molecular weight cut off (MWCO) < 3,500 g mol^{-1}) were purchased from Fisher Scientific. 100 bp DNA ladder (500 μg ml^{-1}) and RNase A (20 mg mL^{-1}) were purchased from New England Biolabs. Blue/orange loading dye (6X) was purchased from Promega. Ultrapure Milli-Q water (resistivity of minimum 18.2

MΩ.cm) was used for solution preparation and dialysis, and nuclease-free water was used for biological assays to avoid the accidental degradation or contamination of dsRNA.

3.3.2 Synthesis of quaternised poly((2-dimethylamino)ethyl methacrylate) macro-CTA

The PQDMAEMA macro-CTA (Q_{110}) was synthesised by aqueous RAFT polymerisation, as shown in the scheme in Figure 3.3A.

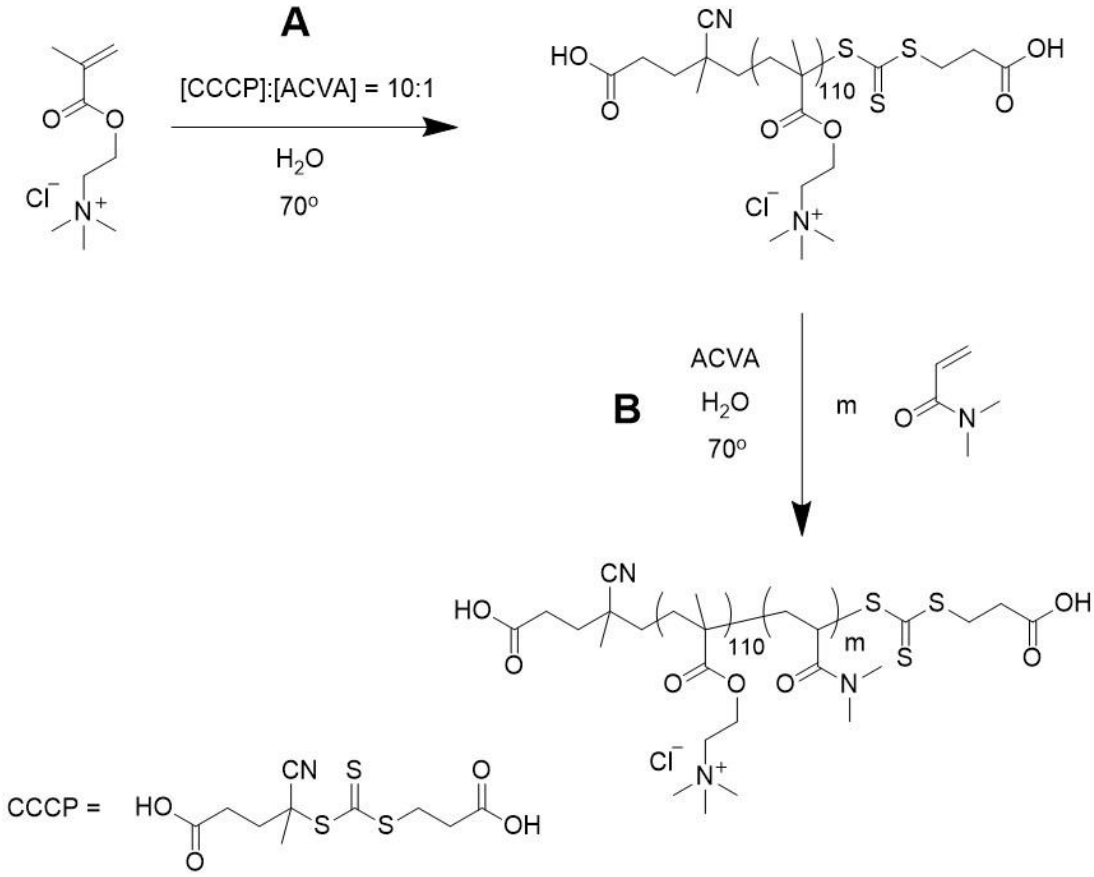

Figure 3.3. Reaction scheme of RAFT polymerisation of the (A) PQDMAEMA macro-CTA (Q_{110}) and subsequently the (B) PQDMAEMA$_{110}$-b-PDMAm (Q_{110}-*b*-D_m) diblock copolymers. Figure created in ChemDraw Prime 17.0.

QDMAEMA (100 g, 80 wt% in H_2O, 385 mmol), CCCP (0.94 g, 3.1 mmol) and ACVA (0.086 g, 0.31 mmol) were dissolved in Milli-Q water, at a ratio of [QDMAEMA]:[CCCP]:[ACVA] = 126:1:0.1 and 50 wt% in solution, pH = 4.3. The solution was degassed with N_2 for 45 min and then stirred at 70 °C for 1.5 h. The reaction was quenched by exposure to air. PQDMAEMA macro-CTA (Q_{110}) was stored at −20 °C to prevent degradation of RAFT chain-

end groups, prior to purification by dialysis against Milli-Q water (MWCO < 3,500 g mol^{-1}) and lyophilisation. The degree of polymerisation (DP), 110, and conversion, 88%, were confirmed with ^{1}H NMR spectroscopy (400 MHz) through comparison of a peak from the pendant amine group (**b**) to a peak from the RAFT-end group (**d**), as demonstrated by Figure 3.4.

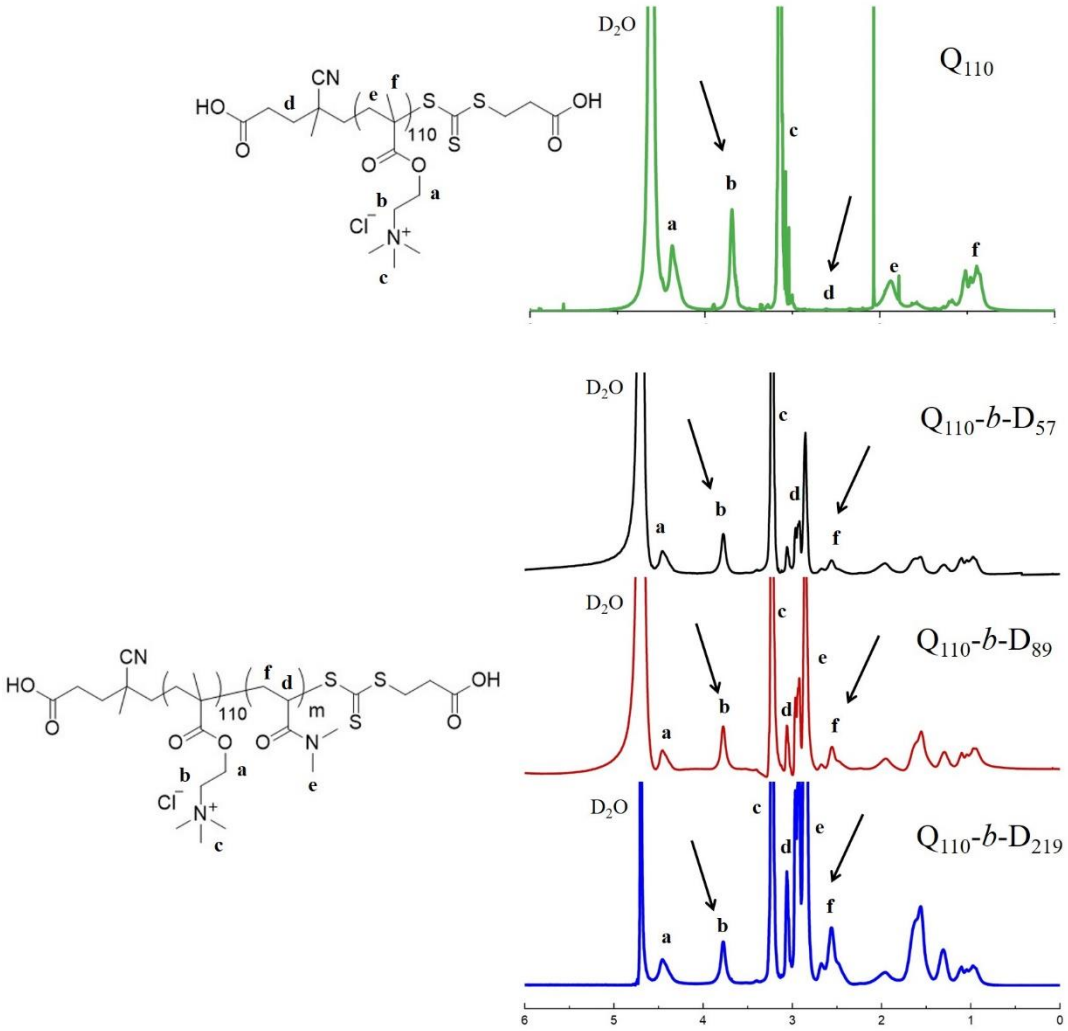

Figure 3.4. ^{1}H NMR spectroscopy (400 MHz) traces of Q_{110} macro-CTA homopolymer, and each diblock copolymer, with key peaks highlighted that were used for peak comparison analysis to calculate degrees of polymerisation.

3.3.1 Synthesis of hydrophilic diblock copolymers

Hydrophilic diblock copolymers were created through chain extension of the previously synthesised Q_{110} macro-CTA, as shown in the scheme in Figure 3.3B. Q_{110} macro-CTA (10 g,

0.38 mmol), ACVA (0.01 g, 0.038 mmol) and DMAm (amount varied to control the DP) were dissolved in Milli-Q water at a ratio of [macro-CTA]:[ACVA] = 1:0.1 and 50 wt% in solution, pH = 6.6. The concentration of DMAm monomer was varied to control the length of the neutral polymer block. The solutions were degassed with N_2 for 45 min and then stirred at 70 °C for 3 h. The reactions were quenched by exposure to air. The solutions were then purified by dialysis against Milli-Q water to remove unreacted monomer (MWCO < 3,500 g mol^{-1}), and lyophilised to yield the PQDMAEMA-*b*-PDMAm (Q_{110}-*b*-D_m) block copolymers as pale yellow powders. The DPs (57, 89 and 219) and conversions (86, 71, 91%, respectively) were confirmed with ^{1}H NMR spectroscopy (400 MHz) through comparison of a characteristic peak from the D block (**f**) with a peak from the pendant amine group (**b**) (Figure 3.4).

3.3.2 Characterisation

3.3.2.1 ^{1}H NMR spectroscopy

Peak comparison was conducted following measurement of samples in D_2O (5 mg mL^{-1}) using a Bruker 400 MHz ^{1}H NMR instrument after purification and lyophilisation. Initial kinetic analysis was conducted with a Spinsolve 60 MHz (see Figure A1 in the Appendix for an example of spectra from this instrument). Conversion was calculated through Eq. 3.1, by comparing the vinyl protons (~ 5 – 7 ppm, no vinyl protons are visible in Figure 3.4 as these spectra were obtained post-purification) to pendant group protons (~ 3.8 or 2.6 ppm, for example **b** or **f** peaks in Figure 3.4, respectively),

$$Conversion\ (\%) = 100\ \times \left(1 - \frac{v_t p_0}{p_t v_0}\right) \qquad \text{Eq. 3.1}$$

Where *p* represents the integral of the peak (~ 3.8 or 2.6 ppm) of the pendant group protons and *v* is the integral of the peaks (~ 5 – 7 ppm) of the vinyl protons, with *t* and *0* representing each time point and the beginning of the reaction, respectively.

3.3.2.2 Aqueous gel permeation chromatography

Molecular weight (MW) and molar mass dispersity (*Đ*) of the polymers were ascertained by aqueous gel permeation chromatography (GPC), using an Agilent 1260 Infinity 2 instrument

equipped with a refractive index detector. Separation was achieved using two PL aquagel-OH Mixed-H columns and an 8 µm guard column (Agilent Technologies). The eluent comprised 0.8 M $NaNO_3$, 0.01 M NaH_2PO_4, 0.05 wt% NaN_3 in Milli-Q water, adjusted to pH 3 using 37% (w/w) HCl. It was eluted at a rate of 1.0 mL min^{-1}. Samples were diluted to 0.5 mg mL^{-1} in the eluent and filtered through a 0.2 µm syringe filter (Sartorius Minisart RC hydrophilic) prior to analysis. MW was calibrated against PEG/PEO standards with molecular weights varying from 106 to 1,500,000 g mol^{-1} (EasiVial PEG/PEO calibration kit, PL2080-0201, Agilent Technologies)[276] and therefore the MW values obtained for the polymers can only be used relative to one another, rather than as an exact MW determination.

3.3.3 Preparation of Q_{110}/dsRNA and Q_{110}-*b*-D_m/dsRNA polyplexes

Q_{110} and Q_{110}-*b*-D_m stock solutions were prepared by dissolving a known mass of polymer in the appropriate volume of Milli-Q water. Solutions were stirred at ~800 RPM for 5 min to ensure complete dissolution. Solutions of dsRNA were prepared through dilution of the 4.68 mg mL^{-1} stock solution with nuclease-free water. Q_{110} or Q_{110}-*b*-D_m/dsRNA polyplexes were formulated by directly mixing specific volumes of the polymer and dsRNA solution to achieve a desired N/P ratio. The N/P ratio, described in Section 2.2, expresses the ratio between the number of ammonium groups present in the Q homopolymer or Q polymer block (as determined through ^{1}H NMR analysis), and the number of phosphate groups present in the dsRNA (for example, 222 bp dsRNA provides 444 phosphate groups per dsRNA molecule). The polymer solutions were added to the dsRNA solution and agitated to mix, before incubating at room temperature (RT) for at least 1.5 h to equilibrate. The pH of the formulations were measured to be pH = 7.4.

3.3.4 Light scattering

Dynamic light scattering: Measurement and fitting of the data was performed as described in Section 2.2.1, viscosity (η) of water used for Stokes-Einstein equation. *Static light scattering:* Collection and fitting of data was performed as described in Section 2.2.1.

For experiments where the salt concentration (C_{NaCl}) was varied, a zeta potential analyser (Zetasizer Nano-ZS, Malvern) was used. A backscatter (173°) detection angle was used with measurements performed in quintuplicate. Data fitting was performed as described in 2.2.1.

3.3.5 Electrophoretic mobility

Aqueous suspensions were prepared at a concentration of 0.1 mg mL^{-1}, 24 h before measurement. Details of instrumentation are described in Section 2.2.2.

3.3.6 Agarose gel electrophoresis

Aliquots of Q_{110} or Q_{110}-*b*-D_m were added to 1 μg dsRNA, in quantities to vary the N/P ratio, with solutions left to incubate at RT for 1.5 h to allow for complexation. When RNase A (0.5 μL, 5 mg mL^{-1}) was added to the polyplex solutions, the samples were incubated at 37 °C for 30 min prior to analysis. Further details of the assay are described in Section 2.3.3.

3.3.7 Fluorescence spectroscopy

Fluorescence intensity was measured in EB exclusion assay, RNase A degradation profiles and fluorimetric NaCl titration assay, as described in Section 2.3.4.

3.3.8 Transmission electron microscopy

Transmission electron microscopy (TEM) was performed as described in Section 2.2.3.

3.4 Results and discussion

3.4.1 Design and characterisation of homopolymer and diblock copolymers

3.4.1.1 Macro-CTA selection

The macro-chain transfer agent (macro-CTA), synthesised first, was chosen as quaternised-PDMAEMA. PQDMAEMA was selected because of its ‘permanent’ positive charge, induced through the quaternised monomer unit (which contains a quaternary amine, see Figure 3.5).

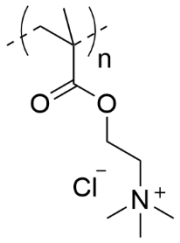

Figure 3.5. Structure of the QDMAEMA repeating monomer unit, drawn in ChemDraw Prime 17.0.

As described in Section 1.7.1.1, PDMAEMA has previously been used as a linear homopolymer for the delivery of DNA and RNA, due to its proton sponge capabilities. The pKa of PDMAEMA typically lies between 7 – 8, therefore it is approximately 50% protonated at physiological pH.[90] However, within the haemolymph and gut of many insects and in the environment where pesticide formulations are applied (such as on the soil or leaves of crops), pH can be extremely variable. For example, Lepidopteran insects typically have very alkaline gut contents[115], and *Drosophila* have variable pH across the gut lumen with an acidic midgut section.[143] Without maintaining a positive charge, the premature release of dsRNA could lead to its degradation and rapid excretion. Replacing PDMAEMA with the permanently cationic PQDMAEMA eliminates this problem, maintaining an electrostatic interaction with polyanions (such as dsRNA) over the entire pH range.

However, the strong binding of an ammonium group-based polycation could pose a problem when considering the release of dsRNA for participation in the RNAi mechanism, or with respect to the endosomal escape of the polyplexes. Nonetheless, there is ambiguity in the literature about the true mechanism by which endosomal escape occurs (outlined in Section 1.7.1). Therefore, further research is required to understand which chemical functionalities incorporated within polymeric delivery vehicles are useful, and which are prohibitive. In this first instance, we chose to ensure strong complexation and binding to dsRNA (and thus protection throughout variable environmental conditions) by selecting a permanently cationic polymer block containing ammonium groups. This is particularly important when considering agrochemical applications in which pH conditions can be more variable.

An additional benefit of using the [2-(methacryloyloxy)ethyl] trimethylammonium chloride monomer (QDMAEMA), and the resulting PQDMAEMA homopolymer, is that both are water-soluble. Water-solubility is desirable for applications such as bio-insecticides as it is critical that the resulting polymer is not inherently toxic, to avoid off-target effects on other species such as the closely related species (to *D. suzukii*), *Drosophila melanogaster*. Water solubility also helps with facile formulation procedures for target assays, and the use of aqueous RAFT polymerisation. Pre-quaternised monomer was chosen to remove the requirement for a post-polymerisation methylation step using methyl iodide, in order to avoid potential remaining toxic contaminants (such as iodide ions) being present in subsequent formulations.

The dsRNA used in this research is significantly longer than the siRNA that is often used in studies concerned with therapeutic applications.[43,113,250,273] Previous research has shown that positively charged diblock copolymers, where the charged block length closely matches the length of the oppositely charged polyanion, form more defined interpolyelectrolyte complexes.[264,277] Unpublished data from our research group also indicated that a PQDMAEMA DP of ~100 – 120 was of sufficient length to complex with 222 bp dsRNA. It is based on these factors that a higher degree of polymerisation was chosen for the charged polymer block (> 100).

3.4.1.2 Kinetic profiling of QDMAEMA RAFT polymerisation

Initially, the kinetics of the aqueous RAFT polymerisation of QDMAEMA was monitored to determine the optimal concentration of reagents in solution with respect to conversion and rate control. Monomer conversion was determined using ^{1}H NMR spectroscopy (60 MHz). The vinyl protons (~5 – 7 ppm) and pendant group protons (~ 3.8 ppm) were compared at *time = t* to *time = 0*, as described in Section 3.3.2.1, to calculate conversion and reaction rate. The

conversions over time in 30 and 50 wt% reaction solutions are shown in Figure 3.6A, and comparative rate plots are shown in Figure 3.6B.

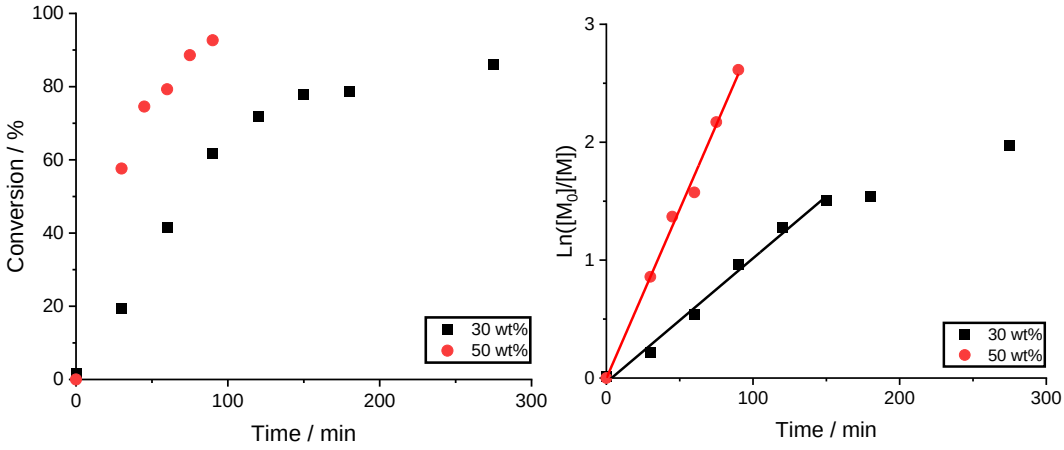

Figure 3.6. (A) Conversion and (B) rate plot of QDMAEMA to PQDMAEMA over time when RAFT polymerisation reactions were run at either 30 wt% or 50 wt% reaction solution concentration.

The data indicated that a 50 wt% reaction solution induces a faster polymerisation of QDMAEMA, in comparison to a 30 wt% reaction solution, with a higher conversion achieved (~ 90%). In the 30 wt% polymerisation, a conversion of ~ 80% is reached after 150 min and the conversion plateaus beyond this reaction time. As shown in the rate plot (Figure 3.6B), this is due to a loss of RAFT control after 150 min, shown by the deviation from a linear relationship. However, at 50 wt%, RAFT control is maintained throughout the reaction, illustrated by the linear relationship in Figure 3.6B. Therefore, a 50 wt% reaction solution was selected for the RAFT polymerisation of QDMAEMA.

3.4.1.3 Hydrophilic diblock copolymer synthesis

As previously mentioned, homopolymers such as PEI and PDMAEMA are typically used as transfection agents. However, these homopolymers have also often caused high cell toxicity. Therefore, modification of polycationic homopolymers such as PEI or PDMAEMA (through branching, post-polymerisation functionalisation or block copolymer synthesis) can be used to mediate toxicity and enhance cellular internalisation.

The Q_{110} macro-CTA was chain extended by three monomers: poly(ethylene glycol) methacrylate ($PEGMA_{300}$), 2-methacryloyloxyethyl phosphorylcholine (MPC) and *N*,*N*-dimethyl acrylamide (DMAm, D); each of which would result in the incorporation of a neutral, hydrophilic polymer block.

In the first instance $PEGMA_{300}$ was chosen, as PEG derivatives are often selected for therapeutic applications due to their biocompatibility. However, during the course of the polymerisation, white particulates became visible. The lower critical solution temperature (LCST) of $PEGMA_{300}$ had been reached at the reaction temperature of 70 °C. PEG methacrylate-based derivatives are amphiphilic, with hydrophilic PEG groups and a hydrophobic backbone of methyl groups. The overall hydrophobicity of PEGMA monomers/polymers can be altered by the number of incorporated PEG units, and therefore their LCSTs may be tuned.[278] Increasing the number of PEG units will increase the LCST, for example $PEGMA_{475}$ (equating to approximately 8 – 9 PEG units) has an LCST of 90 °C. At a reaction temperature of 70 °C, $PEGMA_{300}$ (as tested here) becomes hydrophobic as the hydrogen bonds are disrupted and white particulates (visible to the naked eye) become noticeable. Therefore, as shown in Figure 3.7, the chain extension of Q_{110} macro-CTA with $PEGMA_{300}$ was unsuccessful.

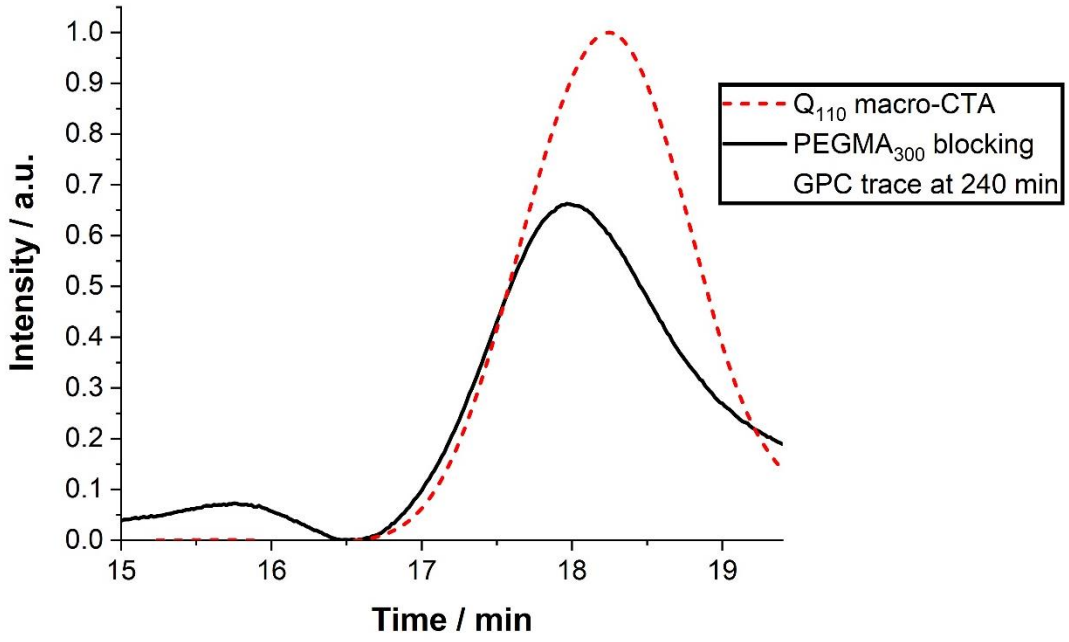

Figure 3.7. GPC trace following the attempted chain extension of Q_{110} macro-CTA by RAFT polymerisation of $PEGMA_{300}$ after a 4 h reaction time.

Secondly, MPC was investigated for its ability to chain extend onto the Q_{110} macro-CTA. MPC is a biocompatible monomer, due to its similarity to the phospholipid bilayer membrane. Whilst the RAFT polymerisation between MPC and Q_{110} was more successful (in comparison to $PEGMA_{300}$), with the GPC trace shifting to shorter retention times (Figure 3.8), there was still the presence of a significant macro-CTA shoulder. This is indicative of remaining, unreacted macro-CTA present in the system.

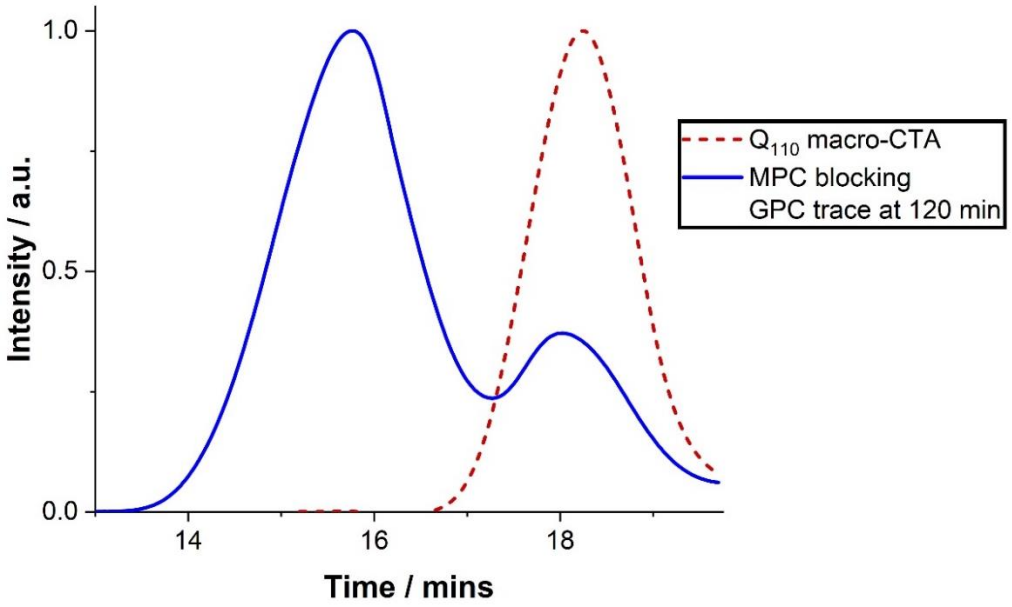

Figure 3.8. GPC trace following attempted RAFT polymerisation between MPC monomer and Q_{110} macro-CTA after a 2 h reaction time.

Finally, DMAm monomer was explored as the neutral polymer block, also due to its biocompatibility.[275] In this instance, the RAFT polymerisation, chain-extending DMAm onto the Q_{110} macro-CTA, was successful, see Figure 3.9.

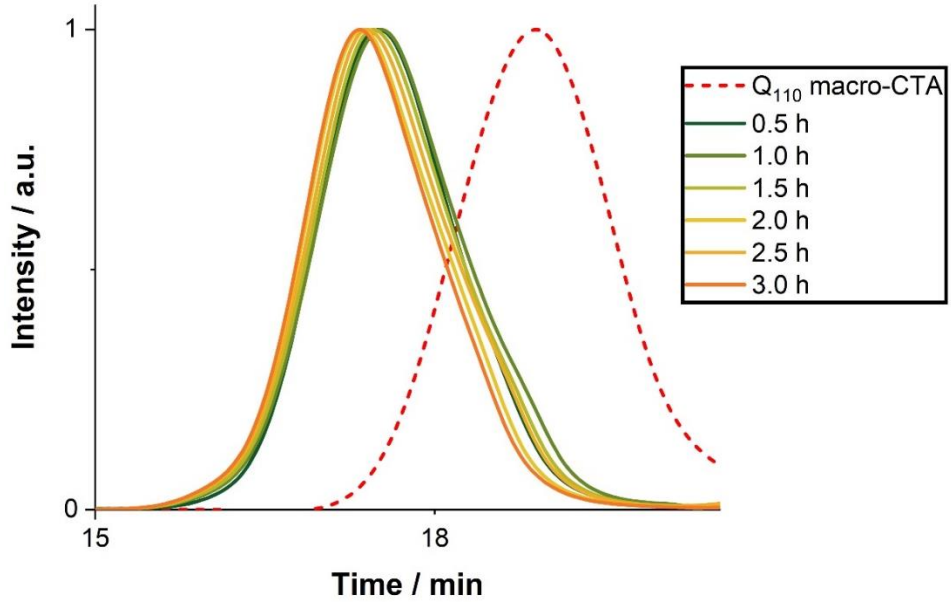

Figure 3.9. GPC traces, following the kinetics of the RAFT polymerisation between DMAm monomer and Q_{110} macro-CTA, over a 3 h period.

As the reaction proceeds from 30 min to 3 h, the GPC peak shifts to shorter retention times. A small macro-CTA shoulder can be seen at 30 min, however this appears to be absent from 2 h onwards. Figure 3.9 highlights that the RAFT polymerisation is rapid, occurring primarily in the first 30 minutes of the reaction time.

3.4.1.4 Synthesis of hydrophilic diblock copolymers by aqueous RAFT solution polymerisation

A series of three hydrophilic diblock copolymers were thus synthesised by aqueous RAFT polymerisation, as illustrated in Figure 3.3. A batch of cationic homopolymer, Q_{110} (M_n = 23100 g mol^{-1}), was first synthesised as a macro-CTA.

The macro-CTA was then chain extended, in aqueous solution by RAFT polymerisation, with *N*,*N*-dimethyl acrylamide (DMAm). The ratio of DMAm monomer to PQDMAEMA macro-CTA was varied in order to tailor the length of the neutral PDMAm (D) polymer block as approximately half, equal and double the length of the cationic polymer block (Q_{110}-*b*-D_{57}, Q_{110}-*b*-D_{89} and Q_{110}-*b*-D_{219} with M_n = 28800, 31900 and 44800 g mol^{-1}, respectively). By first synthesising PQDMAEMA as a macro-CTA, a constant cationic block length was kept between the homopolymer and diblock copolymers, maintaining the same size ratio of dsRNA to cationic charge in later experiments. The influence of the neutral polymer block length could then be investigated in terms of the polymer physicochemical properties, complexation efficiency and the stability of polyplexes formed with dsRNA.

The polycationic homopolymer, Q_{110}, was purified by dialysis and lyophilised separately. The homopolymer and diblock copolymer compositions and molecular weights were determined by ^{1}H NMR spectroscopy (400 MHz, Figure 3.4), detailed in Table 3.1.

Table 3.1. Properties of the homopolymer (macro-CTA) and three hydrophilic diblock copolymers synthesised in this work. [a]MW calculated using the following equation: $M_n(theo.) \approx \frac{[M]_0 - [M]_t}{[CTA]_0} \times M_m + M_{CTA}$ where $[M]_0$ is the initial monomer concentration, $[M]_t$ the monomer concentration at time t, $[CTA]_0$ the initial CTA concentration, M_m the molar mass of the monomer and M_{CTA} the molar mass of CTA.

Polymer code	**Data determined by ^{1}H NMR spectroscopy (400 MHz)**			**Data determined by aqueous-GPC**	
	Monomer conversion / %	**D proportion / mol%**	**M_n by NMR[a] / g mol^{-1}**	**M_n by GPC / g mol^{-1}**	**$Đ$**
Q_{110} (macro-CTA)	88	0	23100	8900	1.48
Q_{110}-*b*-D_{57}	86	34	28800	12600	1.39
Q_{110}-*b*-D_{89}	71	45	31900	16400	1.33
Q_{110}-*b*-D_{219}	91	67	44800	31600	1.23

Molecular composition was calculated through comparison of the relative intensity of an integrated D peak (~ 2.6 ppm) to the intensity of an integrated Q peak (~ 3.8 ppm). Conversion was monitored over the reaction time, as described in Section 3.4.1.2, using a low resolution (60 MHz) ^{1}H NMR instrument and Eq. 3.1. The conversion increased rapidly in the first 30 min and then increased steadily to > 90% until the reaction was quenched by exposure to air after approximately 3 h, see Figure 3.10.

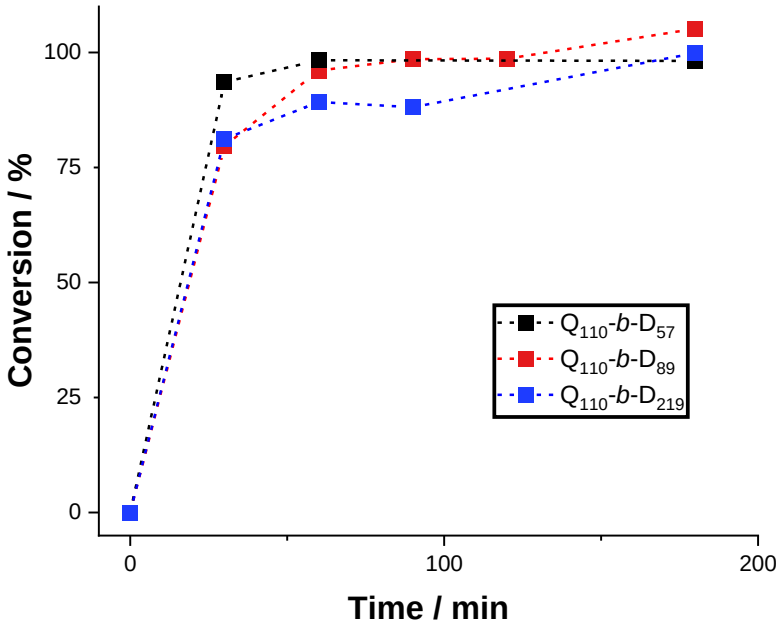

Figure 3.10. Conversion of each chain extension of Q_{110} macro-CTA with DMAm (D, amounts varied to alter final diblock copolymer composition), to synthesise hydrophilic diblock copolymers (Q_{110}-*b*-D_m). Conversion was monitored over time (180 min total reaction time), ascertained by ^{1}H NMR spectroscopy (60 MHz).

Since the polymers synthesised in this work are chemically different in comparison to the polymer standards (*i.e.* PEG/PEO) used to calibrate the aqueous GPC system, their interactions with the column are expected to be different and the molecular weight values obtained with this technique can only be considered as relative values.[279] Thus, to calculate N/P ratios in polyplex formulations, molecular weights derived from ^{1}H NMR spectra were used. Aqueous GPC at the end time-point (3 h) of each RAFT polymerisation (Figure 3.11) showed negligible presence of residual Q_{110} macro-CTA after each chain extension, indicating good blocking efficiencies.

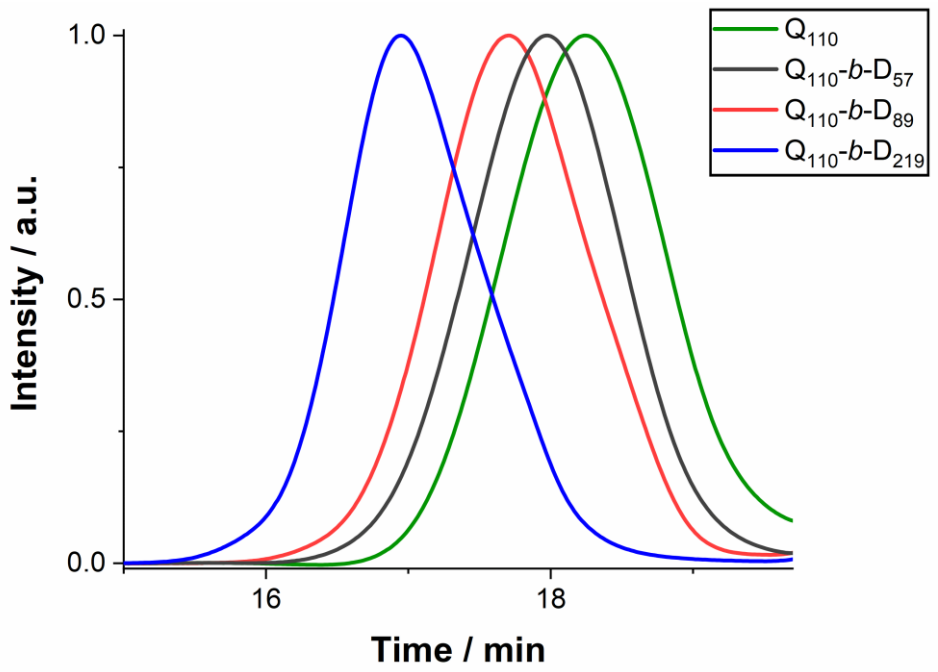

Figure 3.11. GPC chromatogram obtained for the Q_{110} macro-CTA and the series of three hydrophilic diblock copolymers with varying D polymer block degrees of polymerisation. The *y*-axis represents the arbitrary normalised signal from the RI detector.

Molar mass dispersity (*Đ*) of the hydrophilic diblock copolymers ranged from 1.23 to 1.39 (Table 3.1). These values are slightly higher than typically observed for controlled RAFT polymerisations (where Đ ~ 1.1 – 1.3)[220] but are suitable for the intended application.

3.4.2 Polyplex formation and size analysis over variable N/P ratio

The homopolymer and diblock copolymers, once synthesised, were complexed with *Drosophila suzukii*-specific *vha26* dsRNA. Dynamic light scattering (DLS) was employed to confirm the complexation between the positively charged homopolymer or diblock copolymers with dsRNA, and to assess the variability in the resulting size of the assembled polyplexes. DLS also confirmed that there was no sign of assembly of the homopolymer or diblock copolymers in aqueous solution, prior to interaction with dsRNA, with no larger scale structures (e.g. greater than the expected radius of gyration of the polymers on their own) measured.

Normalised intensity auto-correlation (IAC) data obtained for Q_{110}, Q_{110}-*b*-D_{57}, Q_{110}-*b*-D_{89} and Q_{110}-*b*-D_{219} polyplexes with dsRNA at N/P ratios from 1 – 10 was collected across a range of scattering angles. To demonstrate the process of extracting a mean size, the N/P ratio of 5 is shown here as an example in Figure 3.12 (full IAC data at N/P ratio = 5 is shown in Figure A2 in the Appendix).

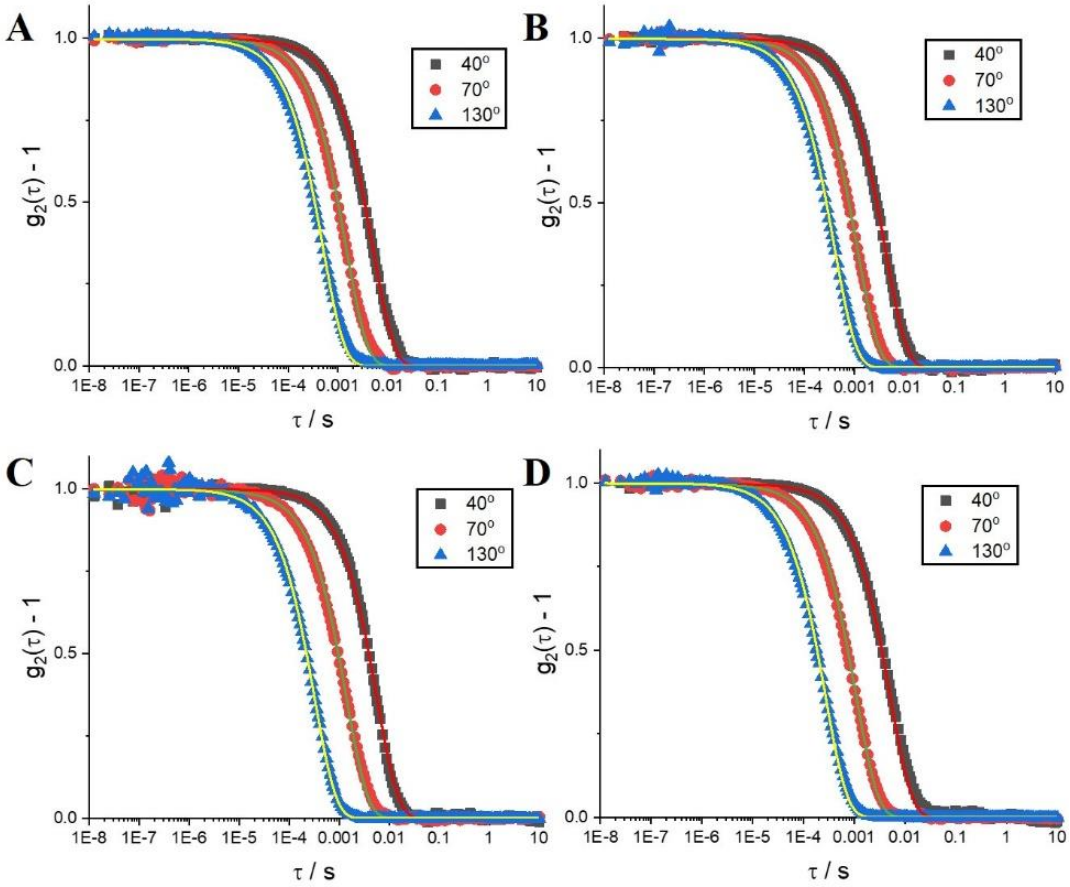

Figure 3.12. Normalised IAC data with single exponential fits obtained using Eq. 3.2 (continuous lines), for 40°, 70° and 130° scattering angles of polyplexes, with polymers of increasing D block lengths: (A) Q_{110}, (B) Q_{110}-*b*-D_{57}, (C) Q_{110}-*b*-D_{89} and (D) Q_{110}-*b*-D_{219}. All samples were measured after 24 h equilibration time and formulated at N/P ratio = 5.

These IAC curves show the presence of a single relaxation mode and were indeed successfully fitted to Eq. 3.2 with $i = 1$.

$$\frac{g_2(\tau) - 1}{\sigma} = \left[A_i exp\left(-\frac{\tau}{\tau_{R,i}}\right)\right]^2 \qquad \text{Eq. 3.2}$$

The coherence factor, σ, allows normalisation of the data so that the *y*-intercept equals 1, and $\tau_{R,i}$ and A_i are the relaxation time and the relative amplitude associated with the relaxation mode i, respectively. Further explanation of IAC data fitting can be found by referring to Section 2.2.1.2.

The obtained relaxation times, τ_R, were then used to calculate the decay rates, $\Gamma = \frac{1}{\tau_R}$, which were plotted against the square of the scattering vector, q^2, as shown in Figure 3.13A. Γ exhibits a q^2-dependence, characteristic of a diffusive behaviour. Hence Eq. 3.3 was used to determine the diffusion coefficient with the *y*-intercept, *B*, not restricted to account for the small uncertainties in the determination of Γ. Assuming a spherical shape for the measured objects, the Stokes-Einstein equation was subsequently used to calculate the hydrodynamic radius, R_H (Eq. 3.4).

$$\Gamma = Dq^2 + B \qquad \text{Eq. 3.3}$$

$$R_H = \frac{kT}{6\pi\eta D} \qquad \text{Eq. 3.4}$$

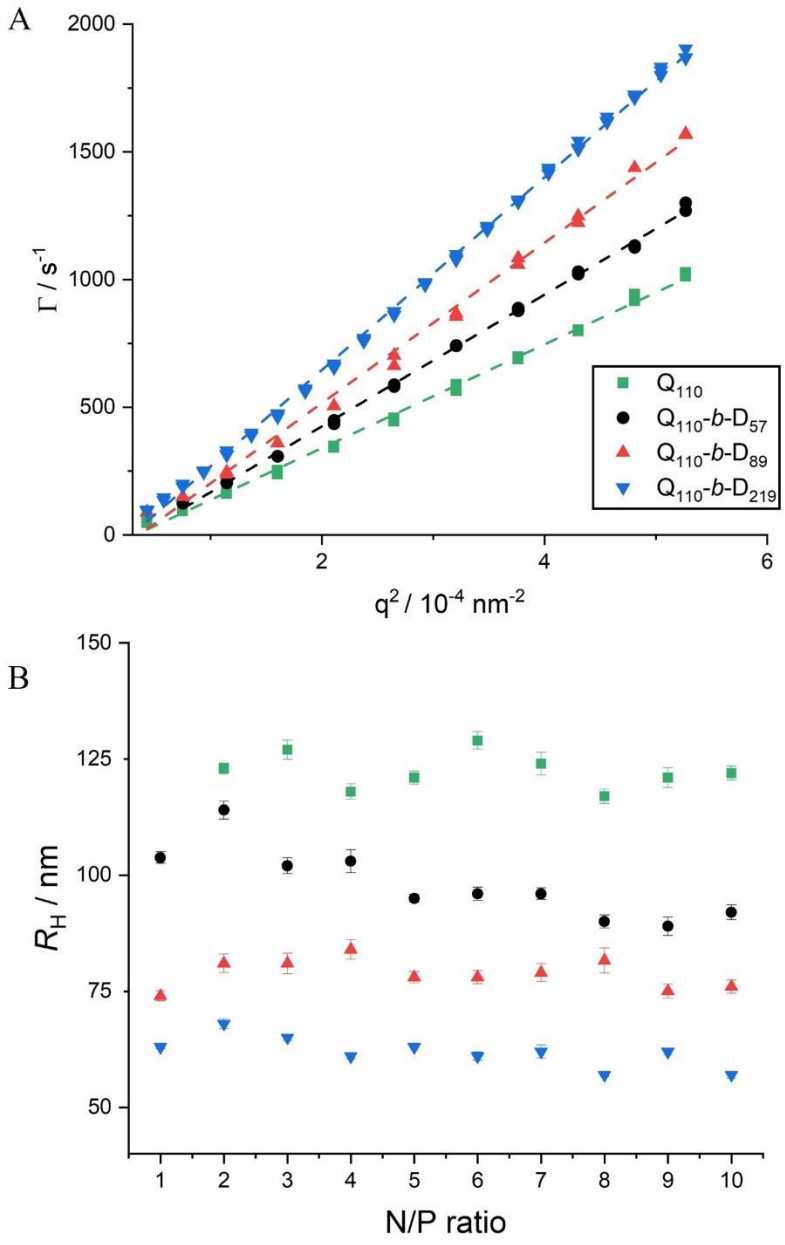

Figure 3.13. (A) Plots of the decay rate, *Γ,* as a function of the squared scattering vector, *q²*, for polyplexes formed with polymers containing increasing D block lengths: Q_{110}, Q_{110}-*b*-D_{57}, Q_{110}-*b*-D_{89} and Q_{110}-*b*-D_{219}. Dashed lines are linear fits of the data and allow the determination of the diffusion coefficient *D* of the scattering objects. All samples were measured after 24 h equilibration time and at N/P ratio = 5. (B) Effective hydrodynamic radii, R_H, of Q_{110}/dsRNA, Q_{110}-*b*-D_{57}/dsRNA, Q_{110}-*b*-D_{89}/dsRNA and Q_{110}-*b*-D_{219}/dsRNA polyplexes measured by dynamic light scattering, over N/P ratios = 1 – 10.

The size of polyplex objects showed minimal variation over N/P ratios = 1 – 10 (Figure 3.13B). Note that no R_H was determined at N/P ratio = 1 for Q_{110}-based polyplexes, as large precipitated aggregates/clusters, visible to the naked eye, formed upon mixing at this particular N/P ratio. Instability of polyplexes prepared through the mixing of two oppositely charged homopolymers (polyelectrolytes) around the isoelectric point is commonly reported in literature,[280] and these experiments further demonstrate the importance of incorporating a neutral block to sterically stabilise the polyplexes when close to charge neutrality. At higher N/P ratios, the polyplexes obtained with the homopolymer appeared to be stable, likely as a result of higher polyplex charge resulting from the imbalance of the overall number of charges between the polymer and the dsRNA, in agreement with previous literature.[281]

Figure 3.13 shows that as the neutral block length is increased, the size of the polyplex objects decreases. The hydrophilic, neutral D polymer block is incorporated to provide steric stabilisation and it likely surrounds the electrostatically-collapsed interpolyelectrolyte core comprising the dsRNA and Q polymer block, as previously predicted by coarse-grained simulation.[263] Beyond steric stabilisation, the assumed hydrophilic corona formed by the D polymer block has the potential to provide enhanced protection for the genetic material.[263] It is important, however, to highlight that in all these systems, the number of dsRNA chains within each of the polyplexes may not be constant, and this will play an important role in determining the size of the resulting polyplexes.

Previous studies on the structure and morphology of interpolyelectrolyte complexes formed between cationic and anionic polyelectrolytes has revealed a dependence on the polymer composition with respect to neutral block length. Their findings show that incorporating a neutral polymer block into one or both polyelectrolyte chains reduces aggregation and can shift the complex structure from vesicles/worm-like cylinders towards star-shaped, more spherical morphologies.[282–284] In particular, Petersen *et al.* studied bPEI-*g*-PEG/pDNA polyplexes and found that incorporating longer PEG blocks resulted in the formation of

smaller sized polyplexes when complexed to pDNA.[269] However, as far as we are aware, the work in this chapter is the first report of decreasing hydrodynamic radii of polyplexes formed between dsRNA and hydrophilic diblock copolymers with increasing neutral block length.

Static light scattering (SLS) was employed to further investigate the size and particle shape of the polyplexes formed between homopolymer or diblock copolymers and dsRNA. SLS was measured at a range of scattering angles to allow the Guinier approximation to be used (as explained in Section 2.2.1.3).[229,230] Guinier plots at low-q values and their respective linear fits and shown in Figure A3 in the Appendix, across a range of N/P ratios (1 – 10). Radii of gyration (R_g) were calculated from the gradient of the linear fits, according to SLS theory. The variation in radius of gyration with varying N/P ratio across the different polyplex samples is highlighted in Figure 3.14A.

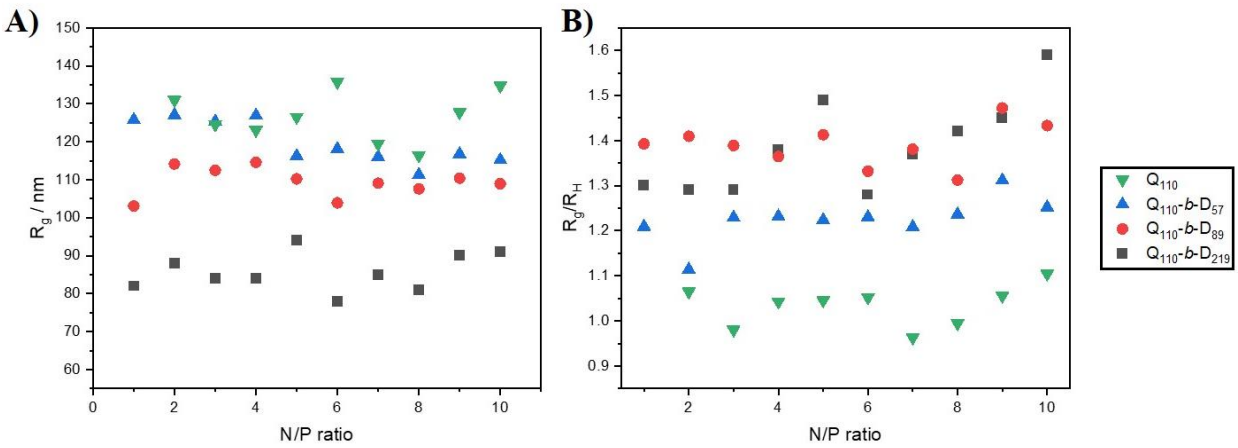

Figure 3.14. (A) Radii of gyration / nm, calculated from Guinier plots (obtained through SLS) across an N/P ratio range of 1 – 10 and (B) ratio of radius of gyration (R_g) with respect to hydrodynamic radius (R_H, measured by DLS) across an N/P ratio range of 1 – 10 for Q_{110}, Q_{110}-*b*-D_{57}, Q_{110}-*b*-D_{89} and Q_{110}-*b*-D_{219} polyplexes with dsRNA.

A similar trend is observed in the radii of gyration to the hydrodynamic radii measured by DLS, with the largest sizes measured for the Q_{110}-based polyplexes and polyplex size decreasing as the neutral D polymer block length is increased. There is also no significant variation in R_g across the N/P ratio range of 1 – 10 for any particular polyplex.

The ρ (R_g/R_H) of the polyplexes was calculated according to Eq. 2.18, as this size ratio can provide important structural information. Q_{110}/dsRNA polyplexes appear to have more spherical morphologies, with ρ values closer to one (Figure 3.14B). Interestingly, as the neutral polymer block length of the participating diblock copolymer is increased, the resulting polyplexes appear to become more rod-like in morphology, as ρ increases above one to up to values of ~ 1.5. Due to size of the hydrodynamic radii measured, the polyplexes are unlikely to be forming simple micelles. Instead, they are more likely to be forming vesicles or structures containing multiple micelles joined together. Thus, the more spherical (ρ ~ 1) Q_{110}-based polyplexes could be forming vesicles, and the diblock copolymer-based polyplexes (particularly as the neutral block length is increased) could be forming rod-like morphologies, possibly through the combination of multiple micellar structures.

These results are corroborated by TEM imaging (Figure 3.15) that visually shows the increasingly rod-like morphologies of polyplexes formed with diblock copolymers with longer neutral D block length.

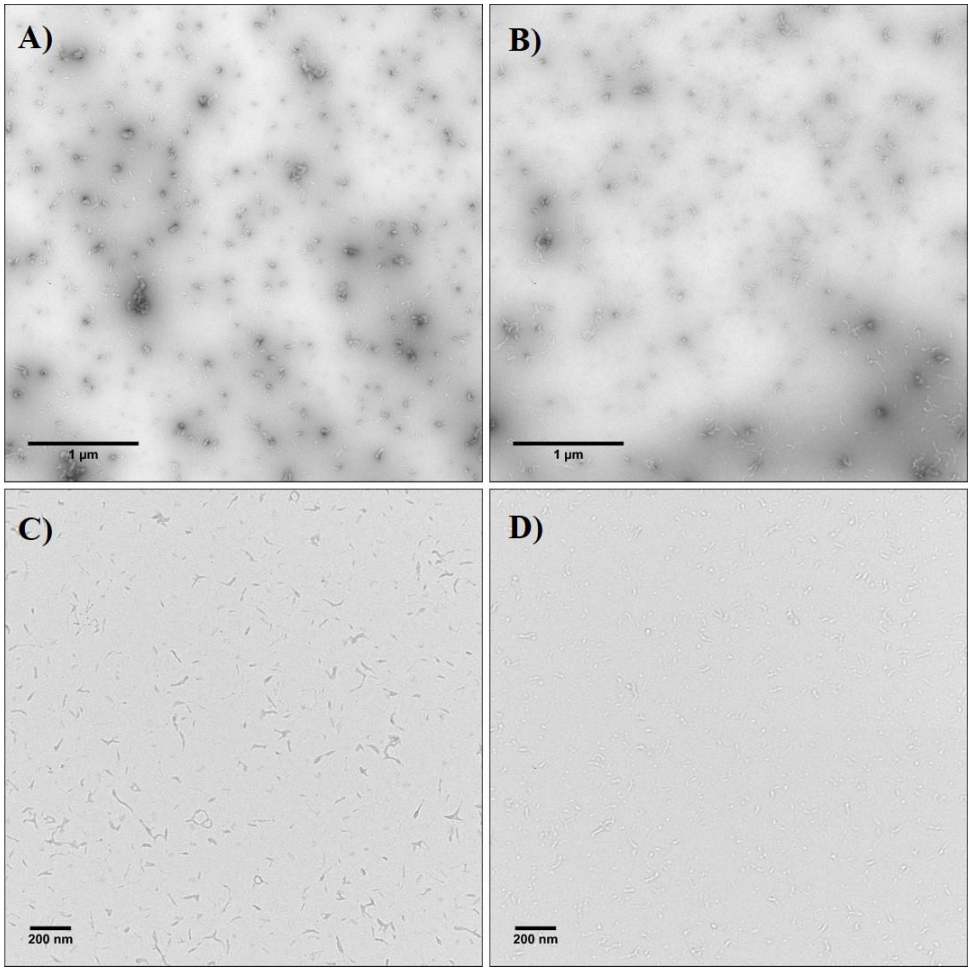

Figure 3.15. Representative TEM images of polyplexes (formulated at N/P ratio = 2) prepared with dsRNA (25 µL, 0.1 mg mL^{-1}) and (A) Q_{110}, (B) Q_{110}-*b*-D_{57}, (C) Q_{110}-*b*-D_{89} and (D) Q_{110}-*b*-D_{219} (0.1 mg mL^{-1}, volume of polymer solution varied to maintain N/P ratio = 2). Solutions were diluted to a final volume of 250 µL, providing an overall polyplex concentration of ~ 30 µg mL^{-1}. 400-mesh carbon-coated copper grids were prepared with 5 µL of sample, prior to washing with Milli-Q water and staining with 1% uranyl acetate. Images were captured using an FEI Tecnai G2-Spirit microscope, with a Gatan Ultrascan 4000 CCD camera, operated at 120 keV with a tungsten filament.

Imaging *via* TEM of systems such as these is challenging and requires a uranyl acetate stain. Images of systems with longer PDMAm chains appear to show more limited contrast (contrast decreases moving from images A through to D in Figure 3.15), perhaps due to less efficient staining of PDMAm with uranyl acetate. The process of drying the polyplexes onto the TEM grid may also have an impact on the morphology of the system, and therefore it is worth appreciating that the structures could be different from their native states when in solution.

3.4.3 Surface charge of polyplexes over variable N/P ratio

The anionic backbone of dsRNA is a prohibitive factor for cell entry due to repulsive electrostatic interactions with negatively charged cell-surface glycosaminoglycans,[285] whereas gene delivery vectors with a positive surface charge can promote genetic material entry into cells.[248,285–288] However, cationic homopolymers can be cytotoxic if their surface charge is too high.[265] Hence, a balance must be found to mitigate against toxicity by lowering cationic charge, whilst still promoting passive entry of dsRNA into cells.

Thus, the electrophoretic mobility (proportional to surface charge) of polyplexes as a function of N/P ratio was measured. As the N/P ratio was increased from 1 to 10, the polyplex electrophoretic mobility increased (Figure 3.16).

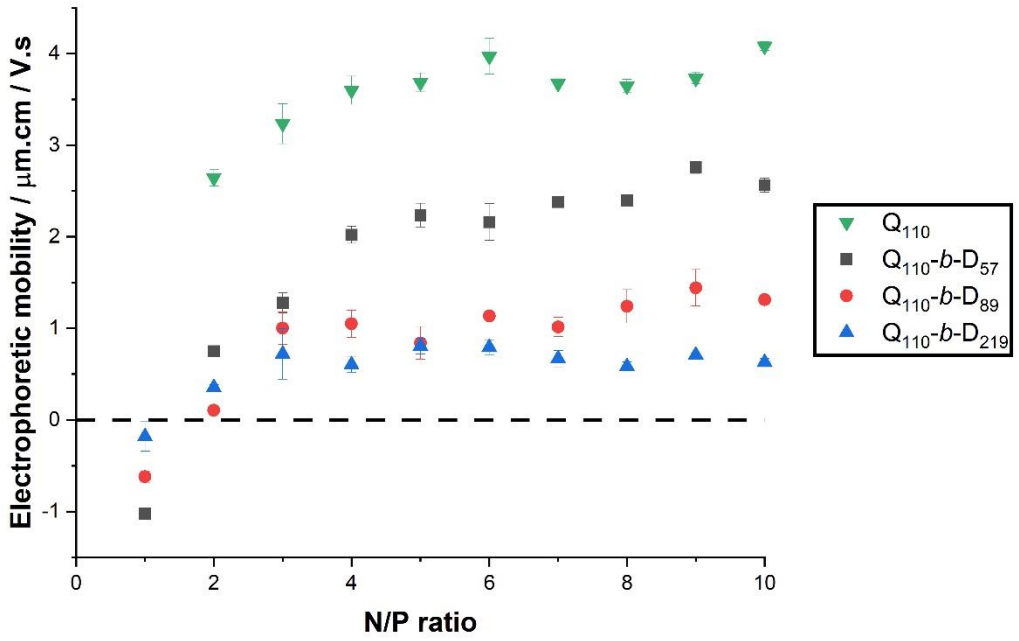

Figure 3.16. Electrophoretic mobility of polyplexes formed with each polymer (Q_{110}, Q_{110}-*b*-D_{57}, Q_{110}-*b*-D_{89} and Q_{110}-*b*-D_{219}) over an N/P ratio range of 1 to 10. Note that no electrophoretic measurement was conducted on polyplexes formed with Q_{110} at N/P ratio = 1, where precipitation/aggregation was observed.

At N/P ratios ≥ 3, the electrophoretic mobility of Q_{110}-*b*-D_{89}/dsRNA and Q_{110}-*b*-D_{219}/dsRNA polyplexes are seen to plateau, likely as a result of no further increase in the polymer to dsRNA

chain ratio. Therefore, polyplex samples with N/P ratios > 3 may contain free polymer chains. Q_{110}/dsRNA and Q_{110}-*b*-D_{57}/dsRNA polyplexes reach this plateau at higher N/P ratios, suggesting that the polyplexes formed with these two polymers, in comparison to Q_{110}-*b*-D_{89} and Q_{110}-*b*-D_{219}-based polyplexes, are able to accommodate additional polymer chains into their structure at higher polymer concentrations. In these cases, the additional chains incorporated within the Q_{110}/dsRNA and Q_{110}-*b*-D_{57}/dsRNA polyplexes, relative to Q_{110}-*b*-D_{89}/dsRNA and Q_{110}-*b*-D_{219}/dsRNA polyplexes, are likely to increase polyplex particle size, which correlates with the larger R_H values, as measured by DLS. At this stage, polyplexes prepared with Q_{110}-*b*-D_{89} and Q_{110}-*b*-D_{219} at N/P ratios ≥ 2 seem to be the best candidates for our application, since their electrophoretic mobility values are lower whilst still endowing a positive surface charge to aid endocytosis.

3.4.4 **Ethidium bromide analysis**

The fluorophore, ethidium bromide (EB), intercalates between the base pairs of DNA/dsRNA. It weakly fluoresces in aqueous solution, but exhibits a strong fluorescence when complexed with intact DNA or dsRNA. EB can therefore be used to monitor whether all, or only a portion, of the DNA/dsRNA is complexed by a polycation.[240,241]

3.4.4.1 Agarose gel retardation

Gel electrophoresis, using agarose gel stained with EB, was performed to assess the complexation of polymers to dsRNA at N/P ratios from 1 to 5. Successful complexation of dsRNA with a polymer is confirmed by the retardation of polyplexes, with the fluorescence from dsRNA-EB confined to the well of the corresponding gel lane, as opposed to migration of free dsRNA. Whereupon partial complexation occurs, a ‘smear’ down the gel lane can be observed, as only a fraction of the dsRNA chains are retarded against migration.[289] Figure 3.17 investigates the complexation of each of the polymers with increasing N/P ratio = 1 – 5.

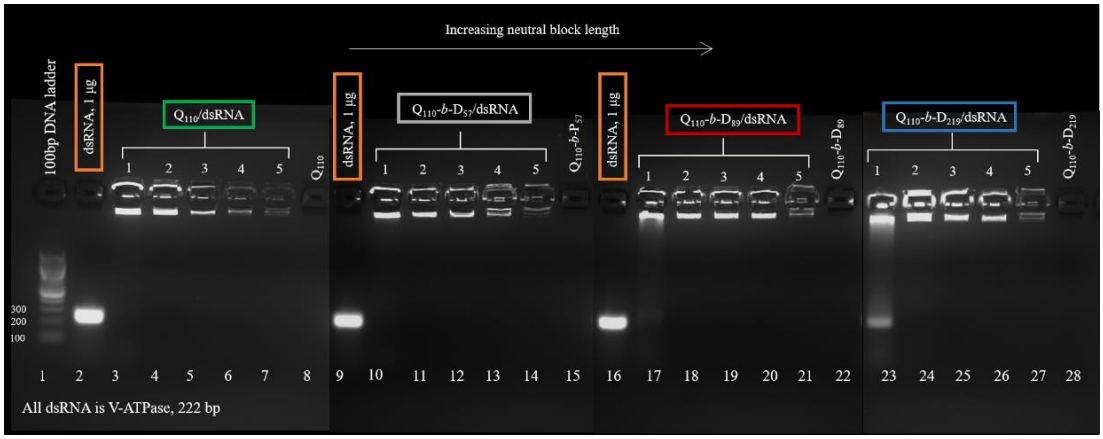

Figure 3.17. Agarose gel electrophoresis of polyplexes formed with each polymer (Q_{110} (lanes 3–7), Q_{110}-*b*-D_{57} (lanes 10–14), Q_{110}-*b*-D_{89} (lanes 17–21) and Q_{110}-*b*-D_{219} (lanes 23–27)) over an N/P ratio range of 1 to 5. 100 bp DNA ladder was used in lane 1, naked dsRNA (1 μg) was added to lanes 2, 9 and 16, and polymers Q_{110}, Q_{110}-*b*-D_{57}, Q_{110}-*b*-D_{89}, and Q_{110}-*b*-D_{219} alone were added to lanes 8, 15, 22 and 28, respectively. The image was collected in four separate images of each part of the gel so that greater focus of the observed fluorescence could be obtained; hence, subtle changes in background colour occurs in different sections of the image.

As indicated by the fluorescent wells, the homopolymer, Q_{110}, retards dsRNA migration at N/P ratios 1 – 5 (see Q_{110}/dsRNA polyplexes on the left side of Figure 3.17). The strength of fluorescence in the wells, however, is also observed to decrease as N/P ratio is increased. This is indicative of stronger binding of the polymer to dsRNA, and will be discussed in more detail in the next section.

Comparing Q_{110}/dsRNA to polyplexes formed with the diblock copolymer with the longest neutral D block, Q_{110}-*b*-D_{219}, a difference can be seen at an N/P ratio = 1. Q_{110}-*b*-D_{219}/dsRNA does not appear to retard the dsRNA migration as successfully as Q_{110}/dsRNA, as illustrated by the smeared fluorescence down the gel lane. This partial migration of dsRNA was reproducible. Multiple gel electrophoresis runs, specifically at an N/P ratio = 1, were performed to confirm this result (see Figure A4 in the Appendix). For diblock copolymer-based polyplexes at an N/P ratio = 1, as D polymer block length is increased, only partial complexation is achieved. A similar phenomenon was identified by Lam *et al.*, with

PDMAEMA-*b*-PMPC diblock copolymers when complexed with plasmid DNA.[231] As the length of the charge-neutral MPC block was increased, higher molar ratios of diblock copolymer were required to reach full complexation. Similarly here, N/P ratios > 1 are required for full complexation of dsRNA chains by longer neutral block length diblock copolymers (Q_{110}-*b*-D_{89} and Q_{110}-*b*-D_{219}).

3.4.4.2 EB exclusion assay

As qualitatively established by agarose gel electrophoresis, fluorescence of EB is quenched at higher N/P ratios. Through complexation of an interacting polycation with DNA/dsRNA, EB cannot intercalate as effectively between the base pairs, hence a decrease in fluorescence is observed. As a result, it is possible to use the quenching of fluorescence as a proxy for monitoring polymer/dsRNA binding/complexation. This phenomenon has been well-documented in literature.[96,238,239,245,289–291]

Quenching of fluorescence can only be determined qualitatively using agarose gel electrophoresis. Thus, fluorescence quenching titrations were performed *via* fluorescence spectroscopy over the N/P ratio range 0 – 10 (N/P ratio = 0 represents dsRNA-EB alone in aqueous solution and is used to quantify I_0, fluorescence intensity at *time = 0*) to quantitatively interpret the exclusion of EB by each polymer. The proportion of quenched fluorescence is interpreted as an indicator of the strength of binding between the homopolymer/diblock copolymer and the dsRNA. These data, presented in Figure 3.18, suggest that an N/P ratio = 2 – 3 is required for maximum fluorescence quenching.

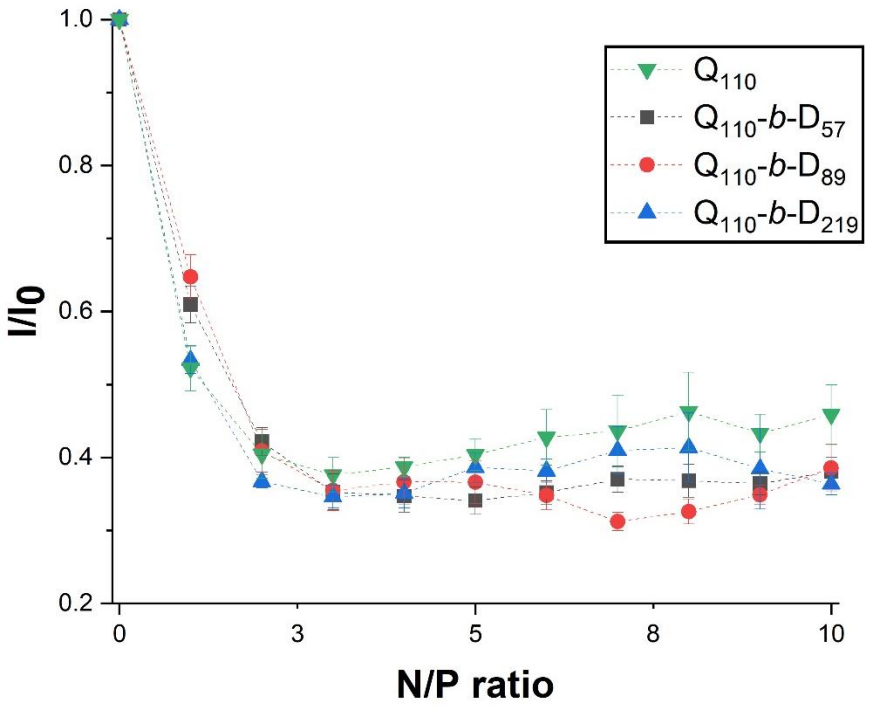

Figure 3.18. Ethidium bromide exclusion from intercalation between dsRNA base pairs, through the complexation of increasing amounts of polymer to dsRNA (increasing N/P ratio). Exclusion was quantitatively assessed through the quenching of fluorescence, measured with a plate reader. Polyplexes were formed between each polymer: Q_{110}, Q_{110}-*b*-D_{57}, Q_{110}-*b*-D_{89} and Q_{110}-*b*-D_{219} and *vha26* dsRNA. Fluorescence intensity has been normalised with respect to initial dsRNA-EB fluorescence (I_0). Dotted lines are included to guide the eye only.

Considering the error associated with the I/I_0 data points, there is no significant difference in the strength of binding between homopolymer and each diblock copolymer with dsRNA (that can be detected using this method). Complete EB exclusion (100% fluorescence quenching) is not achieved with Q_{110} nor the diblock copolymers, which could imply that stronger binding may be possible with alternative polymer designs. For example, Dey *et al.* reported EB exclusion of 90 – 98% between ctDNA and either a poly([3-(methacryloylamino)propyl] trimethylammonium chloride) (PMAPTAC) homopolymer or a series of PMAPTAC-*b*-PEG diblock copolymers.[248] However, such strong binding may also preclude the decomplexation and thus release of dsRNA within cells to incorporate within the RNAi machinery.

3.4.5 **Influence of C_{NaCl} on polyplex binding**

When considering the final application of exogenous dsRNA in agrochemical formulations, one expects many inorganic ions to be present in these environments. To develop an understanding of these systems under relevant conditions, we have investigated the impact of NaCl concentration (C_{NaCl}) on polyplex stability. As demonstrated by fluorimetric titration (Figure 3.19A), increasing the concentration of NaCl in the presence of dsRNA-EB (without complexation by a polymer) causes a decrease in the fluorescence intensity, which has also been previously shown in literature.[238]

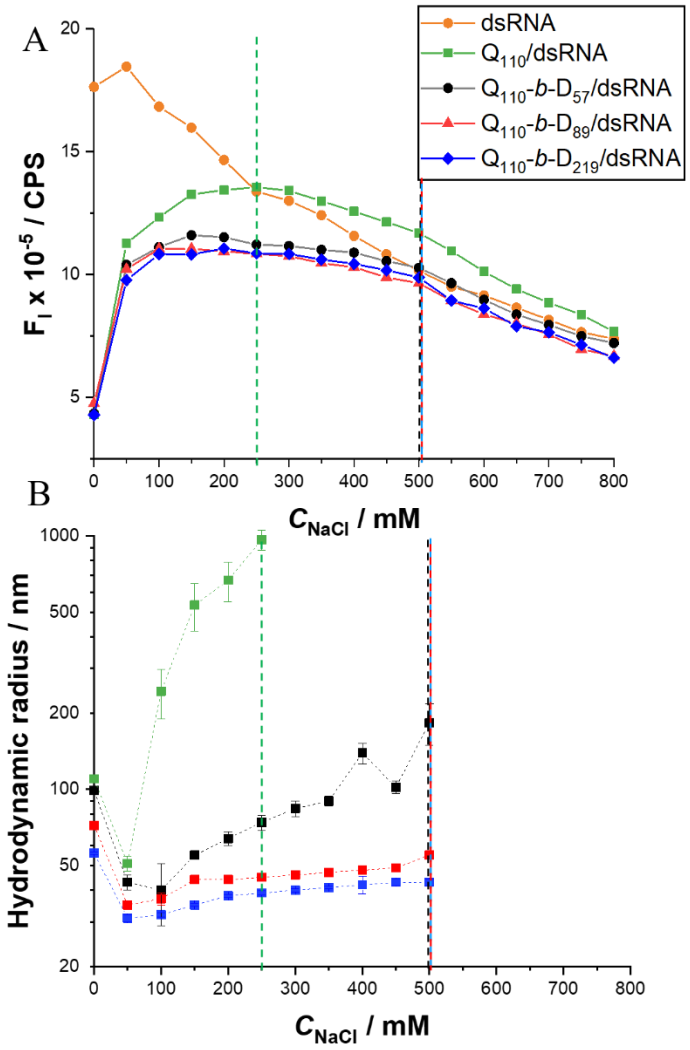

Figure 3.19. (A) Fluorescence intensity (a.u.) of polyplexes formed with either homopolymer or diblock copolymers (N/P ratio = 5) or naked dsRNA with increasing C_{NaCl}. The dsRNA, in the absence of polymer, is shown as the average spread of data following experiments run in quadruplicate. Lines are included to guide the eye only. (B) Average effective hydrodynamic radii (log scale) of Q_{110}/dsRNA, Q_{110}-*b*-D_{57}/dsRNA, Q_{110}-*b*-D_{89}/dsRNA and Q_{110}-*b*-D_{219}/dsRNA based on repeat measurements with increasing NaCl concentration. Dotted vertical lines are included to highlight crossover points with the fluorescence data.

Binding of EB to nucleic acids primarily occurs through the intercalation of base pairs. However, there is also a contribution to binding through electrostatic interaction of the cationic amine site of EB with the anionic phosphate groups. The addition of an electrolyte to naked dsRNA-EB, such as NaCl, weakens the binding of EB through electrostatic interaction, leading to a decrease of the fluorescence intensity of dsRNA-EB with increasing electrolyte

concentration. It is worth noting that this phenomenon has been shown to have a larger impact on dsRNA than DNA.[240,241,245,292]

The fluorescence intensity of polyplexes formed with dsRNA is plotted as a function of NaCl concentration in Figure 3.19A. In order to explain the behaviour of these systems, the results were analysed alongside size analysis to determine the decomplexation point (see Figure 3.19B and corresponding IAC curves in Figure A5 in the Appendix). Prior to addition of NaCl to the polyplex formulations, relative fluorescence intensity of the polyplexes is low as a result of the displacement of EB from dsRNA (and thus fluorescence quenching).[96,238,245,289,290,292]

Transitioning from a salt-free environment to C_{NaCl} = 50 mM, polyplexes appear to form smaller complexes due to chain rearrangement. Similar effects in polyelectrolyte complexes have been observed in literature.[264,293–295] This rearrangement allows increased EB access to intercalate with dsRNA, hence the large increase in fluorescence intensity in the region where C_{NaCl} = 50 – 200 mM.

From C_{NaCl} = 50 mM, light scattering reveals an increase in polyplex size due to electrostatic screening of charge by the addition of competing cations and anions. Charge screening causes swelling of the polyplexes due to osmotic repulsion within the polyplexes themselves.[296] Charge screening will also lead to colloidal instability of the polyplexes. Increased ion concentration leads to shortening of the Debye length of charged particles, thus reducing the barrier to aggregation.[297] Considering the (overall) positively charged polyplexes as charged particles, increasing ion concentration will lead to colloidal instability. This size increase is more pronounced for polyplexes formed by polymers with shorter (or without) D neutral polymer blocks. Petersen *et al.* also found that polyplexes formed between bPEI-*g*-PEG and pDNA swelled in size at C_{NaCl} = 150 mM.[269]

Full decomplexation is characterised as the crossover point beyond which the polyplex samples mimic dsRNA-EB fluorescence, with decreasing intensity upon further increase in C_{NaCl}.[238] Light scattering confirms the instability of polyplexes at this crossover point, beyond which multimodal size distributions are observed (an example of which is shown in Figure A6 in the Appendix) and DLS data can no longer be used. Q_{110}/dsRNA reaches the crossover point at C_{NaCl} ~ 250 mM, whereas the diblock copolymer-based polyplexes do not reach this point until C_{NaCl} ~ 500 mM.

The swelling regime of Q_{110}/dsRNA (C_{NaCl} = 50 – 250 mM) has greater fluorescence intensity than the equivalent regime (C_{NaCl} = 100 – 500 mM) in diblock copolymer/dsRNA samples. This implies that an increased proportion of free dsRNA is available for EB intercalation. We can therefore conclude that the addition of a steric stabilising block plays a role in maintaining complexation with dsRNA as C_{NaCl} is increased, particularly as full decomplexation of diblock copolymer/dsRNA polyplexes is not achieved until C_{NaCl} = 500 mM. In maintaining colloidal stability, one can provide either electrostatic or steric stabilisation. In the case of polyplexes, which are overall positively charged, electrostatics will maintain their stability until a certain ion concentration is reached of the surrounding solution, leading to a reduced aggregation barrier and thus colloidal instability. However, polyplexes formed with diblock copolymers with longer neutral polymer blocks will, in addition, possess steric stability. Thus, these polyplexes maintain their colloidal stability up to higher ion concentrations.

3.4.6 **Protection of dsRNA against degradation by synthetic enzymes**

A major barrier to the successful delivery of exogenous genetic material in agrochemical applications is overcoming the fragility of dsRNA to environmental nucleases. RNase A cleaves dsRNA after every cytosine and uracil, and was thus used to initially investigate the enzymatic degradation and/or protection of dsRNA. Time-resolved fluorescence spectroscopy

quantitatively highlights the dramatic, rapid degradation of dsRNA by RNase A (see Figure 3.20).

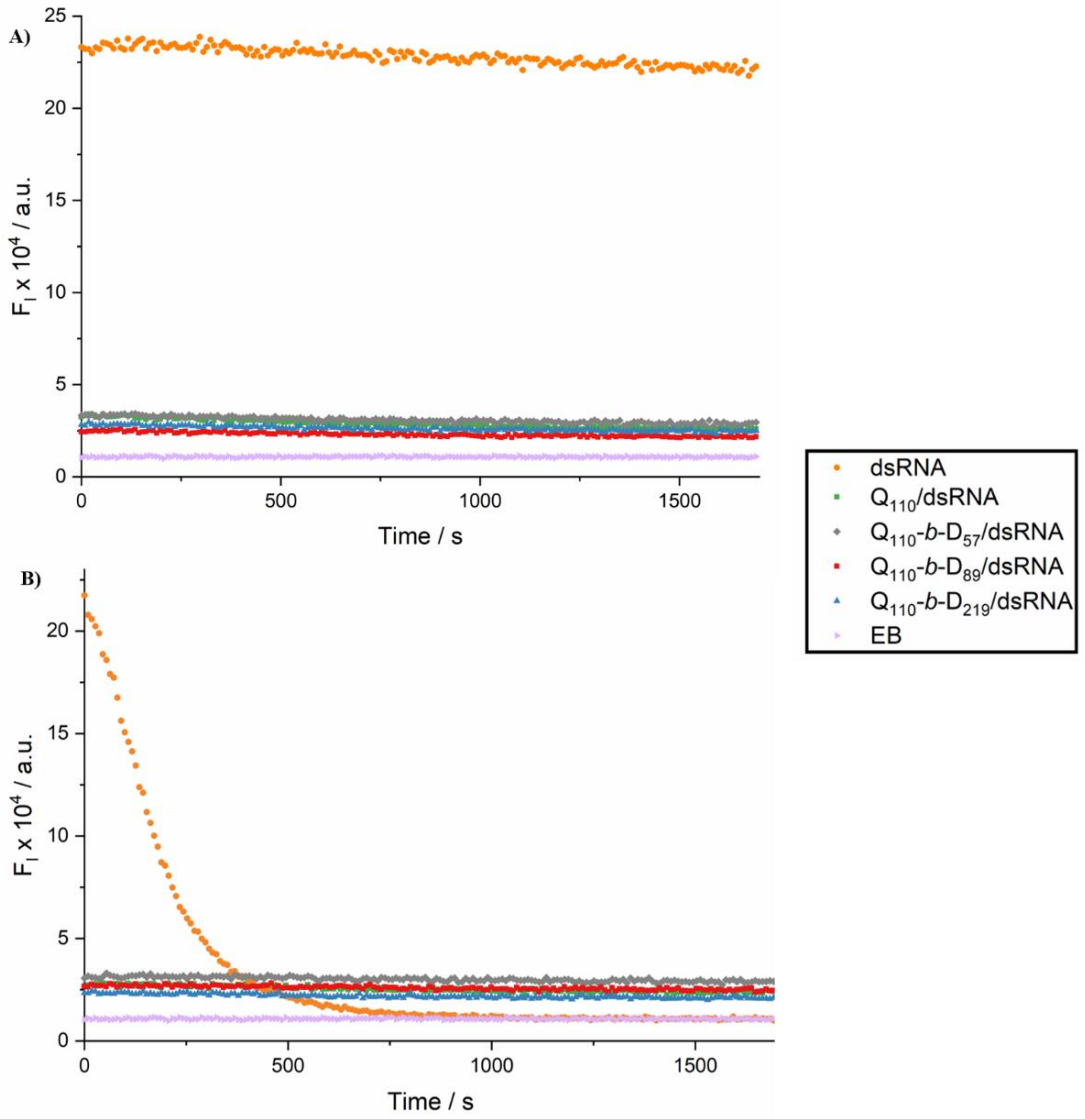

Figure 3.20. Time-resolved fluorescence spectroscopy of dsRNA (orange), Q_{110}/dsRNA polyplex (green), Q_{110}-*b*-D_{57}/dsRNA polyplex (grey), Q_{110}-*b*-D_{89}/dsRNA polyplex (red) and Q_{110}-*b*-D_{219}/dsRNA polyplex (blue), without (A) and with (B) the addition of RNase A. Fluorescence of ethidium bromide (EB) alone in water is shown in pink. Polyplexes were left for 1.5 h to equilibrate. Data is normalised with respect to I_0 (fluorescence intensity at time = 0). Low fluorescence intensity of polyplexes is due to quenching of EB fluorescence after displacement from dsRNA intercalation.

Polyplex fluorescence upon addition of RNase A shows minimal difference to polyplex samples without the addition of RNase A. It is worth noting here that the fluorescence of the

polyplexes (formulated at N/P ratio = 5) is quenched due to the displacement of ethidium bromide as the intercalating species, as explained in previous sections.

To further investigate the level of protection of dsRNA in polyplexes, complexation and proportion of degradation were qualitatively assessed in agarose gel electrophoresis assays over a range of N/P ratios (see Figure 3.21, Figure 3.22, Figure 3.23, and Figure 3.24).

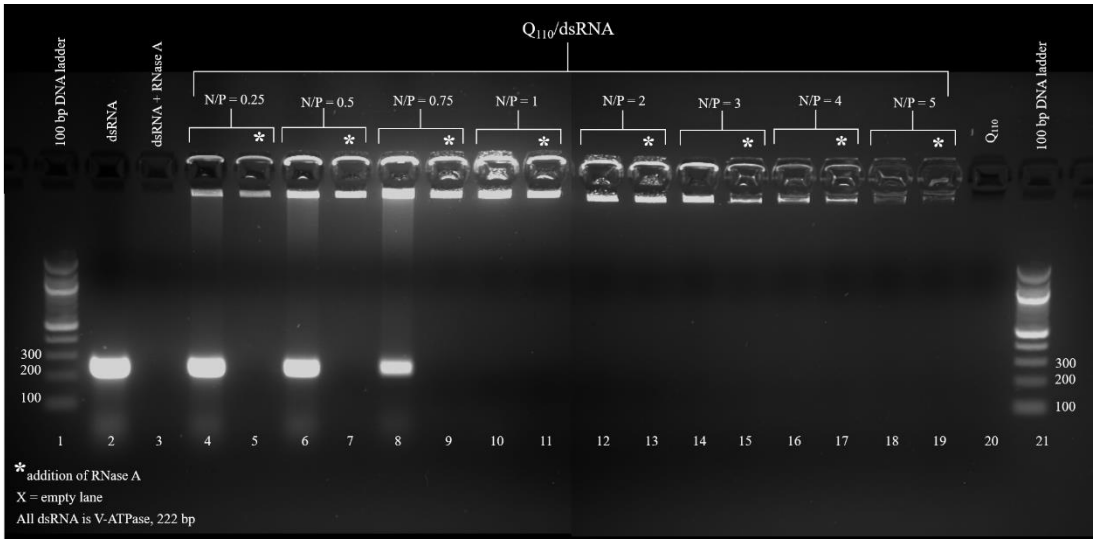

Figure 3.21. Agarose gel electrophoresis of Q_{110}/dsRNA polyplexes at N/P ratio = 0.25, 0.5, 0.75 1, 2, 3, 4 and 5. DsRNA (1 μg, lanes 2 and 3) and the polyplexes were incubated with (indicated by *) and without the presence of RNase A enzyme. 100 bp DNA ladder was used in lanes 1 and 21, and Q_{110} alone was added to lane 20.

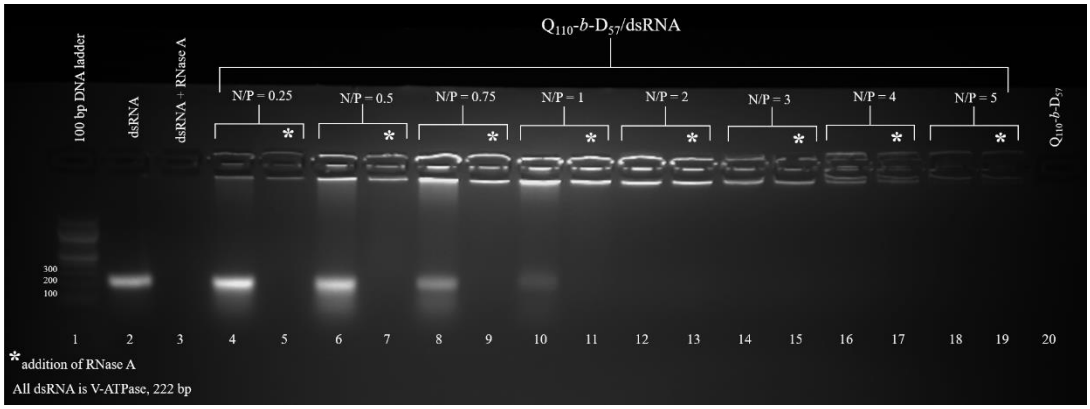

Figure 3.22. Agarose gel electrophoresis of Q_{110}-*b*-D_{57}/dsRNA polyplexes at N/P ratio = 0.25, 0.5, 0.75, 1, 2, 3, 4 and 5. DsRNA (1 µg, lanes 2 and 3) and the polyplexes were incubated with (indicated by *) and without the presence of RNase A enzyme. 100 bp DNA ladder was used in lane 1, and Q_{110}-*b*-D_{57} alone was added to lane 20.

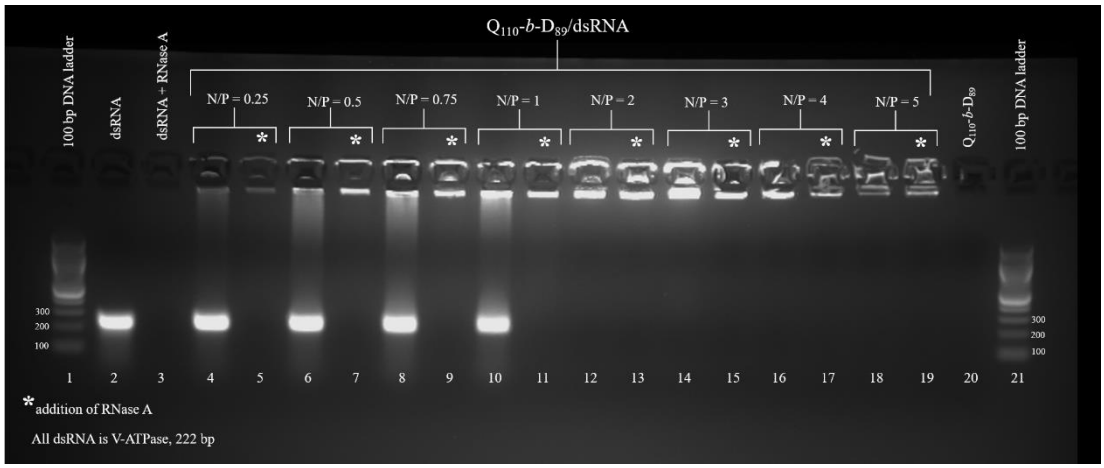

Figure 3.23. Agarose gel electrophoresis of Q_{110}-*b*-D_{89}/dsRNA polyplexes at N/P ratio = 0.25, 0.5, 0.75, 1, 2, 3, 4 and 5. DsRNA (1 µg, lanes 2 and 3) and the polyplexes were incubated with (indicated by *) and without the presence of RNase A enzyme. 100 bp DNA ladder was used in lanes 1 and 21, and Q_{110}-*b*-D_{89} alone was added to lane 20.

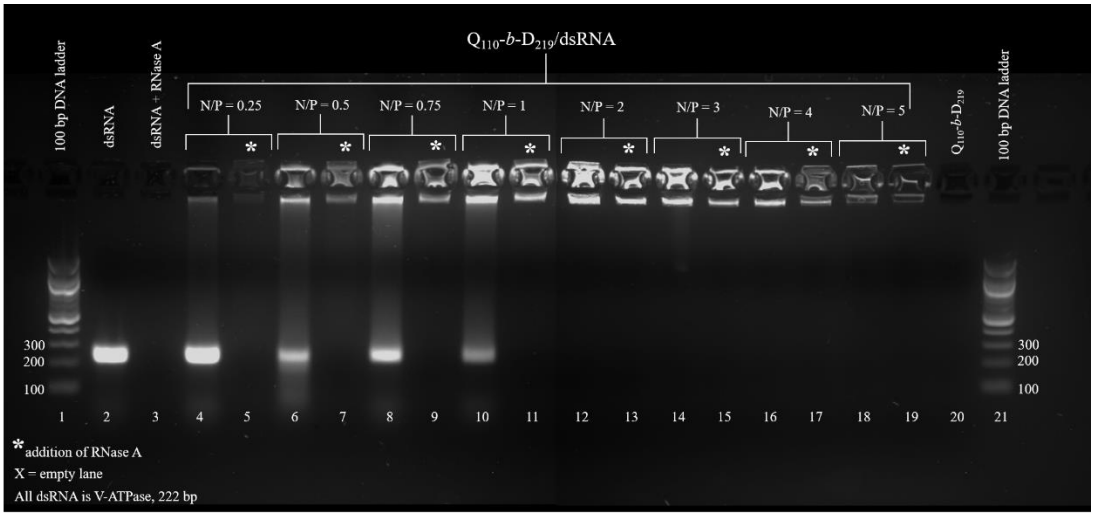

Figure 3.24. Agarose gel electrophoresis of Q_{110}-*b*-D_{219}/dsRNA polyplexes at N/P ratio = 0.25, 0.5, 0.75, 1, 2, 3, 4 and 5. DsRNA (1 μg, lanes 2 and 3) and the polyplexes were incubated with (indicated by *) and without the presence of RNase A enzyme. 100 bp DNA ladder was used in lanes 1 and 21, and Q_{110}-*b*-D_{219} alone was added to lane 20.

In all three diblock copolymer-based polyplexes, an N/P ratio ≥ 2 was required for full complexation and thus full protection of *vha26* dsRNA. Q_{110}/dsRNA, however, also achieved a full retardation of the migration of dsRNA at an N/P ratio = 1, likely due to the aggregation at this N/P ratio, as described in Section 3.4.2. Below these N/P ratios partial complexation occurs, with some dsRNA retarded in the well and a portion of free dsRNA migrating down the gel lane. In these cases, it can be observed that whilst the free dsRNA is degraded (absent fluorescence from sample with added RNase A), the complexed dsRNA remains intact (fluorescence still maintained in well of the gel).

The outcome of these experiments are summarised in Table 3.2, which indicates the complexation state (none, partial or full) of dsRNA by homopolymer and each diblock copolymer at specified N/P ratios, as well as whether dsRNA was degraded through the addition of RNase A.

Table 3.2. Summary of complexation and protection provided to dsRNA by homopolymer and hydrophilic diblock copolymers at different N/P ratios, as evaluated by agarose gel electrophoresis.

N/P ratio		0	1	≥2
dsRNA	dsRNA degraded in presence of RNase A	yes	n.a.	n.a.
Q_{110}/dsRNA	Complexation level	n.a.	partial	full
	dsRNA degraded in presence of RNase A	n.a.	yes	no
Q_{110}-*b*-D_{57}/dsRNA	Complexation level	n.a.	partial	full
	dsRNA degraded in presence of RNase A	n.a.	yes	no
Q_{110}-*b*-D_{89}/dsRNA	Complexation level	n.a.	partial	full
	dsRNA degraded in presence of RNase A	n.a.	yes	no
Q_{110}-*b*-D_{219}/dsRNA	Complexation level	n.a.	partial	full
	dsRNA degraded in presence of RNase A	n.a.	yes	no

Where partial degradation is described, this corresponds to the degradation of dsRNA that was *not* complexed in the control samples (free, migrated dsRNA). Q_{110} and the diblock copolymers provide full protection to dsRNA against degradation by RNase A at N/P ratio ≥ 2, which is promising for both therapeutic and agrochemical applications.

3.4.7 **Impact of dsRNA length on polyplex size and stability**

The dsRNA that was used in this thesis was primarily *vha26* dsRNA, with a length of 222 bp and sequence specific to *Drosophila suzukii* (synthesised by Genolution AgroRNA). However, there are numerous alternative mRNA transcripts that could be targeted, which, when specifically degraded, will induce mortality in *D. suzukii*. The literature is sparse with respect to changing length of nucleic acids, and the subsequent effect on complexation and protection afforded by polymeric delivery vehicles. There are two studies by Jiang *et al.* that detail the

impact of the length of linear and plasmid DNA, however there are no such studies investigating the length of siRNA, hairpin RNA or dsRNA.[259,298] As such, it is important to investigate the impact of changing dsRNA length (i.e. number of base pairs (bp)) on the resulting polyplex size, stability, protective capabilities etc., as many of the desired dsRNA targets will consist of differing numbers of base pairs.

To explore the effect of changing dsRNA length, DLS analysis was conducted (in the same manner as described in Section 3.4.2). Here, polyplexes are formed (at an N/P ratio = 5) between two GFP-specific dsRNAs, with base pair lengths of 590 and 258, and two 'active target' dsRNAs, with base pair lengths of 513 and 228. The dsRNAs were provided by Syngenta; hence the name 'active target' is used to protect their intellectual property, as the length of the dsRNA is our only concern for this body of work. Table 3.3 describes the apparent hydrodynamic radii (in nm) of the polyplexes, formed between the various dsRNAs and Q_{110}, Q_{110}-*b*-D_{57}, Q_{110}-*b*-D_{89} and Q_{110}-*b*-D_{219} polymers, measured by DLS.

Table 3.3. Apparent hydrodynamic radii / nm, by DLS measurement and subsequent fitting and analysis, of polyplexes formed between homopolymer/diblock copolymers and dsRNA of varying base pair numbers (i.e. length). Active target dsRNA is named as such as to maintain the IP rights of Syngenta, who supplied the GFP and active target dsRNA for this work.

	dsRNA				
	V-ATPase	Active target	GFP	Active target	GFP
Base pairs	222	228	258	513	590
Polymer	**Hydrodynamic radii / nm**				
Q_{110}	121	13 / 208	81	19 / 118	31 / 280
Q_{110}-*b*-D_{57}	95	14 / 218	107	81	40
Q_{110}-*b*-D_{89}	78	15 / 105	13 / 108	66	45
Q_{110}-*b*-D_{219}	63	58	49	85	55

All polyplexes were formulated at an N/P ratio = 5. During the fitting and analysis procedure of the raw DLS data (described in detail in Section 2.2.1.2), some of the data required a multi-

exponential fit. In these cases, two exponentials were combined to fit the data, resulting in the determination of two different hydrodynamic radii. These are indicated by the presence of two numbers in Table 3.3.

In particular, complexation with the shorter (228 bp) active target dsRNA caused the appearance of multiple populations within the samples. This could be due to the nature of the dsRNA synthesis, as these dsRNAs were prepared by *in vitro* transcription (IVT). Despite being purified by ethanol precipitation, the dsRNA may still contain a level of impurities that are affecting polyplex formation.

Polyplexes formed with diblock copolymers with shorter neutral D blocks also appeared to induce the formation of multiple populations, more often than polyplexes formed with diblock copolymers containing longer neutral block lengths. Figure 3.25 provides a visual comparison of the apparent hydrodynamic radii of the polyplexes. Polyplexes that formed multiple populations have been excluded from the figure for clarity. Unfortunately, there did not appear to be any significant trends in polyplex size, when comparing between different dsRNA lengths. However, the Q_{110}-*b*-D_{219}-based polyplexes appeared to form the most stable dispersions, with a single population consistently formed across the dsRNAs tested.

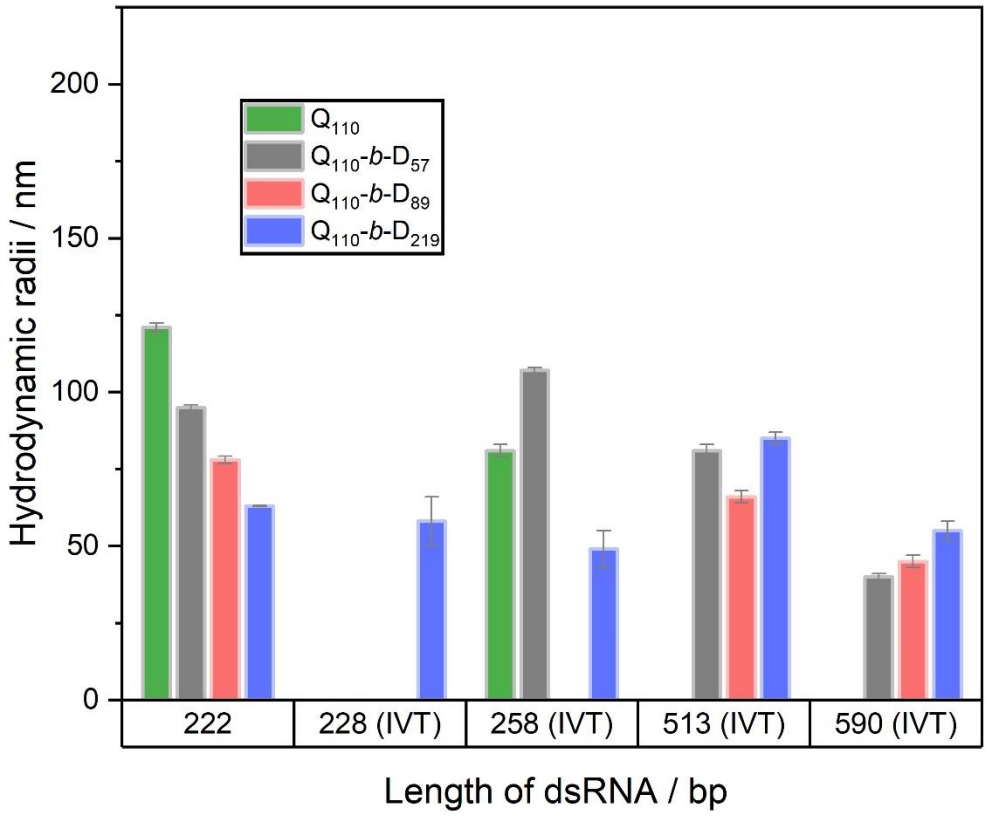

Figure 3.25. A visual comparison of the difference in hydrodynamic radii / nm, by DLS measurement and subsequent fitting and analysis, of polyplexes formed between homopolymer or diblock copolymers and dsRNA of varying base pair numbers (i.e. length). Active target dsRNA is named as such as to maintain the IP rights of Syngenta, who supplied the GFP and active target dsRNA for this work.

The dsRNAs investigated may have different physical properties. The shorter ~200 bp dsRNAs will likely act as rigid rods, however the longer ~500 bp dsRNAs are beyond the persistence length for dsRNA (~260 bp), so will likely be more flexible.[69] The diblock copolymers explored here appear to form single populations of discrete polyplexes with the longer dsRNAs. The flexibility of the longer length dsRNAs may allow for more interaction between the polymers and the dsRNA, inducing enhanced interaction and thus complexation. It is also worth considering the dsRNA structure, as dsRNA is known to be able to form loops and to contain regions of single-stranded chain. The full picture of the structure of each dsRNA used in this work is unknown; therefore this could also contribute to some of the variability in the size and dispersity of the polyplexes formed.

The polydispersity of the polyplexes, Figure 3.26, was measured by DLS through cumulant analysis, as described in Section 2.2.1.2. Cumulant analysis was not used to measure hydrodynamic radii, as this method of analysis is more suited to monodisperse systems. Polydispersity was calculated from DLS measured at a 90° angle.

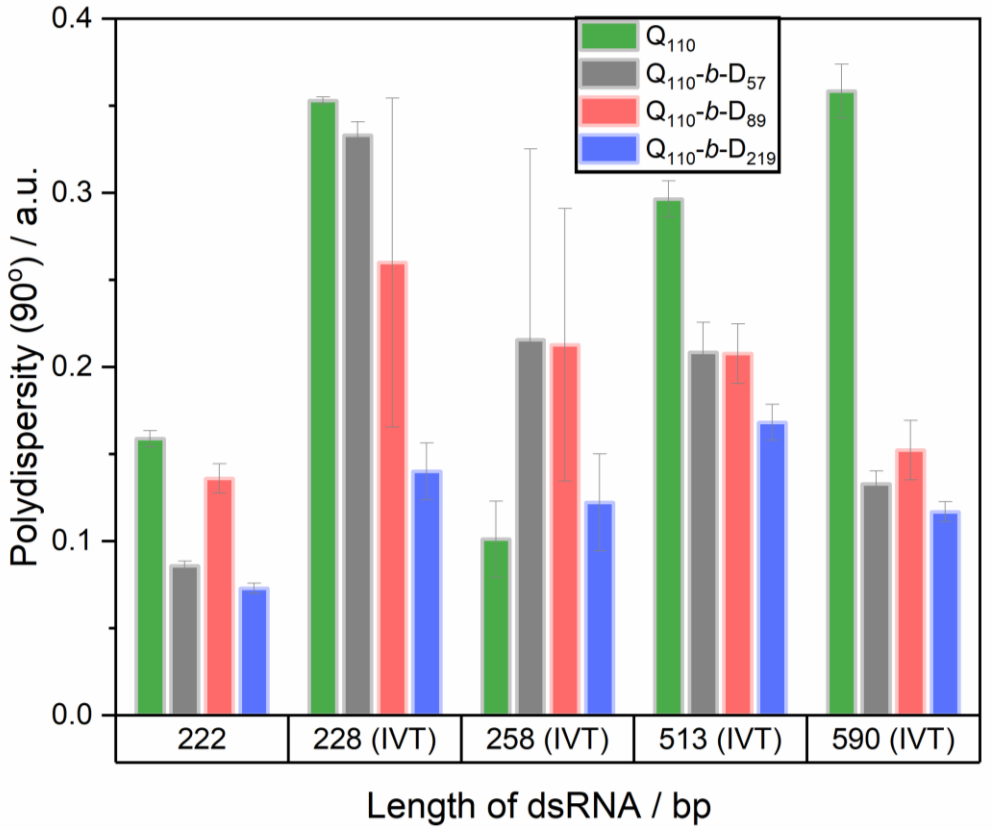

Figure 3.26. A visual comparison of the difference in polydispersity, by DLS measurement performed at 90°, of polyplexes formed between homopolymer or diblock copolymers and dsRNA of varying base pair numbers (i.e. length). Active target dsRNA is named as such as to maintain the IP rights of Syngenta, who supplied the GFP and active target dsRNA for this work.

The homopolymer (Q_{110})-based polyplexes tended to produce the highest level of polydispersity, particularly when complexing with longer dsRNA lengths. Without steric stabilisation (and thus repulsion due to osmotic forces) provided by a neutral polymer block, the complexes are free to form multi-complex bridged particles, which will occur more readily with longer dsRNAs.

Across all dsRNAs, Q_{110}-*b*-D_{219}-based polyplexes exhibited the lowest polydispersity values, remaining below 0.2. Q_{110}-*b*-D_{57} and Q_{110}-*b*-D_{89}-based polyplexes displayed similar polydispersity values that were greater than the values for Q_{110}-*b*-D_{219}-based polyplexes, but usually lower than values for Q_{110}-based polyplexes. These results suggest that incorporating longer length hydrophilic, neutral blocks into diblock copolymers for complexation with dsRNA enhances the stability of the resulting polyplexes. Q_{110}-*b*-D_{219}-based polyplexes consistently formed polyplexes with hydrodynamic radii ≤ 85 nm, and with the lowest levels of polydispersity. Whereas, the diblock copolymers with shorter neutral blocks (or without a neutral block in the case of the homopolymer) had at least one dsRNA with which they formed a polydisperse system of polyplexes with multiple populations. Consistent size and stability of polyplexes is crucial for the formulation development of agrochemicals. It should be noted that there cannot be one single block copolymer that will be able to complex with all dsRNA lengths. It is more likely that there are several candidates for different dsRNAs, but it is preferable if these show suitable complexation over a wide range of dsRNA lengths.

3.5 Conclusion

In this chapter, the synthesis of a polycationic homopolymer and a series of hydrophilic diblock copolymers was successfully achieved *via* aqueous RAFT (co)polymerisation. The final hydrophilic diblock copolymers consisted of a cationic PQDMAEMA (Q) block that was chain extended with varying lengths of PDMAm (D), which acted as a stabilising, neutral polymer block.

Increasing the length of the charge-neutral D polymer block was identified to have an inverse relation to the hydrodynamic radii (R_H) of polyplexes, when complexed with *vha26* dsRNA, as characterised by DLS. The absence of a neutral polymer block led to the largest size (R_H ~ 120 nm) polyplexes, whereas the diblock copolymer with the longest D polymer block formed the smallest size (R_H ~ 60 nm) polyplexes with dsRNA. As the N/P ratio was varied (from 1 to 10), there was no significant impact on polyplex size. However, when formulating at a 1-

to-1 charge ratio (N/P ratio = 1), a neutral polymer block was required to sterically stabilise the polyplexes, to prevent aggregation and precipitation.

The electrostatic interaction between the diblock copolymers, or cationic homopolymer, with *vha26* dsRNA induced the formation of polyplexes that retarded the migration of the nucleic acid through agarose gel above an N/P ratio = 1. The results suggested that diblock copolymers with longer D polymer blocks require higher N/P ratios (increased amount of polymer) to fully complex dsRNA, with only partial complexation at N/P ratio = 1, as qualitatively identified by agarose gel electrophoresis.

Whilst the majority of the work in this chapter was conducted using *Drosophila suzukii*-specific dsRNA (*vha26*), it is also important to understand the impact of changing dsRNA length (number of base pairs) on the size and stability of polyplexes. This is particularly important when considering alternative mRNA transcript targets that may require dsRNAs of different lengths to trigger RNAi. In exploring different dsRNA lengths, it was found that the diblock copolymer with the longest neutral polymer block (Q_{110}-*b*-D_{219}) was capable of forming the most stable (lowest polydispersity) polyplexes with the most consistent sizing (49 – 85 nm). It was also found that incorporating a neutral steric stabilising polymer block provided greater protection against full decomplexation in the presence of competitive salt ions, until C_{NaCl} = 500 mM.

The cationic homopolymer and hydrophilic diblock copolymers were all able to successfully protect dsRNA against degradation by RNase A when complexed at N/P ratio ≥ 2, as shown through agarose gel electrophoresis and fluorescence spectroscopy. However, despite the protective properties exhibited by all of the polymers, the diblock copolymer with the longest neutral polymer block formed the most stable and size-consistent polyplexes. This is particularly important when considering the use of these polyplexes for future agrochemical applications, as consistency across formulations is critical, especially when there are

limitations on the size of the polyplexes with respect to the target pest species and/or cellular internalisation.

Chapter 4. Influence of hydrophobicity on the complexation and protection of dsRNA by ABC triblock copolymers

A portion of the contents of this chapter has been published in *Polymer Chemistry* under the title, 'Linear ABC amphiphilic triblock copolymers for complexation and protection of dsRNA', 10.1039/D2PY00914E.

4.1 Abstract

In this chapter the synthesis and characterisation of linear ABC triblock copolymers, an investigation of their self-assembly in aqueous solution and of their complexation with and protection of double–stranded RNA (dsRNA) is herein reported. The amphiphilic triblock copolymers were synthesised *via* reversible addition-fragmentation chain transfer (RAFT) polymerisation. The precisely controlled polymerisation allowed for modification of the degree of polymerisation of quaternised 2-(dimethylamino)ethyl methacrylate (QDMAEMA, Q), *tert*-butyl acrylamide (*t*BAA, B) and *N*,*N*-dimethyl acrylamide (DMAm, D) polymer blocks, thus tailoring their affinity for the solvent and themselves. Firstly, the polycationic Q homopolymer was synthesised as a macromolecular chain-transfer agent to allow electrostatic interaction with dsRNA. The second block, B, was designed to provide strong anchoring of the assembled structures, and the third polymer block, D, was incorporated to enhance biocompatibility and colloidal stability. As illustrated by ^{1}H NMR spectroscopy, Q-*b*-B-*b*-D linear ABC triblock copolymers were prepared with molecular weights 30, 37 and 44 kDa. The self-assembly of the amphiphilic triblock copolymers in aqueous solution was confirmed by dynamic light scattering (DLS) and transmission electron microscopy (TEM). Furthermore, the potential of these tailored block copolymers as vehicles for dsRNA delivery was

demonstrated through their complexation with dsRNA and subsequent protection against destabilisation at high salt concentration and enzymatic degradation by RNase A, confirmed by ethidium bromide exclusion and agarose gel electrophoresis assays. In addition, the impact of dsRNA length (number of base pairs) was investigated, highlighting the consistent sizing and stability of triblock copolymer-based polyplexes, as opposed to complexes formed with homopolymer or diblock copolymer (Chapter 3) over a range of dsRNAs for different mRNA transcript targets.

4.2 Introduction

Amphiphilic block copolymers are suited as vehicles for cargo delivery in both therapeutic and agrochemical applications. These polymers consist of at least one hydrophilic and one hydrophobic block, which, unlike the hydrophilic diblock copolymers that were synthesised and characterised in Chapter 3, self-assemble in aqueous environments to form aggregated objects such as micelles or vesicles.[299,300]

The advent of controlled 'living' polymerisation in the early 2000s has brought about a number of reversible deactivation radical polymerisation (RDRP) techniques (described in detail in Section 2.1) that allow the precise design of block copolymers.[220,221,301] In these block copolymers, functionality can be tailored through the choice of monomers to suit the intended application.[302,303] In particular, these methods give researchers the ability to precisely control the ratio of blocks within a polymer for a wide range of possible monomers, for example, allowing for control of charge density or amphiphilic nature.

Block copolymers with cationic moieties have been widely explored for their potential for nucleic acid delivery.[135,251,304–307] Nucleic acids are water-soluble molecules with negatively charged phosphate groups along the backbone of the nucleotide chain. The hydrophilicity and anionic character of nucleic acids make them suitable as cargo for polymeric micelles, with

the inclusion of a cationic polymer block as a component of the block copolymer allowing for electrostatic interaction.[246] The DNA or RNA can be carried within the hydrophilic corona of a micelle, or within the hydrophilic core (or on the surface) of a vesicle. In particular, RNA is a fragile biomolecule that can be easily degraded by RNase nucleases present in the environment (e.g. microbial-produced RNases in soil or aquatic environments[60,64,67,68]) and within *in vivo* subjects (e.g. extracellular enzymes in haemolymph and gut juices).[80] Encapsulation of RNA within a polymeric delivery vehicle can provide protection against *ex vivo* or *in vivo* degradation by RNases.[250]

Thus far in the literature, triblock copolymers have not yet been synthesised to complex the longer biomolecule, dsRNA, even though they offer further options (as compared to homopolymers or diblock copolymers) for adding functionality to a block copolymer delivery system. In particular, ABC triblock copolymers, in comparison to homopolymers, diblock copolymers or ABA triblock copolymers, afford additional design opportunities through the incorporation of three unique polymer blocks. Each polymer block can be tailored for a specific purpose, synthesising block copolymers with enhanced properties. Research using triblock copolymers has typically focused on the complexation, protection and delivery of either short-interfering RNA (siRNA) or plasmid-DNA (pDNA). Brissault *et al.* found that for efficient nucleic acid delivery, different polymer architectures were required depending on whether pDNA or siRNA were being complexed. Their report investigated ABA triblock copolymers (where B refers to the hydrophobic polymer block), lPEI$_{50}$-*b*-poly(propylene glycol) (PPG)$_{36}$-*b*-lPEI$_{50}$ and lPEI$_{14}$-*b*-PPG$_{68}$-*b*-lPEI$_{14}$. The water soluble polymer (containing a shorter hydrophobic block, lPEI$_{50}$-*b*-PPG$_{36}$-*b*-lPEI$_{50}$) was more effective for pDNA transfection, whereas the self-assembling triblock copolymer (due to the incorporation of a longer hydrophobic block, lPEI$_{14}$-*b*-PPG$_{68}$-*b*-lPEI$_{14}$) was instead more effective at delivering siRNA for gene knockdown.[308] Plasmid DNA, siRNA and long dsRNA will likely require different polymer architectures for complexation, as they exhibit distinct physical properties from one another, such as rigidity due to differences in their persistence lengths.[69]

Recent studies on the use of amphiphilic triblock copolymers have investigated the impact of the presence, length or structural arrangement of a hydrophilic, neutral polymer block (typically poly(ethylene glycol) (PEG)) on the self-assembled objects themselves or when complexed to pDNA, siRNA or messenger-RNA (mRNA).[251,289,305,309,310] It has been found as a general rule that as hydrophilic block length is increased, the size of the self-assembled objects decreases (with or without complexation with a nucleic acid), which we similarly observed in Chapter 3 with diblock copolymers when complexed with *vha26* dsRNA.[251,309,310] A more compact complex is linked to improved complexation with nucleic acids[311], and the incorporation of a hydrophilic, neutral block has been shown to enhance colloidal stability through steric stabilisation.[251,309] Reports by Cheng *et al.* and Gary *et al.* described the use of ABC triblock copolymers, poly(DMAEMA-*b*-PEGMA-*b*-[diethylaminoethyl methacrylate (DEAEMA)-*co*-BMA]) and PEG-*b*-P*n*BA-*b*-PDMAEMA, for complexation with mRNA or siRNA, respectively. Both reports found that a longer hydrophilic, neutral block (PEG-based in both cases) protected complexes against destabilisation and enhanced gene silencing.[305,309] However, work by Sharma *et al.* showed that the introduction of a PEG block (when comparing PDMAEMA, PDMAEMA-*b*-PEG and PEG-*b*-poly(*n*-butyl acrylate) (P*n*BA)-*b*-PDMAEMA complexes with pDNA) led to a weakened binding to pDNA and less efficient transfection.[289]

There is a clear need for further investigation into the impact of polymer block length, configuration and chemistry on the complexation, stability and protection of nucleic acids when using ABC amphiphilic triblock copolymers, particularly for the delivery of longer dsRNA (in comparison to siRNA or pDNA). It is also worth exploring alternative polymer blocks, such as *N*,*N*-dimethyl acrylamide (DMAm), as some reports have suggested that PEG reduces the cellular uptake of siRNA/DNA.[272–274] As a substitute, PDMAm is easy to synthesise *via* RAFT polymerisation, and is relatively cheap and biocompatible.[275]

In Chapter 3, the use of fully hydrophilic diblock copolymers for the complexation and protection of dsRNA was described. Whilst these polymers were very effective at providing protection to dsRNA against enzymatic degradation by the synthetic enzyme, RNase A, they suffered with a lack of stability in the presence of high salt concentrations (C_{NaCl} > 500 mM) and when complexing different lengths of *in vitro* transcription (IVT) dsRNA. These issues were particularly noticeable in the homopolymer and the diblock copolymers with shorter neutral polymer blocks (D). In coarse-grained simulation by Zhan *et al.*, Figure 4.1, a triblock copolymer (positively charged block is blue, hydrophobic block is green, and hydrophilic, neutral block is pink) is shown interacting with a polyanion (red).

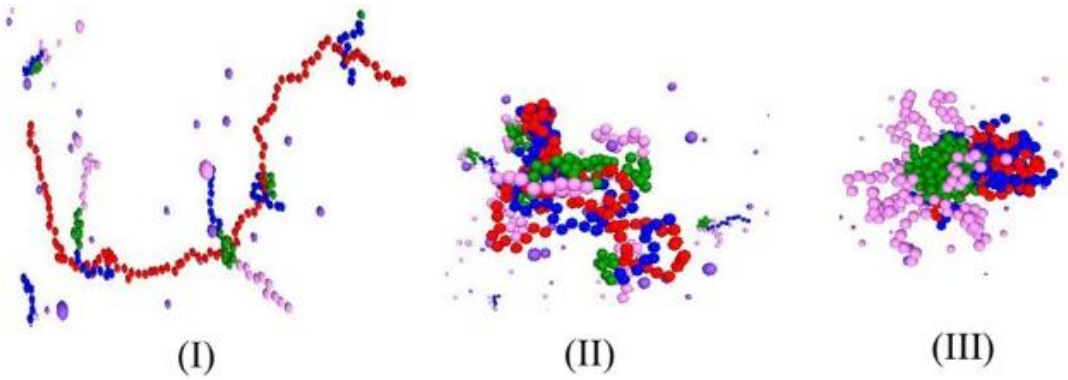

Figure 4.1. Snapshots of the complexation between a triblock copolymer (positively charged block is blue, hydrophobic block is green, and hydrophilic, neutral block is pink) and polyanion (red), as coarse-grained simulated by Zhan *et al.* Reprinted with permission from B. Zhan, K. Shi, Z. Dong, W. Lv, S. Zhao, X. Han, H. Wang and H. Liu, Coarse-Grained Simulation of Polycation/DNA-Like Complexes: Role of Neutral Block, *Mol. Pharmaceutics*, 2015, **12**, 2834–2844. Copyright 2022 American Chemical Society.

The structuring of ABC amphiphilic triblock copolymers by self-assembly induces the formation of compact, discrete complexes with dsRNA, as shown in Figure 4.1(III). Each polymer block has a unique purpose. The hydrophilic, neutral block forms a corona, extending into aqueous solution to provide colloidal stability through steric stabilisation. The corona surrounds a core of hydrophobic block and an interpolyelectrolyte complex core of charged polymer block and dsRNA. The incorporation of a hydrophobic block is used to provide

anchoring for the self-assembled structures, with the aim of enhancing stability of the resulting complexes in the presence of increasing electrolyte concentration and when complexing with dsRNAs of different lengths.

In this chapter, the synthesis and characterisation of a series of novel linear ABC amphiphilic triblock copolymers *via* RAFT polymerisation is described. A cationic and hydrophilic quaternised poly(2-(dimethylamino) ethyl methacrylate) (PQDMAEMA, Q) block was first synthesised as a macromolecular chain-transfer agent (macro-CTA). The macro-CTA was successively chain-extended with a hydrophobic poly(*tert*-butyl acrylamide) (P*t*BAA, B) block and a hydrophilic poly(*N*,*N*-dimethyl acrylamide) (PDMAm, D) block thereafter. The degree of polymerisation (DP), and thus the length, of the B and D blocks were varied in order to modify the extent of hydrophobicity of each amphiphilic triblock copolymer in the series, as well as to explore the influence of each polymer block. The amphiphilic triblock copolymers were characterised by ^{1}H NMR spectroscopy (400 MHz) in order to ascertain conversion and degree of polymerisation by characteristic peak analysis. Subsequently, dynamic light scattering (DLS) and transmission electron microscopy (TEM) were employed in aqueous environments to determine the self-assembling properties of the triblock copolymers and to perform size analysis.

Further to the synthesis and characterisation of the ABC triblock copolymers, the complexation of dsRNA, in salt-free and high salt concentration environments, and the resulting protection against degradation by a RNA-specific nuclease (RNase A) was investigated. The triblock copolymer-based complexes showed enhanced stability in high salt concentration environments (C_{NaCl} > 500 mM), in comparison to previous work on homopolymer and diblock copolymer/dsRNA polyplexes (Chapter 3).[312] A range of different dsRNA lengths were explored for their complexation with the triblock copolymers, to determine the size and polydispersity of the resulting complexes. The complexes showed greater stability and lower polydispersity over the range of dsRNA targets in contrast to

homopolymer and diblock copolymer/dsRNA polyplexes. Therefore, the triblock copolymer-based complexes with dsRNA may prove more suitable for commercial formulations.

4.3 Materials and methods

4.3.1 Materials

[2-(Methacryloyloxy)ethyl] trimethylammonium chloride solution (QDMAEMA, Q, 75 wt% in H_2O), *tert*-butyl acrylamide (*t*BAA, B, 97%), *N*,*N*-dimethylacrylamide (DMAm, D, 99%), sodium chloride (NaCl, 99.5%), D_2O (99.9%), methanol-d_4 (MeOD, 99.8%) and hydrochloric acid (HCl, 12 M) were purchased from Sigma Aldrich. 4-((((2-carboxyethyl)thio)carbonothioyl)thio)-4-cyano-pentanoic acid (CCCP, 95%) was purchased from Boron Molecular. 4,4'-Azobis(4-cyanovaleric acid) (ACVA, 97%) was purchased from Acros Organics. V-ATPase (*vha26*) 222 bp dsRNA was synthesised by Genolution AgroRNA (4.68 µg µL^{-1}), sequence specific to the pest insect, *Drosophila suzukii*. Ethidium bromide (EB, 10 mg mL^{-1}) and regenerated cellulose dialysis membrane (molecular weight cut off (MWCO) < 3,500 g mol^{-1}) were purchased from Fisher Scientific. 100 bp DNA ladder (500 µg ml^{-1}) and RNase A (20 mg mL^{-1}) were purchased from New England Biolabs. Blue/orange loading dye (6X) was purchased from Promega. Ultrapure Milli-Q water (resistivity of minimum 18.2 MΩ.cm) was used for solution preparation and dialysis, and nuclease-free water was used for biological assays to avoid the accidental degradation or contamination of dsRNA.

4.3.2 Synthesis of amphiphilic diblock copolymers

4.3.2.1 Synthesis of quaternised poly(2-dimethylamino ethyl methacrylate) macro-chain transfer agent

The homopolymer Q macro-CTA was synthesised by aqueous RAFT polymerisation, as shown in the scheme in Figure 4.2.

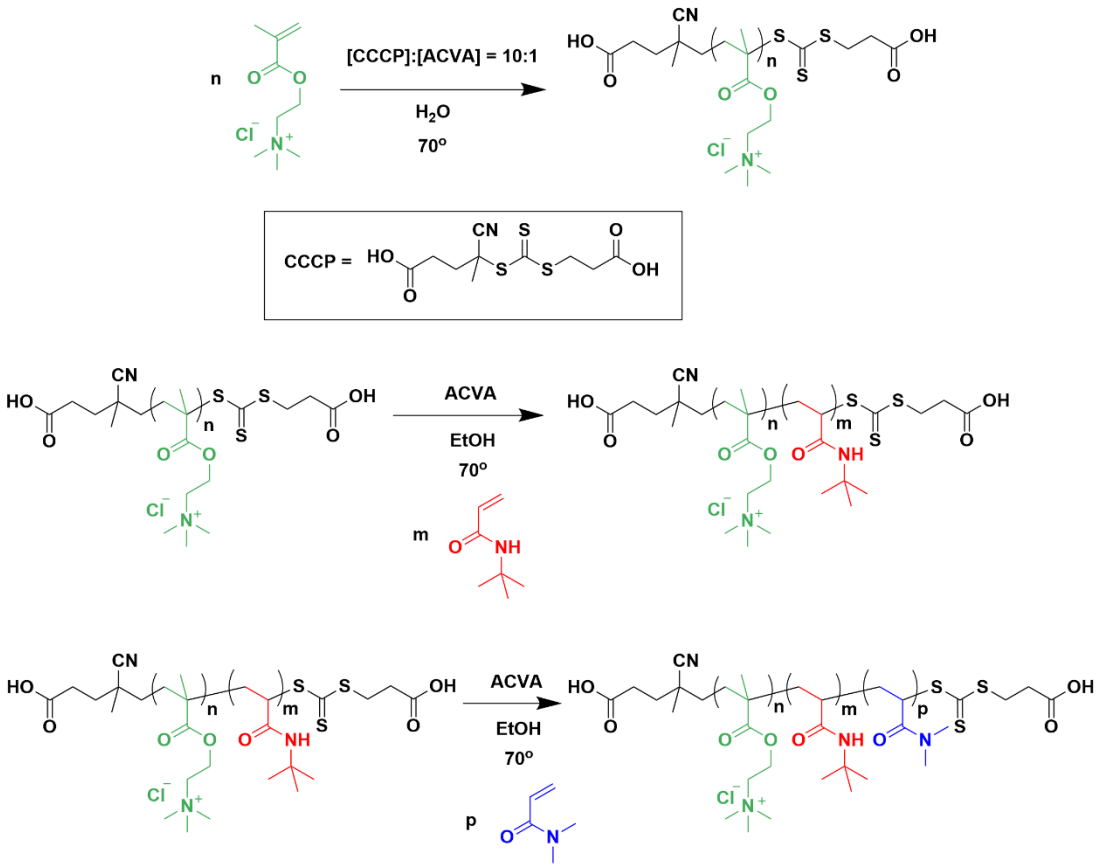

Figure 4.2. Reaction schemes for each stage of the triblock copolymer synthesis. CCCP was the initial chain-transfer agent (CTA) and ACVA was the initiator. The scheme begins with the polymerisation of QDMAEMA as the macro-CTA, then the synthesis of an amphiphilic diblock copolymer by chain extension with *t*BAA, and finally the extension of the diblock copolymer macro-CTA with DMAm to form the linear, amphiphilic ABC triblock copolymer. Figure created in ChemDraw Prime 21.0.

QDMAEMA (6.6 g, 75 wt% in H_2O, 32 mmol), CCCP (78 mg, 0.25 mmol) and ACVA (7.1 mg, 0.025 mmol) were dissolved in Milli-Q water, at a ratio of [QDMAEMA]:[CCCP]:[ACVA] = 126:1:0.1 and 50 wt% in solution, pH = 4.3. The solution was degassed with N_2 and then stirred at 70 °C for 1.5 h. The reaction was quenched by exposure to air. Product was purified by dialysis against Milli-Q water (MWCO < 3,500 g mol^{-1}) and then underwent lyophilisation to produce a pale yellow powder. The resulting macro-CTA had a degree of polymerisation of 100, according to ^1H NMR characterisation.

4.3.2.1 Chain extension of quaternised poly(2-dimethylamino ethyl methacrylate) with tert-butyl acrylamide

Amphiphilic (AB) diblock copolymers were prepared *via* chain extension of the Q_{100} macro-CTA with *tert*-butyl acrylamide (*t*BAA, B) (see scheme in Figure 4.2). An example of the reaction procedure is as follows: Q_{100} macro-CTA (0.40 g, 0.017 mmol), ACVA (1.0 mg, 0.0036 mmol) and *t*BAA (0.11 g, 0.87 mmol) were dissolved in 100% ethanol to 30 wt%, giving a ratio of [*t*BAA]:[macro-CTA]:[ACVA] = 50:1:0.2. The solution was degassed with N_2 for 15 min and then stirred at 70 °C for 24 h before being quenched by exposure to air. The product was purified by dialysis against 100% ethanol (MWCO < 3,500 g mol^{-1}), and remaining solvent was removed by rotary evaporation.

4.3.2.2 Chain extension of amphiphilic diblock copolymers with N,N-dimethyl acrylamide

Linear, amphiphilic ABC triblock copolymers were prepared *via* chain extension of the Q-*b*-B macro-CTA (AB diblock copolymer) with *N,N*-dimethyl acrylamide (DMAm, D, see scheme in Figure 4.2). An example of the reaction procedure is as follows: Q-*b*-B macro-CTA (0.22 g, 0.0080 mmol), ACVA (1.0 mg, 0.0036 mmol) and DMAm (0.10 g, 10 mmol) were dissolved in 100% ethanol to 30 wt%, giving a ratio of [DMAm]:[macro-CTA]:[ACVA] = 250:1:0.4. The solution was degassed with N_2 for 15 min and then stirred at 70 °C for 1.5 h before being quenched by exposure to air. The reaction solution became cloudy after ~ 1 h. The product was purified by dialysis against Milli-Q water (MWCO < 3,500 g mol^{-1}). This solvent switch induced particle formation, and the resulting particles were lyophilised to produce a white powder.

4.3.3 Characterisation

4.3.3.1 ^{1}H NMR spectroscopy

^{1}H NMR spectroscopy was conducted at 400 MHz, post-purification. Q homopolymer was diluted in D_2O, and Q-*b*-B diblock copolymer and Q-*b*-B-*b*-D triblock copolymer were diluted in MeOD, (5 mg mL^{-1}). The DP and conversion (% of target DP) were confirmed in each case

by comparison of characteristic peaks (described in detail in Section 3.3.2.1). Examples of the ^{1}H NMR spectra (Figure 4.3) will be discussed in the Results and Discussion section (4.4.1). Spectra for the other two triblock copolymers can be found in Figure A7 and Figure A8 in the Appendix.

4.3.3.2 Transmission electron microscopy

Transmission electron microscopy (TEM) was performed as described in Section 2.2.3.

2.2.3 Light scattering

4.3.3.3 Triblock copolymer alone in aqueous solution

Triblock copolymer solutions were prepared by directly mixing Q-*b*-B-*b*-D in Milli-Q water to a concentration of 1 mg mL^{-1}.

4.3.3.4 Complexed solutions with dsRNA

Triblock copolymer and dsRNA solutions were prepared through dilution of a mother solution 48 h before measurement. Triblock copolymer-based polyplexes were formulated at a low concentration (0.1 mg mL^{-1}) approx. 24 h before measurement to allow for equilibration time. *Dynamic light scattering:* Fitting of the data was performed using the Levenberg-Marquardt algorithm, with details described in Section 2.2.1.2. *Static light scattering:* Collection and fitting of data was performed as described in Section 2.2.1.3.

4.3.4 Electrophoretic mobility

Aqueous suspensions were prepared (0.1 mg mL^{-1}) 24 h before measurement. Details of instrumentation is described in Section 2.2.2.

4.3.5 Agarose gel electrophoresis

Aliquots of triblock copolymers were added to 1 μg dsRNA, in quantities to vary the N/P ratio, with solutions left to incubate at RT for 1.5 h to allow time for complexation. When RNase A (0.5 μL, 5 mg mL^{-1}) was added to the polyplex solutions, the samples were incubated at 37 °C for 30 min prior to analysis. Further details of the assay are described in Section 2.3.3.

4.3.6 Fluorescence spectroscopy

Details of fluorescence spectroscopy technique and sample preparation are described in Section 2.3.4.

4.4 Results and discussion

4.4.1 Linear ABC amphiphilic triblock copolymer synthesis

Linear, amphiphilic ABC triblock copolymers were synthesised by reversible addition-fragmentation chain transfer (RAFT) polymerisation, allowing control over each polymer block length to produce triblock copolymers with multiple blocks of differing functionalities.

The synthesis of amphiphilic block copolymers can be challenging, as the combination of both hydrophobic and hydrophilic polymer blocks demands careful consideration of solvent choice for their synthesis and subsequent purification methods. The solvent must be carefully selected to ensure solubility of starting reagents and final products, and care must be taken to purify the desired product at each stage of the synthesis.[260] The solubility of monomers, homopolymers, diblock and triblock copolymers were first tested in a variety of solvents to determine the optimal conditions for each stage of the polymerisation, the results of which can be found in Table 4.1.

Table 4.1. Results of solubility assays with monomers and homo-/diblock co-/triblock co-polymers. 'y' indicates that the monomer/polymer is soluble in the solvent, 'y/n' denotes partial solubility, and 'n' indicates that the monomer/polymer is not soluble in the solvent. * denotes that the monomer/polymer is only soluble in the solvent through the addition of a small amount of ethanol.

Solvent	Monomer/Polymer						
	QDMAEMA	PQDMAEMA	*t*BAA	Q-*b*-B	DMAm	Q-*b*-B-*b*-D	Q-*b*-D
H_2O	y	y	n	n	y	n	y
Ethanol	y	y	y	y	y	y	
Acetone	y*	n	y	n			n
Hexane	n	n	n	n			
Methanol		y	y	y			
IPA		n	y				
Toluene		n	y/n				
DCM		n	y				
Diethyl ether			y	n			

RAFT polymerisation was first used to prepare the macro-CTA, Q, in aqueous solution. The product was purified by dialysis in Milli-Q water and lyophilised. The second polymerisation, of the hydrophobic B block, was conducted in 100% ethanol with purification completed by dialysis against 100% ethanol. The resulting amphiphilic diblock copolymer (Q-*b*-B) was isolated by evaporation *in vacuo*. The final polymerisation of the third, hydrophilic polymer block (D) was conducted in 100% ethanol. The final purification was performed by dialysis in Milli-Q water prior to lyophilisation, which is further discussed in the next section (4.4.2).

Due to the charged nature and self-assembly of the triblock copolymers in aqueous solution, gel permeation chromatography (GPC) analysis was inaccessible. The reaction efficiency was instead assessed as a percentage of the target degree of polymerisation (DP) achieved, calculated *via* ^{1}H NMR spectroscopy (400 MHz) as described in Section 4.3.3.1. The ^{1}H NMR spectra at each stage of the synthesis of one of the triblock copolymers (Q_{100}-*b*-B_{44}-*b*-D_{99}) are shown in Figure 4.3 (spectra for the other two triblock copolymers in the series can be found in Figure A7 and Figure A8 of the Appendix, but appear very similar to those in Figure 4.3).

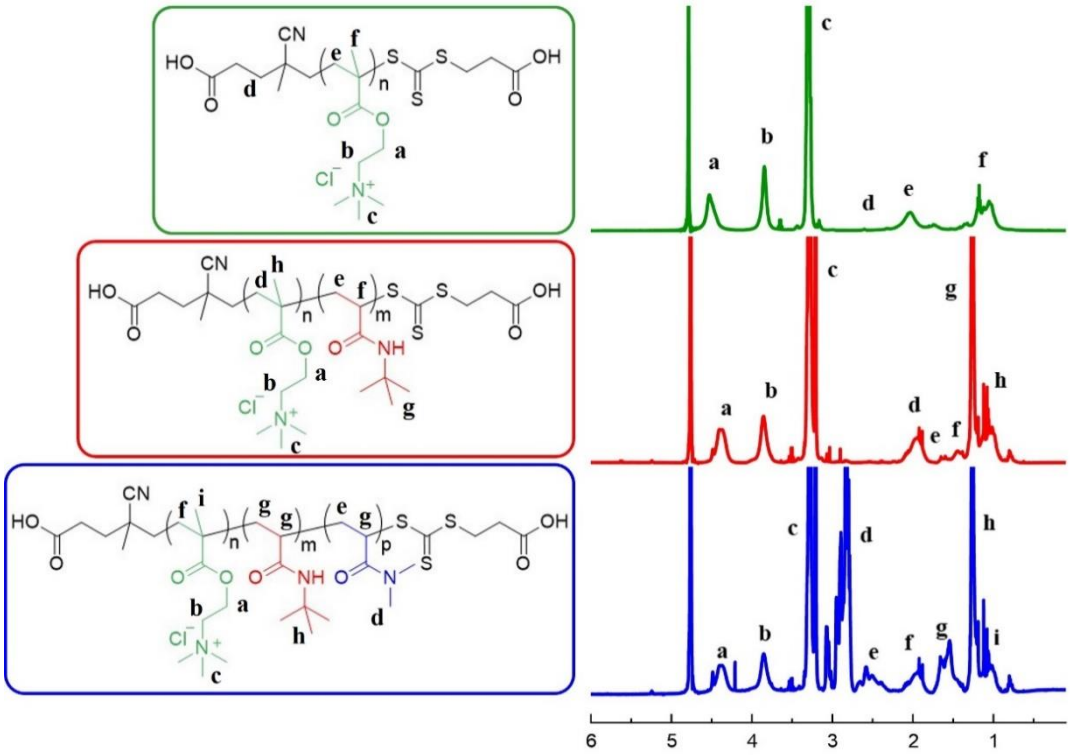

Figure 4.3. Example ^{1}H NMR spectra for each step of the triblock copolymer RAFT polymerisation (Q_{100}-*b*-B_{44}-*b*-D_{99} used as an example here). The chemical structures, drawn in ChemDraw Prime 17.0, are shown on the left, with the corresponding ^{1}H NMR spectrum on the right. Key peaks are identified that were used for peak comparison analysis to calculate the degree of polymerisation.

Peak (**b**) was used to represent the Q block of the triblock copolymer, with peaks (**g**) (in the red spectrum) and (**e**) (in the blue spectrum) representing the B and D blocks, respectively. Molecular weight (M_n) was calculated *via* peak comparison analysis. A summary of the percentage of target DP achieved and composition of each triblock copolymer is detailed in Table 4.2, highlighting the polymer block (Q, B or D) that is of highest relative proportion in each triblock copolymer. A schematic representation of each triblock copolymer is shown in Figure 4.4.

Table 4.2. Summary of the triblock copolymer characterisation, including molecular weight (M_n), conversion (% of target DP) and percentage of each monomer block (by number of units) with respect to the whole polymer, as determined through ^{1}H NMR spectroscopy (400 MHz). The numbers associated with each letter of the triblock copolymer name is related to the degree of polymerisation of each polymer block. For example, Q_{100}-*b*-B_{17}-*b*-D_{212} indicates that a PQDMAEMA block of DP = 100 is connected to a DP = 17 P*t*BAA block and a DP = 212 PDMAm block. The bold % values indicate the highest proportion of that particular polymer block within the series of amphiphilic triblock copolymers synthesised in this work.

Triblock copolymer code	M_n / kDa	Q-block % of target DP	B-block % of target DP	D-block % of target DP	% Q	% B	% D
Q_{100}-*b*-B_{17}-*b*-D_{212}	44.1	80	64	85	30	5	**64**
Q_{100}-*b*-B_{25}-*b*-D_{55}	29.7	80	50	22	**56**	14	31
Q_{100}-*b*-B_{44}-*b*-D_{99}	36.5	80	44	40	41	**18**	41

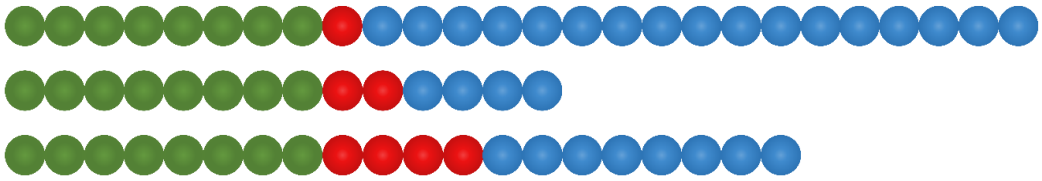

Figure 4.4. Schematic to illustrate the relative proportions of each polymer block with respect to the other triblock copolymers in the series. The top triblock copolymer represents Q_{100}-*b*-B_{17}-*b*-D_{212}, the middle polymer represents Q_{100}-*b*-B_{25}-*b*-D_{55}, and the bottom triblock copolymer represents Q_{100}-*b*-B_{44}-*b*-D_{99}.

4.4.2 Characterisation of triblock copolymers

Following RAFT polymerisation of the final D block of the ABC triblock copolymers in 100% ethanol, purification was accomplished *via* dialysis against Milli-Q water using a MWCO < 3,500 g mol^{-1} regenerated cellulose membrane. Throughout the dialysis procedure, some precipitation was observed during the solvent-switch, as the 100% ethanol was slowly replaced

with Milli-Q water. Lyophilisation of the purified polymer resulted in a dried white-coloured powder, which could be subsequently re-dispersed in pure water with no precipitation observed. Direct mixing of the lyophilised particles into aqueous solution at desired concentration was used to assess the characteristics of the self-assembled triblock copolymers. Particle size analysis was performed *via* DLS measurement of 1 mg mL^{-1} aqueous polymer solutions (Table 4.3).

Table 4.3. Triblock copolymer characteristics (hydrodynamic radius (/ nm) and electrophoretic mobility (/ μm.cm/V.s) alongside their standard errors) when self-assembled in Milli-Q water at a concentration of 1 mg mL^{-1}.

Triblock copolymer code	Hydrodynamic radius of objects in aqueous solution (*c* = 0.1 mg mL^{-1}) / nm^1	Electrophoretic mobility / μm.cm / V.s
Q_{100}-*b*-B_{17}-*b*-D_{212}	119 ± 4	2.3 ± 0.2
Q_{100}-*b*-B_{25}-*b*-D_{55}	214 ± 10	3.5 ± 0.1
Q_{100}-*b*-B_{44}-*b*-D_{99}	154 ± 20	3.2 ± 0.1

These measurements demonstrate that the amphiphilic triblock copolymers form sustainable self-assembled objects with a defined size in aqueous solution. These can also be identified in the transmission electron micrographs presented in Figure 4.5, which suggest a large polydispersity of the self-assembled particles, particularly in the case of the Q_{100}-*b*-B_{25}-*b*-D_{55} triblock copolymer.

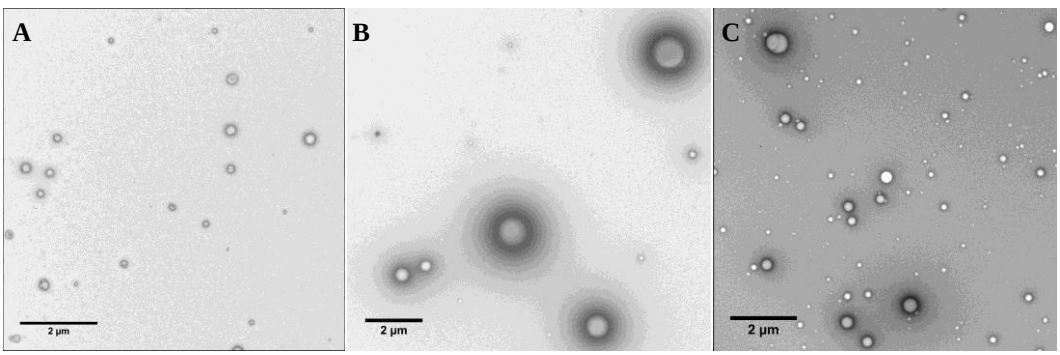

Figure 4.5. TEM micrographs of triblock copolymers, self-assembled in Milli-Q water at 10 mg mL^{-1}. (A) Q_{100}-*b*-B_{17}-*b*-D_{212}, (B) Q_{100}-*b*-B_{25}-*b*-D_{55} and (C) Q_{100}-*b*-B_{44}-*b*-D_{99}.

The average radii (as measured by DLS and TEM) of the self-assembled triblock copolymer structures varies across the series of polymers as follows: $Q_{56}B_{14}D_{31}$ > $Q_{41}B_{18}D_{41}$ > $Q_{30}B_5D_{64}$. The subscript numbers indicating the percentage of each monomer block (by number of units) with respect to the whole polymer. The same order is followed with respect to polydispersity. The triblock copolymer with the greatest relative proportion of hydrophilic, non-ionic D polymer block (Q_{100}-*b*-B_{17}-*b*-D_{212}, with 64% D) forms the smallest size structures, with the least polydispersity (as measured by DLS and visually by TEM, Figure 4.5A). The Q_{100}-*b*-B_{25}-*b*-D_{55} triblock copolymer (with 31% D-block), on the other hand, resulted in the formation of the largest polymeric objects with an average apparent radius of > 200 nm, as measured by DLS. These particles appeared to be the most polydisperse in size when investigated by TEM, with some large objects present with radii ~ 500 nm, Figure 4.5B. Similar results have been reported in literature, with the incorporation of longer hydrophilic, neutral blocks into triblock copolymers inducing the formation of smaller self-assembled objects.[310]

Measuring the electrophoretic mobility of the self-assembled triblock copolymers revealed a positive surface charge in all cases; however, the Q_{100}-*b*-B_{17}-*b*-D_{212} particles had a lower electrophoretic mobility. This is likely due to a dampened positive surface charge as a result of the hydrophilic, neutral block shielding charge on the surface of the self-assembled objects.[310]

4.4.3 Complexation of triblock copolymers with dsRNA

Amphiphilic triblock copolymers can be used as delivery vehicles for genetic material such as double-stranded RNA (dsRNA). The Q-*b*-B-*b*-D triblock copolymers synthesised in this work contain a hydrophilic and positively charged polymer block, Q, which can electrostatically interact with the anionic phosphodiester backbone of the dsRNA. The interaction is entropically favourable due to the release of counterions, and leads to the formation of polyplexes.[262,313]

A common tool used to interpret the strength of dsRNA binding by polycations is the quenching of ethidium bromide (EB) fluorescence.[238,240–245] The relative amount of quenching can be used as a measure of binding strength of the polycation to the genetic material. This method was used in the previous chapter to characterise the complexation of dsRNA with homopolymer/diblock copolymers and is described in detail in Section 2.3.4.

For all three triblock copolymers, as the N/P ratio is increased from 0 (signifying no triblock copolymer added to the dsRNA-EB) to 1 (equal proportion of ammonium to phosphate groups) in Figure 4.6, the fluorescence intensity drastically decreases to 50 – 65%. As the N/P ratio is further increased to 2 – 3, the normalised fluorescence intensity decreases to a plateau (25 – 35%).

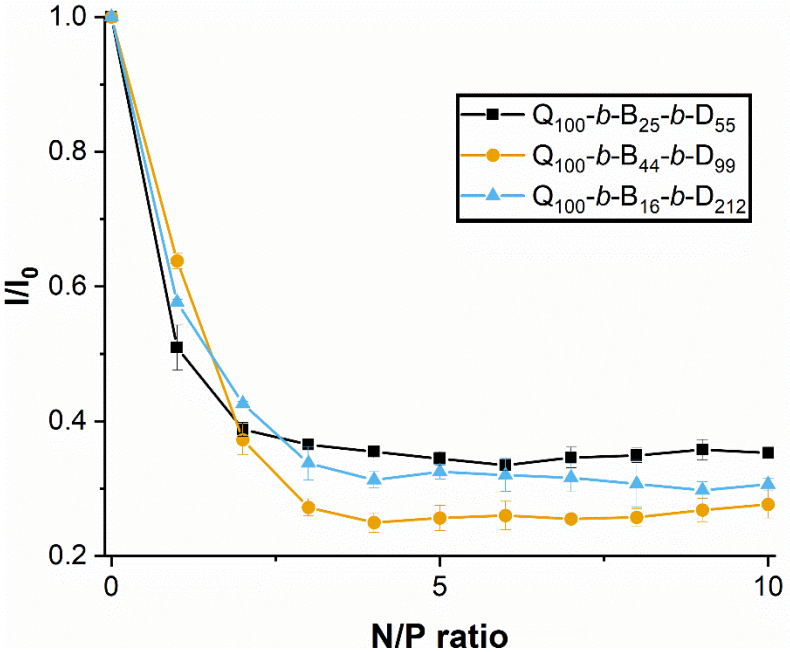

Figure 4.6. Normalised fluorescence intensity (I/I_0, where I_0 is the fluorescence intensity of dsRNA-EB complexes prior to triblock copolymer addition) of polyplexes formed between different amphiphilic triblock copolymers (Q_{100}-*b*-B_{25}-*b*-D_{55}, Q_{100}-*b*-B_{44}-*b*-D_{99} and Q_{100}-*b*-B_{17}-*b*-D_{212}) and 222 bp *vha26* dsRNA at varying N/P ratios 0 – 10. Standard deviation is shown, n = 3.

Interestingly, the Q_{100}-*b*-B_{44}-*b*-D_{99}-based polyplexes appears to quench EB fluorescence more significantly over the N/P ratio = 3 – 8, whereas Q_{100}-*b*-B_{25}-*b*-D_{55} and Q_{100}-*b*-B_{17}-*b*-D_{212}

triblock copolymers are not significantly different from one another (except at a few N/P ratios). These results suggest that a (proportionally) higher hydrophobicity of triblock copolymer may strengthen binding to dsRNA. It has been previously reported in literature that a hydrophilic, neutral block could weaken binding to pDNA. In the report, it was suggested that this is due to the strong hydrophilicity of the neutral block (PEG in this case), which induces excluded-volume interactions between the neutral block chains themselves and the pDNA molecules, which in turn weakens binding between the cationic polymer block and the pDNA chains.[289] However, in this present study it is clear that all three amphiphilic triblock copolymers indeed complex efficiently with dsRNA at N/P ratio ≥ 2, regardless of the length of the hydrophilic polymer block (D).

In addition, the results of the EB assay suggest that the binding of triblock copolymers with dsRNA is stronger in comparison to homopolymer or diblock copolymer (containing the same hydrophilic polymer blocks, Q and D) complexation with dsRNA (as described in Section 3.4.4). The fluorescence quenching of EB is greater in the case of triblock copolymer complexation with dsRNA, with approximately 40% fluorescence at the plateau for homopolymer/diblock copolymer polyplexes, in comparison to ~ 25 – 30% for triblock copolymer polyplexes.

Based on these results, we chose to focus our attention and further characterisation on the N/P ratios 1, 5 and 10 for each triblock copolymer-based polyplex, to provide a broad understanding of these systems. First we measured the hydrodynamic radii of polyplexes, formulated at these N/P ratios, using DLS (see Table 4.4).

Table 4.4. Hydrodynamic radii and standard error (/ nm), as measured by dynamic light scattering, of triblock copolymer polyplexes. Concentration of formulations was 0.1 mg mL^{-1}. * denotes that DLS was not possible due to aggregation/precipitation of the sample.

Apparent hydrodynamic radii / nm			
	N/P ratio		
Triblock copolymer code	1	5	10
Q_{100}-*b*-B_{17}-*b*-D_{212}	91 ± 2	100 ± 4	122 ± 3
Q_{100}-*b*-B_{25}-*b*-D_{55}	*	126 ± 6	160 ± 7
Q_{100}-*b*-B_{44}-*b*-D_{99}	92 ± 5	120 ± 3	134 ± 4

The Q_{100}-*b*-B_{25}-*b*-D_{55}-based polyplexes (at N/P ratio = 1) formed aggregates that were visible to the naked eye. In Chapter 3, a similar phenomenon was observed with the cationic homopolymer, Q_{110}, when electrostatically interacting with dsRNA at a charge ratio close to one (isoelectric point). This is likely due to electro-neutralisation and thus precipitation of the formed complexes.[312] In the case of the Q_{100}-*b*-B_{25}-*b*-D_{55} triblock copolymer, the neutral D block is not long enough to counteract the hydrophobicity introduced by the B block and electro-neutralisation of the Q block upon mixing with the polyanion, dsRNA. Despite the longer hydrophobic B block in the Q_{100}-*b*-B_{44}-*b*-D_{99} polymer, the relative length of the D block appears to be sufficient to stabilise the complexes formed with dsRNA at an N/P ratio = 1. These results indicate that the length (DP) of the neutral, hydrophilic block is critical for the stabilisation of dsRNA-based complexes near the isoelectric point, and, in the case of this polymer block combination, must make up a relative proportion ≥ 31%.

As the N/P ratio is increased from 1 to 10, the average hydrodynamic radii of the polyplexes increases. In comparison to the triblock copolymer structures when self-assembled in aqueous solution (without complexation of dsRNA), the polyplexes measured by DLS are smaller. This suggests that significant chain rearrangement of the initially self-assembled triblock copolymers occurs during the complexation process with dsRNA. This chain rearrangement

is confirmed through TEM (Figure 4.7 and Figure 4.8), which identifies significantly altered structures in comparison to the micellar aggregates observed of the triblock copolymers alone in aqueous solution (Figure 4.5). The self-assembled triblock copolymer structures, as seen in Figure 4.5, are therefore not robust. Following combination with dsRNA the structures easily breakdown to form alternative structures, similar to those found of the diblock copolymer-based polyplexes in Section **Error! Reference source not found.**.

Figure 4.7. Representative TEM images obtained for the three triblock copolymers when complexed with dsRNA (A) Q_{100}-b-B_{17}-b-D_{212}, (B) Q_{100}-b-B_{25}-b-D_{55} and (C) Q_{100}-b-B_{44}-b-D_{99} at N/P ratio = 2. Solutions were formulated at 1 mg mL^{-1}, with 5 μL deposited onto 400-mesh carbon-coated copper grids. Grids were then washed with Milli-Q water and stained with 1% uranyl acetate.

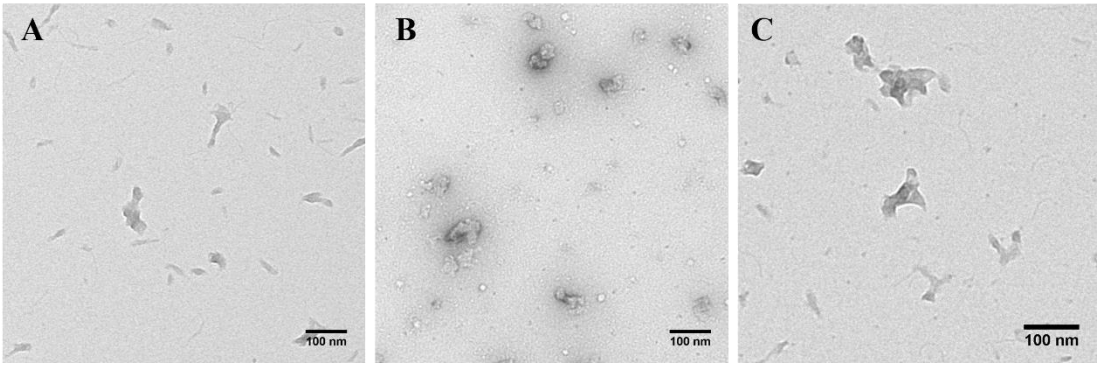

Figure 4.8. Representative TEM images (at higher magnification) obtained for the three triblock copolymers when complexed with dsRNA (A) Q_{100}-b-B_{17}-b-D_{212}, (B) Q_{100}-b-B_{25}-b-D_{55} and (C) Q_{100}-b-B_{44}-b-D_{99}, at N/P ratio = 2. Solutions were formulated at 1 mg mL^{-1}, with 5 μL deposited onto 400-mesh carbon-coated copper grids. Grids were then washed with Milli-Q water and stained with 1% uranyl acetate.

The radius of gyration (R_g) of the polyplexes was measured through static light scattering, determined using cumulant analysis (Guinier plots shown in Figure A9). The radii of gyration present a different picture to that given by the hydrodynamic radii, Table 4.5. At an N/P ratio of 10, the Q_{100}-*b*-B_{25}-*b*-D_{55}-based polyplexes have the largest size, followed by the Q_{100}-*b*-B_{44}-*b*-D_{99} and Q_{100}-*b*-B_{17}-*b*-D_{212} polyplexes. In the case of the polyplexes prepared with triblock copolymers with longer B polymer blocks (Q_{100}-*b*-B_{25}-*b*-D_{55} and Q_{100}-*b*-B_{44}-*b*-D_{99}), the radius of gyration increases as N/P ratio increases, similarly to the hydrodynamic radii (Table 4.4).

Table 4.5. Radii of gyration of triblock copolymer polyplexes (/ nm), as measured by static light scattering. Concentration of formulations was 0.1 mg mL^{-1}. * denotes that DLS was not possible due to aggregation/precipitation of the sample.

Radii of gyration / nm			
	N/P ratio		
Triblock copolymer code	1	5	10
Q_{100}-*b*-B_{17}-*b*-D_{212}	177	158	141
Q_{100}-*b*-B_{25}-*b*-D_{55}	*	180	198
Q_{100}-*b*-B_{44}-*b*-D_{99}	125	146	164

However, the most hydrophilic triblock copolymer (Q_{100}-*b*-B_{17}-*b*-D_{212}) has a decreasing radius of gyration as N/P ratio is increased. This can be interpreted by considering the ρ (R_g/R_H) values that describe the shape of the objects in the system (Table 4.6). In all three triblock copolymer-based polyplexes, the ρ value decreases towards one as N/P ratio increases to 10, suggesting that the objects measured become more 'spherical' with increasing N/P ratio.

Table 4.6. ρ (R_g/R_H), of triblock copolymer polyplexes, as measured by static light scattering. Concentration of formulations was 0.1 mg mL^{-1}. * denotes that DLS was not possible due to aggregation/precipitation of the sample.

ρ (R_g/R_H) values			
	N/P ratio		
Triblock copolymer code	1	5	10
Q_{100}-*b*-B_{17}-*b*-D_{212}	1.90	1.58	1.16
Q_{100}-*b*-B_{25}-*b*-D_{55}	*	1.43	1.24
Q_{100}-*b*-B_{44}-*b*-D_{99}	1.36	1.21	1.22

The Q_{100}-*b*-B_{17}-*b*-D_{212}-based polyplexes at an N/P ratio = 1, however, have a very large ρ value, indicative of a more rod-like morphology. This could explain the large radius of gyration measured at lower N/P ratios for these polyplexes formed with Q_{100}-*b*-B_{17}-*b*-D_{212}, as light scattering analysis assumes spherical morphologies. These results are corroborated by TEM imaging (conducted at an N/P ratio = 2) that visually shows the more 'spherical'-like shape of the Q_{100}-*b*-B_{25}-*b*-D_{55}-based polyplexes in comparison to the polyplexes formed with the triblock copolymer containing a longer neutral, stabilising block, which appears to have less 'spherical', defined shapes.

Further study of the detailed morphologies of the complexes formed between the triblock copolymers and dsRNA is required and future work should focus on additional transmission electron microscopy and small-angle X-ray/neutron scattering to elucidate their in-depth structure. Initial steps to perform these experiments were taken, but due to time limitations we were not able to fully investigate.

As N/P ratio is increased from 1 – 10, the polyplexes undergo a negative to positive charge inversion, as shown in Figure 4.9.

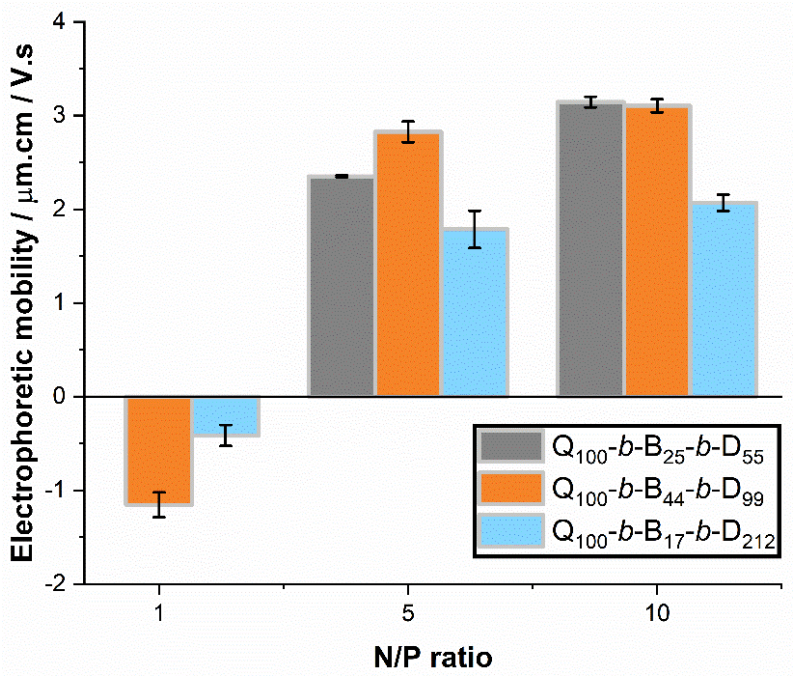

Figure 4.9. Electrophoretic mobility of polyplexes, at N/P ratio 1, 5 and 10. Triblock copolymer solutions were kept at constant concentration (0.1 mg mL^{-1}), with dsRNA concentration varied to alter the N/P ratio. Formulations were prepared at least 24 h prior to measurements, which were taken at 25 ± 0.5 °C. Standard deviation is shown, n = 3.

At an N/P ratio = 1, Q_{100}-*b*-B_{44}-*b*-D_{99} and Q_{100}-*b*-B_{17}-*b*-D_{212}-based polyplexes have electrophoretic mobility's that are close to 0 or slightly negative. As N/P ratio is increased to 5 and 10, Q_{100}-*b*-B_{44}-*b*-D_{99} and Q_{100}-*b*-B_{17}-*b*-D_{212}-based polyplexes have positive electrophoretic mobility that is not significantly different over this N/P ratio range. However, Q_{100}-*b*-B_{25}-*b*-D_{55}-based polyplexes show a slight increase in electrophoretic mobility between N/P ratio 5 and 10. The N/P ratio at which an electrophoretic mobility plateau occurs corresponds to 'full' complexation, i.e. the minimum concentration of polymer able to complex all dsRNA chains present in solution. These results suggest that Q_{100}-*b*-B_{25}-*b*-D_{55} polyplexes may require higher N/P ratios for full complexation, however with limited data one cannot draw significant conclusions, particularly as EB exclusion (Figure 4.6) confirmed that an N/P ratio = 2 was satisfactory for full complexation.

Q_{100}-*b*-B_{17}-*b*-D_{212}-based polyplexes, similarly to their un-complexed form, have a dampened surface charge in comparison to Q_{100}-*b*-B_{25}-*b*-D_{55} and Q_{100}-*b*-B_{44}-*b*-D_{99} polyplexes, likely due to shielding of charge by the hydrophilic, non-ionic D polymer block.[251,309,310]

4.4.4 **Protection of dsRNA against enzymatic degradation**

Following characterisation of the complexation between the amphiphilic triblock copolymers with dsRNA, the protection afforded to the complexed dsRNA was tested using the synthetic enzyme, RNase A. As a biomolecule, RNA is inherently unstable and susceptible to degradation in the environment or upon application in agrochemical settings.[60,64] Thus, to ensure successful delivery and to minimise loss of dsRNA during the delivery process, the dsRNA must be suitably protected to prevent enzymatic degradation.

In the case of all three triblock copolymer polyplexes, an N/P ratio ≥ 2 was required (as demonstrated by EB exclusion assay, Figure 4.6) for full complexation. This is further confirmed by the retardation of dsRNA-EB fluorescence in agarose gel electrophoresis at N/P ratio ≥ 2 (shown in Figure 4.10, Figure 4.11, and Figure 4.12, lanes 13, 14 and 14, respectively). Prior to an N/P ratio = 2, smearing is observed down the gel lane, indicating only a partial complexation with remaining free dsRNA able to migrate down the gel lane.

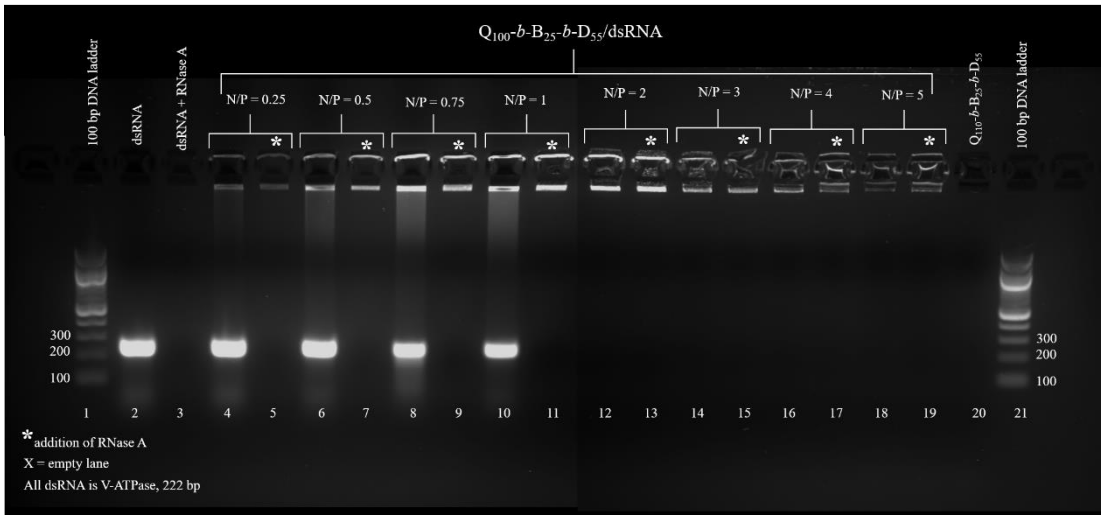

Figure 4.10. Agarose gel electrophoresis of Q_{100}-b-B_{25}-b-D_{55}/dsRNA polyplexes at N/P ratio = 0.25, 0.5, 0.75, 1, 2, 3, 4 and 5. DsRNA (1 µg, lanes 2 and 3) and the polyplexes were incubated with (indicated by *) and without the presence of RNase A enzyme. 100 bp DNA ladder was used in lanes 1 and 21, and Q_{100}-b-B_{25}-b-D_{55} alone was added to lane 20.

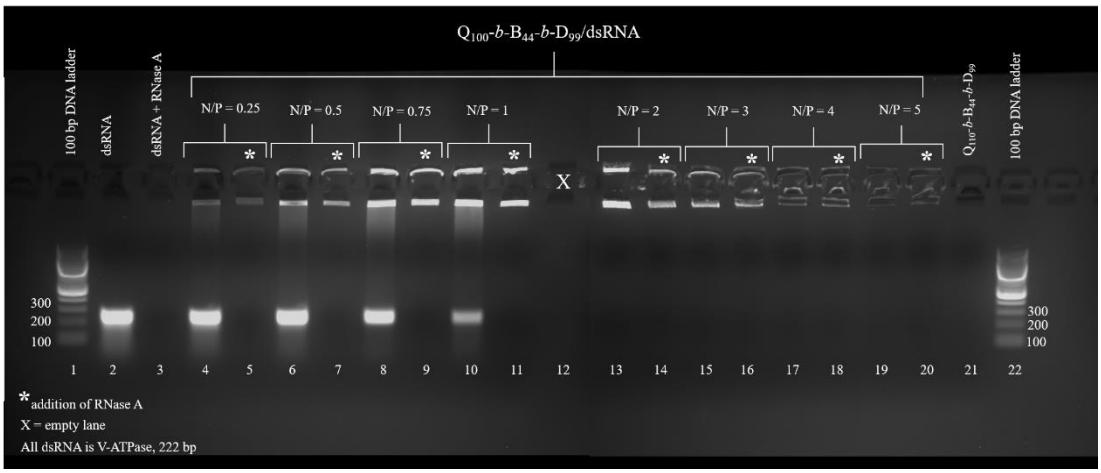

Figure 4.11. Agarose gel electrophoresis of Q_{100}-b-B_{44}-b-D_{99}/dsRNA polyplexes at N/P ratio = 0.25, 0.5, 0.75, 1, 2, 3, 4 and 5. DsRNA (1 µg, lanes 2 and 3) and the polyplexes were incubated with (indicated by *) and without the presence of RNase A enzyme. 100 bp DNA ladder was used in lanes 1 and 22, and Q_{100}-b-B_{44}-b-D_{99} alone was added to lane 21.

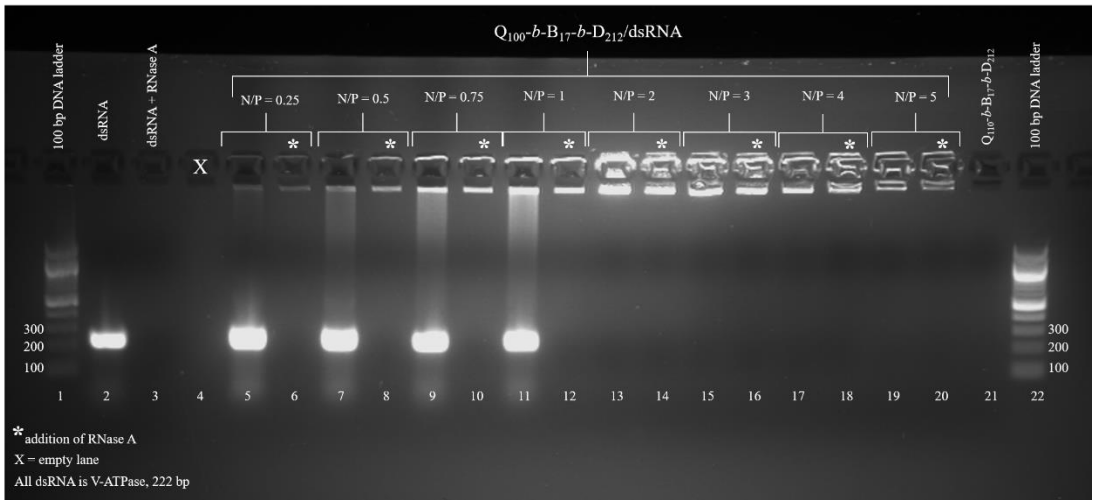

Figure 4.12. Agarose gel electrophoresis of Q_{100}-b-B_{17}-b-D_{212}/dsRNA polyplexes at N/P ratio = 0.25, 0.5, 0.75, 1, 2, 3, 4 and 5. DsRNA (1 μg, lanes 2 and 3) and the polyplexes were incubated with (indicated by *) and without the presence of RNase A enzyme. 100 bp DNA ladder was used in lanes 1 and 22, and Q_{100}-b-B_{17}-b-D_{212} alone was added to lane 21.

The fluorescence intensity (normalised with respect to dsRNA alone), of the free dsRNA that migrated through the gel, is shown in Figure 4.13, as a more quantitative comparison of complexation from the agarose gel images.

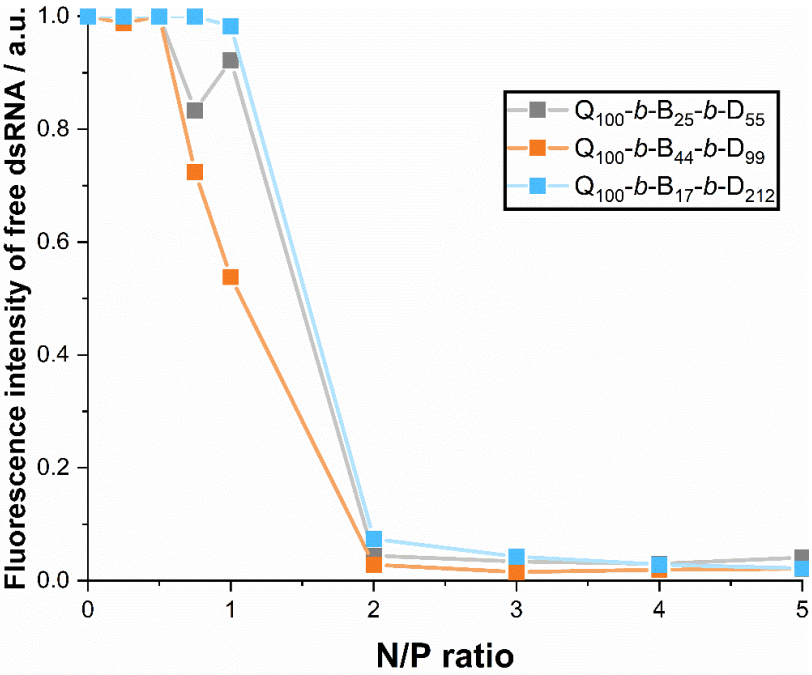

Figure 4.13. Proportion of free dsRNA that has migrated down the gel lane, when complexed with each triblock copolymer, as determined *via* agarose gel electrophoresis fluorescence intensity (Figure 4.10, Figure 4.11 and Figure 4.12). Data were normalised against naked dsRNA fluorescence and calculations were run using ImageJ.

The intensity of free dsRNA was measured *via* ImageJ analysis of the gel images at the corresponding ~ 200 bp location of the gel lane. The sharp decrease in the amount of free dsRNA at N/P ratio = 2 in Figure 4.13 further demonstrates that an N/P ratio ≥ 2 is required for full complexation. There is a decrease in free dsRNA at N/P ratios = 0.75 and 1, particularly in the case of Q_{100}-*b*-B_{44}-*b*-D_{99}-based polyplexes. This complements EB exclusion data (Figure 4.6) that suggests a stronger binding between Q_{100}-*b*-B_{44}-*b*-D_{99} and dsRNA in comparison to the other triblock copolymers in the series.

Similar to both the homopolymer and diblock copolymer polyplexes, when each triblock copolymer was complexed with dsRNA, the proportion of dsRNA that was complexed appeared to remain intact following incubation with RNase A. This is shown by the maintenance of fluorescence intensity in the well of the gel lane. When dsRNA was not

complexed with triblock copolymer (e.g. migrated down the gel lane), it was fully degraded by RNase A, as illustrated by the complete absence of fluorescence.

The protection of dsRNA against degradation by RNase A over time was assessed using fluorescence spectroscopy. Likewise to the homopolymer and diblock copolymer polyplexes in Section 3.4.6, Figure 4.14 shows the quenching of EB fluorescence through the complexation of triblock copolymers with dsRNA.

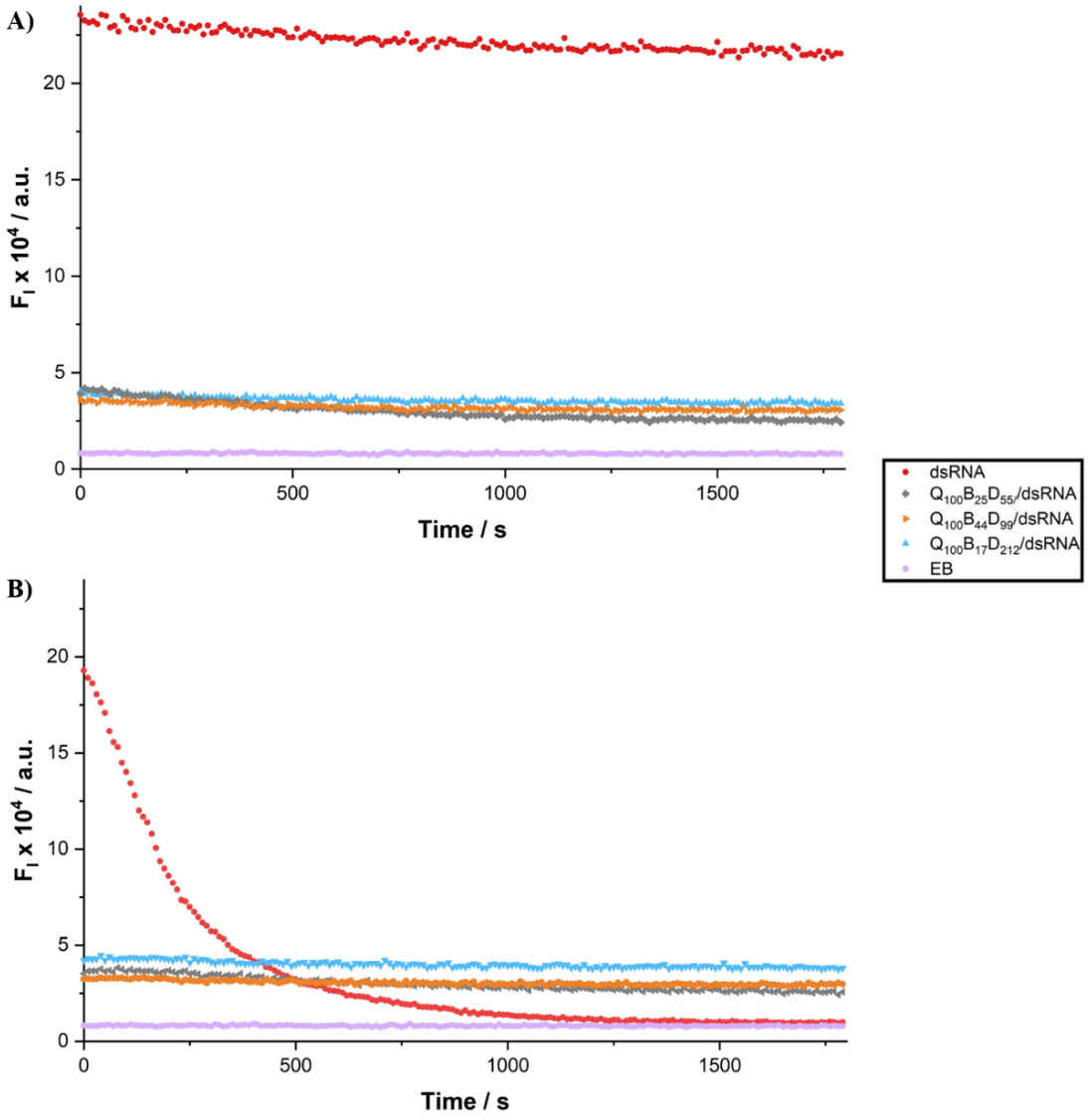

Figure 4.14. Time-resolved fluorescence spectroscopy of dsRNA (red), Q_{100}-*b*-B_{25}-*b*-D_{55}/dsRNA polyplex (grey), Q_{100}-*b*-B_{44}-*b*-D_{99}/dsRNA polyplex (orange) and Q_{100}-*b*-B_{17}-*b*-D_{212}/dsRNA polyplex (blue) without (A) and with (B) the addition of RNase A. Polyplexes were left for 1.5 h to equilibrate. Low fluorescence intensity of polyplexes is due to quenching of EB fluorescence after displacement from dsRNA intercalation.

Whilst naked dsRNA (shown in red) exhibits a strong fluorescence in the absence of RNase A (A), this fluorescence is rapidly extinguished within 5 – 15 min after the addition of RNase A (B) as the dsRNA is fully degraded. It is noted that there is a subtle decrease in fluorescence of the Q_{100}-*b*-B_{25}-*b*-D_{55}/dsRNA polyplexes over time, but this is observed in both the presence and absence of RNase A, and could be due to chain rearrangement within the system, or it

could be within experimental error as the decrease is minimal. The level of fluorescence of the triblock copolymer/dsRNA polyplexes is maintained regardless of the presence (B) or absence (A) of the synthetic RNase A enzyme. Thus, we can conclude that the dsRNA is protected against enzymatic degradation.

4.4.5 Impact of salt concentration on polyplex stability

In addition to investigating the protection of dsRNA against enzymatic degradation by RNase A, it was important to consider the impact of bulk salt concentration on the stability of the polyplexes, as formulations for both therapeutic and agrochemical applications typically contain electrolytes as part of a buffer solution, or adjuvants to aid application. Here, NaCl is used as a simple model salt to increase the ionic strength of the aqueous bulk in which the complexes are dispersed, and the resulting changes in hydrodynamic radii are measured *via* DLS.

Despite the stronger binding between Q_{100}-*b*-B_{44}-*b*-D_{99} and dsRNA in salt-free, aqueous environments, the resulting polyplexes appear to be the least stable as NaCl concentration (C_{NaCl}) increases, as shown in Figure 4.15.

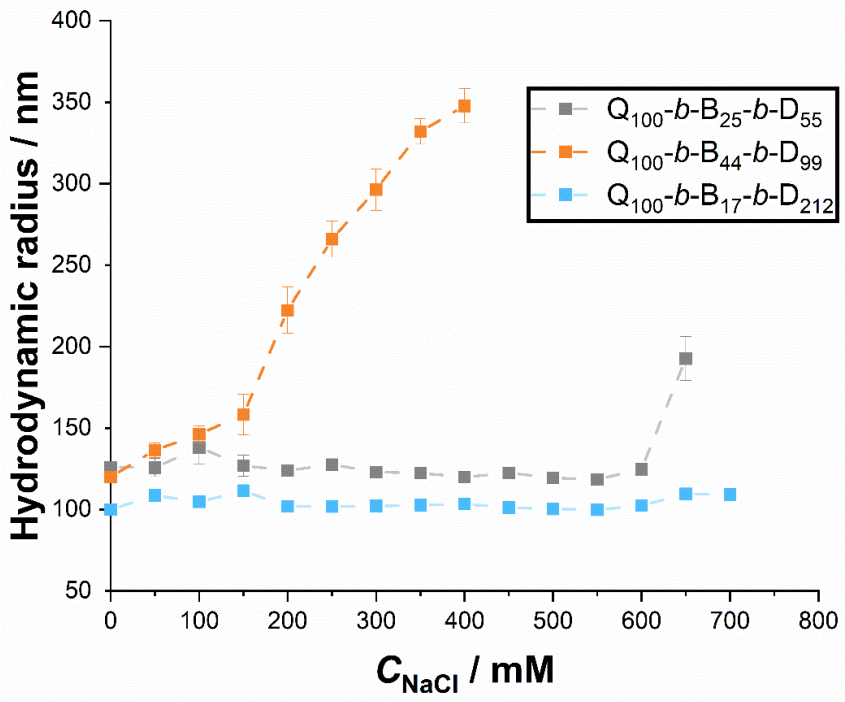

Figure 4.15. Apparent hydrodynamic radii of polyplexes formed between dsRNA and each triblock copolymer, formulated at an N/P ratio = 5, measured with DLS, as NaCl concentration is increased from 0 to 700 mM.

Above C_{NaCl} = 150 mM, the apparent average hydrodynamic radius of the Q_{100}-*b*-B_{44}-*b*-D_{99}-based polyeplexes steadily increases, suggesting that charge screening from the increased ionic strength of the solution is causing aggregation between the polyplexes.

Q_{100}-*b*-B_{25}-*b*-D_{55} and Q_{100}-*b*-B_{17}-*b*-D_{212}-based polyplexes, however, remain stable, maintaining a consistent hydrodynamic radius until C_{NaCl} = 650 – 700 mM. In comparison to the results presented in Chapter 3 (Section 3.4.5) on the salt stability of homopolymer and diblock copolymer-based polyplexes, the two triblock copolymers with the highest proportion of hydrophilic polymer blocks (Q or D, respectively) are stable over a greater NaCl concentration range.[312] Sharma *et al.* investigated a PEG_{113}-*b*-P*n*BA_{100}-*b*-$PDMAEMA_{128}$ triblock copolymer in comparison to a PEG_{113}-*b*-$PDMAEMA_{142}$ diblock copolymer and a $PDMAEMA_{127}$ homopolymer. They found, similarly to the results presented here, that the amphiphilic triblock copolymer-based polyplexes stabilised pDNA more efficiently than the

diblock copolymer or homopolymer polyplexes. They also discovered that the triblock copolymer more effectively protected the pDNA against degradation by DNase enzymes.[289]

Sharma *et al.* demonstrate the resistance of their ABC triblock copolymer-based complexes with pDNA, to aggregation in salt over a period of 1 h. However, a salt concentration of 150 mM only is examined.[289] Whilst this may be suitable for some therapeutic applications (for example, mammalian Na^+ and Cl^- extracellular concentrations reach 145 mM and 116 mM, respectively[314,315]), demonstrating stability at higher salt concentration (as is shown here) is valuable for assessing such formulations that might be required for commercial products, particularly in the agrochemical industry that requires the addition of adjuvants to product formulations.

4.4.6 Impact of dsRNA length on polyplex size and stability

As described in Section 3.4.7, it is important to investigate the impact of changing dsRNA length (number of base pairs) on the resulting complexes, as there are many different mRNA transcripts that can be targeted for a single pest insect species, which require dsRNAs of different lengths to trigger RNAi. It is likely that different polymer designs will be required for varying dsRNA lengths, however versatility is desirable and the ability of the triblock copolymers to complex with different dsRNA lengths is thus assessed here. The apparent hydrodynamic radii of polyplexes formed (at N/P ratio = 5) with *in vitro* transcription (IVT) dsRNAs (short and long GFP and ‘active target’ dsRNA) have been measured, and are compared in Figure 4.16.

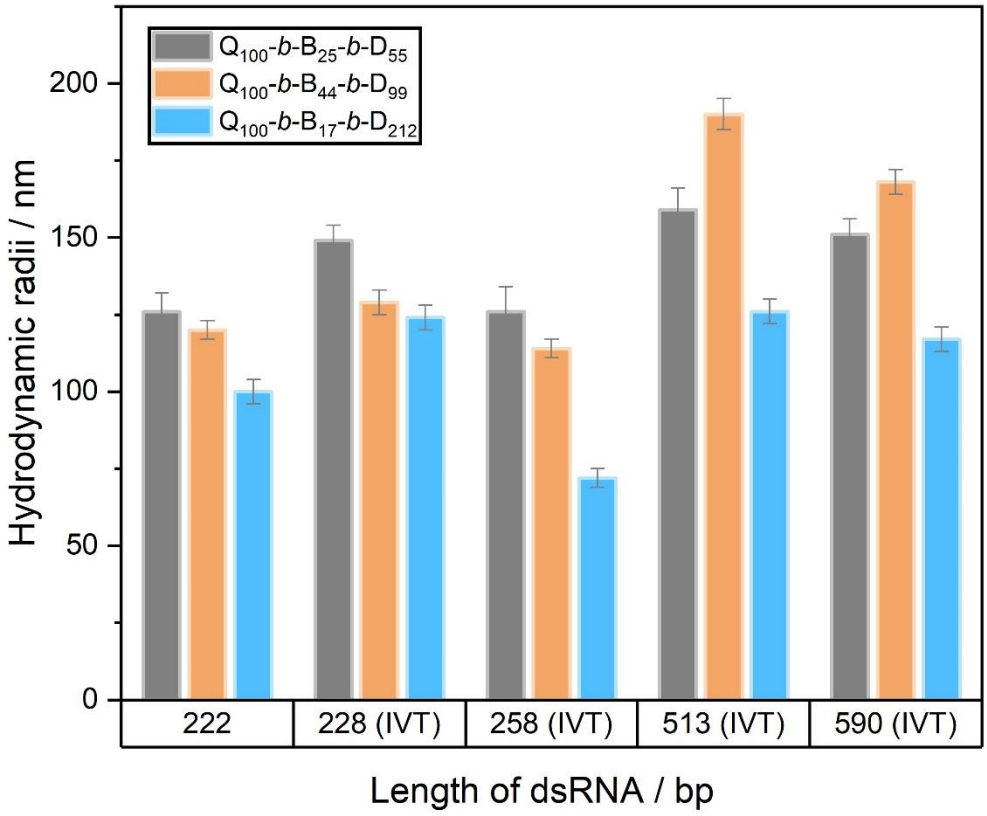

Figure 4.16. A visual comparison of the difference in hydrodynamic radii (/ nm) of polyplexes formed between the series of triblock copolymers prepared in this work, and dsRNAs of varying base pair numbers (i.e. length) at an N/P ratio = 5.

The data show similar patterns across the range of dsRNAs when complexed with each triblock copolymer. The most compact polyplexes, as measured by DLS, were those formed with the Q_{100}-*b*-B_{17}-*b*-D_{212} polymer, the most hydrophilic triblock copolymer of the series. This trend is similar to the pattern found of the homopolymer/diblock copolymer polyplexes described in Chapter 3, in which the diblock copolymer with the longest hydrophilic, neutral block (Q_{110}-*b*-D_{219}) formed the most compact polyplexes (49 – 85 nm across the spectrum of dsRNAs).

Triblock copolymer/dsRNA polyplexes appear to be somewhat influenced by dsRNA length, with the shorter (~200 bp), more rigid dsRNAs resulting in the formation of polyplexes with smaller apparent hydrodynamic radii than polyplexes formed with the longer (~500 bp), more flexible dsRNAs. This trend is repeated across polyplexes formed with all three triblock copolymers of the series. A similar pattern was observed in a study by Jiang *et al*., in which

the authors used an AB diblock copolymer (*hydrophilic-hydrophobic*, PDMAEMA$_{27}$-*b*-poly(*n*-butyl methacrylate) (P*n*BMA)$_{14}$) micelle to complex with linear and plasmid DNA (lDNA and pDNA, respectively) of different lengths. The authors found that increasing the length of both lDNA and pDNA induced the formation of larger complexes, when formulated at N/P ratio > 1. They suggest that this is due to increased bridging between the complexes, and the formation of multiple-complex particles. Jiang *et al.* also discovered that longer DNA molecules enhance the stability of complexes close to the isoelectric point, due to the additional steric repulsions from the longer chains/loops.[258,259,298]

The three shorter (~200 bp) dsRNAs, when complexed with Q$_{100}$-*b*-B$_{25}$-*b*-D$_{55}$ (forming the most hydrophobic polyplexes after complexation), formed the largest polyplexes. This was followed by Q$_{100}$-*b*-B$_{44}$-*b*-D$_{99}$, and then the smallest (most compact) polyplexes were formed with the most hydrophilic triblock copolymer (Q$_{100}$-*b*-B$_{17}$-*b*-D$_{212}$). However, the trend is altered when longer dsRNAs are used; the Q$_{100}$-*b*-B$_{44}$-*b*-D$_{99}$ triblock copolymer (the triblock copolymer with the longest hydrophobic B block) forms the largest polyplexes.

The polydispersity, Figure 4.17, of each polyplex system was measured by DLS (at a 90° angle), and calculated through cumulant analysis as described in Section 2.2.1.3. In all triblock copolymer-based polyplex samples, the polydispersity remained consistently between 0.10 and 0.25.

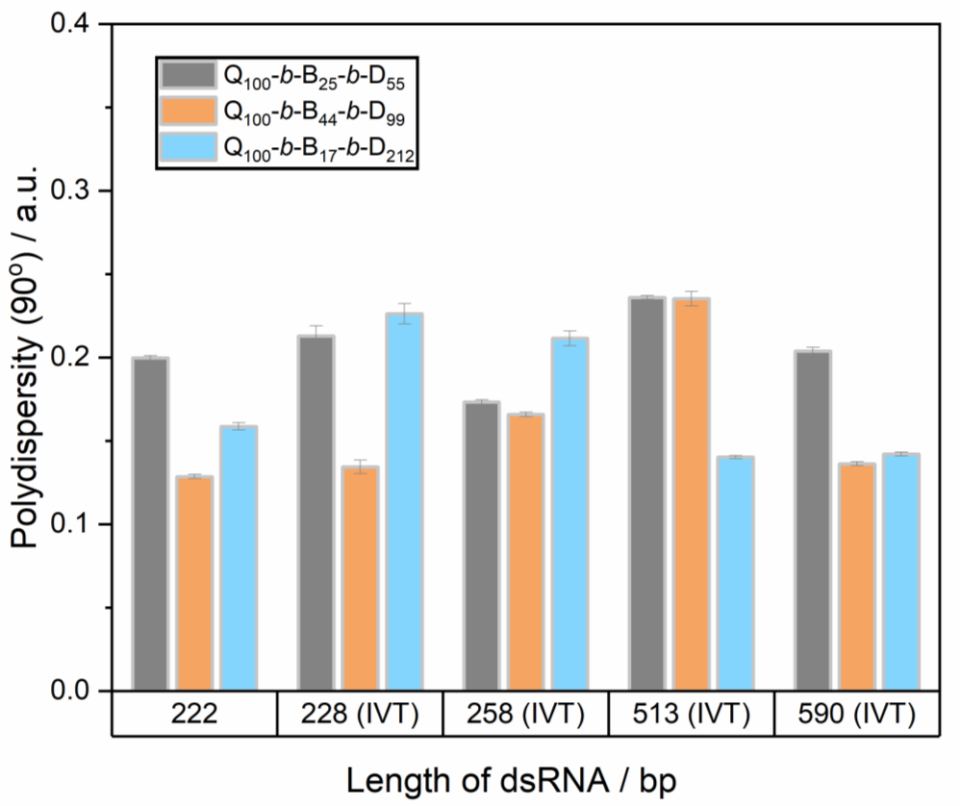

Figure 4.17. A visual comparison of the difference in polydispersity, by DLS measurement performed at 90°, of polyplexes formed between triblock copolymers and dsRNAs of varying base pair numbers (i.e. length) at an N/P ratio = 5.

Polydispersity of the polyplexes was generally much lower than the values of polydispersity calculated for homopolymer/diblock copolymer polyplexes formed with the IVT dsRNAs (except in the case of Q_{110}-*b*-D_{219}-based polyplexes). This suggests that triblock copolymer-based polyplexes with dsRNA tend to be more stable against aggregation and have more consistent sizing across a range of dsRNA lengths, in comparison to homopolymer or diblock copolymer-based polyplexes (particularly when compared to complexes formed with diblock copolymers with shorter neutral block lengths). This general result complements data in the previous section on the stability of the polyplexes in increasing salt concentrations (Section 4.4.5), where the triblock copolymer-based polyplexes showed greater stability at higher NaCl concentrations, in comparison to homopolymer and diblock copolymer polyplexes. The triblock copolymers may provide greater stability to the resulting complexes with dsRNA due to the presence of an anchoring hydrophobic polymer block, which induces self-assembling

properties. Whilst chain rearrangement occurs upon complexation with dsRNA, the design of the triblock copolymers to incorporate a hydrophobic polymer block has achieved the aim of providing additional support, shown by the enhanced stability of the resulting complexes.

4.4.7 **Comparison to homopolymer and diblock copolymers**

Comparing the complexation of the linear ABC amphiphilic triblock copolymers to the complexation of hydrophilic 'A' homopolymer and 'AC' diblock copolymers with *vha26* dsRNA, a similar pattern was observed. The agarose gel electrophoresis assays are combined in Figure 4.18, to show a comparison of the partial/full complexation of polymers with dsRNA, and their protection/degradation in the presence or absence of RNase A.[312]

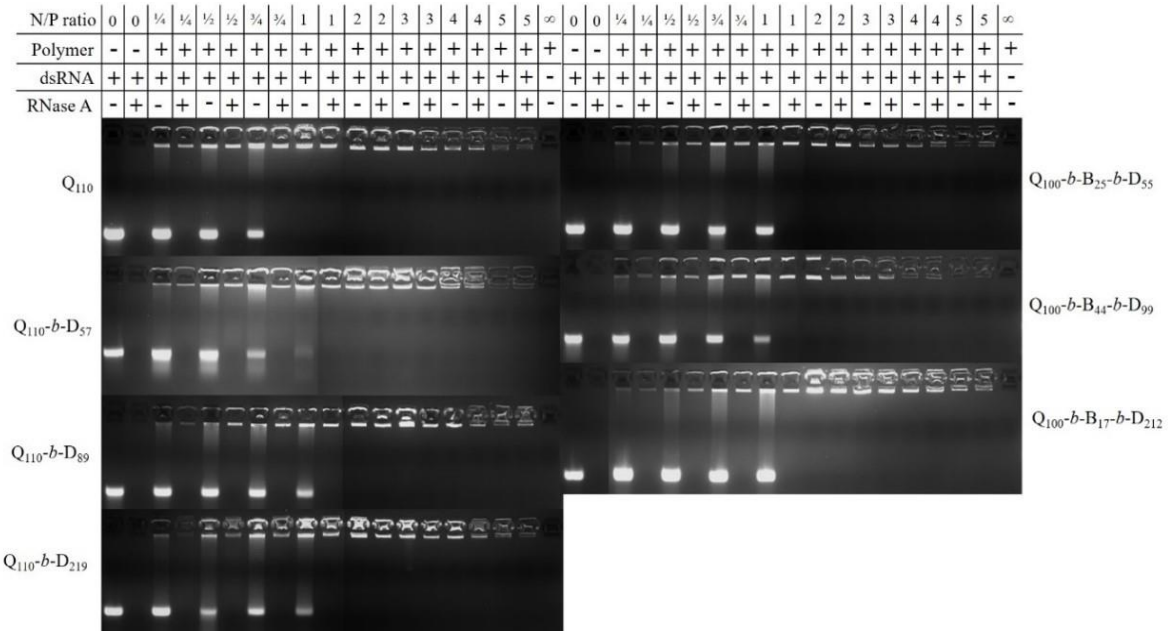

Figure 4.18. Comparison of the complexation and protection provided to *vha26* dsRNA by Q_{110}, Q_{110}-*b*-D_{57}, Q_{110}-*b*-D_{89}, Q_{110}-*b*-D_{219}, Q_{110}-*b*-B_{25}-*b*-D_{55}, Q_{110}-*b*-B_{44}-*b*-D_{99}, or Q_{110}-*b*-B_{17}-*b*-D_{212}, at N/P ratios = 0 (naked dsRNA), ¼, ½, 1, 2, 3, 4, 5 and ∞ (polymer alone), against degradation by RNase A. Presence or absence of polymer, dsRNA or RNase A is indicated by + (present) and – (absent) symbols.

An N/P ratio = 1 was only sufficient to provide 'full' retardation of dsRNA by the Q_{110} homopolymer, however, full complexation was achieved at an N/P ratio ≥ 2 for all remaining polymers. This phenomenon appears to be common throughout literature, where an N/P ratio

of 2 is often found to correspond to efficient binding of the nucleic acid to polycations.[116,316–319] However, the exact N/P ratio value can sometimes fluctuate depending on the specific polymer design/composition; for example, Li *et al.* found that a higher N/P ratio of 5 was required for their AC diblock copolymers (poly(2-deoxy-2-methacrylamido glucopyranose)-*b*-poly(methacrylate amine)) with secondary amine derivatives, in comparison to similar AC diblock copolymers with either primary or quaternary amine groups.[320]

The hydrodynamic radii of polyplexes formed between the homopolymer/diblock copolymers and *vha26* dsRNA ranged from 57 – 125 nm, and showed no significant variability in size across an N/P ratio range of 1 – 10. In comparison, whilst the triblock copolymer/dsRNA complexes exhibited similar hydrodynamic radii to the homopolymer/diblock copolymer-based polyplexes, they indeed showed variation in size with changing N/P ratio, with an increase in hydrodynamic radii as N/P ratio was increased.

As expected, the homopolymer/diblock copolymers did not exhibit self-assembly prior to the addition of dsRNA, whereas the triblock copolymers showed self-assembly in aqueous solution. However, the similarity in size of homopolymer or diblock copolymer/dsRNA polyplexes and triblock copolymer/dsRNA polyplexes suggests that the triblock copolymers undergo substantial chain rearrangement in order to complex with dsRNA. This is corroborated by TEM imaging that indicates the breakdown of the self-assembled micellar structures observed of the triblock copolymers (when formulated alone in aqueous solution), when complexed with dsRNA.

The benefit of designing amphiphilic triblock copolymers for the complexation and protection of dsRNA can only be observed when considering the stability of these complexes against increased NaCl concentration (increased ionic strength), and when complexing with a variety of dsRNA lengths for alternative mRNA transcript targets. The more hydrophilic triblock copolymer-based polyplexes showed increased stability, in comparison to homopolymer and

diblock copolymer-based polyplexes, in the presence of salt concentrations up to C_{NaCl} = 700 mM. All three triblock copolymer-based polyplexes showed greater consistency with respect to size and polydispersity when complexed with dsRNAs of varying base pair length (other than when comparing to the diblock copolymer with the longest neutral block length, which also showed consistent size/polydispersity when complexed with different dsRNAs). This can be understood as due to the anchoring and self-assembly induced by the hydrophobic polymer block (B), as intended by the design of the triblock copolymers. Thus, amphiphilic triblock copolymers exhibit greater flexibility for complexation with a wider range of dsRNA targets.

4.5 Conclusion

In this chapter, the synthesis of novel linear ABC triblock copolymers by RAFT polymerisation, and their formation of self-assembled objects in aqueous solution has been demonstrated. The potential of these amphiphilic triblock copolymers as polymeric delivery vehicles for dsRNA was examined, and the impact of the proportion of each polymer block was investigated: hydrophilic, cationic PQDMAEMA (Q), hydrophobic P*t*BAA (B) and hydrophilic, neutral PDMAm (D).

The D block was found to be the most important for the formation of compact polyplexes, and influenced the electrophoretic mobility of the particles by dampening the overall surface charge. This proved beneficial in producing polyplexes with greater stability at high salt concentrations, reaching up to 700 mM NaCl concentration before disassembly/aggregation. In comparison, the hydrophobic B block was found to induce the strongest binding to dsRNA by EB exclusion assay and agarose gel electrophoresis, however, the corresponding polyplexes were only stable until C_{NaCl} = 150 mM. The triblock copolymer with the highest proportion of charged Q block formed the most polydisperse and the largest polyplex objects when complexed with dsRNA. It was discovered that, in the series of triblock copolymers tested

here, a relative proportion of ≥ 31 % hydrophilic, neutral polymer block is required to stabilise polyplexes at an N/P ratio = 1.

All three amphiphilic triblock copolymers were able to complex with *vha26* dsRNA at N/P ratios ≥ 2, and successfully protected the dsRNA against enzymatic degradation by RNase A. Amphiphilic ABC triblock copolymers could therefore be envisioned as useful delivery vehicles for dsRNA, with optimised architecture to prevent destabilisation at high salt concentrations and enhanced stability for complexes formed with a variety of dsRNA lengths for commercially viable agrochemical applications.

Chapter 5. Efficacy of polyplexes in biologically-relevant environments: *ex vivo* dsRNA protection and *in vitro* and *in vivo* delivery

A portion of this chapter has been published as a pre-print for peer-review in *Journal of Pest Science*, under the title 'Effective delivery and selective insecticidal activity of double-stranded RNA *via* complexation with diblock copolymer varies with polymer block composition', 10.21203/rs.3.rs-2272882/v1.

5.1 Abstract

Chemical insecticides are an important tool to control damaging pest infestations. However, lack of species specificity, the rise of resistance to these pesticides and the demand for biological alternatives with improved eco-toxicity profiles means that formulations with new mode-of-actions are required. RNA interference (RNAi)-based strategies, that use double-stranded RNA (dsRNA) as a species-specific bio-insecticide, offer an attractive solution that addresses these issues. Many species, such as the Asiatic pest fruit fly *Drosophila suzukii*, are recalcitrant to RNAi when dsRNA is orally administered, due to the degradation by gut nucleases and slow cellular uptake pathways. Thus, delivery vehicles that protect dsRNA and deliver it to insect gut cells are highly desirable. In this chapter, to demonstrate the efficiency of the polymer delivery systems developed in the previous chapters, the *ex vivo* protection of dsRNA against enzymatic degradation by haemolymph and gut enzymes is studied. Flow cytometry is then used to investigate the cellular uptake of Cy3-labelled dsRNA, with confocal microscopy confirming cytoplasmic delivery after complexation. Significantly decreased

survival of *D. suzukii* larvae was induced following oral feeding of complexes, only when formed with a diblock copolymer containing a long neutral block length (1:2 cationic block: neutral block, Q_{110}-*b*-D_{219}). However, there was no toxicity when the same formulation was fed to the closely related *Drosophila melanogaster*. In addition, *D. suzukii* gut imaging demonstrated a prolonged gut lumen exposure to dsRNA when complexed to Q_{110}-*b*-D_{219}. Despite *in vitro* cell uptake of Q_{110}-*b*-D_{219}/dsRNA polyplexes in HEK-293T cells and specific *in vivo D. suzukii* mortality, a luciferase protein assay in a transformed Sf9 cell line with Q_{110}-*b*-D_{219}/dsRNA polyplexes revealed no significant induction of luciferase mRNA degradation. Thus, we provide evidence that, in order to take full advantage of the promising strategy of complexing dsRNA with block copolymers for RNAi-based pest control, optimisation of the polymer composition is essential for RNAi success.

5.2 Introduction

Double-stranded RNA (dsRNA) is a versatile biomolecule with applications in both therapeutic and agrochemical fields. In recent years, the use of dsRNA as a species-specific bio-insecticide has been the subject of intense investigation due to the need for pest control agents with new mode-of-actions and improved biosafety profiles to counter the rise in resistance to commonly used chemical pesticides and the widespread eco-toxicity concerns with the field-use of such chemicals.[17,21,24–26,29,321,321,322,322,323] The specificity of RNAi induced by the application of exogenous dsRNA offers a promising biological alternative to current chemical insecticides to address the aforementioned concerns.

RNAi, induced by dsRNA, acts within the cell cytoplasm causing post-transcriptional degradation of mRNA. The judicious choice of the dsRNA sequence can provide a bio-chemical that is highly specific to the pest insect species, with a low risk of off-target toxicity.[40,41] For an in-depth explanation of the RNAi mechanism, please refer to Section 1.4 or published literature reviews.[35,40,44,44,45,65,304,324]

Prior work with *Drosophila suzukii* has shown a failed induction of RNAi when the insects were fed naked dsRNA, whilst exhibiting effective RNAi when dsRNA was administered by microinjection.[53,58] A similar issue in RNAi efficacy is observed in many other insect pest species, such as those of the lepidopteran or coleopteran orders.[51,59,63,72,74] This phenomenon can be explained by the degradation of dsRNA by RNases in the haemolymph, saliva and digestive tract of the insect, or within the environment (e.g. by microbial-produced RNases in the soil) prior to ingestion.[35,60–62,64–66,70,216,304] Another cause of poor RNAi induction is the low cellular uptake of dsRNA. This is particularly relevant in *Drosophila* as they lack the SID-1-like transporter protein that ordinarily provides a faster cellular uptake pathway in comparison to endocytosis.[48,115,198,199,304,325,326] Therefore, a method of delivery must be employed to provide effective protection for dsRNA against enzymatic degradation, and facilitate its efficient uptake through the cellular membrane.

For agrochemical bio-insecticide applications, recent research by Parsons *et al.*[114] and Christiaens *et al.*[115] targeting *Spodoptera,* used guanidinium-functionalised homopolymers or (co)polymers, respectively, to orally deliver dsRNA (described in detail in Section 1.7.1.3). The strongly basic guanidine moieties are particularly important for lepidopteran species, due to their alkaline gut contents.[61,62,79,115] Lichtenberg *et al.* also recently illustrated the delivery of dsRNA, however their protocol utilised the soaking (rather than oral feeding) of *C. elegans* with chitosan as the protective vehicle.[327] As far as we are aware, the work in this chapter represents the first study to use *block* copolymers to orally deliver dsRNA for bio-insecticidal applications.

Here, we report the effectiveness of the polymethacrylate-based homopolymer and series of diblock and triblock copolymers, synthesised *via* RAFT polymerisation (as described in Chapters 3 and 4) to protect *vha26* dsRNA from nuclease attack in the gut of *Drosophila suzukii,* the important insect pest of fruit.[89,220] *Vha26* codes for the 26 kDa E subunit of the vacuolar H^+-ATPase and has been shown to be a valid insecticidal target for RNAi in several

insect species, including *D. suzukii*.[58,328] The polymers contain quaternised ammonium groups, possessing a permanent positive charge in order to electrostatically interact with the anionic phosphodiester backbone of dsRNA.[265] The resulting interaction forms polyplexes that were characterised in terms of their ability to complex with dsRNA at varying N/P ratios (see Sections 3.4.4 and 4.4.3).

Following investigation into the influence of N/P ratio on complexation characteristics in Chapters 3 and 4, the formulations were analysed for their capacity to provide protection to the dsRNA against *ex vivo* enzymatic degradation by *Drosophila suzukii* adult and 3rd instar larvae (L3) gut enzymes. The cell viability of each polymer was assessed in mammalian HEK-293T and insect Sf9 cells *via* 3-(4,5-dimethylthiazol-2-yl)-5-(3-carboxymethoxyphenyl)-2-(4-sulfophenyl)-2H-tetrazolium (MTS) assay. Flow cytometry was then used to investigate the enhanced interaction of polymer-complexed Cy3-labelled dsRNA with HEK-293T cells, and confocal microscopy was employed to confirm uptake and perinuclear localisation.

A luciferase-based assay in transformed Sf9 cells was performed with Q_{110}-*b*-D_{219}/dsRNA polyplexes to determine if specific mRNA degradation could be induced in an insect cell line. Finally, *in vivo* oral feeding of 1st and 2nd instar (L1/L2) larvae was completed, with survival rate of *D. suzukii* and *D. melanogaster* assessed to identify species-specific mortality. . Gut sections of *D. suzukii* L3 larvae were then dissected and imaged after oral feeding with either Q_{110}-*b*-D_{219}/dsRNA polyplexes or naked Cy3-labelled dsRNA, to reveal the time-resolved *in vivo* ingestion and exposure of larvae to Cy3-labelled dsRNA. The results discovered here suggest that block copolymers are a promising potential candidate to protect and deliver dsRNA for bio-insecticidal applications; however, tailored polymer design and characterisation optimisation is required for successful RNAi induction.

5.3 Materials and methods

5.3.1 Materials

Homopolymer, Q_{110}, and block copolymers, Q_{110}-*b*-D_{57}, Q_{110}-*b*-D_{89}, Q_{110}-*b*-D_{219}, Q_{110}-*b*-B_{25}-*b*-D_{55}, Q_{110}-*b*-B_{44}-*b*-D_{99}, and Q_{110}-*b*-B_{12}-*b*-D_{212} were synthesised as described in Chapter 3 and 4. Dulbecco's Modified Eagle's Medium (DMEM) (supplemented with 10X Fetal Bovine Serum (FBS) and 1X Penicillin-Streptomycin (P/S)), 10X phosphate-buffered saline (PBS), paraformaldehyde (4%), ethanol (100%) and 3-(4,5-dimethylthiazol-2-yl)-5-(3-carboxymethoxyphenyl)-2-(4-sulfophenyl)-2H-tetrazolium (MTS, CellTiter 96® AQueous One Solution Cell Proliferation Assay) were purchased from Promega. *Vha26* (V-ATPase) 222 bp dsRNA was synthesised by Genolution AgroRNA (4.68 μg μL^{-1}), sequence specific to the pest insect, *Drosophila suzukii*.[58] Long and short luciferase dsRNA and poly(vinyl sulfonate) (PVS) was provided by Syngenta. ESF 921 media was purchased from Expression Systems. 7-Aminoactinomycin D (7-AAD) and ProLong™ Gold Antifade Mountant with 4′,6-diamidino-2-phenylindole (DAPI) were purchased from Thermo Fisher Scientific. Transformed Sf9 cells were provided by Oxford Expression Technologies Ltd. HEK-293T cells were provided by Dr Martin Stacey from the University of Leeds. Label IT® Tracker™ Intracellular Nucleic Acid Localization Kit Cy3 was purchased from Mirus Bio. Nuclease-free water (VWR) was used for biological assays to avoid the accidental degradation or contamination of dsRNA.

5.3.1 *Ex vivo* degradation assays

Intestines were dissected from 3rd instar *D. suzukii* larvae (L3), after 2 h starvation, and homogenised in Milli-Q water using a plastic homogeniser (30× intestines / 100 μL). *D. suzukii* adult male and female flies were starved by withholding food for 2 h before dissection. The intestine was removed from mixed sex flies and homogenised as described above in Milli-Q water (7× intestines / 100 μL). All homogenates were centrifuged at 13,000 RPM for 20 min to remove debris, and the supernatant was collected and stored at -20 °C until required.

Pre-determined aliquots of Q, Q-*b*-D or Q-*b*-B-*b*-D polymers were added to 1 μg dsRNA, to provide an N/P ratio = 2.5. Solutions were incubated at RT for 1.5 h to allow for complexation, and a solution of dsRNA alone (naked) in nuclease-free water was also prepared. Solutions of adult or L3 guts (7.1 or 1.6 μL, respectively, equivalent to ½ a gut per 1 μg dsRNA (i.e. per gel lane), sufficient to fully degrade naked dsRNA as confirmed by gel electrophoresis in Section 5.4.2[329,330]) was added to polyplex and naked dsRNA solutions. The samples were then incubated for 30 min (adult guts) or 24 h (L3 larval guts) at 26 °C. Each solution was loaded (with 2 μL of 6X blue/orange loading dye) onto a 2% (w/v) agarose gel stained with ethidium bromide (EB, 20 ng mL^{-1}), prepared with 1X TAE (Tris base, acetic acid and EDTA) buffer. Assays were run for 25 min at 90 V. An aliquot of 100 bp DNA ladder (1 μL, combined with 1 μL 6X purple non-SDS dye and 4 μL nuclease-free water, NEB) was run for comparison. The gel was imaged under a UV transilluminator at 365 nm.

5.3.2 Mammalian cell culture

HEK-293T cells were cultured in 75 cm^2 flasks within a 37 °C, 5% CO_2 and 95 % relative humidity (RH) incubator. Media was Dulbecco's Modified Eagle's Medium (DMEM) supplemented with FBS (10% v/v) and 1% penicillin/streptomycin (P/S, 100 μg mL^{-1} and 100 μg mL^{-1}, respectively). Cell confluence was monitored and cells were passaged as required (approx. every 2-3 days).

5.3.3 Sf9 cell culture

Sf9 cells (New England Biolabs (UK) Ltd) and transformed Sf9 cells (Oxford Expression Technologies Ltd) were cultured in 75 cm^2 flasks within a 26 °C, 60 %RH incubator. Media was ESF 921 supplemented with 1% penicillin/streptomycin (P/S, 100 μg mL^{-1} and 100 μg mL^{-1}, respectively). Cell confluence was monitored and cells were passaged as required (approx. every 2-3 days).

5.3.4 **Cell viability assays**

5.3.4.1 Mammalian HEK-293T cells

HEK-293T cells were seeded onto a 96-well plate 24 h prior to treatment, at seeding density ~10,000 cells/well, to allow cells to reach ~40,000 cells/well. Q_{110}, Q_{110}-*b*-D_{57}, Q_{110}-*b*-D_{89}, Q_{110}-*b*-D_{219}, Q_{110}-*b*-B_{25}-*b*-D_{55}, Q_{110}-*b*-B_{44}-*b*-D_{99} and Q_{110}-*b*-B_{17}-*b*-D_{212} at varying concentrations (0.01 – 10 mg mL^{-1}) were added to each well, with nuclease-free water applied as the untreated control. 6 μL of treatment (either polymer or nuclease-free water control solution) was added to each well, containing a total volume 150 μL to maintain < 5 v/v% nuclease-free water addition to the cells. Cells were incubated at 37 °C, 5% CO_2, 95 %RH for 24 h. Media was then removed, and fresh DMEM media was added alongside 3-(4,5-dimethylthiazol-2-yl)-5-(3-carboxymethoxyphenyl)-2-(4-sulfophenyl)-2H-tetrazolium (MTS, 20 μL). Cells were incubated with MTS for 2 h prior to analysis with a plate reader at 495 nm (absorption). Cells treated with nuclease-free water only were normalised to 100% cell viability, and other treatments were normalised with respect to the cells in nuclease-free water. The assay was performed in triplicate.

5.3.4.2 Insect Sf9 cells

Sf9 cells (New England Biolabs (UK) Ltd) were seeded onto 96-well plates, 2 days prior, at a seeding density of ~20,000 cells/well. Q_{110}-*b*-D_{219} was assessed as the most promising construct, due to the compactness of its resulting polyplexes. A range of polymer concentrations (0.01 – 2 mg mL^{-1}) were prepared in ESF 921 media. Aliquots (100 μL/well) at each concentration were added to Sf9 cell 96-well plates with 3 replicates, and incubated for 24 h at 26 °C, 60 %RH. Subsequently, MTS (20 μL) was added to each well and the cells were incubated for 4 h prior to analysis with a plate reader at 495 nm (absorption). Cells treated with ESF 921 media (1% P/S) only were normalised to 100% cell viability and other treatments were normalised with respect to cells in ESF 921 media. A complete repeat experiment was conducted, containing triplicate wells of the different variables in each repeat.

5.3.5 **Labelling of dsRNA with Cy3 fluorophore**

Labelling of dsRNA with a Cy3 fluorophore was conducted as per standard protocol according to the Label IT® Tracker™ Intracellular Nucleic Acid Localization Kit, and purification was performed by precipitation in ethanol and stored at -20 °C until required.

5.3.6 **Flow cytometry**

HEK-293T cells were seeded onto a 12-well plate, at seeding density ~10,000 cells/well, 24 h prior to allow cells to reach ~50,000 cells/well. Polyplexes were prepared 24 h prior to treatment, through the addition of Cy3-labeled *vha26* dsRNA (20 μL, 50 ng μL^{-1}) to each polymer solution (20 μL). Polymers were dissolved in nuclease-free water at varying concentrations, in order to maintain an N/P ratio of 5 when a 20 μL aliquot was added: Q_{110} = 163 ng μL^{-1}, Q_{110}-*b*-D_{57} = 202 ng μL^{-1}, Q_{110}-*b*-D_{89} = 225 ng μL^{-1}, Q_{110}-*b*-D_{219} = 315 ng μL^{-1}, Q_{110}-*b*-B_{25}-*b*-D_{55} = 230 ng μL^{-1}, Q_{110}-*b*-B_{44}-*b*-D_{99} = 282 ng μL^{-1}, Q_{110}-*b*-B_{17}-*b*-D_{212} = 342 ng μL^{-1}. All solutions were prepared using RNase-free and DNase-free Eppendorf tubes and filter pipette tips to minimise dsRNA degradation. Polyplexes, Cy3-labelled dsRNA-only and polymer-only solutions were individually applied to wells containing HEK-293T cells in the 12-well plate. Nuclease-free water was included in the absence of either polymer/dsRNA, and a nuclease-free water control was conducted. Fresh DMEM media was added to the wells alongside the treatments (40 μL) to maintain < 5 v/v% nuclease-free water to media ratio. After 4 h, cells were placed on ice and then lifted from wells by physical disturbance. Cells were pelleted by centrifugation and media/treatment was removed before washing and resuspension of cells in fresh, ice-cold DMEM media, alongside 1% 7-aminoactinomycin D (7-AAD) as a dead cell stain, when required. Cy3-positive cells were analysed by flow cytometry using a CytoFLEX S (Beckman Coulter) with filters set at 561 nm excitation, 585 nm emission wavelengths. Data were analysed using FlowJo software and all experiments were performed in duplicate.

5.3.7 Confocal microscopy

Cells were cultured on microscope slides introduced to the 12-well plate prior to cell seeding. A polyplex solution of Q_{110}-*b*-D_{219}/dsRNA was prepared as a model example, and HEK-293T cells were seeded as described above. After a 4 h incubation period of the cells with polyplex, Cy3-labelled dsRNA, polymer or nuclease-free water, media was removed and the slides were washed with 1X PBS, before fixing with 4% paraformaldehyde. Slides were mounted with a DAPI-stain liquid mountant (ProLong™ Gold Antifade Mountant with DAPI) to prepare for cell imaging on a confocal microscope (Zeiss LSM700).

5.3.8 Luciferase protein assay

Transformed Sf9 cells with eGFP and luciferase expression (Oxford Expression Technologies Ltd) were seeded onto 96-well plates 2 days prior, at a seeding density of ~20,000 cells/well. Cells were seeded in ESF 921 media (1% P/S). Q_{110}-*b*-D_{219}/dsRNA polyplexes (used as a promising construct with the most compact polyplexes) of varying N/P ratios (0.25, 0.5, 1, 3 and 5) were prepared with both long and short luciferase dsRNA (40 μg/well, dsRNA provided by Syngenta) in TC-100 serum-free media, with ~30 min for complexation. Polyplex solutions (100 μL) were added to Sf9 cell 96-well plates with 3 replicates, and incubated. After 4 h, the media was removed from the cells and replaced with regular media (ESF 921 with 1% P/S). The Sf9 cells were then incubated at 26 °C, 60 %RH for another 44 h (48 h total incubation). Cells with regular media (ESF 921 with 1% P/S) were included as a control, as well as GeneJuice® solution (4 μL/well) as a positive control. Naked long and short luciferase dsRNA (N/P ratio = 0) was also incubated with cells at the same concentration as polyplex solutions. The 96-well plate was read for eGFP fluorescence using a BioTek Cytation 3 imaging plate reader. The Sf9 cells were subsequently lysed using cell lysis buffer for 30 min and incubated at 37 °C. Cell contents were removed from wells through physical disturbance and pipetting. 25 μL of this solution was diluted with 175 uL of water in a white clear-bottomed 96-well plate. The bioluminescence was measured using a plate reader. This bioluminescence reading

was then normalised against the BSA concentration in each well (using a Pierce™ BCA Protein Assay Kit) to calculate the reduction in luciferase expression.

5.3.9 *D. suzukii* and *D. melanogaster* husbandry

D. suzukii and *D. melanogaster* were maintained on a yeast-based diet (Lancashire recipe), prepared through the combination of the following: Milli-Q water (2 L) fine oatmeal (148 g), molasses (100 g), yeast (16.8 g), agar (16.8 g) and the *Drosophila* anti-fungal agent monohydroxybenzoic acid (MHPB, also referred to as Tegosept or Nipagin, 68 mL, 10% in 100% ethanol). Flies were kept in standard fly bottles or cages and stored in an incubator set to 26 °C, 60 %RH. Flies were transferred using CO_2 as adults or with a paintbrush as larvae.

5.3.10 Oral feeding of *Drosophila*

In order to collect synchronised-instar larvae, *D. suzukii* (or *D. melanogaster*) adults were transferred to cages with fresh diet, and incubated at 26 °C, 60 %RH to produce eggs. Adults were removed after 24 h and larvae were left to hatch from the laid eggs. 1st and 2nd instar (L1/L2) *D. suzukii* and *D. melanogaster* larvae were collected after 24 h and isolated to starve on moist filter paper for 3 h prior to addition to treated diets.

Vha26 222 bp dsRNA (4.68 mg mL^{-1}, 8 μL, 37 μg) was complexed with an equal volume (8 μL) of polymer in each polyplex formulation, ensuring an N/P ratio = 5 by varying polymer concentration. For example: 8 μL of Q_{110}-*b*-D_{219} at 29.5 mg mL^{-1}. Polyplexes were incubated for 1.5 h at RT to equilibrate, see Figure 5.1 that illustrates the necessity for an equilibration period (particularly when formulating at high concentrations, such as those used in biological assays) to allow complexes to re-disperse after their initial electrostatic interaction.

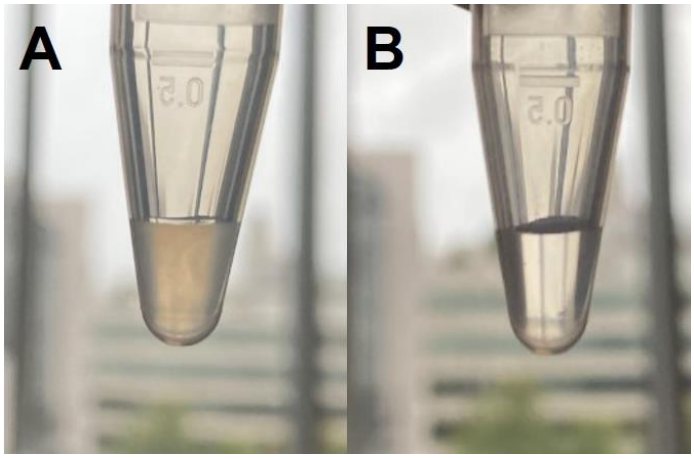

Figure 5.1. (A) Q_{110}-*b*-D_{219}/dsRNA solution upon initial mixing before addition to diet for oral feeding of *Drosophila*. (B) The same Q_{110}-*b*-D_{219}/dsRNA polyplex solution after 1.5 h equilibration time, polyplexes have re-dispersed following complexation at high concentration in nuclease-free water.

Each solution (16 μL) was then added to 50 mg of diet (as described in previous section) and mixed thoroughly for an even distribution, allowing 30 min to incorporate. Nuclease-free water (16 μL) was added to diet as the untreated control. Five starved L1/L2 larvae were then transferred to each 50 mg treated (or untreated control) diet, n = 25 total per assay repeat. Larvae were removed from treated diet after 24 h of feeding, and transferred to fresh untreated diet. The *D. suzukii* (or *D. melanogaster*) were then monitored for the next 15 days for survival. Larvae mortality was assessed by the failure to reach the pupal stage and the absence of any live larvae in or on the surface of the food. Mortality was identified between the larval and pupal stage, however *Drosophila* were monitored until adult eclosion to ensure all mortality was accounted for. Survival results were averaged across assays repeated in duplicate and normalised against untreated diet-fed *D. suzukii*. Standard deviation was calculated and represented as error bars on plots. Statistical significance was determined using binary logistic regression performed in SPSS Statistics 26.

5.3.11 **Digestive tract *in vivo* imaging**

3rd instar (L3) *D. suzukii* larvae were starved for 3 h on moist filter paper. Solutions of polyplex (50 μL, Q_{110}-*b*-D_{219}/Cy3-labelled dsRNA), Cy3-labelled dsRNA and blue dye were prepared, at a 5% sucrose concentration. To prepare polyplex dispersions, Q_{110}-*b*-D_{219} (20 μL, 315 ng

μL^{-1}) was added to Cy3-labelled dsRNA (20 μL, 50 ng μL^{-1}) and allowed to equilibrate for 1.5 h for complexation alongside 20% sucrose solution (10 μL, to achieve 5% final sucrose concentration). Five starved L3 larvae were then transferred to a dispersion of polyplex (20 μL, N/P ratio = 5), dsRNA (20 μL, 50 ng μL^{-1}) or blue dye (20 μL) for 1 h, 4 h and 24 h. Feeding was confirmed by the presence of blue dye within the gut of the control (blue dye-fed) larvae. The larval intestines (guts) were then dissected from the body and submerged in 4% paraformaldehyde to fix for 24 h before mounting with anti-fade DAPI-stain mounting fluid. Fluorescence and confocal microscopy images were then taken.

5.4 Results and discussion

5.4.1 Polymer synthesis

Linear homopolymer, a series of hydrophilic diblock copolymers and a series of amphiphilic ABC triblock copolymers were synthesised by RAFT polymerisation, as described in detail in Chapters 3 and 4 and in brief below.

The polymethacrylate-based polymer block was poly[2-(methacryloyloxy)ethyl] trimethylammonium chloride (Q), possessing a quaternised ammonium group and thus a positive charge regardless of pH conditions (a 'strong' polyelectrolyte). The Q polymer block was purified as a homopolymer (Q_{110}) for comparison to the diblock and triblock copolymers. To prepare the hydrophilic diblock copolymers, the Q block was synthesised as a macro-chain-transfer agent (macro-CTA) and chain extended with poly(*N*,*N*-dimethyl acrylamide) (D). The cationic macro-CTA length was kept constant (DP ~ 110), and a series of three diblock copolymers were synthesised with varying neutral D polymer block lengths (DP ~ 57, 89 and 219). For the amphiphilic triblock copolymers, the Q macro-CTA chain length was kept constant (DP ~ 100) and chain extended first with a hydrophobic poly(*tert*-butyl acrylamide) (B) block to varying chain lengths (DP ~ 25, 44 and 17). The Q-*b*-B amphiphilic diblock copolymers were purified as new macro-CTAs and chain extended with varying chain lengths

of hydrophilic D polymer blocks (DP ~ 55, 99 and 212, respectively). Polymer characterisation is described in detail in Sections 3.3.2 and 4.3.3.

5.4.2 *Ex vivo* protection of dsRNA against degradation by *D. suzukii* gut enzymes

The cationic ammonium moieties of the polymer Q block (present in the homopolymer, diblock copolymers and triblock copolymers) are the basis for the complexation of the polymers with dsRNA, through the electrostatic interaction with the anionic phosphate groups of the phosphodiester-bonded backbone. The relative proportions of polymer/dsRNA were varied in order to ascertain the optimal N/P ratio for full complexation (≥ 2), which is described in Sections 3.4.4 and 4.4.3 for the homopolymer/diblock copolymers and triblock copolymers, respectively.

The protective properties of the homopolymer, diblock copolymers and triblock copolymers are evident, following *ex vivo* degradation assessments in agarose gel electrophoresis, the first of which is shown in Figure 5.2.

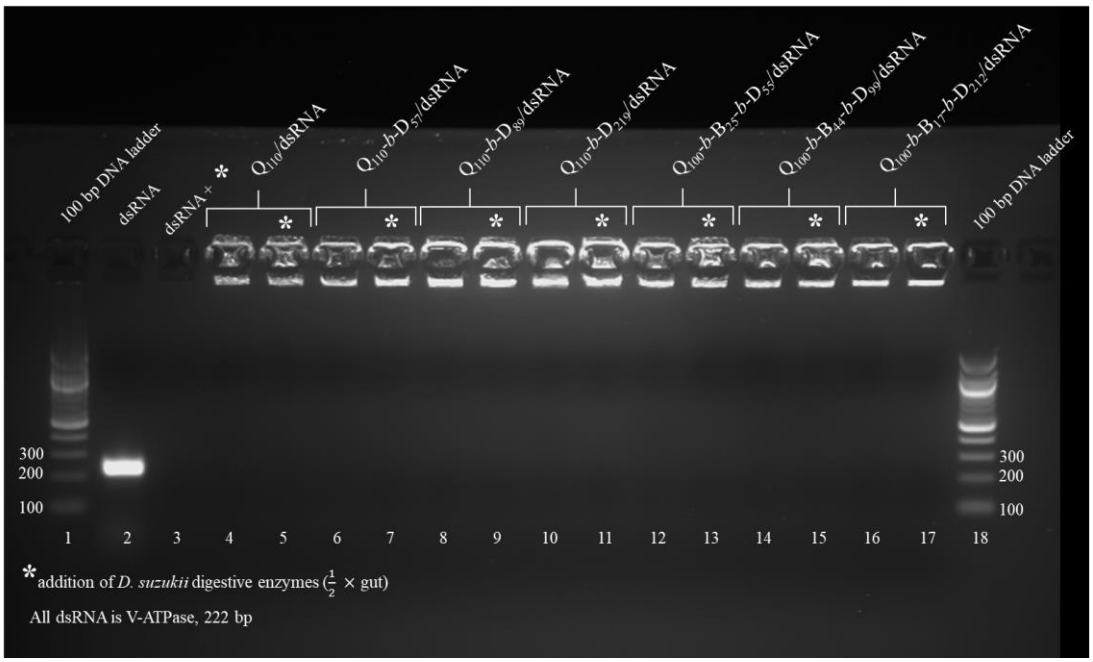

Figure 5.2. Agarose gel electrophoresis of homopolymer (Q, lanes 4 and 5), diblock copolymer (Q-*b*-D, lanes 6, 7 and 8, 9 and 10, 11) and triblock copolymer (Q-*b*-B-*b*-D, lanes 12, 13 and 14, 15 and 16, 17) complexes with dsRNA at an N/P ratio = 2.5. DsRNA was run in lanes 2 and 3. Homogenised gut of adult flies (equivalent of ½ a gut) was added to lanes 3, 5, 7, 9, 11, 13, 15 and 17, annotated with a *. A 100 bp DNA ladder was run for comparison in lanes 1 and 18.

D. suzukii gut enzymes were collected through the tissue homogenisation and centrifugation of the guts of starved *D. suzukii* adults and L3 larvae. The equivalent of ½ a gut's worth of enzymes was used per 1 μg dsRNA (i.e. per gel lane), which was sufficient to fully degrade naked *vha26* dsRNA, as indicated for the adult gut enzymes by the complete absence of fluorescent band at the ~200 bp location on the gel (Figure 5.2, lane 3).

After 30 min (at 26 °C) incubation with adult *D. suzukii* gut enzymes, the naked *vha26* dsRNA was completely degraded (Figure 5.2, lane 3). In contrast, gut enzymes extracted from L3 *D. suzukii* larvae required a longer, 24 h incubation with *vha26* dsRNA for complete degradation (see Figure 5.3).

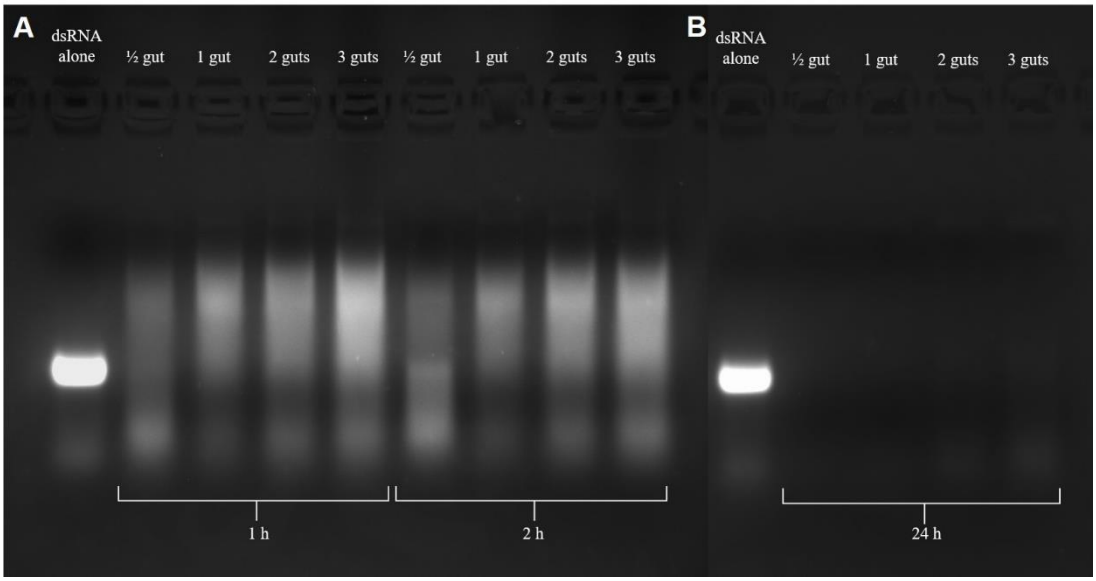

Figure 5.3. Agarose gel electrophoresis of dsRNA alone and dsRNA incubated with the homogenised guts of L3 *D. suzukii* larvae added to the equivalent of ½ gut, 1 gut, 2 guts, or 3 guts. Samples of dsRNA were incubated with the L3 larvae gut enzymes for either (A) 1 h, 2 h or (B) 24 h. Image B was a separate agarose gel, following incubation of the dsRNA for 24 h, hence the subtle background colour change that may be noticeable.

As described by Yoon *et al.*, late-stage L3 larvae (and pupae) express lower levels of dsRNases in comparison to early-stage L1 or L2 larvae and the adult flies.[331] This explains why the *vha26* dsRNA was only partially degraded through incubation with L3 larvae gut enzymes after 1 h or 2 h (Figure 5.3A), in contrast to the full degradation obtained after incubation for 30 min with the adult *D. suzukii* gut enzymes (Figure 5.2). However, 24 h incubation with L3 larvae gut enzymes appears to be sufficient to completely degrade *vha26* dsRNA (Figure 5.3B), indicated by the total absence of fluorescence.

As shown in both Figure 5.2 and Figure 5.4, the homopolymer, diblock copolymers and the triblock copolymers were able to form complexes with dsRNA at an N/P ratio = 2.5, illustrated by the retardation of dsRNA migration in the agarose gel (fluorescence is maintained in the well of the gel, with no smear apparent along the gel lane).

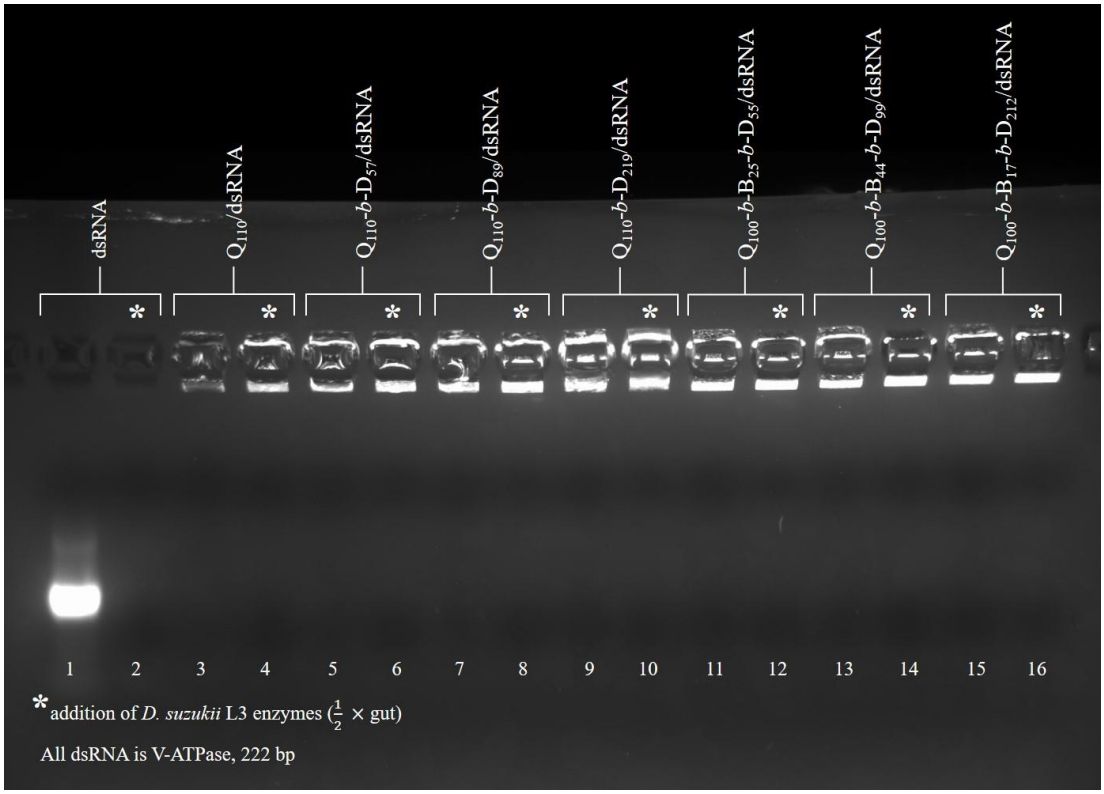

Figure 5.4. Agarose gel electrophoresis of homopolymer (Q, lanes 3 and 4), diblock copolymer (Q-*b*-D, lanes 5, 6 and 7, 8 and 9, 10) and triblock copolymer (Q-*b*-B-*b*-D, lanes 11, 12 and 13, 14 and 15, 16) complexes with dsRNA at an N/P ratio = 2.5. DsRNA was run in lanes 1 and 2. Homogenised gut of L3 larvae (equivalent of ½ a gut) was added to lanes 2, 4, 6, 8, 10, 12, 14 and 16, annotated with a *.

All of the complexes formed between the polymers and dsRNA maintained strong fluorescence (and therefore stability of dsRNA) in the wells of the agarose gel following incubation with *D. suzukii* adult gut enzymes for 30 min (Figure 5.2), and incubation with *D. suzukii* L3 larval gut enzymes for 24 h (Figure 5.4).

There are limited examples in literature of the polymer-induced protection of dsRNA against enzymatic degradation.[64,250] Therefore, the results shown here illustrate the potential of these block copolymers for the delivery of intact dsRNA to *D. suzukii* for bio-insecticidal applications, as they are capable of protecting the genetic material from degradation by enzymes in the gut after oral feeding.

5.4.3 Cell viability in mammalian and insect cells

HEK-293T cells are widely used in the study of gene delivery to cells in culture and are used here for comparison with results from similar studies designed for therapeutic applications.[332–334] Thus, prior to an exploration of the *in vitro* capabilities of the polyplexes, it was important to assess cell viability following incubation with each of the polymer constructs. An insect-specific cell line, Sf9, was later acquired and therefore cell viability was also performed in Sf9 cells with the most promising diblock copolymer candidate, Q_{110}-*b*-D_{219}.

5.4.3.1 Mammalian HEK-293T cells

The cell viability of homopolymer, diblock copolymers and triblock copolymers was assessed *via* MTS assay with HEK-293T cells, in which the concentrations of stock polymer solutions were varied to assess the concentration dependence of polymer cytotoxicity, Figure 5.5.

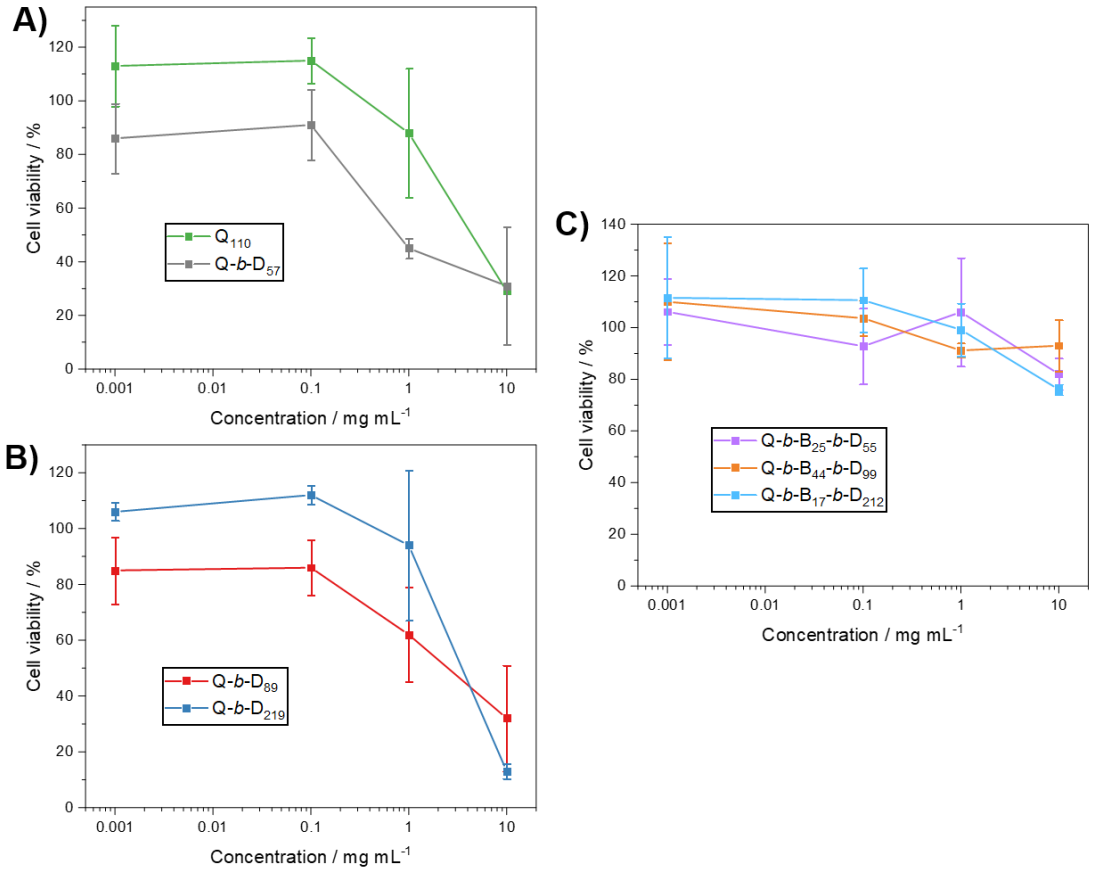

Figure 5.5. Cell viability of HEK-293T cells, normalised with respect to untreated cells, *via* MTS assay with (A) homopolymer (Q_{110}) and diblock copolymer (Q_{110}-*b*-D_{57}), (B) diblock copolymers (Q_{110}-*b*-D_{89} and Q_{110}-*b*-D_{219}) and (C) triblock copolymers (Q_{110}-*b*-B_{25}-*b*-D_{55}, Q_{110}-*b*-B_{44}-*b*-D_{99} and Q_{110}-*b*-B_{17}-*b*-D_{212}). Concentration of stock polymer solution added to cell culture was varied from 0.01 – 10 mg mL^{-1}. Cell viability was assessed in triplicate after 24 h incubation. Error bars represent standard deviation, and lines are drawn here to guide the eye.

The cells were incubated with the polymer solutions for 24 h. The highest stock solution concentrations (10 mg mL^{-1}) induced a significant decrease in cell viability. A tenfold decrease in stock concentration (1 mg mL^{-1}) showed more variable results between the polymers, whilst 0.1 and 0.01 mg mL^{-1} stock concentrations showed >85% viability in all samples. There were some cases of >100% cell viability, which are most likely due to cell proliferation due to pipetting error as they were not significant and within error. In the case of 0.1 mg mL^{-1} stock concentration, the final polymer concentration in each well (total volume, 150 µL) was 4 ng $µL^{-1}$ and thus confirmed that a polymer concentration of approximately 4 ng $µL^{-1}$ (as used in

in vitro assays) is suitable in terms of cell viability, even after a 24 h incubation period. It is notable that the triblock copolymers, even at a high stock concentration of 10 mg mL^{-1}, showed a greater cell viability than homopolymer or diblock copolymers.

5.4.3.2 Insect Sf9 cells

Cell viability of the Q_{110}-*b*-D_{219} diblock copolymer (chosen as a promising construct with the most compact polyplexes) was assessed *via* MTS assay in insect Sf9 cells, at concentrations 0.01 – 2 mg mL^{-1}.

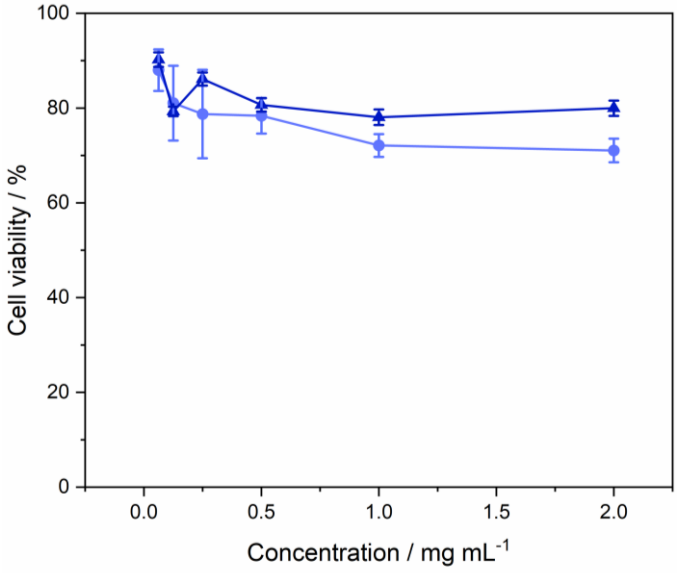

Figure 5.6. Cell viability of Sf9 cells with increasing polymer (Q_{110}-*b*-D_{219}) concentration, normalised with respect to untreated cells *via* MTS assay. Concentration of diblock copolymer solution added to cell culture was varied from 0.01 – 2 mg mL^{-1}. The different shade of colour represents a repeat with Sf9 cells of different passage number, within each repeat viability was assessed in triplicate. Error bars represent standard deviation, and lines are drawn here to guide the eye.

Across the concentration range tested, in Figure 5.6, the cell viability remains high (>70%) throughout with no significant decrease as polymer concentration is increased.

5.4.4 **Complexation with homopolymer, diblock copolymer or triblock copolymer enhances *in vitro* uptake of dsRNA in HEK-293T cells**

Following confirmation that the Q, Q-*b*-D and Q-*b*-B-*b*-D polymers complex with dsRNA and provide sufficient protection against *ex vivo* enzymatic degradation, and establishing a suitable

concentration (~4 ng μL^{-1}) for maintaining sufficient cell viability, the *in vitro* delivery potential of the polyplexes was determined. Cellular uptake was thus assessed in HEK-293T cells, using flow cytometry and confocal microscopy.

Flow cytometry. After a 4 h incubation period with Cy3-labelled dsRNA alone or complexed with Q, Q-*b*-D or Q-*b*-B-*b*-D polymers, cells were fixed and analysed for fluorescence intensity at 585 nm. There was a large shift in the mean fluorescence intensity of cells treated with polyplexes (formulated at N/P ratio = 5). In comparison, cells treated with naked Cy3-labelled dsRNA alone did not cause a significant increase in fluorescence intensity. Gating strategies to exclude dead cells and cell doublets are shown in Figure 5.7, Figure 5.8 and Figure 5.9.

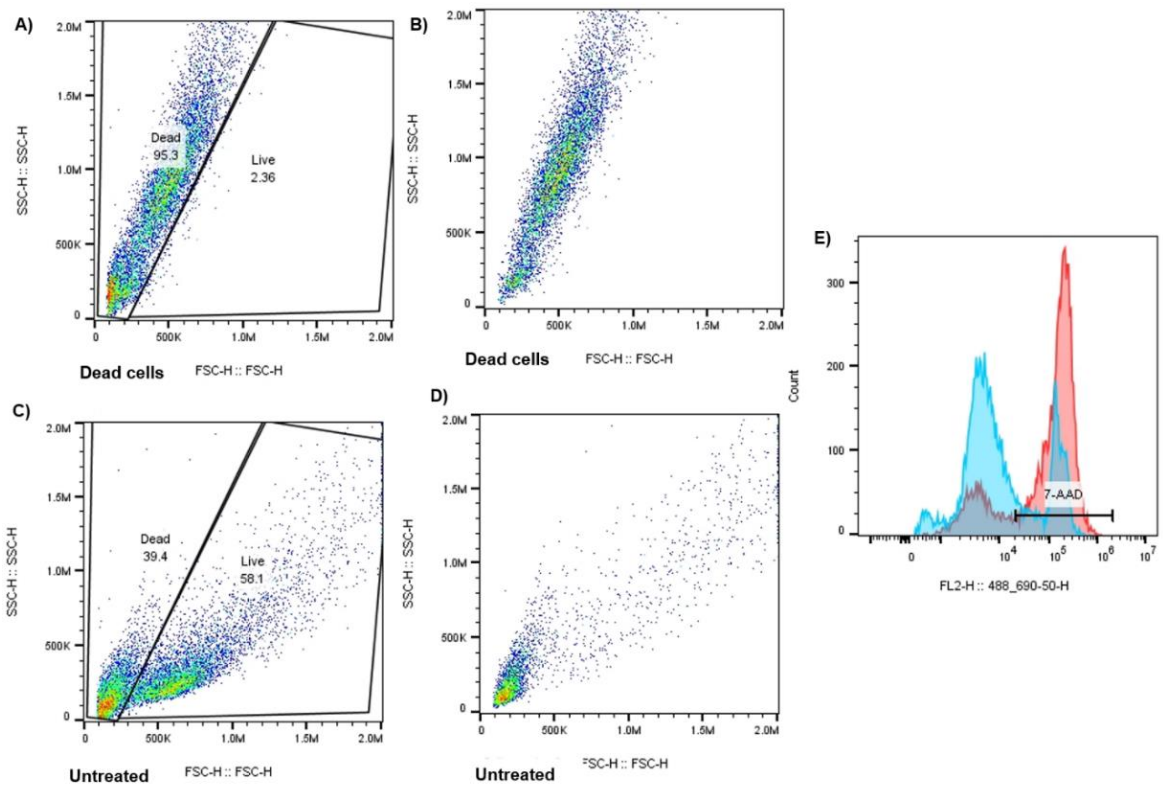

Figure 5.7. Cells were killed by heating for 30 min at 90 °C in a heating block, in order to confirm dead cell appearance in dot plots and intensity plots. (A) and (C) show FSC/SSC dot plots of samples of dead cells and untreated cells, respectively, with live/dead gating shown. (B) and (D) show FSC/SSC dot plots following 7-AAD discrimination of dead cells and untreated cells, respectively, with gating illustrated in (E), which shows a histogram of 7-AAD fluorescence intensity in dead cells (red) and untreated cells (blue).

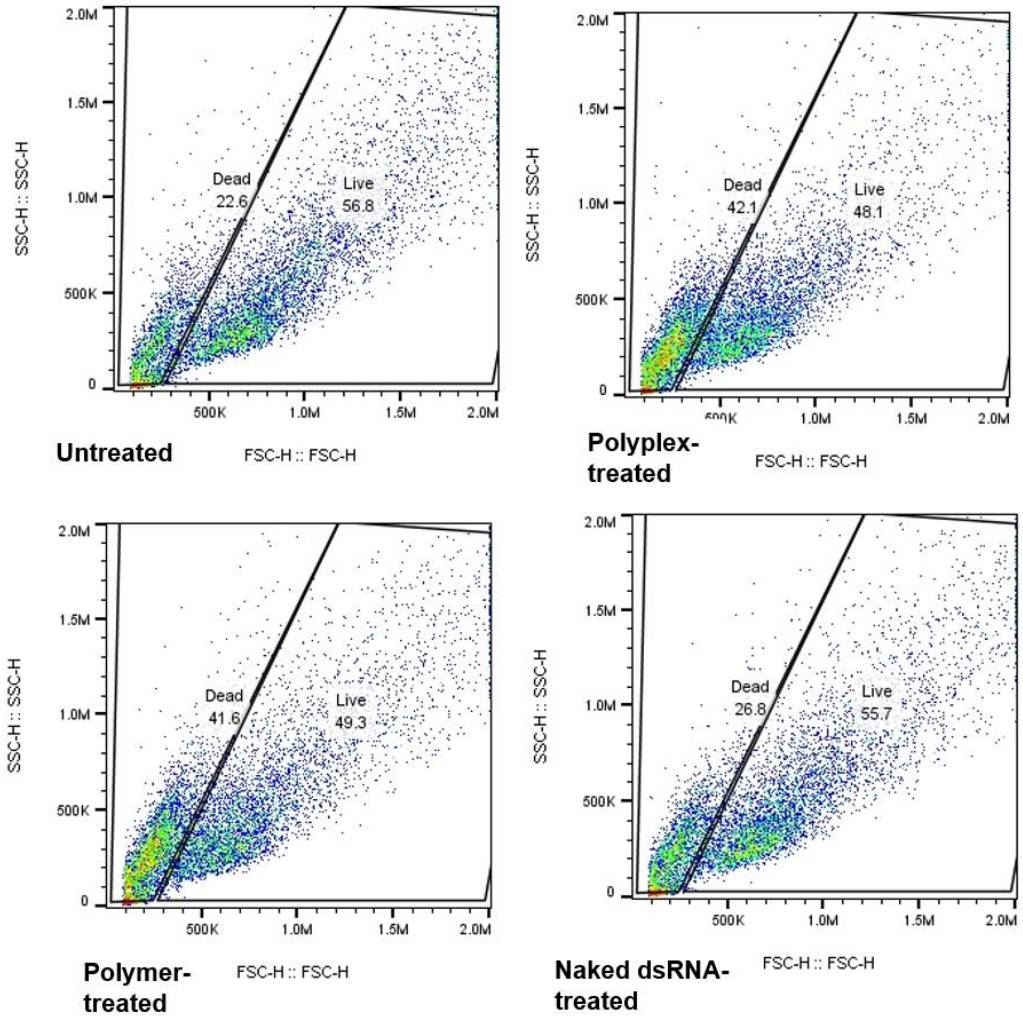

Figure 5.8. FSC/SSC (forward scatter height/side scatter height) dot plots of a representative sample of untreated cells, Q_{110}-*b*-D_{219}-based polyplex-treated cells, Q_{110}-*b*-D_{219} polymer-treated cells and naked dsRNA-treated cells (as indicated by titles in bottom left hand corner of graphs). Live/dead gating is shown. Q_{110}-*b*-D_{219} is used here as an example, other complexes and polymers showed similar dot-plots (see Figure A10 in Appendix).

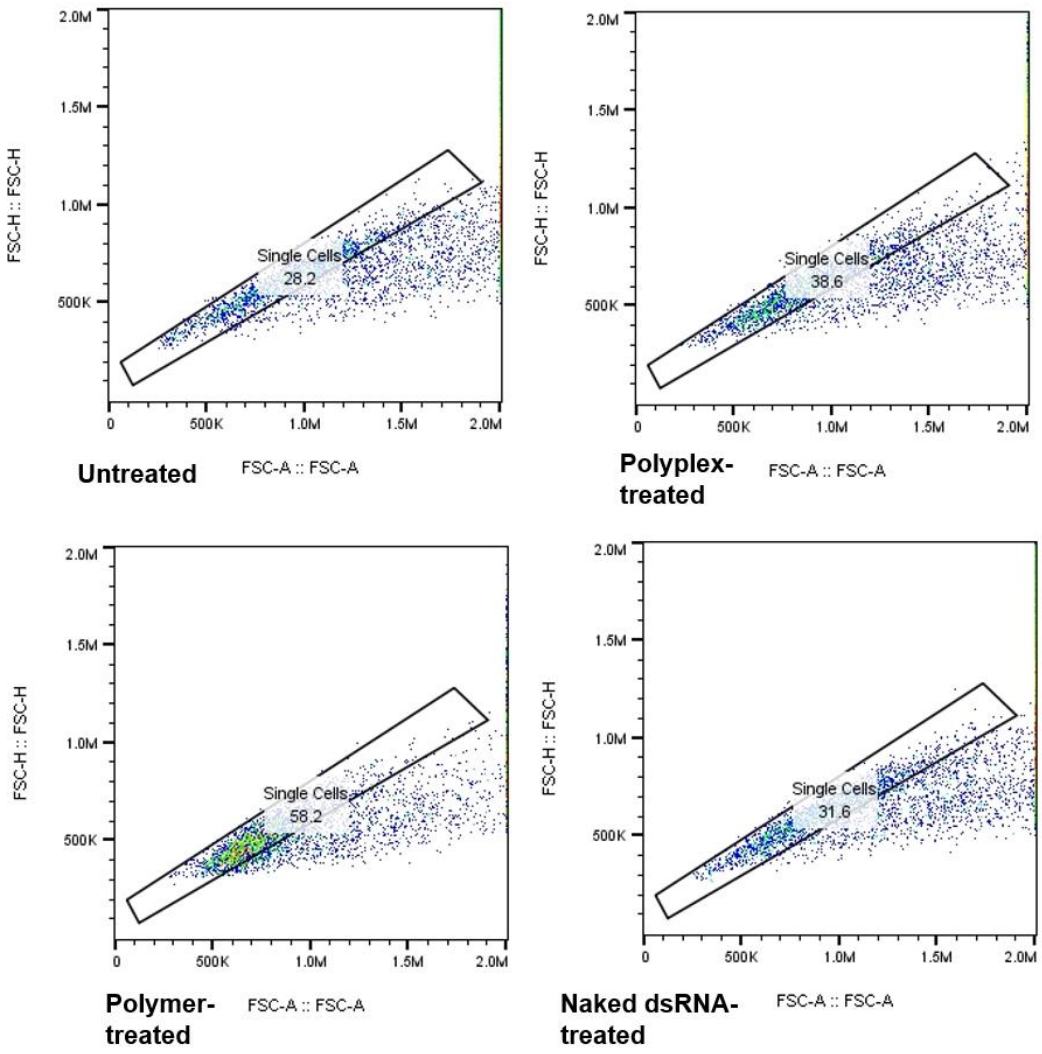

Figure 5.9. FSC-H/FSC-A (forward scatter height/forward scatter area) dot plots of a representative sample of untreated cells, Q_{110}-*b*-D_{219}-based polyplex-treated cells, Q_{110}-*b*-D_{219} polymer-treated cells and naked dsRNA-treated cells (as indicated by titles in bottom left hand corner of graphs). Gating of single cells is shown. Q_{110}-*b*-D_{219} is used here as an example, other complexes and polymers showed similar dot-plots (see Figure A10 in Appendix).

Upon incubation of mammalian HEK-293T cells with Q, Q-*b*-D or Q-*b*-B-*b*-D-based complexes with Cy3-labelled dsRNA, in contrast to naked Cy3-labelled dsRNA alone, there was a significant increase in fluorescence intensity, Figure 5.10. Full flow cytometry data are shown in Figure A10 in the Appendix.

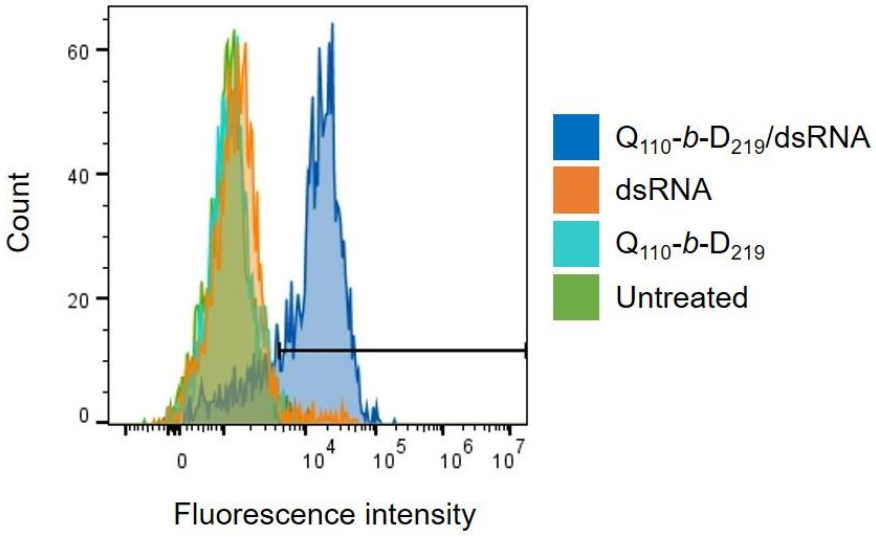

Figure 5.10. Histogram of the Cy3 fluorescence intensity in HEK-293T cells that were untreated, or incubated with Cy3-labelled dsRNA alone or complexed with Q_{110}-*b*-D_{219} diblock copolymer. Q_{110}-*b*-D_{219} used as example here, other polymer-based complexes with dsRNA showed similar increases in fluorescence intensity (see Figure A10 in the Appendix). The gating is shown by a black line, as >95th percentile of the negative control.

The gating, as shown in Figure 5.10, was used to assess the percentage of Cy3 positive HEK-293T cells. The calculated percentage of Cy3 positive live, single cells upon incubation with each treatment (polyplexes, polymers alone or naked Cy3-labelled dsRNA) is shown in Figure 5.11.

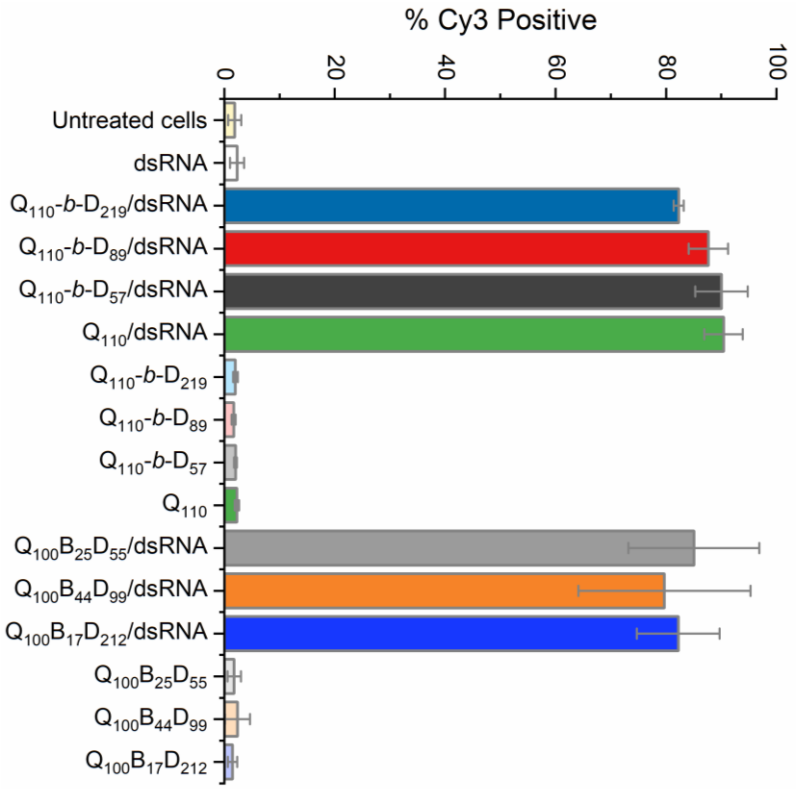

Figure 5.11. Percentage of Cy3 positive events, determined *via* flow cytometry of untreated or treated HEK-293T cells, which demonstrates that complexation of Cy3-labelled dsRNA with homopolymer, diblock copolymer or triblock copolymer greatly enhances interaction with eukaryotic cells. Standard deviation shown by error bars from assays performed in duplicate.

Over 80% of single, live HEK-293T cells exhibited a significant increase in fluorescence, and thus cell interaction, when incubated with polymer/Cy3-labelled dsRNA polyplexes (regardless of which polymer was used for complex formulation) as compared to less than 5% of live, single cells showing a shift in Cy3 fluorescence in the case of HEK-293T cells incubated with naked Cy3-labelled dsRNA, polymer alone, or when untreated. There was no significant difference between the percentage of Cy3 positive cells following incubation with the different polyplexes.

To confirm that the increase in Cy3 fluorescence, measured by flow cytometry, upon treatment with polyplexes was not simply due to these structures adhering to the cell surface, confocal laser scanning microscopy was conducted, using Q_{110}-*b*-D_{219}/dsRNA polyplexes as a

representative sample (as there was no significant difference between the different polyplexes used as part of the flow cytometry data).

Confocal microscopy: Z-stack images of representative HEK-293T cells were captured after incubation with Q_{110}-*b*-D_{219}/Cy3-labelled dsRNA polyplexes, naked Cy3-labelled dsRNA, Q_{110}-*b*-D_{219} alone or nuclease-free water (untreated), Figure 5.12.

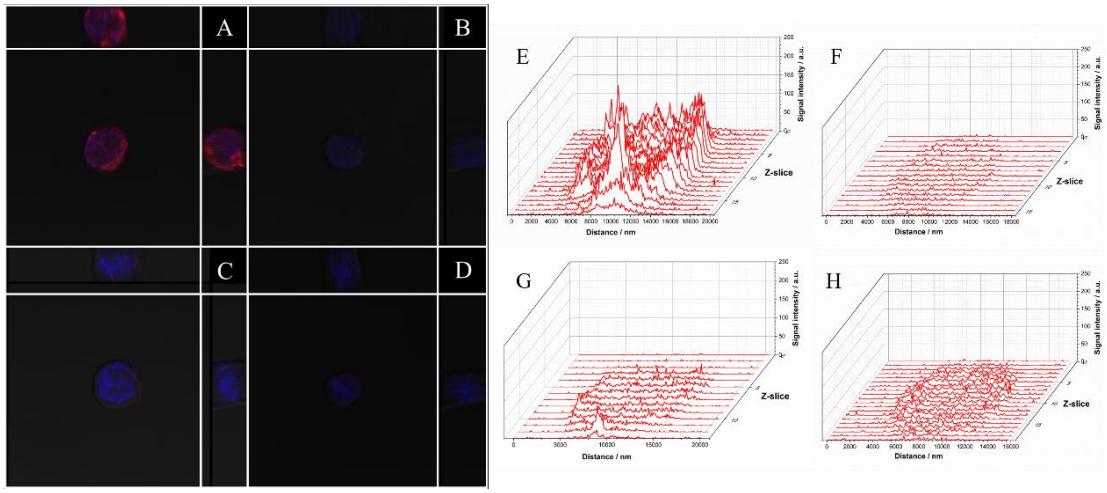

Figure 5.12. Representative confocal and light microscopy merged images (left) of mid-section Z-slices of HEK-293Tcells treated with (A) Q_{110}-*b*-D_{219}/dsRNA, (B) dsRNA, (B) Q_{110}-*b*-D_{219}, (C) dsRNA and (D) water. The images show the red fluorescence of Cy3-labelled dsRNA. DAPI was used as the mountant to stain the nuclei and can be seen fluorescing blue. Images are a representative sample of the cell population. Orthogonal projections are shown above and to the right of the primary image. Histogram profiles (right) of Cy3 fluorescence intensity, at each Z-slice across a horizontal middle line of cell images are shown for HEK-293T cells treated with (E) Q_{110}-*b*-D_{219}/dsRNA, (F) Q_{110}-*b*-D_{219} alone, (G) Cy3-labelled dsRNA and (H) nuclease-free water.

Orthogonal mid-section images of representative cells alongside histogram profiles mapping the Cy3 fluorescence intensity at each Z-slice confirm the perinuclear delivery of Cy3-labelled dsRNA when cells were incubated with Q_{110}-*b*-D_{219}/Cy3-labelled dsRNA. Figure 5.13 shows a cluster of HEK-293T cells after incubation with Q_{110}-*b*-D_{219}/Cy3-labelled dsRNA, further confirming the cellular uptake and perinuclear delivery.

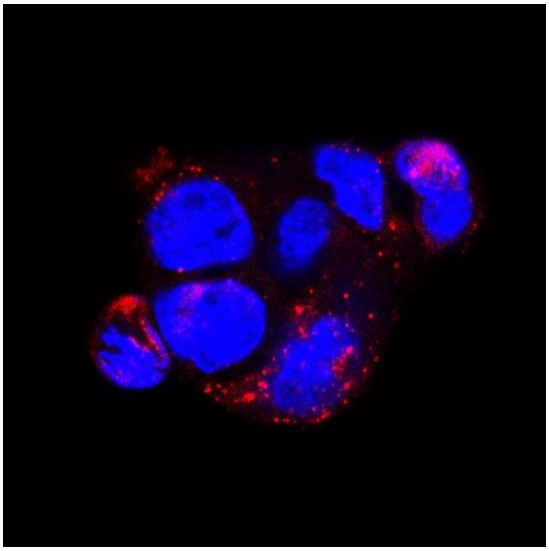

Figure 5.13. Confocal image of mid-section slice through a cluster of HEK-293T cells, showing DAPI staining of nuclei and Cy3 fluorescence of *vha26* dsRNA, following incubation of the cells with Q_{110}-*b*-D_{219}/Cy3-labelled dsRNA polyplexes.

The confocal images clearly identify that the Cy3-labelled dsRNA is confined within the plasma membrane and not simply adhering to the cell surface. The Cy3 signal mapping highlights the strong Cy3 signal in the cell incubated with Q_{110}-*b*-D_{219}/Cy3-labelled dsRNA polyplexes, suggesting an efficient uptake of Cy3-labelled dsRNA. The increase in Cy3 fluorescence intensity in HEK-293T cells, determined *via* flow cytometry assay, after incubation with Q_{110}-*b*-D_{219}/dsRNA polyplexes is therefore likely as a result of cell uptake. A much lower intensity of Cy3 fluorescence was recorded in cells treated with naked dsRNA, and no significant fluorescence was observed in cells treated with Q_{110}-*b*-D_{219} alone or when untreated (beyond the background auto-fluorescence of the cells). The more efficient cellular uptake of dsRNA to the cell cytoplasm when delivered as part of a polyplex, in comparison to free dsRNA, is likely due to the positive charge of the polyplexes (when formulated at N/P ratio > 1), as electrostatic repulsion from the negative charges of the cell membrane has previously been described as a barrier to cell entry for dsRNA.[288,290]

There are few examples in literature of cell uptake studies using fluorescently labelled dsRNA polyplexes. A study by Christiaens *et al.* investigated the penetration of CF203 cells by FITC-

labelled poly(2-(aminoethyl) methacrylate-*co*-guanylated-methacrylate)/Cy3-labelled dsRNA polyplexes.[115] The authors discovered, similarly to the results described here, the perinuclear localisation of dsRNA when delivered *via* complexation with polymer, in comparison to only a small proportion of dsRNA that was internalised when incubated with cells alone. They also found that the FITC labelled-polymer was located in the outer region of the cytoplasm, close to the cell membrane. Future work in this area should explore co-localisation techniques, such as Förster resonance energy transfer (FRET), to discover under which conditions the polymer and dsRNA remain complexed/decomplexed.

5.4.5 Complexation of dsRNA with diblock copolymer for *in vitro* mRNA degradation in transformed Sf9 cells

To verify the cellular internalisation of polyplexes in an insect-specific cell line and to test their capability to induce specific mRNA degradation, transformed Sf9 cells (Oxford Expression Technologies Ltd) were cultured for a luciferase protein assay (in collaboration with Dr. J. Y. Rho and Prof. S. Perrier at the University of Warwick). The transformed Sf9 cells included luciferase and eGFP genes, allowing for specific degradation of luciferase mRNA by luciferase-specific dsRNA without affecting eGFP expression. The reporter system had been previously optimised in Sf9 cells; hence these were used rather than the more relevant *Drosophila* S2 cells.

The diblock copolymer, Q_{110}-*b*-D_{219}, was tested as the most promising polymer construct. The amount of luciferase protein produced in the transformed Sf9 cells, following incubation with Q_{110}-*b*-D_{219}/dsRNA (assessed using both long and short luciferase dsRNA) polyplexes at N/P ratio 0.25 – 5, naked long and short luciferase dsRNA (N/P ratio = 0, used as a negative control), or GeneJuice® (used as a positive control) is highlighted in Figure 5.14A with eGFP expression in the same Sf9 cells shown in Figure 5.14B. The protein production in cells without treatment (CO) are also shown as an additional control.

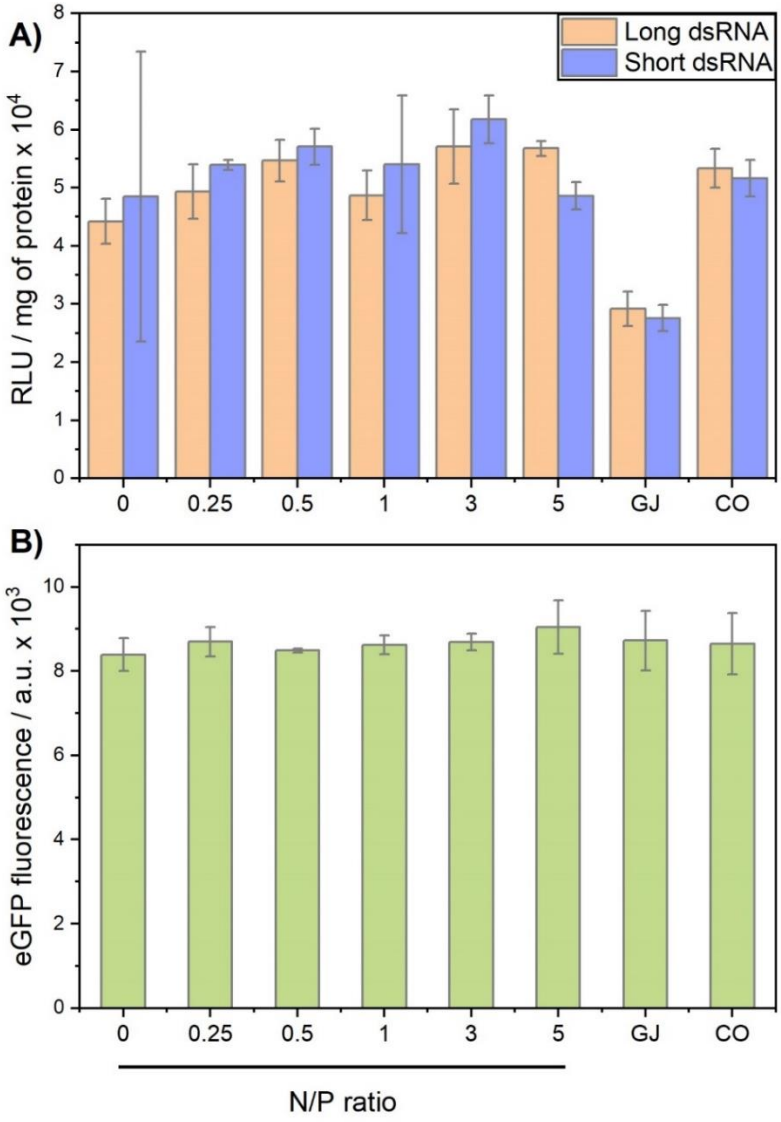

Figure 5.14. (A) Luciferase relative protein production and (B) eGFP expression in transformed Sf9 cells, either untreated (CO) or after incubation with GeneJuice® (GJ), long and short luciferase dsRNA (N/P ratio = 0, negative control), or polyplexes prepared with long/short luciferase dsRNA at N/P ratios from 0.25 – 5.

Figure 5.14B provides assurance that total protein production was not affected by the luciferase dsRNA, with eGFP expression remaining high in all cases without significant difference in expression across the different samples.

Both naked dsRNA (N/P ratio = 0, negative control) and the polyplexes (N/P ratios = 0.25 – 5) did not significantly reduce the luciferase protein production in comparison to the positive

control, GeneJuice®. These results indicate that the release/decomplexation of dsRNA from the polyplexes may not be very efficient, as cellular internalisation of the polyplexes in HEK-293T cells (at an N/P ratio = 5) was far superior than that of naked dsRNA, yet there was no reduction in luciferase protein production induced by the polyplexes, which would have indicated significant degradation of target luciferase mRNA in cells.

5.4.6 Complexation with diblock copolymer enhances uptake of dsRNA *in vivo*

The effectiveness of polyplexes for *in vivo* delivery of dsRNA to *D. suzukii* was studied using larval and pupal toxicity as a surrogate readout. *Drosophila* diet was mixed with polyplex formulations (at an N/P ratio = 5), naked *vha26* dsRNA, polymer alone, or nuclease-free water (untreated). Early instar (L1/L2) larvae were starved for 3 h before transfer to the various treated diets for 24 h and then monitored on fresh, untreated diet for 15 days. The oral feeding process is described visually in Figure 5.15.

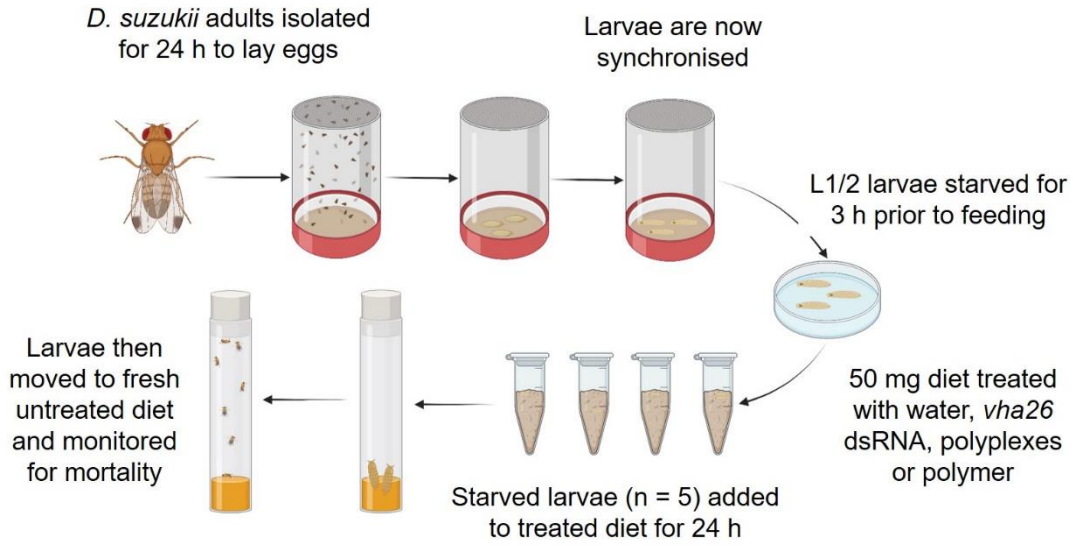

Figure 5.15. Schematic description of the oral feeding protocol for *Drosophila*. The adult flies (male and female) were allowed to mate for 24 h in a feeding chamber, before removal to produce synchronised eggs and subsequently larvae. The larvae were taken at an early 1st/2nd instar (L1/L2) stage for maximum feeding capacity and starved on moist filter paper for 3 h prior to transferral to treated or untreated artificial diet. Five larvae were placed onto 50 mg of diet for 24 h, before removal to fresh artificial (untreated) diet. The *D. suzukii* were then monitored for 15 days for survival. Image produced in BioRender.

The normalised (with respect to untreated diet-fed *D. suzukii* or *D. melanogaster*) survival rate of *D. suzukii* (or *D. melanogaster*) is shown in Figure 5.16. Mortality was scored by the number of L1/L2 larvae that failed to reach the pupal stage of development.

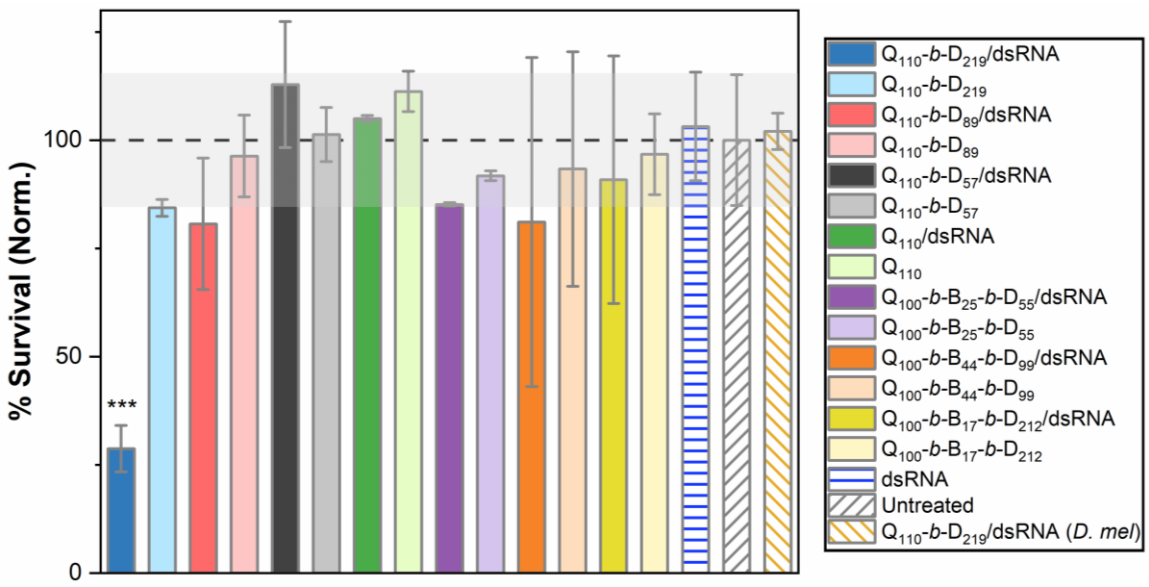

Figure 5.16. Survival of *D. suzukii* after feeding larvae (L1/L2) for 24 h on a diet treated with polyplexes, naked dsRNA or polymers alone, as well as survival of *D. melanogaster* larvae (L1/L2) when diet was treated with Q_{110}-*b*-D_{219}/dsRNA polyplex. Survival was assessed over 15 days by the failure to reach the pupal stage, and the absence of any live larvae in or on the surface of the food. Results were normalised against larvae fed on diet treated with nuclease-free water (untreated). Error bars represent standard deviation, and the grey box represents the standard deviation of the survival of larvae fed diet treated with nuclease-free water (untreated), n = 50. *** indicates a P value ≤ .0001 according to binary logistic regression.

A significantly decreased survival was observed in *D. suzukii* larvae treated with Q_{110}-*b*-D_{219}/dsRNA polyplexes, to ~30%. In contrast, larvae fed diet treated with polyplexes formed with homopolymer, diblock copolymers with shorter neutral block lengths or triblock copolymers, or larvae fed diet treated with naked dsRNA, polymers only, or nuclease-free water, did not show any significant effect on survival. It is important to note that the presence of polymer in the diet did not induce larval toxicity or visually prevent feeding. Binary logistic regression indicated a significant association between larvae fed Q_{110}-*b*-D_{219}/dsRNA polyplex-treated diet and survival to the pupal stage ($p \leq .0001$), with a substantial decrease in the odds of survival. No significant effect of feeding other complex-treated diets, naked dsRNA-treated diets or polymer only-treated diets, compared to untreated diet, was observed.

The *vha26* dsRNA used in this study was designed to specifically target *D. suzukii* V-ATPase subunit transcripts. As expected, feeding the Q_{110}-*b*-D_{219}/dsRNA polyplex to the closely-related species, *D. melanogaster*, did not result in any significant lethality, thus there is no off-target toxicity on this species.

Whilst feeding naked dsRNA generates systemic RNAi in some insect species (e.g. hemipterans), other species (e.g. dipterans) are resistant to orally administered dsRNA.[40,48,51,55,72,77,335] Here, the larval toxicity assay confirms a previous report that feeding naked *vha26* dsRNA alone to *D. suzukii* larvae does not result in significant mortality.[58] In contrast, larvae fed a diet treated with polyplexes prepared by complexation of *vha26* dsRNA with Q_{110}-*b*-D_{219}, resulted in high mortality (~70%). However, complexation with the other tested polymers (homopolymer, other diblock copolymers or triblock copolymers) did not increase mortality. It is worth noting that results for the assays with Q_{100}-*b*-B_{44}-*b*-D_{99}/dsRNA and Q_{100}-*b*-B_{44}-*b*-D_{99}-fed larvae were more variable. This is likely due to the nature of *in vivo* biological data, and is not presumed to be significant.

Whilst *in vivo* experimentation can lead to variable results (hence the need for repetition), the effect on survival was maintained when administering Q_{110}-*b*-D_{219}-based polyplexes and was shown to be statistically significant. These results indicate a potential correlation between the length of the diblock copolymer neutral block and the resulting toxicity. The research presented in Chapter 3 revealed that dsRNA-based polyplexes prepared with diblock copolymers of increasing neutral block length, resulted in the formation of more compact polyplexes (smaller effective hydrodynamic radii). Thus, we can speculate that the size of the Q_{110}-*b*-D_{219}/dsRNA polyplexes facilitates dsRNA uptake by the *D. suzukii* cells to elicit a strong RNAi response and larval lethality. This work adds to a body of research that suggests that the incorporation of a longer hydrophilic neutral polymer block can indeed enhance the delivery of nucleic acids.[289,298,309]

A further hypothesis is that the Q_{110}-*b*-D_{219}-based polyplexes appear to require (slightly) higher N/P ratios to induce full complexation, and the binding to Q_{110}-*b*-D_{219} did not appear to be as strong when visually assessed in agarose gel electrophoresis (Figure 3.17). This could suggest that the polyplexes formed with Q_{110}-*b*-D_{219} are able to decomplex more easily (in comparison to other complexes in this work) once cellular internalisation has occurred, thus the dsRNA can more readily participate in the RNAi machinery.

These hypotheses are corroborated by Kim *et al.*, who investigated the delivery of pDNA by combinations of α-poly(L-lysine) (strongly binding) and ε-poly(L-lysine) (weakly binding) polymers.[336] They discovered that smaller, more compact polyplexes were able to deliver more pDNA to cells, and they also found that polyplexes that were too tightly bound resulted in poor release of pDNA and low transfection efficiencies. This could further explain the results from the luciferase protein study, in which Q_{110}-*b*-D_{219}-based polyplexes were not found to be effective at degrading mRNA, despite enhanced *in vitro* uptake demonstrated in HEK-293T cells. These results highlight the importance of block copolymer design, as the size of the resulting complexes and decomplexation capability of the complexing-polymer are clearly important properties for successful induction of RNAi. Therefore, future work should focus on exploring alternative polymer designs to produce smaller-sized polyplexes (e.g. investigating longer neutral block lengths) and polymers with decomplexation capabilities (e.g. incorporation of a self-hydrolysing cationic polymer block).

5.4.1 *In vivo D. suzukii* gut imaging

In order to begin to interpret the successful induced mortality of *D. suzukii* larvae following consumption of a diet treated with Q_{110}-*b*-D_{219}-based polyplexes, in comparison to the lack of toxicity associated with the oral feeding of *vha26* dsRNA, the *in vivo* delivery of Cy3-labelled *vha26* dsRNA (either naked, or complexed to Q_{110}-*b*-D_{219}) to 3rd instar (L3) *D. suzukii* larvae

was investigated *via* fluorescence microscopy/confocal laser scanning microscopy of the insect guts.

A time-resolved study was conducted, feeding L3 larvae for 1 h, 4 h and 24 h, to investigate the journey of the dsRNA through the gut during the entire feeding protocol (oral feeding was conducted over a 24 h period). Figure 5.17A shows light and fluorescence microscopy images of L3 gut sections following feeding with Cy3-labelled dsRNA with or without complexation to Q_{110}-*b*-D_{219}, at 1 h, 4 h, and 24 h time-points.

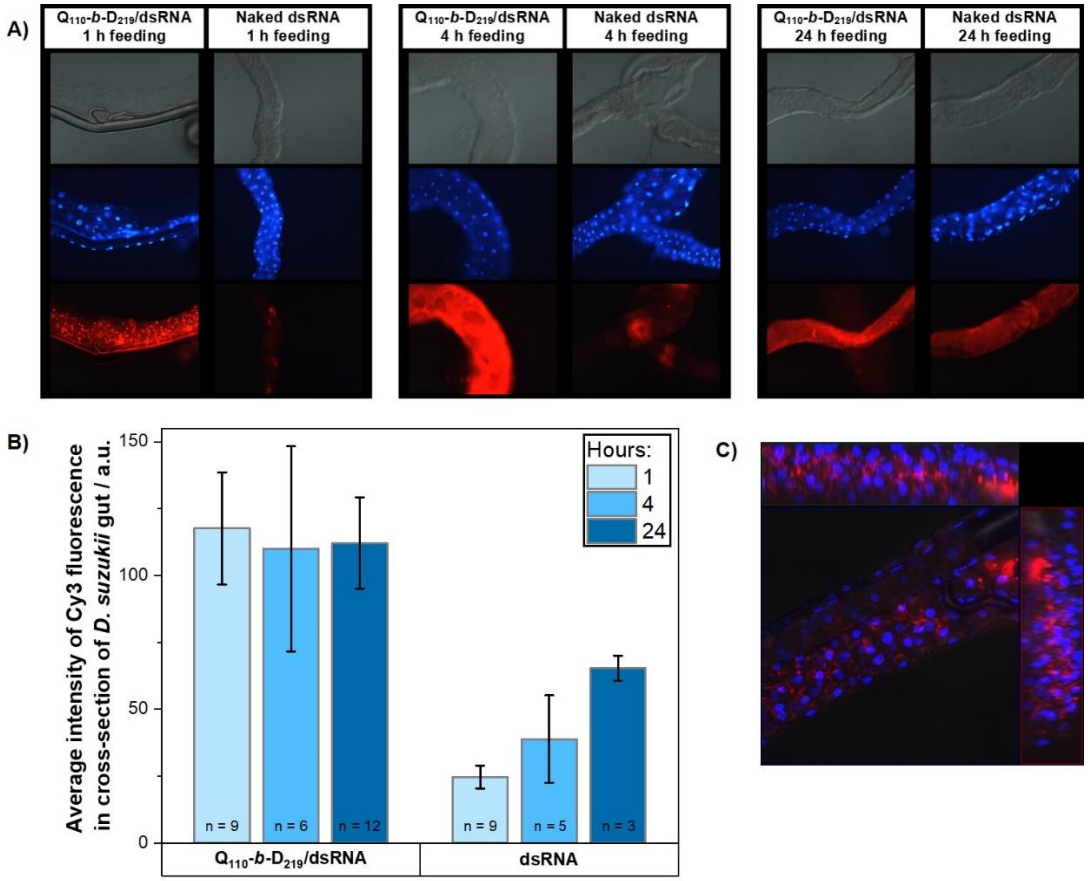

Figure 5.17. (A) Time-resolved images of Cy3-labelled dsRNA feeding assay. Each figure shows light microscopy images (top), DAPI-staining (middle) and Cy3 fluorescence (bottom). On the left-hand side of each figure is the guts from *D. suzukii* larvae fed Q_{110}-*b*-D_{219}/dsRNA polyplex, and the right-hand side of each figure is the guts from larvae fed dsRNA alone. 1 h, 4 h and 24 h feeding time-points are shown, with increasing time moving from left to right. Identical microscope settings (e.g. exposure time) were used throughout image gathering between samples. (B) Average Cy3 fluorescence intensity measured across gut sections (of fluorescence microscopy images, as shown in (A)) of *D. suzukii* L3 larvae fed either Q_{110}-*b*-D_{219}/dsRNA polyplexes or Cy3-labelled dsRNA. The number of total images used to generate the average intensity is indicated by the 'n' number, and standard deviation is shown by error bars. (C) Confocal microscopy image in middle section of the gut of *D. suzukii* L3 larvae, following 1 h feeding with Q_{110}-*b*-D_{219}/dsRNA polyplex with Cy3-labelled dsRNA. Orthogonal images are shown above and to the right of the central image.

Through the time-resolved study imaging, it appears that a greater amount of Cy3 (red) fluorescence is present in the guts of larvae fed Q_{110}-*b*-D_{219}/dsRNA polyplexes, with enhanced fluorescence particularly when feeding is conducted over a shorter time period.

Between 3 – 12 images were captured of larval guts for each time-point/treatment (fewer images were taken when little fluorescence could be identified), and these images were analysed for their fluorescence intensity across the gut section, perpendicular to the direction of the gut lumen (an example of how this was achieved in the Zeiss ZEN blue software is shown in Figure A11 in the Appendix). An average intensity was calculated across the range of gut images, and these averages are presented in Figure 5.17B. These results complement the images in Figure 5.17A, suggesting that feeding L3 larvae Q_{110}-*b*-D_{219}/dsRNA polyplexes enhances the Cy3 fluorescence detected in the larval guts at all time-points. When Cy3-labelled dsRNA was not complexed, the intensity of fluorescence in the larval guts increased as feeding occurred for longer time periods (24 h, as opposed to 1 or 4 h).

Confocal microscopy was used to image the larval gut sections, Figure 5.17C, to assess whether the Cy3-labelled dsRNA was simply remaining in the gut lumen or entering into the gut cells. Whilst the fluorescence appears to surround the gut cells, it is challenging to confirm whether cellular uptake has truly occurred. However it can be confirmed that the fluorescence is, at the very least, confined within the gut lumen. It can thus be concluded that the increased resistance of the Q_{110}-*b*-D_{219}/dsRNA polyplexes to degradation leads to longer retention in the gut lumen, and the extensive dsRNA breakdown (when dsRNA is un-protected) results in faster excretion in the faeces. Further investigation is required to confirm whether the dsRNA is transported from the gut lumen to the gut cells successfully, and whether this differs from the transport of dsRNA within the other polyplex formulations.

5.5 Conclusion

In this chapter, the delivery of *Drosophila suzukii*-specific double-stranded RNA for bio-insecticidal application using a hydrophilic diblock copolymer has been demonstrated, for the first time.

A polycationic homopolymer, a series of hydrophilic diblock copolymers, and a series of amphiphilic triblock copolymers were assessed. The previous Chapters 3 and 4 demonstrated the use of agarose gel electrophoresis to identify the optimal N/P ratio for full complexation, which indicated that an N/P ratio ≥ 2 was required for sufficient complexation of the polymers with 222bp *vha26* dsRNA. In this chapter, agarose gel electrophoresis assays showed the effective protection of dsRNA against *ex vivo* degradation by *D. suzukii* gut enzymes from adult flies and 3rd instar larvae, through complexation with each of the polymers.

Delivery of Cy3-labelled dsRNA was successfully shown *in vitro* in HEK-293T cells through flow cytometry, with confocal laser scanning microscopy confirming the perinuclear localisation of the dsRNA when complexed to the diblock copolymer, Q_{110}-*b*-D_{219}. The promising construct, Q_{110}-*b*-D_{219}, was explored to identify whether its complexation with luciferase dsRNA could induce specific mRNA degradation of luciferase mRNA in transformed Sf9 cells. However, there was not a significant decrease in luciferase protein production following the application of naked dsRNA or Q_{110}-*b*-D_{219}-based polyplexes.

In vivo orally administered naked *vha26* dsRNA to early instar *D. suzukii* larvae, as expected, did not induce RNAi to significantly affect the survival rates of larvae to pupal or adult eclosion stages. However, upon complexation of the dsRNA to the diblock copolymer, Q_{110}-*b*-D_{219}, the orally administered formulation induced a statistically significant decrease in the survival of the *D. suzukii* larvae. No off-target effects were observed when *D. melanogaster* larvae were fed Q_{110}-*b*-D_{219}/dsRNA, and *in vivo* gut imaging confirmed that the Q_{110}-*b*-D_{219} polymer enhances the retention of dsRNA in the gut lumen, preventing the degradation and rapid excretion of dsRNA in the faeces. Complexation of *vha26* dsRNA with other block copolymers did not result in an enhanced mortality of the *D. suzukii*. This suggests that the size of polyplexes has an impact on the efficacy of dsRNA delivery in *D. suzukii*, as Q_{110}-*b*-D_{219} was previously shown to form the most compact polyplexes. It also might suggest that the decomplexation capability of dsRNA from block copolymers plays an important role in

inducing effective RNAi, as Q_{110}-*b*-D_{219}/dsRNA polyplexes were previously found to complex less efficiently with dsRNA, requiring higher N/P ratios for full complexation. Referring back to Figure 4.1 (coarse-grained simulation by Zhan *et al.*[263]), the predicted structure of the triblock copolymer/dsRNA complexes does not appear to provide additional protection to the dsRNA, any more than that of a homopolymer (Figure 3.1). Hence, this could explain the low *in vivo* efficacy of triblock copolymer-based polyplexes in this thesis.

These results suggest that hydrophilic diblock copolymers are promising candidates for the complexation, protection and delivery of dsRNA for bio-insecticidal applications, but that optimisation of the polymer composition (particularly the stabilising, neutral polymer block) is required for successful RNAi *in vivo*.

Conclusions and Future Outlook

5.6 Conclusions

The overarching aim of the research conducted for this thesis was to design, synthesise, characterise, and biologically assess block copolymers, for their ability to complex with and protect species-specific double-stranded RNA for insecticidal RNA interference in *Drosophila suzukii*.

In Chapter 3, aqueous RAFT (co)polymerisation was used to prepare a polycationic PQDMAEMA (Q) homopolymer, a portion of which was subsequently chain-extended with PDMAm (D), acting as a neutral polymer block, to create a series of hydrophilic diblock copolymers in a fast, efficient, and cost-effective synthesis. Polymer characterisation was carried out using ^{1}H NMR spectroscopy and gel permeation chromatography, which revealed that quaternised poly(2-dimethylamino)ethyl methacrylate-*block*-poly(*N*,*N*-dimethyl acrylamide) (Q-*b*-D) diblock copolymers can be synthesised to high conversion with moderate levels of dispersity. Dynamic light scattering (DLS), electrophoretic mobility measurements and fluorescence spectroscopy were used to characterise the complexation between *vha26* dsRNA (species-specific to *Drosophila suzukii*) and homopolymer/diblock copolymer in terms of size, surface charge, binding ability and stability in the presence of increasing salt concentration. The homopolymer and the series of diblock copolymers were able to electrostatically interact with dsRNA to form distinct polyplexes that were fully complexed above an N/P ratio = 1. The neutral polymer block, D, enhanced the colloidal stability of the polyplexes when formulated close to the isoelectric point, likely by providing steric stabilisation to avoid aggregation and precipitation (as observed when complexing the dsRNA at N/P ratio = 1 to the homopolymer alone). It was discovered that, as the length of the neutral polymer block was increased, more compact polyplexes (with smaller apparent hydrodynamic radii) were formed over the N/P ratio range 1 – 10. In the presence of high salt concentrations,

and when formulating polyplexes using different lengths of dsRNA, which is valuable when exploring alternative mRNA transcript targets, the hydrophilic diblock copolymer with the longest length of neutral polymer block (1:2 cationic to neutral block) remained the most stable. The Q_{110}-*b*-D_{219} polymer was stable, with no significant aggregation or decomplexation, until C_{NaCl} = 500 mM, and it was also able to complex with dsRNAs of different lengths, forming monodisperse, compact polyplexes with hydrodynamic radii 49 – 85 nm. Agarose gel electrophoresis and fluorescence spectroscopy were used to explore the protection of dsRNA provided by the homopolymer and diblock copolymers, against degradation by the synthetic enzyme, RNase A. When prepared at an N/P ratio to provide full complexation (N/P ratio ≥ 2), polyplexes formed with homopolymer or diblock copolymer were all able to protect *vha26* dsRNA against enzymatic degradation.

In Chapter 4, careful consideration and selection of solvent and purification conditions ensured the synthesis of a series of linear, amphiphilic triblock copolymers by RAFT polymerisation, to high conversion. The quaternised poly(2-dimethylamino)ethyl methacrylate macro-chain transfer agent (macro-CTA) was synthesised first (Q), followed by chain extension with a hydrophobic polymer block, poly(*tert*-butyl acrylamide) (B). The amphiphilic diblock copolymer, quaternised poly(2-dimethylamino)ethyl methacrylate-*block*-poly(*tert*-butyl acrylamide) (Q-*b*-B), was isolated and purified before acting as a new macro-CTA for chain extension with the neutral polymer block, poly(*N*,*N*-dimethyl acrylamide) (D). Different degrees of polymerisation were targeted with each polymer block to alter the amphiphilicity across the series. Following purification and lyophilisation, the poly(2-dimethylamino)ethyl methacrylate-*block*-poly(*tert*-butyl acrylamide)-*block*-poly(*N*,*N*-dimethyl acrylamide) (Q-*b*-B-*b*-D) triblock copolymers were characterised alone in aqueous solution using DLS, transmission electron microscopy (TEM), and electrophoretic mobility measurements. The triblock copolymers self-assembled in aqueous solution, with the smallest and least polydisperse structures formed by the triblock copolymer with the longest neutral polymer block. Through the introduction of *vha26* dsRNA, the triblock copolymers underwent

significant chain rearrangement to form less spherical polyplexes with smaller apparent hydrodynamic radii. The triblock copolymer with the longest hydrophobic polymer block appeared to induce the strongest binding to dsRNA, however, the resulting polyplexes were the least stable in the presence of increasing salt concentration. The triblock copolymers with the longer hydrophilic polymer blocks enhanced the stability of the polyplexes, preventing aggregation and decomplexation until C_{NaCl} = 700 mM. In addition, all three of the triblock copolymers showed greater size consistency and lower polydispersity when complexed with dsRNA of varying lengths, in comparison to the polyplexes prepared in Chapter 3. All of the amphiphilic triblock copolymers were able to successfully protect *vha26* dsRNA from degradation by the synthetic enzyme, RNase A, when fully complexed at N/P ratio ≥ 2.

In Chapter 5, the polycationic homopolymer, series of hydrophilic diblock copolymers and series of ABC linear, amphiphilic triblock copolymers were assessed in biologically relevant environments, to investigate their ability to perform as polymeric delivery vehicles for dsRNA as RNAi-induced species-specific *Drosophila suzukii* control agents. The gut enzymes from *D. suzukii* adult flies and late stage 3rd instar (L3) larvae were extracted through dissection and tissue homogenisation. *Ex vivo* protection of *vha26* dsRNA was determined through agarose gel electrophoresis of the polyplexes following incubation with the gut enzymes. Naked *vha26* dsRNA was fully degraded by adult gut enzymes after 30 min incubation, and L3 larvae gut enzymes after 24 h. When polyplexes were incubated with gut enzymes for 30 min or 24 h for adult and L3 larvae gut enzymes, respectively, the *vha26* dsRNA was protected against enzymatic degradation. *In vitro* studies followed the *ex vivo* assays, beginning by ascertaining cell viability with increasing polymer concentration in mammalian HEK-293T and insect Sf9 cells. Using MTS assays, it was found that the polymers did not significantly affect the cell viability at concentrations < 1 mg mL^{-1}. Flow cytometry and confocal laser scanning microscopy were then used to identify the cellular uptake of polyplexes in HEK-293T cells. *Vha26* dsRNA was labelled with the fluorophore Cy3, and complexed with each polymer before incubating with HEK-293T cells. Flow cytometry revealed an enhanced Cy3

fluorescence of cells when incubated with polyplexes, in comparison to cells incubated with naked Cy3-labelled dsRNA alone. Over 75% of the single, live cells, incubated with polyplexes exhibited this enhanced fluorescence. Q_{110}-*b*-D_{219}, used as an example, was incubated as a polyplex with Cy3-labelled dsRNA with HEK-293T cells before confocal microscopy imaging. This identified the perinuclear localisation of the Cy3-labelled dsRNA in the HEK-293T cells when complexed to polymer, and thus cellular internalisation was confirmed. A transformed Sf9 cell line, possessing eGFP and luciferase genes, was used to measure luciferase protein production following incubation with long and short luciferase dsRNA. When delivered alone or in Q_{110}-*b*-D_{219}-based polyplexes, neither the long nor short luciferase dsRNA significantly decreased luciferase protein production. This suggests that the release of dsRNA from these polyplexes may not be very efficient, as cellular internalisation of the polyplexes in HEK-293T cells was superior to that of naked dsRNA, yet the polyplexes failed to significantly reduce luciferase protein production in comparison to the positive control. Following *in vitro* studies, an *in vivo* environment was explored. Oral feeding of *Drosophila suzukii* and the closely related species *Drosophila melanogaster* was performed, by feeding 1st and 2nd instar early stage larvae diet treated by mixing with polyplexes (at an N/P ratio of 5), naked *vha26* dsRNA, or the polymers alone. It was discovered that *only* the Q_{110}-*b*-D_{219}-based polyplexes, the hydrophilic diblock copolymer with the longest neutral polymer block, induced a significant decrease in larvae survival, with mortality reaching ~70%. In contrast, upon feeding diet treated with Q_{110}-*b*-D_{219}/dsRNA polyplexes to *D. melanogaster*, no significant impact on survival, and therefore no off-target toxicity, was observed. These results indicate that the compactness of the polyplexes could play a significant role in the successful *in vivo* delivery of dsRNA, as the Q_{110}-*b*-D_{219}/dsRNA polyplexes were found to form complexes with the smallest hydrodynamic radius. It could also be the case that more rod-like morphologies lead to enhanced delivery of dsRNA, as the Q_{110}-*b*-D_{219}/dsRNA polyplexes were found to form less spherical structures when investigated using SLS and TEM. In addition, Q_{110}-*b*-D_{219} appeared to require higher N/P ratios (i.e. more polymer chains) to fully complex with dsRNA, perhaps indicating a weaker binding and thus an increased

likelihood of decomplexation after cell penetration (in comparison to other complexes in this work). *In vivo* gut imaging of L3 larvae fed Q_{110}-*b*-D_{219}/Cy3-labelled dsRNA and naked Cy3-labelled dsRNA revealed that Q_{110}-*b*-D_{219} enhances the presence of Cy3-labelled dsRNA in the gut lumen. This indicates that the protection of dsRNA by Q_{110}-*b*-D_{219} against degradation leads to longer retention in the gut lumen, with the degradation of naked dsRNA resulting in faster excretion.

5.7 Future Outlook

Whilst the research conducted throughout this thesis has contributed to an enhanced knowledge base in some areas, it has, as expected, opened up many further questions. The homopolymer, diblock copolymers and triblock copolymers synthesised in this work indeed successfully protect dsRNA against enzymatic degradation; however, they do not consistently influence the survival of *D. suzukii* following oral feeding. This could be due to the strong complexation of the permanently charged cationic groups, preventing decomplexation within the cells so that the dsRNA cannot take part in the RNAi mechanism to induce mRNA degradation. Synthesis of block copolymers with the capability to release dsRNA once the target location has been reached is highly desirable. For example, Cook *et al.* synthesised branched polymers with a self-hydrolysing polymer group. The polymers charge density reduces over time, resulting in the slow release of dsRNA.[116] Preparation of polymers with monomers that can decrease the interaction strength with dsRNA within cells would prove invaluable. In addition, it is important for future work to be mindful of the persistence of the synthesised polymers within the environment after their application. Incorporation of a biodegradation mechanism, and the use of more renewable materials, would significantly lessen the environmental impact of the formulations.[337,338]

Synthesising carefully designed block copolymers allows the precise manufacture of polymers with desired functionalities; however, this process can be laborious and slow. Kumar *et al.*, with a focus on therapeutic applications, have reported their use of machine learning to screen a combinatorial polymer library for effective pDNA delivery, creating a set of design rules for future polymer synthesis.[339] Following a similar approach for agrochemical applications would be worthwhile to enable a more rapid assessment of polymer viability and identify beneficial polymer properties more efficiently.

Being able to specifically identify the co-localisation of polymeric delivery vehicles and their cargo (i.e. dsRNA) would be advantageous. In the case of polyplexes, one would be able to determine under which conditions (for example, the presence of competing ions or adjuvants, or under varying pH) the polymer and dsRNA remain complexed, and where, in *in vitro* or *in vivo* environments, the dsRNA is receiving protection provided by the polymer. Gómez-Varela *et al.* have developed fluorescence cross-correlation spectroscopy (FCCS) methods as a tool to assess the degree of association between liposomes and pDNA, as well as size of the lipoplexes.[340] Utilising either FCCS or a Förster resonance energy transfer (FRET) system (with Cy5 covalently attached to the polymer, alongside Cy3-labelled dsRNA), would aid the identification of the co-localisation of the polymer and dsRNA, opening up a plethora of new insights.

References

1 M. Hauser, A historic account of the invasion of Drosophila suzukii (Matsumura) (Diptera: Drosophilidae) in the continental United States, with remarks on their identification, *Pest Management Science*, 2011, **67**, 1352–1357.

2 CABI: Invasive Species Compendium, https://www.cabi.org/isc/datasheet/109283#C5BAAABC-FCFC-41A8-8B47-609B6182DB37, (accessed 20 July 2022).

3 Lifemap: NCBI Version, https://lifemap-ncbi.univ-lyon1.fr/?tid=28584.

4 M. K. Asplen, G. Anfora, A. Biondi, D.-S. Choi, D. Chu, K. M. Daane, P. Gibert, A. P. Gutierrez, K. A. Hoelmer, W. D. Hutchison, R. Isaacs, Z.-L. Jiang, Z. Kárpáti, M. T. Kimura, M. Pascual, C. R. Philips, C. Plantamp, L. Ponti, G. Vétek, H. Vogt, V. M. Walton, Y. Yu, L. Zappalà and N. Desneux, Invasion biology of spotted wing Drosophila (Drosophila suzukii): a global perspective and future priorities, *J Pest Sci*, 2015, **88**, 469–494.

5 S. Tochen, D. T. Dalton, N. Wiman, C. Hamm, P. W. Shearer and V. M. Walton, Temperature-Related Development and Population Parameters for Drosophila suzukii (Diptera: Drosophilidae) on Cherry and Blueberry, *Environmental Entomology*, 2014, **43**, 501–510.

6 J. C. Lee, X. Wang, K. M. Daane, K. A. Hoelmer, R. Isaacs, A. A. Sial and V. M. Walton, Biological Control of Spotted-Wing Drosophila (Diptera: Drosophilidae)—Current and Pending Tactics, *J Integr Pest Manag*, , DOI:10.1093/jipm/pmz012.

7 H. K. Dweck, G. J. Talross, W. Wang and J. R. Carlson, Evolutionary shifts in taste coding in the fruit pest Drosophila suzukii, *eLife*, 2021, **10**, e64317.

8 R. E. Goodhue, M. Bolda, D. Farnsworth, J. C. Williams and F. G. Zalom, Spotted wing drosophila infestation of California strawberries and raspberries: economic analysis of potential revenue losses and control costs, *Pest Management Science*, 2011, **67**, 1396–1402.

9 M. P. Bolda, R. E. Goodhue and F. G. Zalom, Spotted Wing Drosophila: Potential Economic Impact of a Newly Established Pest, *Giannini Foundation of Agricultural Economics, University of California*, 5–8.

10 D. B. Walsh, M. P. Bolda, R. E. Goodhue, A. J. Dreves, J. Lee, D. J. Bruck, V. M. Walton, S. D. O'Neal and F. G. Zalom, Drosophila suzukii (Diptera: Drosophilidae): Invasive Pest of Ripening Soft Fruit Expanding its Geographic Range and Damage Potential, *J Integr Pest Manag*, 2011, **2**, G1–G7.

11 G. De Ros, G. Anfora, A. Grassi and C. Ioriatti, The potential economic impact of Drosophila suzukii on small fruits production in Trentino (Italy)., *The potential economic impact of Drosophila suzukii on small fruits production in Trentino (Italy).*, 2013, **91**, 317–321.

12 Expert Working Group for performing PRA on Drosophila suzukii, https://www.eppo.int/MEETINGS/2010_meetings/https%3A%2F%2Fwww.eppo.int%2FMEETINGS%2F2010_meetings%2Fp_ewg_drosophila_suzukii, (accessed 28 November 2022).

13 M. A. Rogers, E. C. Burkness and W. D. Hutchison, Evaluation of high tunnels for management of Drosophila suzukii in fall-bearing red raspberries: Potential for reducing insecticide use, *J Pest Sci*, 2016, **89**, 815–821.

14 C. Small, I. Paddibhatla, R. Rajwani and S. Govind, An Introduction to Parasitic Wasps of Drosophila and the Antiparasite Immune Response, *J Vis Exp*, 2012, 3347.

15 C. Kim-Jo, J.-L. Gatti and M. Poirié, Drosophila Cellular Immunity Against Parasitoid Wasps: A Complex and Time-Dependent Process, *Frontiers in Physiology*.

16 B. J. M. Häussling, J. Lienenlüke and J. Stökl, The preference of Trichopria drosophilae for pupae of Drosophila suzukii is independent of host size, *Sci Rep*, 2021, **11**, 995.
17 B. E. Gress and F. G. Zalom, Identification and risk assessment of spinosad resistance in a California population of Drosophila suzukii, *Pest Management Science*, 2019, **75**, 1270–1276.
18 A. Singla, H. Barmota, S. Kumar Sahoo and B. Kaur Kang, Influence of neonicotinoids on pollinators: A review, *Journal of Apicultural Research*, 2021, **60**, 19–32.
19 E. Oerke, Crop losses to pests, *The Journal of Agricultural Science*, 2006, **144**, 31–43.
20 S. Chakraborty and A. C. Newton, Climate change, plant diseases and food security: an overview, *Plant Pathology*, 2011, **60**, 2–14.
21 B. Borel, Resistance is exhausting the agricultural arsenal against insects, weeds and disease. New biological approaches could help., *Nature*, 2017, **543**, 302–304.
22 S. Sharma, R. Kooner and R. Arora, in *Breeding Insect Resistant Crops for Sustainable Agriculture*, eds. R. Arora and S. Sandhu, Springer, Singapore, 2017, pp. 45–66.
23 Arthropod Pesticide Resistance Database, https://www.pesticideresistance.org/index.php, (accessed 7 May 2020).
24 B. E. Tabashnik, D. Mota-Sanchez, M. E. Whalon, R. M. Hollingworth and Y. Carrière, Defining Terms for Proactive Management of Resistance to Bt Crops and Pesticides, *J Econ Entomol*, 2014, **107**, 496–507.
25 T. C. Sparks and R. Nauen, IRAC: Mode of action classification and insecticide resistance management, *Pesticide Biochemistry and Physiology*, 2015, **121**, 122–128.
26 D. Mota-Sanchez and J. C. Wise, ESA, 2017.
27 M. J. Windley, V. Herzig, S. A. Dziemborowicz, M. C. Hardy, G. F. King and G. M. Nicholson, Spider-Venom Peptides as Bioinsecticides, *Toxins (Basel)*, 2012, **4**, 191–227.
28 E. Y. T. Nakasu, S. M. Williamson, M. G. Edwards, E. C. Fitches, J. A. Gatehouse, G. A. Wright and A. M. R. Gatehouse, Novel biopesticide based on a spider venom peptide shows no adverse effects on honeybees, *Proceedings of the Royal Society B: Biological Sciences*, 2014, **281**, 20140619.
29 S. D. Frank and J. F. Tooker, Opinion: Neonicotinoids pose undocumented threats to food webs, *PNAS*, , DOI:10.1073/pnas.2017221117.
30 W. H. McGaughey, Problems of insect resistance to Bacillus thuringiensis, *Agriculture, Ecosystems & Environment*, 1994, **49**, 95–102.
31 J. G. Scott, Unraveling the mystery of spinosad resistance in insects, *Journal of Pesticide Science*, 2008, **33**, 221–227.
32 A. Bravo, S. Likitvivatanavong, S. S. Gill and M. Soberón, Bacillus thuringiensis: A story of a successful bioinsecticide, *Insect Biochemistry and Molecular Biology*, 2011, **41**, 423–431.
33 M. S. T. Abbas, Genetically engineered (modified) crops (Bacillus thuringiensis crops) and the world controversy on their safety, *Egyptian Journal of Biological Pest Control*, 2018, **28**, 52.
34 V. S. V. Santos and B. B. Pereira, Properties, toxicity and current applications of the biolarvicide spinosad, *Journal of Toxicology and Environmental Health, Part B*, 2020, **23**, 13–26.
35 J. G. Scott, K. Michel, L. C. Bartholomay, B. D. Siegfried, W. B. Hunter, G. Smagghe, K. Y. Zhu and A. E. Douglas, Towards the elements of successful insect RNAi, *J. Insect Physiol.*, 2013, **59**, 1212–1221.
36 E. Vogel, D. Santos, L. Mingels, T.-W. Verdonckt and J. V. Broeck, RNA Interference in Insects: Protecting Beneficials and Controlling Pests, *Front. Physiol.*, , DOI:10.3389/fphys.2018.01912.
37 O. Christiaens, S. Whyard, A. M. Vélez and G. Smagghe, Double-Stranded RNA Technology to Control Insect Pests: Current Status and Challenges, *Front. Plant Sci.*, , DOI:10.3389/fpls.2020.00451.
38 S. Yan, B. Ren, B. Zeng and J. Shen, Improving RNAi efficiency for pest control in crop species, *BioTechniques*, 2020, **68**, 283–290.

39 C. Khajuria, S. Ivashuta, E. Wiggins, L. Flagel, W. Moar, M. Pleau, K. Miller, Y. Zhang, P. Ramaseshadri, C. Jiang, T. Hodge, P. Jensen, M. Chen, A. Gowda, B. McNulty, C. Vazquez, R. Bolognesi, J. Haas, G. Head and T. Clark, Development and characterization of the first dsRNA-resistant insect population from western corn rootworm, Diabrotica virgifera virgifera LeConte, *PLOS ONE*, 2018, **13**, e0197059.
40 D. R. G. Price and J. A. Gatehouse, RNAi-mediated crop protection against insects, *Trends Biotechnol.*, 2008, **26**, 393–400.
41 H. Huvenne and G. Smagghe, Mechanisms of dsRNA uptake in insects and potential of RNAi for pest control: A review, *Journal of Insect Physiology*, 2010, **56**, 227–235.
42 A. Fire, S. Xu, M. K. Montgomery, S. A. Kostas, S. E. Driver and C. C. Mello, Potent and specific genetic interference by double-stranded RNA in Caenorhabditis elegans, *Nature*, 1998, **391**, 806–811.
43 D. Smith, A. C. Holley and C. L. McCormick, RAFT-synthesized copolymers and conjugates designed for therapeutic delivery of siRNA, *Polym. Chem.*, 2011, **2**, 1428–1441.
44 R. Katoch, A. Sethi, N. Thakur and L. L. Murdock, RNAi for Insect Control: Current Perspective and Future Challenges, *Appl Biochem Biotechnol*, 2013, **171**, 847–873.
45 M. R. Joga, M. J. Zotti, G. Smagghe and O. Christiaens, RNAi Efficiency, Systemic Properties, and Novel Delivery Methods for Pest Insect Control: What We Know So Far, *Front. Physiol.*, , DOI:10.3389/fphys.2016.00553.
46 N. Kunte, E. McGraw, S. Bell, D. Held and L.-A. Avila, Prospects, challenges and current status of RNAi through insect feeding, *Pest Management Science*, 2020, **76**, 26–41.
47 S. Liu, M. Jaouannet, D. A. Dempsey, J. Imani, C. Coustau and K.-H. Kogel, RNA-based technologies for insect control in plant production, *Biotechnology Advances*, 2020, **39**, 107463.
48 S. Whyard, A. D. Singh and S. Wong, Ingested double-stranded RNAs can act as species-specific insecticides, *Insect Biochemistry and Molecular Biology*, 2009, **39**, 824–832.
49 N. Yu, O. Christiaens, J. Liu, J. Niu, K. Cappelle, S. Caccia, H. Huvenne and G. Smagghe, Delivery of dsRNA for RNAi in insects: an overview and future directions, *Insect Science*, 2013, **20**, 4–14.
50 S. Kang, D. Shin, M. Y. Noh, J. S. Peters, C. T. Smartt, Y. S. Han and Y. S. Hong, Optimization of double-stranded RNAi intrathoracic injection method in Aedes aegypti, *Entomol Res*, 2018, **48**, 269–278.
51 J. A. Baum, T. Bogaert, W. Clinton, G. R. Heck, P. Feldmann, O. Ilagan, S. Johnson, G. Plaetinck, T. Munyikwa, M. Pleau, T. Vaughn and J. Roberts, Control of coleopteran insect pests through RNA interference, *Nat Biotechnol*, 2007, **25**, 1322–1326.
52 J. W. Pridgeon, L. Zhao, J. J. Becnel, D. A. Strickman, G. G. Clark and K. J. Linthicum, Topically Applied AaeIAP1 Double-Stranded RNA Kills Female Adults of Aedes aegypti, *Journal of Medical Entomology*, 2008, **45**, 414–420.
53 S. Whyard, C. N. Erdelyan, A. L. Partridge, A. D. Singh, N. W. Beebe and R. Capina, Silencing the buzz: a new approach to population suppression of mosquitoes by feeding larvae double-stranded RNAs, *Parasites & Vectors*, 2015, **8**, 96.
54 N. Killiny, S. Hajeri, S. Tiwari, S. Gowda and L. L. Stelinski, Double-Stranded RNA Uptake through Topical Application, Mediates Silencing of Five CYP4 Genes and Suppresses Insecticide Resistance in Diaphorina citri, *PLOS ONE*, 2014, **9**, e110536.
55 D. M. Galdeano, M. C. Breton, J. R. S. Lopes, B. W. Falk and M. A. Machado, Oral delivery of double-stranded RNAs induces mortality in nymphs and adults of the Asian citrus psyllid, Diaphorina citri, *PLoS One*, , DOI:10.1371/journal.pone.0171847.
56 J. E. Webb and R. A. Green, On the Penetration of Insecticides Through the Insect Cuticle, *Journal of Experimental Biology*, 1945, **22**, 8–20.
57 B. Mamta and M. V. Rajam, RNAi technology: a new platform for crop pest control, *Physiol Mol Biol Plants*, 2017, **23**, 487–501.

58 C. N. T. Taning, O. Christiaens, N. Berkvens, H. Casteels, M. Maes and G. Smagghe, Oral RNAi to control Drosophila suzukii: laboratory testing against larval and adult stages, *J Pest Sci*, 2016, **89**, 803–814.
59 O. Christiaens, L. Swevers and G. Smagghe, DsRNA degradation in the pea aphid (Acyrthosiphon pisum) associated with lack of response in RNAi feeding and injection assay, *Peptides*, 2014, **53**, 307–314.
60 S. Dubelman, J. Fischer, F. Zapata, K. Huizinga, C. Jiang, J. Uffman, S. Levine and D. Carson, Environmental Fate of Double-Stranded RNA in Agricultural Soils, *PLOS ONE*, 2014, **9**, e93155.
61 J. N. Shukla, M. Kalsi, A. Sethi, K. E. Narva, E. Fishilevich, S. Singh, K. Mogilicherla and S. R. Palli, Reduced stability and intracellular transport of dsRNA contribute to poor RNAi response in lepidopteran insects, *RNA Biology*, 2016, **13**, 656–669.
62 I. K. Singh, S. Singh, K. Mogilicherla, J. N. Shukla and S. R. Palli, Comparative analysis of double-stranded RNA degradation and processing in insects, *Sci Rep*, 2017, **7**, 17059.
63 Y. Peng, K. Wang, W. Fu, C. Sheng and Z. Han, Biochemical Comparison of dsRNA Degrading Nucleases in Four Different Insects, *Front Physiol*, , DOI:10.3389/fphys.2018.00624.
64 R. Whitfield, A. Anastasaki, N. P. Truong, A. B. Cook, M. Omedes-Pujol, V. Loczenski Rose, T. A. H. Nguyen, J. A. Burns, S. Perrier, T. P. Davis and D. M. Haddleton, Efficient Binding, Protection, and Self-Release of dsRNA in Soil by Linear and Star Cationic Polymers, *ACS Macro Lett.*, 2018, **7**, 909–915.
65 A. M. Cooper, K. Silver, J. Zhang, Y. Park and K. Y. Zhu, Molecular mechanisms influencing efficiency of RNA interference in insects, *Pest Management Science*, 2019, **75**, 18–28.
66 K. Y. Zhu and S. R. Palli, Mechanisms, Applications, and Challenges of Insect RNA Interference, *Annual Review of Entomology*, 2020, **65**, 293–311.
67 J. R. Fischer, F. Zapata, S. Dubelman, G. M. Mueller, J. P. Uffman, C. Jiang, P. D. Jensen and S. L. Levine, Aquatic fate of a double-stranded RNA in a sediment-–water system following an over-water application, *Environmental Toxicology and Chemistry*, 2017, **36**, 727–734.
68 P. Bachman, J. Fischer, Z. Song, E. Urbanczyk-Wochniak and G. Watson, Environmental Fate and Dissipation of Applied dsRNA in Soil, Aquatic Systems, and Plants, *Frontiers in Plant Science*.
69 D. J. Gary, N. Puri and Y.-Y. Won, Polymer-based siRNA delivery: Perspectives on the fundamental and phenomenological distinctions from polymer-based DNA delivery, *Journal of Controlled Release*, 2007, **121**, 64–73.
70 J.-S. Yoon, D. Gurusamy and S. R. Palli, Accumulation of dsRNA in endosomes contributes to inefficient RNA interference in the fall armyworm, Spodoptera frugiperda, *Insect Biochem. Mol. Biol.*, 2017, **90**, 53–60.
71 D. Gurusamy, K. Mogilicherla, J. N. Shukla and S. R. Palli, Lipids help double-stranded RNA in endosomal escape and improve RNA interference in the fall armyworm, Spodoptera frugiperda, *Archives of Insect Biochemistry and Physiology*, 2020, **104**, e21678.
72 O. Terenius, A. Papanicolaou, J. S. Garbutt, I. Eleftherianos, H. Huvenne, S. Kanginakudru, M. Albrechtsen, C. An, J.-L. Aymeric, A. Barthel, P. Bebas, K. Bitra, A. Bravo, F. Chevalier, D. P. Collinge, C. M. Crava, R. A. de Maagd, B. Duvic, M. Erlandson, I. Faye, G. Felföldi, H. Fujiwara, R. Futahashi, A. S. Gandhe, H. S. Gatehouse, L. N. Gatehouse, J. M. Giebultowicz, I. Gómez, C. J. P. Grimmelikhuijzen, A. T. Groot, F. Hauser, D. G. Heckel, D. D. Hegedus, S. Hrycaj, L. Huang, J. J. Hull, K. Iatrou, M. Iga, M. R. Kanost, J. Kotwica, C. Li, J. Li, J. Liu, M. Lundmark, S. Matsumoto, M. Meyering-Vos, P. J. Millichap, A. Monteiro, N. Mrinal, T. Niimi, D. Nowara, A. Ohnishi, V. Oostra, K. Ozaki, M. Papakonstantinou, A. Popadic, M. V. Rajam, S. Saenko, R. M. Simpson, M. Soberón, M. R. Strand, S. Tomita, U. Toprak, P. Wang, C. W. Wee, S. Whyard, W. Zhang, J. Nagaraju, R. H. Ffrench-Constant, S.

Herrero, K. Gordon, L. Swevers and G. Smagghe, RNA interference in Lepidoptera: an overview of successful and unsuccessful studies and implications for experimental design, *J. Insect Physiol.*, 2011, **57**, 231–245.
73 S. R. Palli, RNA interference in Colorado potato beetle: steps toward development of dsRNA as a commercial insecticide, *Curr Opin Insect Sci*, 2014, **6**, 1–8.
74 F. Zhu, J. Xu, R. Palli, J. Ferguson and S. R. Palli, Ingested RNA interference for managing the populations of the Colorado potato beetle, Leptinotarsa decemlineata, *Pest Manag. Sci.*, 2011, **67**, 175–182.
75 N. Wynant, H. Verlinden, B. Breugelmans, G. Simonet and J. Vanden Broeck, Tissue-dependence and sensitivity of the systemic RNA interference response in the desert locust, Schistocerca gregaria, *Insect Biochemistry and Molecular Biology*, 2012, **42**, 911–917.
76 N. Wynant, D. Santos and J. Vanden Broeck, Biological mechanisms determining the success of RNA interference in insects, *Int Rev Cell Mol Biol*, 2014, **312**, 139–167.
77 O. Christiaens and G. Smagghe, The challenge of RNAi-mediated control of hemipterans, *Current Opinion in Insect Science*, 2014, **6**, 15–21.
78 M. Mulot, S. Boissinot, B. Monsion, M. Rastegar, G. Clavijo, D. Halter, N. Bochet, M. Erdinger and V. Brault, Comparative Analysis of RNAi-Based Methods to Down-Regulate Expression of Two Genes Expressed at Different Levels in Myzus persicae, *Viruses*, , DOI:10.3390/v8110316.
79 R.-B. Guan, H.-C. Li, Y.-J. Fan, S.-R. Hu, O. Christiaens, G. Smagghe and X.-X. Miao, A nuclease specific to lepidopteran insects suppresses RNAi, *J. Biol. Chem.*, 2018, **293**, 6011–6021.
80 K. Wang, Y. Peng, J. Pu, W. Fu, J. Wang and Z. Han, Variation in RNAi efficacy among insect species is attributable to dsRNA degradation in vivo, *Insect Biochemistry and Molecular Biology*, 2016, **77**, 1–9.
81 R. Zhou, I. Hotta, A. M. Denli, P. Hong, N. Perrimon and G. J. Hannon, Comparative Analysis of Argonaute-Dependent Small RNA Pathways in Drosophila, *Molecular Cell*, 2008, **32**, 592–599.
82 V. Mongelli and M.-C. Saleh, Bugs Are Not to Be Silenced: Small RNA Pathways and Antiviral Responses in Insects, *Annual Review of Virology*, 2016, **3**, 573–589.
83 K. Matyjaszewski, Atom Transfer Radical Polymerization (ATRP): Current Status and Future Perspectives, *Macromolecules*, 2012, **45**, 4015–4039.
84 G. Y. Wu and C. H. Wu, Receptor-mediated in vitro gene transformation by a soluble DNA carrier system, *J. Biol. Chem.*, 1987, **262**, 4429–4432.
85 O. Boussif, F. Lezoualc'h, M. A. Zanta, M. D. Mergny, D. Scherman, B. Demeneix and J. P. Behr, A versatile vector for gene and oligonucleotide transfer into cells in culture and in vivo: polyethylenimine, *PNAS*, 1995, **92**, 7297–7301.
86 J.-Y. Cherng, P. van de Wetering, H. Talsma, D. J. A. Crommelin and W. E. Hennink, Effect of Size and Serum Proteins on Transfection Efficiency of Poly ((2-dimethylamino)ethyl Methacrylate)-Plasmid Nanoparticles, *Pharm Res*, 1996, **13**, 1038–1042.
87 A. R. Klemm, D. Young and J. B. Lloyd, Effects of Polyethyleneimine on Endocytosis and Lysosome Stability, *Biochemical Pharmacology*, 1998, **56**, 41–46.
88 U. Lungwitz, M. Breunig, T. Blunk and A. Göpferich, Polyethylenimine-based non-viral gene delivery systems, *European Journal of Pharmaceutics and Biopharmaceutics*, 2005, **60**, 247–266.
89 S. Agarwal, Y. Zhang, S. Maji and A. Greiner, PDMAEMA based gene delivery materials, *Materials Today*, 2012, **15**, 388–393.
90 P. van de Wetering, N. J. Zuidam, M. J. van Steenbergen, O. A. G. J. van der Houwen, W. J. M. Underberg and W. E. Hennink, A Mechanistic Study of the Hydrolytic Stability of Poly(2-(dimethylamino)ethyl methacrylate), *Macromolecules*, 1998, **31**, 8063–8068.

91 A. von Harpe, H. Petersen, Y. Li and T. Kissel, Characterization of commercially available and synthesized polyethylenimines for gene delivery, *Journal of Controlled Release*, 2000, **69**, 309–322.
92 J. D. Ziebarth and Y. Wang, Understanding the protonation behavior of linear polyethylenimine in solutions through Monte Carlo simulations, *Biomacromolecules*, 2010, **11**, 29.
93 J.-H. Choi, S.-O. Kim, E. Linardy, E. C. Dreaden, V. P. Zhdanov, P. T. Hammond and N.-J. Cho, Influence of pH and Surface Chemistry on Poly(l-lysine) Adsorption onto Solid Supports Investigated by Quartz Crystal Microbalance with Dissipation Monitoring, *J. Phys. Chem. B*, 2015, **119**, 10554–10565.
94 T. Bus, A. Traeger and U. S. Schubert, The great escape: how cationic polyplexes overcome the endosomal barrier, *J. Mater. Chem. B*, 2018, **6**, 6904–6918.
95 R. A. Jones, M. H. Poniris and M. R. Wilson, pDMAEMA is internalised by endocytosis but does not physically disrupt endosomes, *Journal of Controlled Release*, 2004, **96**, 379–391.
96 A. M. Funhoff, C. F. van Nostrum, G. A. Koning, N. M. E. Schuurmans-Nieuwenbroek, D. J. A. Crommelin and W. E. Hennink, Endosomal Escape of Polymeric Gene Delivery Complexes Is Not Always Enhanced by Polymers Buffering at Low pH, *Biomacromolecules*, 2004, **5**, 32–39.
97 A. Akinc, M. Thomas, A. M. Klibanov and R. Langer, Exploring polyethylenimine-mediated DNA transfection and the proton sponge hypothesis, *The Journal of Gene Medicine*, 2005, **7**, 657–663.
98 M. Thomas and A. M. Klibanov, Enhancing polyethylenimine's delivery of plasmid DNA into mammalian cells, *Proceedings of the National Academy of Sciences*, 2002, **99**, 14640–14645.
99 S. Vaidyanathan, K. B. Anderson, R. L. Merzel, B. Jacobovitz, M. P. Kaushik, C. N. Kelly, M. A. van Dongen, C. A. Dougherty, B. G. Orr and M. M. Banaszak Holl, Quantitative Measurement of Cationic Polymer Vector and Polymer–pDNA Polyplex Intercalation into the Cell Plasma Membrane, *ACS Nano*, 2015, **9**, 6097–6109.
100 S. Vaidyanathan, B. G. Orr and M. M. Banaszak Holl, Role of Cell Membrane–Vector Interactions in Successful Gene Delivery, *Acc. Chem. Res.*, 2016, **49**, 1486–1493.
101 C. K. Choudhury, A. Kumar and S. Roy, Characterization of Conformation and Interaction of Gene Delivery Vector Polyethylenimine with Phospholipid Bilayer at Different Protonation State, *Biomacromolecules*, 2013, **14**, 3759–3768.
102 Z. ur Rehman, D. Hoekstra and I. S. Zuhorn, Mechanism of Polyplex- and Lipoplex-Mediated Delivery of Nucleic Acids: Real-Time Visualization of Transient Membrane Destabilization without Endosomal Lysis, *ACS Nano*, 2013, **7**, 3767–3777.
103 J. Cai, Y. Yue, Y. Wang, Z. Jin, F. Jin and C. Wu, Quantitative study of effects of free cationic chains on gene transfection in different intracellular stages, *Journal of Controlled Release*, 2016, **238**, 71–79.
104 A. Shakya, C. A. Dougherty, Y. Xue, H. M. Al-Hashimi and M. M. Banaszak Holl, Rapid Exchange Between Free and Bound States in RNA–Dendrimer Polyplexes: Implications on the Mechanism of Delivery and Release, *Biomacromolecules*, 2016, **17**, 154–164.
105 S. Vaidyanathan, J. Chen, B. G. Orr and M. M. Banaszak Holl, Cationic Polymer Intercalation into the Lipid Membrane Enables Intact Polyplex DNA Escape from Endosomes for Gene Delivery, *Mol. Pharmaceutics*, 2016, **13**, 1967–1978.
106 A. Mecke, I. J. Majoros, A. K. Patri, J. R. Baker, M. M. Banaszak Holl and B. G. Orr, Lipid Bilayer Disruption by Polycationic Polymers: The Roles of Size and Chemical Functional Group, *Langmuir*, 2005, **21**, 10348–10354.
107 W. T. Godbey, K. K. Wu and A. G. Mikos, Poly(ethylenimine)-mediated gene delivery affects endothelial cell function and viability, *Biomaterials*, 2001, **22**, 471–480.
108 P. van de Wetering, J.-Y. Cherng, H. Talsma and W. E. Hennink, Relation between transfection efficiency and cytotoxicity of poly(2-(dimethylamino)ethyl methacrylate)/plasmid complexes, *Journal of Controlled Release*, 1997, **49**, 59–69.

109 D. Fischer, Y. Li, B. Ahlemeyer, J. Krieglstein and T. Kissel, In vitro cytotoxicity testing of polycations: influence of polymer structure on cell viability and hemolysis, *Biomaterials*, 2003, **24**, 1121–1131.
110 L. E. Prevette, D. G. Mullen and M. M. Banaszak Holl, Polycation-Induced Cell Membrane Permeability Does Not Enhance Cellular Uptake or Expression Efficiency of Delivered DNA, *Mol. Pharmaceutics*, 2010, **7**, 870–883.
111 C. V. Synatschke, A. Schallon, V. Jérôme, R. Freitag and A. H. E. Müller, Influence of Polymer Architecture and Molecular Weight of Poly(2-(dimethylamino)ethyl methacrylate) Polycations on Transfection Efficiency and Cell Viability in Gene Delivery, *Biomacromolecules*, 2011, **12**, 4247–4255.
112 A. T. Silva, A. Nguyen, C. Ye, J. Verchot and J. H. Moon, Conjugated polymer nanoparticles for effective siRNA delivery to tobacco BY-2 protoplasts, *BMC Plant Biology*, 2010, **10**, 291.
113 K. H. Parsons, A. C. Holley, G. A. Munn, A. S. Flynt and C. L. McCormick, Block ionomer complexes consisting of siRNA and aRAFT-synthesized hydrophilic-block-cationic copolymers II: the influence of cationic block charge density on gene suppression, *Polym. Chem.*, 2016, **7**, 6044–6054.
114 K. H. Parsons, M. H. Mondal, C. L. McCormick and A. S. Flynt, Guanidinium-Functionalized Interpolyelectrolyte Complexes Enabling RNAi in Resistant Insect Pests, *Biomacromolecules*, 2018, **19**, 1111–1117.
115 O. Christiaens, M. G. Tardajos, Z. L. Martinez Reyna, M. Dash, P. Dubruel and G. Smagghe, Increased RNAi Efficacy in Spodoptera exigua via the Formulation of dsRNA With Guanylated Polymers, *Front. Physiol.*, , DOI:10.3389/fphys.2018.00316.
116 A. B. Cook, R. Peltier, M. Hartlieb, R. Whitfield, G. Moriceau, J. A. Burns, D. M. Haddleton and S. Perrier, Cationic and hydrolysable branched polymers by RAFT for complexation and controlled release of dsRNA, *Polym. Chem.*, 2018, **9**, 4025–4035.
117 C. Arigita, N. J. Zuidam, D. J. A. Crommelin and W. E. Hennink, Association and Dissociation Characteristics of Polymer/DNA Complexes Used for Gene Delivery, *Pharm Res*, 1999, **16**, 1534–1541.
118 J. Y. Cherng, H. Talsma, R. Verrijk, D. J. Crommelin and W. E. Hennink, The effect of formulation parameters on the size of poly-((2-dimethylamino)ethyl methacrylate)-plasmid complexes, *Eur J Pharm Biopharm*, 1999, **47**, 215–224.
119 W. T. Godbey, K. K. Wu and A. G. Mikos, Size matters: Molecular weight affects the efficiency of poly(ethylenimine) as a gene delivery vehicle, *Journal of Biomedical Materials Research*, 1999, **45**, 268–275.
120 K. Kunath, A. von Harpe, D. Fischer, H. Petersen, U. Bickel, K. Voigt and T. Kissel, Low-molecular-weight polyethylenimine as a non-viral vector for DNA delivery: comparison of physicochemical properties, transfection efficiency and in vivo distribution with high-molecular-weight polyethylenimine, *Journal of Controlled Release*, 2003, **89**, 113–125.
121 J. M. Layman, S. M. Ramirez, M. D. Green and T. E. Long, Influence of Polycation Molecular Weight on Poly(2-dimethylaminoethyl methacrylate)-Mediated DNA Delivery In Vitro, https://pubs.acs.org/doi/pdf/10.1021/bm9000124, (accessed 7 August 2020).
122 C. Lu, Z. Li, L. Chang, Z. Dong, P. Guo, G. Shen, Q. Xia and P. Zhao, Efficient Delivery of dsRNA and DNA in Cultured Silkworm Cells for Gene Function Analysis Using PAMAM Dendrimers System, *Insects*, , DOI:10.3390/insects11010012.
123 Y. Zheng, Y. Hu, S. Yan, H. Zhou, D. Song, M. Yin and J. Shen, A polymer/detergent formulation improves dsRNA penetration through the body wall and RNAi-induced mortality in the soybean aphid Aphis glycines, *Pest Management Science*, 2019, **75**, 1993–1999.
124 Z. Xu, B. He, W. Wei, K. Liu, M. Yin, W. Yang and J. Shen, Highly water-soluble perylenediimide-cored poly(amido amine) vector for efficient gene transfection, *J. Mater. Chem. B*, 2014, **2**, 3079–3086.

125 D. Shen, F. Zhou, Z. Xu, B. He, M. Li, J. Shen, M. Yin and C. An, Systemically interfering with immune response by a fluorescent cationic dendrimer delivered gene suppression, *J. Mater. Chem. B*, 2014, **2**, 4653–4659.
126 L. Jiang, L. Ding, B. He, J. Shen, Z. Xu, M. Yin and X. Zhang, Systemic gene silencing in plants triggered by fluorescent nanoparticle-delivered double-stranded RNA, *Nanoscale*, 2014, **6**, 9965–9969.
127 B. He, Y. Chu, M. Yin, K. Müllen, C. An and J. Shen, Fluorescent Nanoparticle Delivered dsRNA Toward Genetic Control of Insect Pests, *Advanced Materials*, 2013, **25**, 4580–4584.
128 C. H. Edwards, C. R. Christie, A. Masotti, A. Celluzzi, A. Caporali and E. M. Campbell, Dendrimer-coated carbon nanotubes deliver dsRNA and increase the efficacy of gene knockdown in the red flour beetle Tribolium castaneum, *Scientific Reports*, 2020, **10**, 12422.
129 X. Liao, G. Walden, N. D. Falcon, S. Donell, M. J. Raxworthy, M. Wormstone, G. P. Riley and A. Saeed, A direct comparison of linear and star-shaped poly(dimethylaminoethyl acrylate) polymers for polyplexation with DNA and cytotoxicity in cultured cell lines, *European Polymer Journal*, 2017, **87**, 458–467.
130 P. Cotanda, D. B. Wright, M. Tyler and R. K. O'Reilly, A comparative study of the stimuli-responsive properties of DMAEA and DMAEMA containing polymers, *Journal of Polymer Science Part A: Polymer Chemistry*, 2013, **51**, 3333–3338.
131 E. Schönemann, A. Laschewsky and A. Rosenhahn, Exploring the Long-Term Hydrolytic Behavior of Zwitterionic Polymethacrylates and Polymethacrylamides, *Polymers (Basel)*, , DOI:10.3390/polym10060639.
132 S. Ros, J. Wang, N. A. D. Burke and H. D. H. Stöver, A Mechanistic Study of the Hydrolysis of Poly[N,N-(dimethylamino)ethyl acrylates] as Charge-Shifting Polycations, *Macromolecules*, , DOI:10.1021/acs.macromol.9b02272.
133 D. T. Auguste, K. Furman, A. Wong, J. Fuller, S. P. Armes, T. J. Deming and R. Langer, Triggered release of siRNA from poly(ethylene glycol)-protected, pH-dependent liposomes, *Journal of Controlled Release*, 2008, **130**, 266–274.
134 S. Lin, F. Du, Y. Wang, S. Ji, D. Liang, L. Yu and Z. Li, An Acid-Labile Block Copolymer of PDMAEMA and PEG as Potential Carrier for Intelligent Gene Delivery Systems, *Biomacromolecules*, 2008, **9**, 109–115.
135 A. J. Convertine, C. Diab, M. Prieve, A. Paschal, A. S. Hoffman, P. H. Johnson and P. S. Stayton, pH-Responsive Polymeric Micelle Carriers for siRNA Drugs, *Biomacromolecules*, 2010, **11**, 2904–2911.
136 M. J. Manganiello, C. Cheng, A. J. Convertine, J. D. Bryers and P. S. Stayton, Diblock copolymers with tunable pH transitions for gene delivery, *Biomaterials*, 2012, **33**, 2301–2309.
137 Z. Cao, H. Xiao, L. Li, M. Liu, G. Lin, P. Zhai, K.-T. Yong, X. Wang and G. Xu, The Codelivery of siRNA and QDs by pH-Responsive Micelle for Hepatoma Cancer Cells, *Front. Pharmacol.*, , DOI:10.3389/fphar.2019.01194.
138 W. B. Liechty, R. L. Scheuerle, J. E. Vela Ramirez and N. A. Peppas, Cytoplasmic delivery of functional siRNA using pH-Responsive nanoscale hydrogels, *International Journal of Pharmaceutics*, 2019, **562**, 249–257.
139 E. Vivès, J. Schmidt and A. Pèlegrin, Cell-penetrating and cell-targeting peptides in drug delivery, *Biochimica et Biophysica Acta (BBA) - Reviews on Cancer*, 2008, **1786**, 126–138.
140 G. Cermenati, I. Terracciano, I. Castelli, B. Giordana, R. Rao, F. Pennacchio and M. Casartelli, The CPP Tat enhances eGFP cell internalization and transepithelial transport by the larval midgut of Bombyx mori (Lepidoptera, Bombycidae), *Journal of Insect Physiology*, 2011, **57**, 1689–1697.
141 Y.-J. Chen, B. R. Liu, Y.-H. Dai, C.-Y. Lee, M.-H. Chan, H.-H. Chen, H.-J. Chiang and H.-J. Lee, A gene delivery system for insect cells mediated by arginine-rich cell-penetrating peptides, *Gene*, 2012, **493**, 201–210.

142 F.-X. Gillet, R. A. Garcia, L. L. P. Macedo, E. V. S. Albuquerque, M. C. M. Silva and M. F. Grossi-de-Sa, Investigating Engineered Ribonucleoprotein Particles to Improve Oral RNAi Delivery in Crop Insect Pests, *Front. Physiol.*, , DOI:10.3389/fphys.2017.00256.
143 C. T. J. Ferguson, A. A. Al-Khalaf, R. E. Isaac and O. J. Cayre, pH-responsive polymer microcapsules for targeted delivery of biomaterials to the midgut of Drosophila suzukii, *PLoS ONE*, 2018, **13**, e0201294.
144 T. F. Abelha, C. A. Dreiss, M. A. Green and L. A. Dailey, Conjugated polymers as nanoparticle probes for fluorescence and photoacoustic imaging, *J. Mater. Chem. B*, 2020, **8**, 592–606.
145 J. H. Moon, E. Mendez, Y. Kim and A. Kaur, Conjugated polymer nanoparticles for small interfering RNA delivery, *Chem. Commun.*, 2011, **47**, 8370–8372.
146 H. J. Fisk and A. M. Dandekar, in *Transgenic Plants: Methods and Protocols*, ed. L. Peña, Humana Press, Totowa, NJ, 2004, pp. 79–90.
147 M. R. Davey, P. Anthony, J. B. Power and K. C. Lowe, Plant protoplasts: status and biotechnological perspectives, *Biotechnology Advances*, 2005, **23**, 131–171.
148 M. Fromm, L. P. Taylor and V. Walbot, Expression of genes transferred into monocot and dicot plant cells by electroporation, *PNAS*, 1985, **82**, 5824–5828.
149 F. Wang, H. Chen, Z. Liu, F. Mi, X. Fang, J. Liu, M. Wang, P. K. Lo and Q. Li, Conjugated polymer dots for biocompatible siRNA delivery, *New J. Chem.*, 2019, **43**, 14443–14449.
150 J. Haensler and F. C. Szoka, Polyamidoamine cascade polymers mediate efficient transfection of cells in culture, *Bioconjugate Chem.*, 1993, **4**, 372–379.
151 S. Yamano, J. Dai and A. M. Moursi, Comparison of Transfection Efficiency of Nonviral Gene Transfer Reagents, *Mol Biotechnol*, 2010, **46**, 287–300.
152 P. Kesharwani, S. Banerjee, U. Gupta, M. C. I. Mohd Amin, S. Padhye, F. H. Sarkar and A. K. Iyer, PAMAM dendrimers as promising nanocarriers for RNAi therapeutics, *Materials Today*, 2015, **18**, 565–572.
153 N. Mitter, E. A. Worrall, K. E. Robinson, P. Li, R. G. Jain, C. Taochy, S. J. Fletcher, B. J. Carroll, G. Q. (Max) Lu and Z. P. Xu, Clay nanosheets for topical delivery of RNAi for sustained protection against plant viruses, *Nature Plants*, 2017, **3**, 1–10.
154 E. A. Worrall, A. Bravo-Cazar, A. T. Nilon, S. J. Fletcher, K. E. Robinson, J. P. Carr and N. Mitter, Exogenous Application of RNAi-Inducing Double-Stranded RNA Inhibits Aphid-Mediated Transmission of a Plant Virus, *Front. Plant Sci.*, , DOI:10.3389/fpls.2019.00265.
155 X. Xu, Z. Li, X. Zhao, L. Keen and X. Kong, Calcium phosphate nanoparticles-based systems for siRNA delivery, *Regen Biomater*, 2016, **3**, 187–195.
156 I. Roy, S. Mitra, A. Maitra and S. Mozumdar, Calcium phosphate nanoparticles as novel non-viral vectors for targeted gene delivery, *International Journal of Pharmaceutics*, 2003, **250**, 25–33.
157 S. Das, N. Debnath, Y. Cui, J. Unrine and S. R. Palli, Chitosan, Carbon Quantum Dot, and Silica Nanoparticle Mediated dsRNA Delivery for Gene Silencing in Aedes aegypti: A Comparative Analysis, *ACS Appl. Mater. Interfaces*, 2015, **7**, 19530–19535.
158 B. Mostaghaci, J. Susewind, G. Kickelbick, C.-M. Lehr and B. Loretz, Transfection system of amino-functionalized calcium phosphate nanoparticles: in vitro efficacy, biodegradability, and immunogenicity study, *ACS Appl Mater Interfaces*, 2015, **7**, 5124–5133.
159 Z. Elhaj Baddar, D. Gurusamy, J. Laisney, P. Tripathi, S. R. Palli and J. M. Unrine, Polymer-Coated Hydroxyapatite Nanocarrier for Double-Stranded RNA Delivery, *J. Agric. Food Chem.*, 2020, **68**, 6811–6818.
160 K. L. Kozielski, S. Y. Tzeng and J. J. Green, Bioengineered Nanoparticles for siRNA delivery, *Wiley Interdiscip Rev Nanomed Nanobiotechnol*, 2013, **5**, 449–468.
161 J. Laisney, D. Gurusamy, Z. E. Baddar, S. R. Palli and J. M. Unrine, RNAi in Spodoptera frugiperda Sf9 Cells via Nanomaterial Mediated Delivery of dsRNA: A

Comparison of Poly-l-arginine Polyplexes and Poly-l-arginine-Functionalized Au Nanoparticles, *ACS Appl. Mater. Interfaces*, 2020, **12**, 25645–25657.
162 E. M. Wessel, J. M. Tomich and R. B. Todd, Biodegradable Drug-Delivery Peptide Nanocapsules, *ACS Omega*, 2019, **4**, 20059–20063.
163 L. A. Avila, R. Chandrasekar, K. E. Wilkinson, J. Balthazor, M. Heerman, J. Bechard, S. Brown, Y. Park, S. Dhar, G. R. Reeck and J. M. Tomich, Delivery of Lethal dsRNAs in Insect Diets by Branched Amphiphilic Peptide Capsules., *J Control Release*, 2018, **273**, 139–146.
164 K. Numata, M. Ohtani, T. Yoshizumi, T. Demura and Y. Kodama, Local gene silencing in plants via synthetic dsRNA and carrier peptide, *Plant Biotechnology Journal*, 2014, **12**, 1027–1034.
165 M. Lakshmanan, Y. Kodama, T. Yoshizumi, K. Sudesh and K. Numata, Rapid and Efficient Gene Delivery into Plant Cells Using Designed Peptide Carriers, *Biomacromolecules*, 2013, **14**, 10–16.
166 S. M. Barros, S. K. Whitaker, P. Sukthankar, L. A. Avila, S. Gudlur, M. Warner, E. I. C. Beltrão and J. M. Tomich, A review of solute encapsulating nanoparticles used as delivery systems with emphasis on branched amphipathic peptide capsules, *Archives of Biochemistry and Biophysics*, 2016, **596**, 22–42.
167 S. de M. Barros, L. A. Avila, S. K. Whitaker, K. E. Wilkinson, P. Sukthankar, E. I. C. Beltrão and J. M. Tomich, Branched Amphipathic Peptide Capsules: Different Ratios of the Two Constituent Peptides Direct Distinct Bilayer Structures, Sizes, and DNA Transfection Efficiency, *Langmuir*, 2017, **33**, 7096–7104.
168 S. M. Barros, R. Chandrasekar, K. E. Wilkinson-Nutsch, P. Yoonseong, G. Reeck, J. M. Tomich and L. A. Avila, Delivery of Lethal dsRNAs in Insect Diets by Branched Amphiphilic Peptide Capsules, *The FASEB Journal*, 2019, **33**, 785.4-785.4.
169 J. M. Tomich, E. Wessel, J. Choi and L. A. Avila, in *Nucleic Acid Nanotheranostics*, Elsevier, 2019, pp. 247–276.
170 N. J. Yang and M. J. Hinner, Getting Across the Cell Membrane: An Overview for Small Molecules, Peptides, and Proteins, *Methods Mol Biol*, 2015, **1266**, 29–53.
171 A. D. Frankel and C. O. Pabo, Cellular uptake of the tat protein from human immunodeficiency virus, *Cell*, 1988, **55**, 1189–1193.
172 A. Joliot, C. Pernelle, H. Deagostini-Bazin and A. Prochiantz, Antennapedia homeobox peptide regulates neural morphogenesis, *PNAS*, 1991, **88**, 1864–1868.
173 E. Vivès, P. Brodin and B. Lebleu, A Truncated HIV-1 Tat Protein Basic Domain Rapidly Translocates through the Plasma Membrane and Accumulates in the Cell Nucleus, *J. Biol. Chem.*, 1997, **272**, 16010–16017.
174 N. Unnamalai, B. G. Kang and W. S. Lee, Cationic oligopeptide-mediated delivery of dsRNA for post-transcriptional gene silencing in plant cells, *FEBS Letters*, 2004, **566**, 307–310.
175 K. Numata and D. L. Kaplan, Silk-Based Gene Carriers with Cell Membrane-Destabilizing Peptides, *Biomacromolecules*, 2010, **11**, 3189–3195.
176 I. Serrano-Sevilla, Á. Artiga, S. G. Mitchell, L. De Matteis and J. M. de la Fuente, Natural Polysaccharides for siRNA Delivery: Nanocarriers Based on Chitosan, Hyaluronic Acid, and Their Derivatives, *Molecules*, , DOI:10.3390/molecules24142570.
177 X. Zhang, J. Zhang and K. Y. Zhu, Chitosan/double-stranded RNA nanoparticle-mediated RNA interference to silence chitin synthase genes through larval feeding in the African malaria mosquito (Anopheles gambiae), *Insect Molecular Biology*, 2010, **19**, 683–693.
178 D. Gurusamy, K. Mogilicherla and S. R. Palli, Chitosan nanoparticles help double-stranded RNA escape from endosomes and improve RNA interference in the fall armyworm, Spodoptera frugiperda, *Archives of Insect Biochemistry and Physiology*, 2020, **104**, e21677.
179 X. Zhang, K. Mysore, E. Flannery, K. Michel, D. W. Severson, K. Y. Zhu and M. Duman-Scheel, Chitosan/Interfering RNA Nanoparticle Mediated Gene Silencing in

Disease Vector Mosquito Larvae, *JoVE (Journal of Visualized Experiments)*, 2015, e52523.
180 G. Theerawanitchpan, N. Saengkrit, W. Sajomsang, P. Gonil, U. Ruktanonchai, S. Saesoo, T. W. Flegel and V. Saksmerprome, Chitosan and its quaternized derivative as effective long dsRNA carriers targeting shrimp virus in Spodoptera frugiperda 9 cells, *Journal of Biotechnology*, 2012, **160**, 97–104.
181 D. Ramesh Kumar, P. Saravana Kumar, M. R. Gandhi, N. A. Al-Dhabi, M. G. Paulraj and S. Ignacimuthu, Delivery of chitosan/dsRNA nanoparticles for silencing of wing development vestigial (vg) gene in Aedes aegypti mosquitoes, *International Journal of Biological Macromolecules*, 2016, **86**, 89–95.
182 R. K. Dhandapani, D. Gurusamy, J. L. Howell and S. R. Palli, Development of CS-TPP-dsRNA nanoparticles to enhance RNAi efficiency in the yellow fever mosquito, Aedes aegypti, *Scientific Reports*, 2019, **9**, 1–11.
183 A. Guţoaia, L. Schuster, S. Margutti, S. Laufer, B. Schlosshauer, R. Krastev, D. Stoll and H. Hartmann, Fine-tuned PEGylation of chitosan to maintain optimal siRNA-nanoplex bioactivity, *Carbohydrate Polymers*, 2016, **143**, 25–34.
184 W. E. Rudzinski, A. Palacios, A. Ahmed, M. A. Lane and T. M. Aminabhavi, Targeted delivery of small interfering RNA to colon cancer cells using chitosan and PEGylated chitosan nanoparticles, *Carbohydrate Polymers*, 2016, **147**, 323–332.
185 P. Sun, W. Huang, M. Jin, Q. Wang, B. Fan, L. Kang and Z. Gao, Chitosan-based nanoparticles for survivin targeted siRNA delivery in breast tumor therapy and preventing its metastasis, *Int J Nanomedicine*, 2016, **11**, 4931–4945.
186 V. Iranpur Mobarakeh, M. H. Modarressi, P. Rahimi, A. Bolhassani, E. Arefian, F. Atyabi and R. Vahabpour, Optimization of chitosan nanoparticles as an anti-HIV siRNA delivery vehicle, *International Journal of Biological Macromolecules*, 2019, **129**, 305–315.
187 M. Malhotra, C. Tomaro-Duchesneau and S. Prakash, Synthesis of TAT peptide-tagged PEGylated chitosan nanoparticles for siRNA delivery targeting neurodegenerative diseases, *Biomaterials*, 2013, **34**, 1270–1280.
188 S. Park, E. J. Jeong, J. Lee, T. Rhim, S. K. Lee and K. Y. Lee, Preparation and characterization of nonaarginine-modified chitosan nanoparticles for siRNA delivery, *Carbohydrate Polymers*, 2013, **92**, 57–62.
189 F. Yang, W. Huang, Y. Li, S. Liu, M. Jin, Y. Wang, L. Jia and Z. Gao, Anti-tumor effects in mice induced by survivin-targeted siRNA delivered through polysaccharide nanoparticles, *Biomaterials*, 2013, **34**, 5689–5699.
190 P. L. Felgner, T. R. Gadek, M. Holm, R. Roman, H. W. Chan, M. Wenz, J. P. Northrop, G. M. Ringold and M. Danielsen, Lipofection: a highly efficient, lipid-mediated DNA-transfection procedure, *PNAS*, 1987, **84**, 7413–7417.
191 R. W. Malone, P. L. Felgner and I. M. Verma, Cationic liposome-mediated RNA transfection, *Proc. Natl. Acad. Sci. U.S.A.*, 1989, **86**, 6077–6081.
192 J. Sparks, G. Slobodkin, M. Matar, R. Congo, D. Ulkoski, A. Rea-Ramsey, C. Pence, J. Rice, D. McClure, K. J. Polach, E. Brunhoeber, L. Wilkinson, K. Wallace, K. Anwer and J. G. Fewell, Versatile cationic lipids for siRNA delivery, *J Control Release*, 2012, **158**, 269–276.
193 S. Zhang, D. Zhi and L. Huang, Lipid-based vectors for siRNA delivery, *J Drug Target*, 2012, **20**, 724–735.
194 T. Friedmann, A brief history of gene therapy, *Nature Genetics*, 1992, **2**, 93–98.
195 N. J. Zuidam, D. Hirsch-Lerner, S. Margulies and Y. Barenholz, Lamellarity of cationic liposomes and mode of preparation of lipoplexes affect transfection efficiency, *Biochimica et Biophysica Acta (BBA) - Biomembranes*, 1999, **1419**, 207–220.
196 Y. Barenholz, Liposome application: problems and prospects, *Current Opinion in Colloid & Interface Science*, 2001, **6**, 66–77.
197 H. Y. Xue, P. Guo, W.-C. Wen and H. L. Wong, Lipid-Based Nanocarriers for RNA Delivery, *Curr Pharm Des*, 2015, **21**, 3140–3147.

198 M. Saleh, R. P. van Rij, A. Hekele, A. Gillis, E. Foley, P. H. O'Farrell and R. Andino, The endocytic pathway mediates cell entry of dsRNA to induce RNAi silencing, *Nat Cell Biol*, 2006, **8**, 793–802.
199 J. Ulvila, M. Parikka, A. Kleino, R. Sormunen, R. A. Ezekowitz, C. Kocks and M. Rämet, Double-stranded RNA Is Internalized by Scavenger Receptor-mediated Endocytosis in Drosophila S2 Cells, *J. Biol. Chem.*, 2006, **281**, 14370–14375.
200 Y.-H. Lin, J.-H. Huang, Y. Liu, X. Belles and H.-J. Lee, Oral delivery of dsRNA lipoplexes to German cockroach protects dsRNA from degradation and induces RNAi response, *Pest Management Science*, 2017, **73**, 960–966.
201 J.-H. Huang, Y. Liu, Y.-H. Lin, X. Belles and H.-J. Lee, Practical Use of RNA Interference: Oral Delivery of Double-stranded RNA in Liposome Carriers for Cockroaches, *J Vis Exp*, , DOI:10.3791/57385.
202 Y. Zhang, J. Cui, Y. Zhou, J. Cao, H. Gong, H. Zhang and J. Zhou, Liposome mediated double-stranded RNA delivery to silence ribosomal protein P0 in the tick Rhipicephalus haemaphysaloides, *Ticks and Tick-borne Diseases*, 2018, **9**, 638–644.
203 N. L. Castellanos, G. Smagghe, R. Sharma, E. E. Oliveira and O. Christiaens, Liposome encapsulation and EDTA formulation of dsRNA targeting essential genes increase oral RNAi-caused mortality in the Neotropical stink bug Euschistus heros, *Pest Management Science*, 2019, **75**, 537–548.
204 J. de la Fuente, K. M. Kocan, C. Almazán and E. F. Blouin, RNA interference for the study and genetic manipulation of ticks, *Trends in Parasitology*, 2007, **23**, 427–433.
205 G. Barry, P. Alberdi, E. Schnettler, S. Weisheit, A. Kohl, J. K. Fazakerley and L. Bell-Sakyi, Gene silencing in tick cell lines using small interfering or long double-stranded RNA, *Exp Appl Acarol*, 2013, **59**, 319–338.
206 D. T. Auguste, S. P. Armes, K. R. Brzezinska, T. J. Deming, J. Kohn and R. K. Prud'homme, pH triggered release of protective poly(ethylene glycol)-b-polycation copolymers from liposomes, *Biomaterials*, 2006, **27**, 2599–2608.
207 K. A. Howard, U. L. Rahbek, X. Liu, C. K. Damgaard, S. Z. Glud, M. Ø. Andersen, M. B. Hovgaard, A. Schmitz, J. R. Nyengaard, F. Besenbacher and J. Kjems, RNA Interference in Vitro and in Vivo Using a Novel Chitosan/siRNA Nanoparticle System, *Molecular Therapy*, 2006, **14**, 476–484.
208 A. Eguchi, B. R. Meade, Y.-C. Chang, C. T. Fredrickson, K. Willert, N. Puri and S. F. Dowdy, Efficient siRNA delivery into primary cells by a peptide transduction domain–dsRNA binding domain fusion protein, *Nature Biotechnology*, 2009, **27**, 567–571.
209 N. J. Treat, D. Smith, C. Teng, J. D. Flores, B. A. Abel, A. W. York, F. Huang and C. L. McCormick, Guanidine-Containing Methacrylamide (Co)polymers via aRAFT: Toward a Cell-Penetrating Peptide Mimic, *ACS Macro Lett.*, 2012, **1**, 100–104.
210 Z. Tan, Y. Jiang, M. S. Ganewatta, R. Kumar, A. Keith, K. Twaroski, T. Pengo, J. Tolar, T. P. Lodge and T. M. Reineke, Block Polymer Micelles Enable CRISPR/Cas9 Ribonucleoprotein Delivery: Physicochemical Properties Affect Packaging Mechanisms and Gene Editing Efficiency, *Macromolecules*, 2019, **52**, 8197–8206.
211 Q. Bai, J. Liu, J. Tang, Z. Li, X. Zheng and Q. Chen, Redox-Responsive Polymeric RNAi Based on Multivalent Conjugation of siRNA for Improved Intracellular Delivery, *Bioconjugate Chem.*, 2019, **30**, 2777–2781.
212 D. Wang, J. Lin, F. Jia, X. Tan, Y. Wang, X. Sun, X. Cao, F. Che, H. Lu, X. Gao, J. C. Shimkonis, Z. Nyoni, X. Lu and K. Zhang, Bottlebrush-architectured poly(ethylene glycol) as an efficient vector for RNA interference in vivo, *Science Advances*, 2019, **5**, eaav9322.
213 H. Li-Byarlay, Y. Li, H. Stroud, S. Feng, T. C. Newman, M. Kaneda, K. K. Hou, K. C. Worley, C. G. Elsik, S. A. Wickline, S. E. Jacobsen, J. Ma and G. E. Robinson, RNA interference knockdown of DNA methyl-transferase 3 affects gene alternative splicing in the honey bee, *PNAS*, 2013, **110**, 12750–12755.
214 M. W. Thairu, I. H. Skidmore, R. Bansal, E. Nováková, T. E. Hansen, H. Li-Byarlay, S. A. Wickline and A. K. Hansen, Efficacy of RNA interference knockdown using

aerosolized short interfering RNAs bound to nanoparticles in three diverse aphid species, *Insect Molecular Biology*, 2017, **26**, 356–368.
215 J. G. Lundgren and J. J. Duan, RNAi-Based Insecticidal Crops: Potential Effects on Nontarget Species, *BioScience*, 2013, **63**, 657–665.
216 K. M. Parker, V. Barragán Borrero, D. M. van Leeuwen, M. A. Lever, B. Mateescu and M. Sander, Environmental Fate of RNA Interference Pesticides: Adsorption and Degradation of Double-Stranded RNA Molecules in Agricultural Soils, *Environ. Sci. Technol.*, 2019, **53**, 3027–3036.
217 J. Romeis and F. Widmer, Assessing the Risks of Topically Applied dsRNA-Based Products to Non-target Arthropods, *Front Plant Sci*, , DOI:10.3389/fpls.2020.00679.
218 M. Szwarc, 'Living' Polymers, *Nature*, 1956, **178**, 1168–1169.
219 G. Moad, E. Rizzardo and S. H. Thang, Living Radical Polymerization by the RAFT Process – A Second Update, *Aust. J. Chem.*, 2009, **62**, 1402–1472.
220 S. Perrier, 50th Anniversary Perspective: RAFT Polymerization—A User Guide, *Macromolecules*, 2017, **50**, 7433–7447.
221 D. J. Keddie, A guide to the synthesis of block copolymers using reversible-addition fragmentation chain transfer (RAFT) polymerization, *Chem. Soc. Rev.*, 2014, **43**, 496–505.
222 A. El Jundi, S. J. Buwalda, Y. Bakkour, X. Garric and B. Nottelet, Double hydrophilic block copolymers self-assemblies in biomedical applications, *Advances in Colloid and Interface Science*, 2020, **283**, 102213.
223 H. Feng, X. Lu, W. Wang, N.-G. Kang and J. W. Mays, Block Copolymers: Synthesis, Self-Assembly, and Applications, *Polymers (Basel)*, 2017, **9**, 494.
224 M. Kamachi, M. Kurihara and J. K. Stille, Synthesis of Block Polymers for Desalination Membranes. Preparation of Block Copolymers of 2-Vinylpyridine and Methacrylic Acid or Acrylic Acid, *Macromolecules*, 1972, **5**, 161–167.
225 B. V. K. J. Schmidt, Double Hydrophilic Block Copolymer Self-Assembly in Aqueous Solution, *Macromolecular Chemistry and Physics*, 2018, **219**, 1700494.
226 H. Cölfen, Double-Hydrophilic Block Copolymers: Synthesis and Application as Novel Surfactants and Crystal Growth Modifiers, *Macromolecular Rapid Communications*, 2001, **22**, 219–252.
227 D. E. Koppel, Analysis of Macromolecular Polydispersity in Intensity Correlation Spectroscopy: The Method of Cumulants, *J. Chem. Phys.*, 1972, **57**, 4814–4820.
228 A. Scotti, W. Liu, J. S. Hyatt, E. S. Herman, H. S. Choi, J. W. Kim, L. A. Lyon, U. Gasser and A. Fernandez-Nieves, The CONTIN algorithm and its application to determine the size distribution of microgel suspensions, *J. Chem. Phys.*, 2015, **142**, 234905.
229 J. Pencer and F. R. Hallett, Effects of Vesicle Size and Shape on Static and Dynamic Light Scattering Measurements, *Langmuir*, 2003, **19**, 7488–7497.
230 K. Haydukivska, V. Blavatska and J. Paturej, Universal size ratios of Gaussian polymers with complex architecture: radius of gyration vs hydrodynamic radius, *Sci Rep*, 2020, **10**, 14127.
231 J. K. W. Lam, Y. Ma, S. P. Armes, A. L. Lewis, T. Baldwin and S. Stolnik, Phosphorylcholine–polycation diblock copolymers as synthetic vectors for gene delivery, *Journal of Controlled Release*, 2004, **100**, 293–312.
232 S. Caccia, M. Casartelli and G. Tettamanti, The amazing complexity of insect midgut cells: types, peculiarities, and functions, *Cell Tissue Res*, 2019, **377**, 505–525.
233 G. Overend, Y. Luo, L. Henderson, A. E. Douglas, S. A. Davies and J. A. T. Dow, Molecular mechanism and functional significance of acid generation in the Drosophila midgut, *Sci Rep*, , DOI:10.1038/srep27242.
234 R. R. Dubreuil, Copper cells and stomach acid secretion in the Drosophila midgut, *The International Journal of Biochemistry & Cell Biology*, 2004, **36**, 742–752.
235 J.-P. Sumner, J. A. T. Dow, F. G. P. Earley, U. Klein, D. Jäger and H. Wieczorek, Regulation of Plasma Membrane V-ATPase Activity by Dissociation of Peripheral Subunits (∗), *Journal of Biological Chemistry*, 1995, **270**, 5649–5653.

236 D. Francis and A. S. Ghabrial, Compensatory branching morphogenesis of stalk cells in the Drosophila trachea, *Development*, 2015, **142**, 2048–2057.
237 Y. Guo, Z. Wang, A. Carter, K. Kaiser and J. A. T. Dow, Characterisation of vha26, the Drosophila gene for a 26 kDa E-subunit of the vacuolar ATPase, *Biochimica et Biophysica Acta (BBA) - Biomembranes*, 1996, **1283**, 4–9.
238 V. A. Izumrudov, M. V. Zhiryakova and A. A. Goulko, Ethidium Bromide as a Promising Probe for Studying DNA Interaction with Cationic Amphiphiles and Stability of the Resulting Complexes, *Langmuir*, 2002, **18**, 10348–10356.
239 M. V. Zhiryakova and V. A. Izumrudov, A fluorescent method based on the competitive displacement of intercalated dyes for the study of DNA polyelectrolyte complexes: Advantages and prospects, *Polym. Sci. Ser. A*, 2007, **49**, 1290–1301.
240 M. J. Waring, Complex formation between ethidium bromide and nucleic acids, *Journal of Molecular Biology*, 1965, **13**, 269–282.
241 J.-B. Lepecq and C. Paoletti, A fluorescent complex between ethidium bromide and nucleic acids: Physical—Chemical characterization, *Journal of Molecular Biology*, 1967, **27**, 87–106.
242 J. Olmsted and D. R. Kearns, Mechanism of ethidium bromide fluorescence enhancement on binding to nucleic acids, *Biochemistry*, 1977, **16**, 3647–3654.
243 R. J. Douthart, J. P. Burnett, F. W. Beasley and B. H. Frank, Binding of ethidium bromide to double-stranded ribonucleic acid, *Biochemistry*, 1973, **12**, 214–220.
244 W. Chen, N. J. Turro and D. A. Tomalia, Using Ethidium Bromide To Probe the Interactions between DNA and Dendrimers, *Langmuir*, 2000, **16**, 15–19.
245 R. Galindo-Murillo and T. E. Cheatham III, Ethidium bromide interactions with DNA: an exploration of a classic DNA–ligand complex with unbiased molecular dynamics simulations, *Nucleic Acids Research*, 2021, **49**, 3735–3747.
246 M. Thomas and A. M. Klibanov, Non-viral gene therapy: polycation-mediated DNA delivery, *Appl Microbiol Biotechnol*, 2003, **62**, 27–34.
247 D. Fischer, T. Bieber, Y. Li, H.-P. Elsässer and T. Kissel, A Novel Non-Viral Vector for DNA Delivery Based on Low Molecular Weight, Branched Polyethylenimine: Effect of Molecular Weight on Transfection Efficiency and Cytotoxicity, *Pharm Res*, 1999, **16**, 1273–1279.
248 D. Dey, S. Kumar, R. Banerjee, S. Maiti and D. Dhara, Polyplex Formation between PEGylated Linear Cationic Block Copolymers and DNA: Equilibrium and Kinetic Studies, *J. Phys. Chem. B*, 2014, **118**, 7012–7025.
249 R. J. Dalal, R. Kumar, M. Ohnsorg, M. Brown and T. M. Reineke, Cationic Bottlebrush Polymers Outperform Linear Polycation Analogues for pDNA Delivery and Gene Expression, *ACS Macro Lett.*, 2021, **10**, 886–893.
250 C. W. Scales, F. Huang, N. Li, Y. A. Vasilieva, J. Ray, A. J. Convertine and C. L. McCormick, Corona-Stabilized Interpolyelectrolyte Complexes of SiRNA with Nonimmunogenic, Hydrophilic/Cationic Block Copolymers Prepared by Aqueous RAFT Polymerization †, *Macromolecules*, 2006, **39**, 6871–6881.
251 Y. Jiang, T. P. Lodge and T. M. Reineke, Packaging pDNA by Polymeric ABC Micelles Simultaneously Achieves Colloidal Stability and Structural Control, *J. Am. Chem. Soc.*, 2018, **140**, 11101–11111.
252 S. Jung, T. P. Lodge and T. M. Reineke, Complexation between DNA and Hydrophilic-Cationic Diblock Copolymers, *J. Phys. Chem. B*, 2017, **121**, 2230–2243.
253 A. Blanazs, S. P. Armes and A. J. Ryan, Self-Assembled Block Copolymer Aggregates: From Micelles to Vesicles and their Biological Applications, *Macromolecular Rapid Communications*, 2009, **30**, 267–277.
254 J.-F. Berret, B. Vigolo, R. Eng, P. Hervé, I. Grillo and L. Yang, Electrostatic Self-Assembly of Oppositely Charged Copolymers and Surfactants: A Light, Neutron, and X-ray Scattering Study, *Macromolecules*, 2004, **37**, 4922–4930.
255 A. Guzik and P. Raffa, Direct synthesis via RAFT of amphiphilic diblock polyelectrolytes facilitated by the use of a polymerizable ionic liquid as a monomer, *Polym. Chem.*, , DOI:10.1039/D1PY00801C.

256 A. V. Korobko, C. Backendorf and J. R. C. van der Maarel, Plasmid DNA Encapsulation within Cationic Diblock Copolymer Vesicles for Gene Delivery, *J. Phys. Chem. B*, 2006, **110**, 14550–14556.
257 S. Kozuka, K. Kuroda, K. Ishihara and S. Yusa, Interpolymer association of amphiphilic diblock copolymers bearing pendant siloxane and phosphorylcholine groups, *Journal of Polymer Science Part A: Polymer Chemistry*, 2019, **57**, 1500–1507.
258 D. Sprouse, Y. Jiang, J. E. Laaser, T. P. Lodge and T. M. Reineke, Tuning Cationic Block Copolymer Micelle Size by pH and Ionic Strength, *Biomacromolecules*, 2016, **17**, 2849–2859.
259 Y. Jiang, D. Sprouse, J. E. Laaser, Y. Dhande, T. M. Reineke and T. P. Lodge, Complexation of Linear DNA and Poly(styrenesulfonate) with Cationic Copolymer Micelles: Effect of Polyanion Flexibility, *J. Phys. Chem. B*, 2017, **121**, 6708–6720.
260 M. H. Stenzel, C. Barner-Kowollik, T. P. Davis and H. M. Dalton, Amphiphilic Block Copolymers Based on Poly(2-acryloyloxyethyl phosphorylcholine) Prepared via RAFT Polymerisation as Biocompatible Nanocontainers, *Macromolecular Bioscience*, 2004, **4**, 445–453.
261 S. P. Armes, S. Perrier and P. B. Zetterlund, Introduction to polymerisation-induced self assembly, *Polym. Chem.*, 2021, **12**, 8–11.
262 M. A. Cohen Stuart, N. A. M. Besseling and R. G. Fokkink, Formation of Micelles with Complex Coacervate Cores, *Langmuir*, 1998, **14**, 6846–6849.
263 B. Zhan, K. Shi, Z. Dong, W. Lv, S. Zhao, X. Han, H. Wang and H. Liu, Coarse-Grained Simulation of Polycation/DNA-Like Complexes: Role of Neutral Block, *Mol. Pharmaceutics*, 2015, **12**, 2834–2844.
264 D. V. Pergushov, A. H. E. Müller and F. H. Schacher, Micellar interpolyelectrolyte complexes, *Chem. Soc. Rev.*, 2012, **41**, 6888–6901.
265 W. T. Godbey and A. G. Mikos, Recent progress in gene delivery using non-viral transfer complexes, *Journal of Controlled Release*, 2001, **72**, 115–125.
266 S. Pirotton, C. Muller, N. Pantoustier, F. Botteman, S. Collinet, C. Grandfils, G. Dandrifosse, P. Degée, P. Dubois and M. Raes, Enhancement of Transfection Efficiency Through Rapid and Noncovalent Post-PEGylation of Poly(Dimethylaminoethyl Methacrylate)/DNA Complexes, *Pharm Res*, 2004, **21**, 1471–1479.
267 D. Oupický, Č. Koňák and K. Ulbrich, Preparation of DNA complexes with diblock copolymers of poly[N(2-hydroxypropyl)methacrylamide] and polycations, *Materials Science and Engineering: C*, 1999, **7**, 59–65.
268 V. Toncheva, M. A. Wolfert, P. R. Dash, D. Oupicky, K. Ulbrich, L. W. Seymour and E. H. Schacht, Novel vectors for gene delivery formed by self-assembly of DNA with poly(l-lysine) grafted with hydrophilic polymers, *Biochimica et Biophysica Acta (BBA) - General Subjects*, 1998, **1380**, 354–368.
269 H. Petersen, P. M. Fechner, A. L. Martin, K. Kunath, S. Stolnik, C. J. Roberts, D. Fischer, M. C. Davies and T. Kissel, Polyethylenimine-graft-Poly(ethylene glycol) Copolymers: Influence of Copolymer Block Structure on DNA Complexation and Biological Activities as Gene Delivery System, *Bioconjugate Chem.*, 2002, **13**, 845–854.
270 U. Rungsardthong, M. Deshpande, L. Bailey, M. Vamvakaki, S. P. Armes, M. C. Garnett and S. Stolnik, Copolymers of amine methacrylate with poly(ethylene glycol) as vectors for gene therapy, *Journal of Controlled Release*, 2001, **73**, 359–380.
271 G. P. Tang, J. M. Zeng, S. J. Gao, Y. X. Ma, L. Shi, Y. Li, H.-P. Too and S. Wang, Polyethylene glycol modified polyethylenimine for improved CNS gene transfer: effects of PEGylation extent, *Biomaterials*, 2003, **24**, 2351–2362.
272 P. Harvie, F. M. P. Wong and M. B. Bally, Use of Poly(ethylene glycol)–Lipid Conjugates to Regulate the Surface Attributes and Transfection Activity of Lipid–DNA Particles, *J. Pharm. Sci.*, 2000, **89**, 652–663.
273 Y. Bao, Y. Jin, P. Chivukula, J. Zhang, Y. Liu, J. Liu, J.-P. Clamme, R. I. Mahato, D. Ng, W. Ying, Y. Wang and L. Yu, Effect of PEGylation on Biodistribution and Gene Silencing of siRNA/Lipid Nanoparticle Complexes, *Pharm Res*, 2013, **30**, 342–351.

274 J. J. F. Verhoef and T. J. Anchordoquy, Questioning the Use of PEGylation for Drug Delivery, *Drug Deliv Transl Res*, 2013, **3**, 499–503.
275 M. P. Algi and O. Okay, Highly stretchable self-healing poly(N,N-dimethylacrylamide) hydrogels, *European Polymer Journal*, 2014, **59**, 113–121.
276 PEO/PEG Standards | Agilent, https://www.agilent.com/en/product/gpc-sec-columns/gpc-sec-standards/peo-peg-standards, (accessed 26 January 2022).
277 A. Harada and K. Kataoka, Chain Length Recognition: Core-Shell Supramolecular Assembly from Oppositely Charged Block Copolymers, *Science*, 1999, **283**, 65–67.
278 M. Luzon, C. Boyer, C. Peinado, T. Corrales, M. Whittaker, L. Tao and T. P. Davis, Water-soluble, thermoresponsive, hyperbranched copolymers based on PEG-methacrylates: Synthesis, characterization, and LCST behavior, *Journal of Polymer Science Part A: Polymer Chemistry*, 2010, **48**, 2783–2792.
279 S. Mori and H. G. Barth, *Size Exclusion Chromatography*, Springer Science & Business Media, 1999.
280 Y. H. Kim, K. Lee and S. Li, Nucleic Acids Based Polyelectrolyte Complexes: Their Complexation Mechanism, Morphology, and Stability, *Chem. Mater.*, 2021, **33**, 7923–7943.
281 R. Zhang and B. I. Shklovskii, Phase diagram of solution of oppositely charged polyelectrolytes, *Physica A: Statistical Mechanics and its Applications*, 2005, **352**, 216–238.
282 S. Sakamoto, Y. Sanada, M. Sakashita, K. Nishina, K. Nakai, S. Yusa and K. Sakurai, Chain-length dependence of polyion complex architecture bearing phosphobetaine block explored using SAXS and FFF-MALS, *Polym J*, 2014, **46**, 617–622.
283 J. R. Magana, C. C. M. Sproncken and I. K. Voets, On Complex Coacervate Core Micelles: Structure-Function Perspectives, *Polymers*, 2020, **12**, 1953.
284 A. Zintchenko, H. Dautzenberg, K. Tauer and V. Khrenov, Polyelectrolyte Complex Formation with Double Hydrophilic Block Polyelectrolytes: Effects of the Amount and Length of the Neutral Block, *Langmuir*, 2002, **18**, 1386–1393.
285 M. Ruponen, P. Honkakoski, M. Tammi and A. Urtti, Cell-surface glycosaminoglycans inhibit cation-mediated gene transfer, *The Journal of Gene Medicine*, 2004, **6**, 405–414.
286 K. A. Mislick and J. D. Baldeschwieler, Evidence for the role of proteoglycans in cation-mediated gene transfer, *PNAS*, 1996, **93**, 12349–12354.
287 L. Stamatatos, R. Leventis, M. J. Zuckermann and J. R. Silvius, Interactions of cationic lipid vesicles with negatively charged phospholipid vesicles and biological membranes, *Biochemistry*, 1988, **27**, 3917–3925.
288 M. Hanzlíková, M. Ruponen, E. Galli, A. Raasmaja, V. Aseyev, H. Tenhu, A. Urtti and M. Yliperttula, Mechanisms of polyethylenimine-mediated DNA delivery: free carrier helps to overcome the barrier of cell-surface glycosaminoglycans, *The Journal of Gene Medicine*, 2011, **13**, 402–409.
289 R. Sharma, J.-S. Lee, R. C. Bettencourt, C. Xiao, S. F. Konieczny and Y.-Y. Won, Effects of the incorporation of a hydrophobic middle block into a PEG-polycation diblock copolymer on the physicochemical and cell interaction properties of the polymer-DNA complexes, *Biomacromolecules*, 2008, **9**, 3294–3307.
290 T. Bieber, W. Meissner, S. Kostin, A. Niemann and H.-P. Elsasser, Intracellular route and transcriptional competence of polyethylenimine–DNA complexes, *Journal of Controlled Release*, 2002, **82**, 441–454.
291 X. Liu, J. W. Yang and D. M. Lynn, Addition of 'Charge-Shifting' Side Chains to Linear Poly(ethyleneimine) Enhances Cell Transfection Efficiency, *Biomacromolecules*, 2008, **9**, 2063–2071.
292 V. A. Izumrudov and M. V. Zhiryakova, Stability of DNA-containing interpolyelectrolyte complexes in water-salt solutions, *Macromolecular Chemistry and Physics*, 1999, **200**, 2533–2540.
293 V. Starchenko, M. Müller and N. Lebovka, Sizing of PDADMAC/PSS Complex Aggregates by Polyelectrolyte and Salt Concentration and PSS Molecular Weight, *J. Phys. Chem. B*, 2012, **116**, 14961–14967.

294 H. Wu, J. M. Ting, O. Werba, S. Meng and M. V. Tirrell, Non-equilibrium phenomena and kinetic pathways in self-assembled polyelectrolyte complexes, *J. Chem. Phys.*, 2018, **149**, 163330.
295 H. Dautzenberg and W. Jaeger, Effect of charge density on the formation and salt stability of polyelectrolyte complexes, *Macromolecular Chemistry and Physics*, 2002, **203**, 2095–2102.
296 Y. Li, H.-L. Dong, J.-S. Zhang, C. Lin and Z.-J. Tan, Effective Repulsion Between Oppositely Charged Particles in Symmetrical Multivalent Salt Solutions: Effect of Salt Valence, *Frontiers in Physics*, 2021, **9**, 372.
297 J. Polte, Fundamental growth principles of colloidal metal nanoparticles – a new perspective, *CrystEngComm*, 2015, **17**, 6809–6830.
298 Y. Jiang, T. M. Reineke and T. P. Lodge, Complexation of DNA with Cationic Copolymer Micelles: Effects of DNA Length and Topology, *Macromolecules*, 2018, **51**, 1150–1160.
299 D. Lombardo, M. A. Kiselev, S. Magazù and P. Calandra, Amphiphiles Self-Assembly: Basic Concepts and Future Perspectives of Supramolecular Approaches, *Advances in Condensed Matter Physics*, 2015, **2015**, e151683.
300 Y. Xiao, K. Shi, Y. Qu, B. Chu and Z. Qian, Engineering Nanoparticles for Targeted Delivery of Nucleic Acid Therapeutics in Tumor, *Mol Ther Methods Clin Dev*, 2018, **12**, 1–18.
301 D. J. Keddie, G. Moad, E. Rizzardo and S. H. Thang, RAFT Agent Design and Synthesis, *Macromolecules*, 2012, **45**, 5321–5342.
302 A. C. Holley, K. H. Parsons, W. Wan, D. F. Lyons, G. R. Bishop, J. J. Correia, F. Huang and C. L. McCormick, Block ionomer complexes consisting of siRNA and aRAFT-synthesized hydrophilic-block-cationic copolymers: the influence of cationic block length on gene suppression, *Polym. Chem.*, 2014, **5**, 6967–6976.
303 H. Willcock and R. K. O'Reilly, End group removal and modification of RAFT polymers, *Polym. Chem.*, 2010, **1**, 149–157.
304 C. E. Pugsley, R. E. Isaac, N. J. Warren and O. J. Cayre, Recent Advances in Engineered Nanoparticles for RNAi-Mediated Crop Protection Against Insect Pests, *Front. Agron.*, , DOI:10.3389/fagro.2021.652981.
305 D. J. Gary, H. Lee, R. Sharma, J.-S. Lee, Y. Kim, Z. Y. Cui, D. Jia, V. D. Bowman, P. R. Chipman, L. Wan, Y. Zou, G. Mao, K. Park, B.-S. Herbert, S. F. Konieczny and Y.-Y. Won, Influence of Nano-Carrier Architecture on in Vitro siRNA Delivery Performance and in Vivo Biodistribution: Polyplexes vs Micelleplexes, *ACS Nano*, 2011, **5**, 3493–3505.
306 Z. Tan, Y. Jiang, W. Zhang, L. Karls, T. P. Lodge and T. M. Reineke, Polycation Architecture and Assembly Direct Successful Gene Delivery: Micelleplexes Outperform Polyplexes via Optimal DNA Packaging, *J. Am. Chem. Soc.*, 2019, **141**, 15804–15817.
307 A. W. York, S. E. Kirkland and C. L. McCormick, Advances in the synthesis of amphiphilic block copolymers via RAFT polymerization: Stimuli-responsive drug and gene delivery, *Advanced Drug Delivery Reviews*, 2008, **60**, 1018–1036.
308 B. Brissault, C. Leborgne, D. Scherman, C. Guis and A. Kichler, Synthesis of Poly(propylene glycol)-block-Polyethylenimine Triblock Copolymers for the Delivery of Nucleic Acids, *Macromolecular Bioscience*, 2011, **11**, 652–661.
309 C. Cheng, A. J. Convertine, P. S. Stayton and J. D. Bryers, Multifunctional triblock copolymers for intracellular messenger RNA delivery, *Biomaterials*, 2012, **33**, 6868–6876.
310 T. K. Endres, M. Beck-Broichsitter, O. Samsonova, T. Renette and T. H. Kissel, Self-assembled biodegradable amphiphilic PEG–PCL–lPEI triblock copolymers at the borderline between micelles and nanoparticles designed for drug and gene delivery, *Biomaterials*, 2011, **32**, 7721–7731.
311 T. Segura and J. A. Hubbell, Synthesis and in Vitro Characterization of an ABC Triblock Copolymer for siRNA Delivery, *Bioconjugate Chem.*, 2007, **18**, 736–745.

312 C. E. Pugsley, R. E. Isaac, Nicholas. J. Warren, J. S. Behra, K. Cappelle, R. Dominguez-Espinosa and Olivier. J. Cayre, Protection of Double-Stranded RNA via Complexation with Double Hydrophilic Block Copolymers: Influence of Neutral Block Length in Biologically Relevant Environments, *Biomacromolecules*, , DOI:10.1021/acs.biomac.2c00136.
313 V. Incani, A. Lavasanifar and H. Uludağ, Lipid and hydrophobic modification of cationic carriers on route to superior gene vectors, *Soft Matter*, 2010, **6**, 2124–2138.
314 H. Lodish, A. Berk, S. L. Zipursky, P. Matsudaira, D. Baltimore and J. Darnell, *Intracellular Ion Environment and Membrane Electric Potential*, W H Freeman & Co, New York, 2000.
315 B. Liu, B. Poolman and A. J. Boersma, Ionic Strength Sensing in Living Cells, *ACS Chem. Biol.*, 2017, **12**, 2510–2514.
316 V. Chrysostomou, A. Forys, B. Trzebicka, C. Demetzos and S. Pispas, Structure of micelleplexes formed between QPDMAEMA-b-PLMA amphiphilic cationic copolymer micelles and DNA of different lengths, *European Polymer Journal*, 2022, **166**, 111048.
317 C. Cokca, F. J. Hack, D. Costabel, K. Herwig, J. Hülsmann, P. Then, R. Heintzmann, D. Fischer and K. Peneva, PEGylation of Guanidinium and Indole Bearing Poly(methacrylamide)s – Biocompatible Terpolymers for pDNA Delivery, *Macromolecular Bioscience*, 2021, **21**, 2100146.
318 D. J. Gary, J. B. Min, Y. Kim, K. Park and Y.-Y. Won, The Effect of N/P Ratio on the In Vitro and In Vivo Interaction Properties of PEGylated Poly(2-(dimethylamino)ethyl methacrylate)-Based siRNA Complexes, *Macromol Biosci*, 2013, **13**, 1059–1071.
319 I. Y. Perevyazko, M. Bauer, G. M. Pavlov, S. Hoeppener, S. Schubert, D. Fischer and U. S. Schubert, Polyelectrolyte Complexes of DNA and Linear PEI: Formation, Composition and Properties, *Langmuir*, 2012, **28**, 16167–16176.
320 H. Li, M. A. Cortez, H. R. Phillips, Y. Wu and T. M. Reineke, Poly(2-deoxy-2-methacrylamido glucopyranose)-b-Poly(methacrylate amine)s: Optimization of Diblock Glycopolycations for Nucleic Acid Delivery, *ACS Macro Lett.*, 2013, **2**, 230–235.
321 J. O. Disi and A. A. Sial, Laboratory Selection and Assessment of Resistance Risk in Drosophila suzukii (Diptera: Drosophilidae) to Spinosad and Malathion, *Insects*, 2021, **12**, 794.
322 C. Deans and W. D. Hutchison, Propensity for resistance development in the invasive berry pest, spotted-wing drosophila (Drosophila suzukii), under laboratory selection, *Pest Management Science*, , DOI:10.1002/ps.7139.
323 G. Tait, S. Mermer, D. Stockton, J. Lee, S. Avosani, A. Abrieux, G. Anfora, E. Beers, A. Biondi, H. Burrack, D. Cha, J. C. Chiu, M.-Y. Choi, K. Cloonan, C. M. Crava, K. M. Daane, D. T. Dalton, L. Diepenbrock, P. Fanning, F. Ganjisaffar, M. I. Gómez, L. Gut, A. Grassi, K. Hamby, K. A. Hoelmer, C. Ioriatti, R. Isaacs, J. Klick, L. Kraft, G. Loeb, M. V. Rossi-Stacconi, R. Nieri, F. Pfab, S. Puppato, D. Rendon, J. Renkema, C. Rodriguez-Saona, M. Rogers, F. Sassù, T. Schöneberg, M. J. Scott, M. Seagraves, A. Sial, S. Van Timmeren, A. Wallingford, X. Wang, D. A. Yeh, F. G. Zalom and V. M. Walton, Drosophila suzukii (Diptera: Drosophilidae): A Decade of Research Towards a Sustainable Integrated Pest Management Program, *J Econ Entomol*, 2021, **114**, 1950–1974.
324 S. J. Fletcher, P. T. Reeves, B. T. Hoang and N. Mitter, A Perspective on RNAi-Based Biopesticides, *Front. Plant Sci.*, , DOI:10.3389/fpls.2020.00051.
325 K. Cappelle, C. F. R. de Oliveira, B. V. Eynde, O. Christiaens and G. Smagghe, The involvement of clathrin-mediated endocytosis and two Sid-1-like transmembrane proteins in double-stranded RNA uptake in the Colorado potato beetle midgut, *Insect Molecular Biology*, 2016, **25**, 315–323.
326 S. C. Miller, S. J. Brown and Y. Tomoyasu, Larval RNAi in Drosophila?, *Dev Genes Evol*, 2008, **218**, 505–510.
327 S. S. Lichtenberg, K. Nuti, J. DeRouchey, O. V. Tsyusko and J. M. Unrine, Efficacy of chitosan/double-stranded RNA polyplex nanoparticles for gene silencing under variable environmental conditions, *Environ. Sci.: Nano*, 2020, **7**, 1582–1592.

328 K. A. Murphy, C. A. Tabuloc, K. R. Cervantes and J. C. Chiu, Ingestion of genetically modified yeast symbiont reduces fitness of an insect pest via RNA interference, *Scientific Reports*, 2016, **6**, 22587.
329 H. Song, J. Zhang, D. Li, A. M. W. Cooper, K. Silver, T. Li, X. Liu, E. Ma, K. Y. Zhu and J. Zhang, A double-stranded RNA degrading enzyme reduces the efficiency of oral RNA interference in migratory locust, *Insect Biochemistry and Molecular Biology*, 2017, **86**, 68–80.
330 J.-Z. Chen, Y.-X. Jiang, M.-W. Li, J.-W. Li, B.-H. Zha and G. Yang, Double-Stranded RNA-Degrading Enzymes Reduce the Efficiency of RNA Interference in Plutella xylostella, *Insects*, 2021, **12**, 712.
331 J.-S. Yoon, S.-J. Ahn, C. M. Flinn and M.-Y. Choi, Identification and functional analysis of dsRNases in spotted-wing drosophila, Drosophila suzukii, *Archives of Insect Biochemistry and Physiology*, 2021, **107**, e21822.
332 B. Khurana, A. K. Goyal, A. Budhiraja, D. Aora and S. P. Vyas, Lipoplexes versus nanoparticles: pDNA/siRNA delivery, *Drug Delivery*, 2013, **20**, 57–64.
333 M. Martínez-Negro, K. Kumar, A. L. Barrán-Berdón, S. Datta, P. Kondaiah, E. Junquera, S. Bhattacharya and E. Aicart, Efficient Cellular Knockdown Mediated by siRNA Nanovectors of Gemini Cationic Lipids Having Delocalizable Headgroups and Oligo-Oxyethylene Spacers, *ACS Appl. Mater. Interfaces*, 2016, **8**, 22113–22126.
334 X. Chen, L. S. Mangala, C. Rodriguez-Aguayo, X. Kong, G. Lopez-Berestein and A. K. Sood, RNA Interference–Based Therapy and Its Delivery Systems, *Cancer Metastasis Rev*, 2018, **37**, 107–124.
335 S. D. Desai, Y.-J. Eu, S. Whyard and R. W. Currie, Reduction in deformed wing virus infection in larval and adult honey bees (Apis mellifera L.) by double-stranded RNA ingestion, *Insect Molecular Biology*, 2012, **21**, 446–455.
336 K. Kim, H. S. Hwang, M. S. Shim, Y.-Y. Cho, J. Y. Lee, H. S. Lee and H. C. Kang, Controlling complexation/decomplexation and sizes of polymer-based electrostatic pDNA polyplexes is one of the key factors in effective transfection, *Colloids and Surfaces B: Biointerfaces*, 2019, **184**, 110497.
337 F. L. Hatton, Recent advances in RAFT polymerization of monomers derived from renewable resources, *Polym. Chem.*, 2020, **11**, 220–229.
338 A. Samir, F. H. Ashour, A. A. A. Hakim and M. Bassyouni, Recent advances in biodegradable polymers for sustainable applications, *npj Mater Degrad*, 2022, **6**, 1–28.
339 R. Kumar, N. Le, F. Oviedo, M. E. Brown and T. M. Reineke, Combinatorial Polycation Synthesis and Causal Machine Learning Reveal Divergent Polymer Design Rules for Effective pDNA and Ribonucleoprotein Delivery, *JACS Au*, , DOI:10.1021/jacsau.1c00467.
340 A. I. Gómez-Varela, R. Gaspar, A. Miranda, J. L. Assis, R. H. F. Valverde, M. Einicker-Lamas, B. F. B. Silva and P. A. A. De Beule, Fluorescence cross-correlation spectroscopy as a valuable tool to characterize cationic liposome-DNA nanoparticle assembly, *J Biophotonics*, 2021, **14**, e202000200.

Appendix

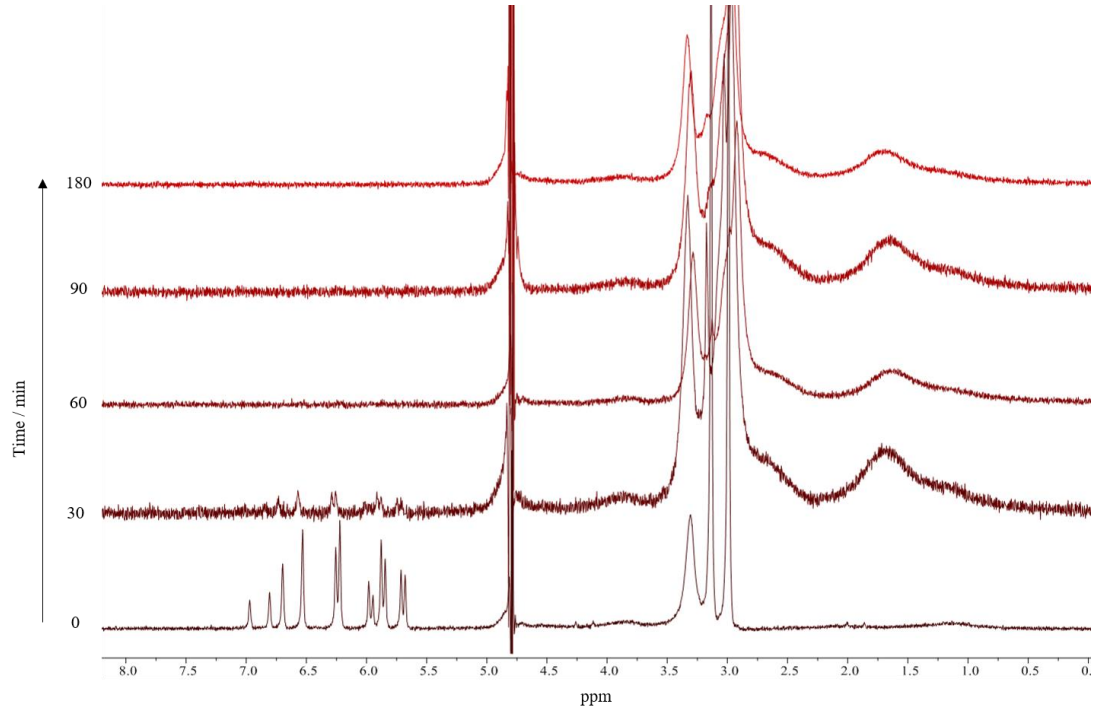

Figure A1. Stacked ^{1}H NMR (60 MHz) spectra showing the conversion of *N*,*N*-dimethyl acrylamide monomer, to poly(*N*,*N*-dimethyl acrylamide) (D) polymerised as a second block onto the PQDMAEMA (Q) macro-CTA (Q_{110}-*b*-D_{219} used as an example here). The peaks at 5.5 – 7.0 ppm at *t = 0* are attributed to the vinyl protons of the monomer unit. The decrease and eventual absence of these peaks after 30 min indicates the successful polymerisation of D, with very low levels of monomer remaining prior to purification.

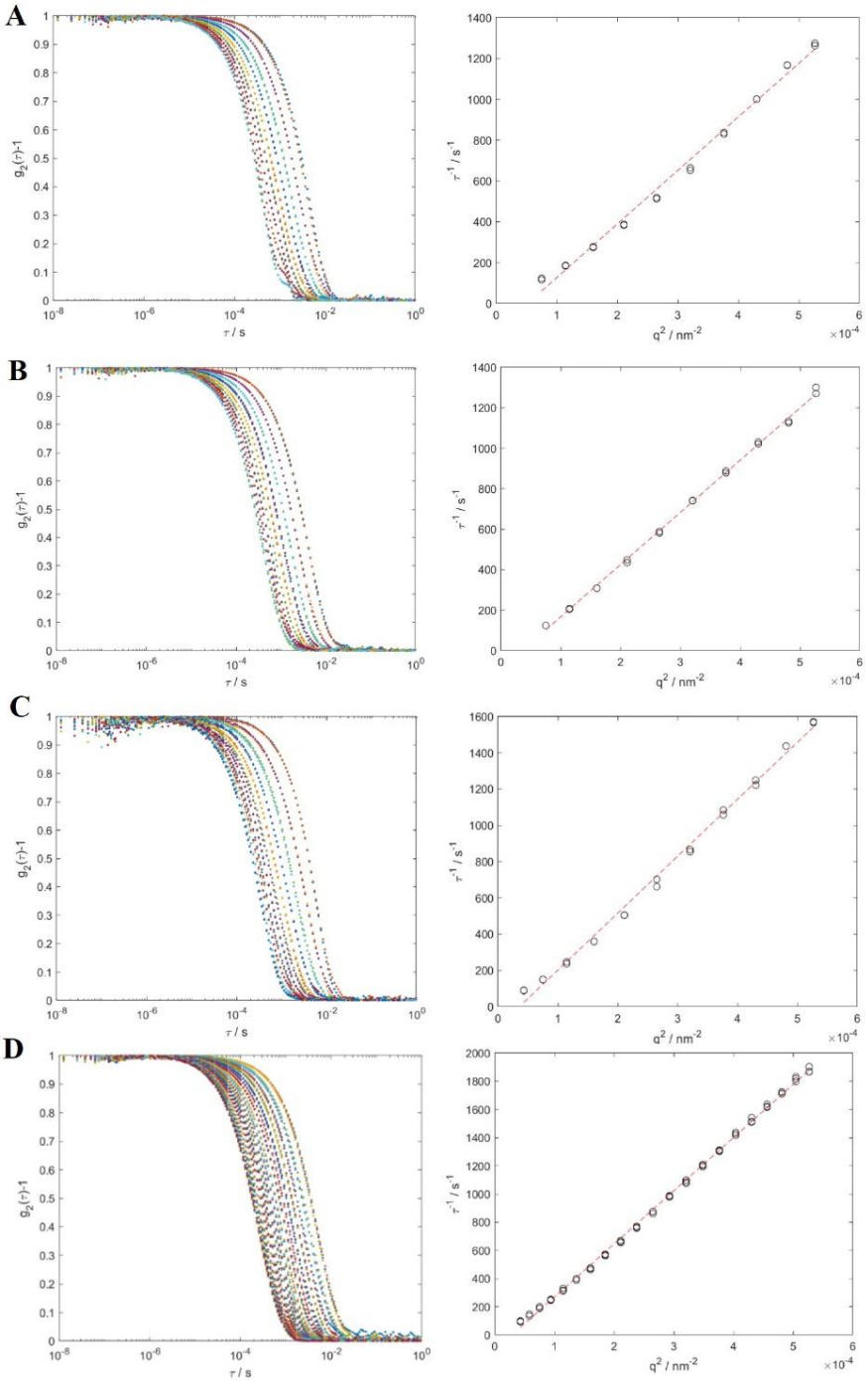

Figure A2. DLS data collected of homopolymer or diblock copolymer-based polyplexes, formulated at an N/P ratio = 5, after 24 h equilibration time. (Left) Normalised intensity auto-correlation (IAC) data measured by DLS at scattering angles 30 – 130°. Angle increases from right to left, with measurements in triplicate (not all visible due to overlap of similar data points). (Right) Plots of the decay rate, Γ, against the squared scattering vector, q^2. Dashed lines are fits to, $\Gamma = Dq^2 + B$, where the *y*-intercept, *B*, is not restricted to account for a small uncertainty in the values of Γ. (A) Q_{110}/dsRNA, (B) Q_{110}-*b*-D_{57}/dsRNA, (C) Q_{110}-*b*-D_{89}/dsRNA, (D) Q_{110}-*b*-D_{219}/dsRNA.

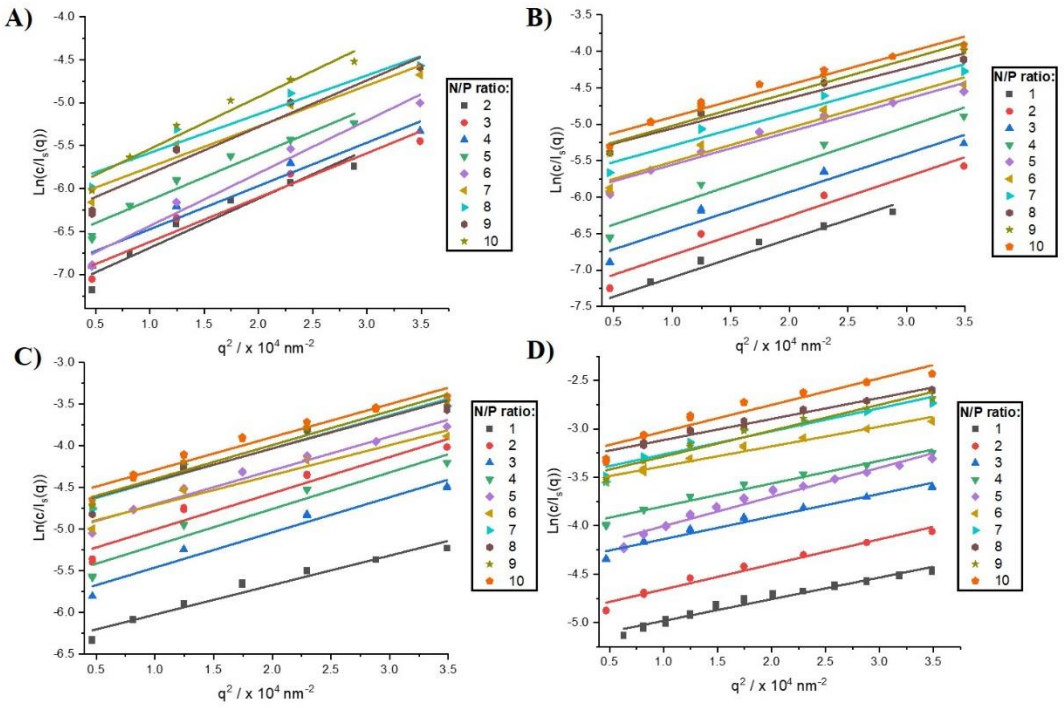

Figure A3. Guinier plots for (A) Q_{110}, (B) Q_{110}-*b*-D_{57}, (C) Q_{110}-*b*-D_{89} and (D) Q_{110}-*b*-D_{219} polyplexes with *vha26* dsRNA, across N/P ratios 1 – 10, with their respective linear fits.

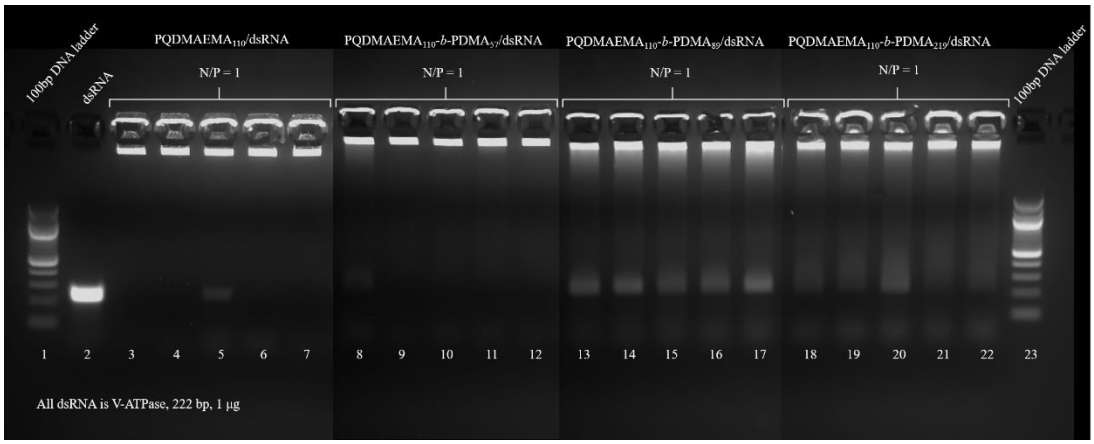

Figure A4. Agarose gel electrophoresis replicates at N/P ratio = 1 for each homopolymer or diblock copolymer-based polyplex with *vha26* dsRNA, as follows: Q_{110} (lanes 3–7), Q_{110}-*b*-D_{57} (lanes 8–12), Q_{110}-*b*-D_{89} (lanes 13–17) and Q_{110}-*b*-D_{219} (lanes 18–22). Naked dsRNA (1 µg) was run in lane 2, and 100 bp DNA ladder was run in lanes 1 and 23 for comparison. The image was collected in four separate images of each part of the gel, so that greater focus of the observed fluorescence could be obtained; hence, subtle changes in background colour occurs in different sections of the image.

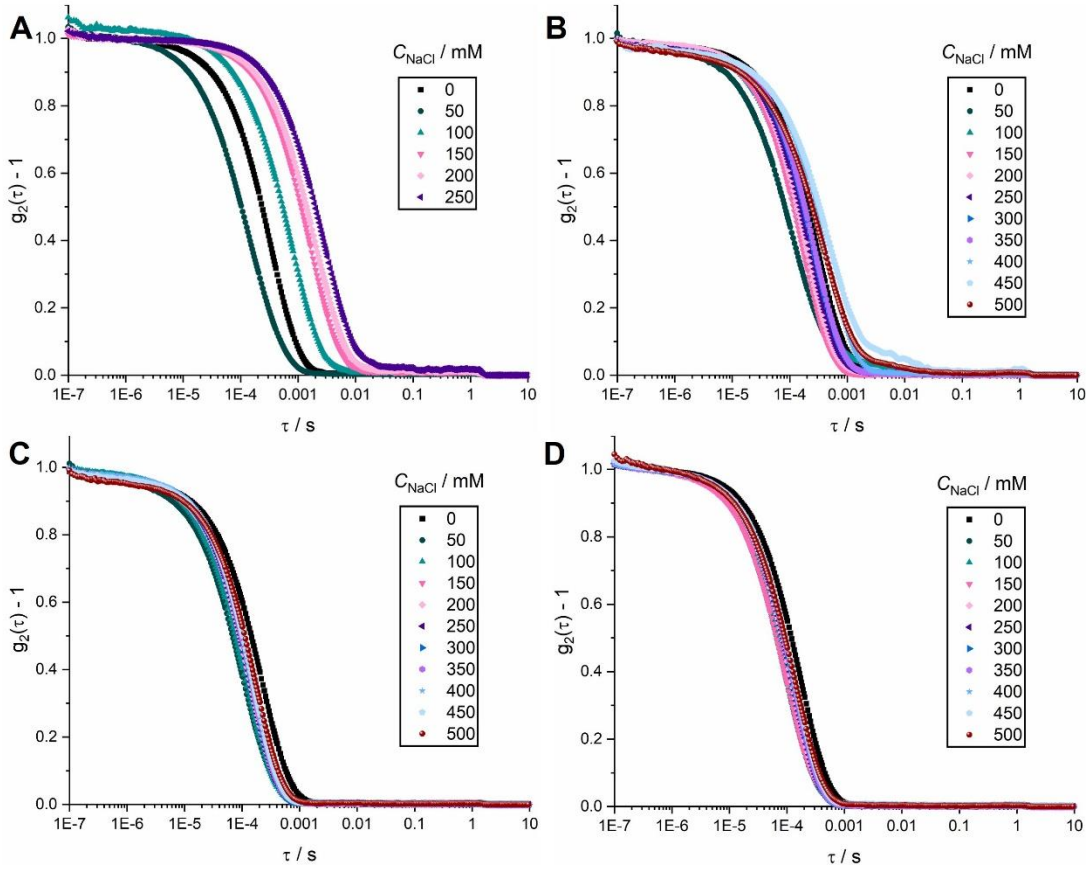

Figure A5. Intensity auto-correlation curves for each homopolymer or diblock copolymer-based polyplex (A) Q_{110}/dsRNA, (B) Q_{110}-*b*-D_{57}/dsRNA, (C) Q110-*b*-D_{89}/dsRNA and (D) Q_{110}-*b*-D_{219}/dsRNA), with variation in the C_{NaCl}.

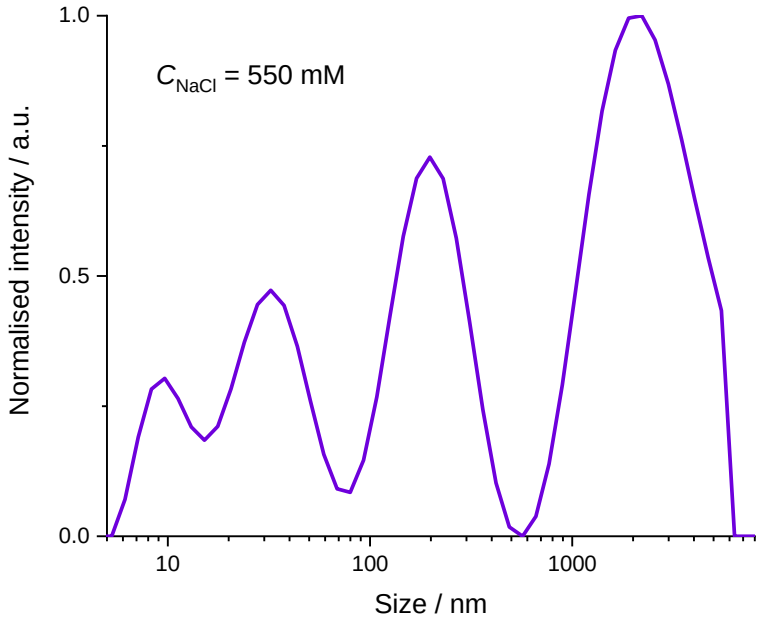

Figure A6. Size distribution measured of a Q_{110}-*b*-D_{57}/dsRNA polyplex formulation (N/P ratio = 5) after incubation in 550 mM NaCl concentration aqueous solution. Shown here as an example of the multimodal distributions measured by DLS upon decomplexation/aggregation of the polyplexes once a particular electrolyte concentration is reached. Size distribution produced by the Zetasizer software, using CONTIN analysis.

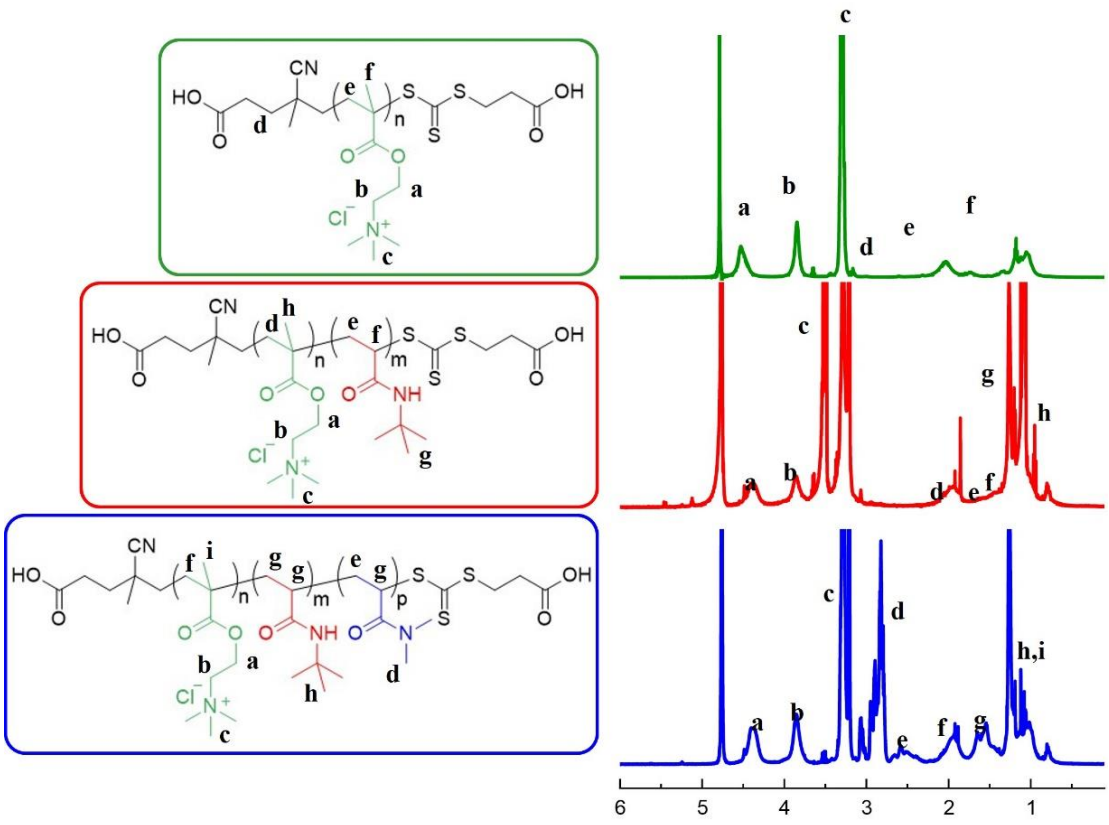

Figure A7. ^{1}H NMR (400 MHz) spectra of the homopolymer Q_{100} (green), the diblock copolymer Q_{100}-*b*-B_{25} (red) and the triblock copolymer Q_{100}-*b*-B_{25}-*b*-D_{55} (blue).

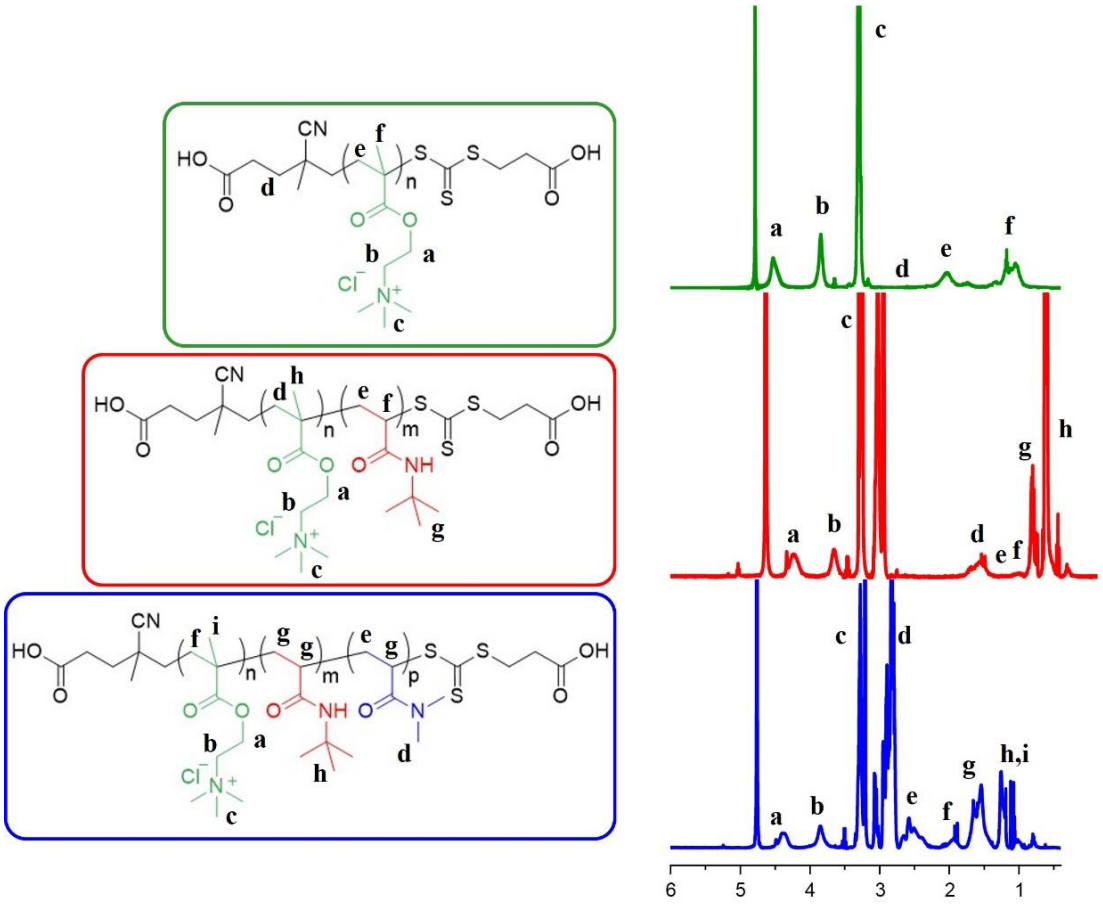

Figure A8. ^{1}H NMR (400 MHz) spectra of the homopolymer Q_{100} (green), the diblock copolymer Q_{100}-*b*-B_{17} (red) and the triblock copolymer Q_{100}-*b*-B_{17}-*b*-D_{212} (blue).

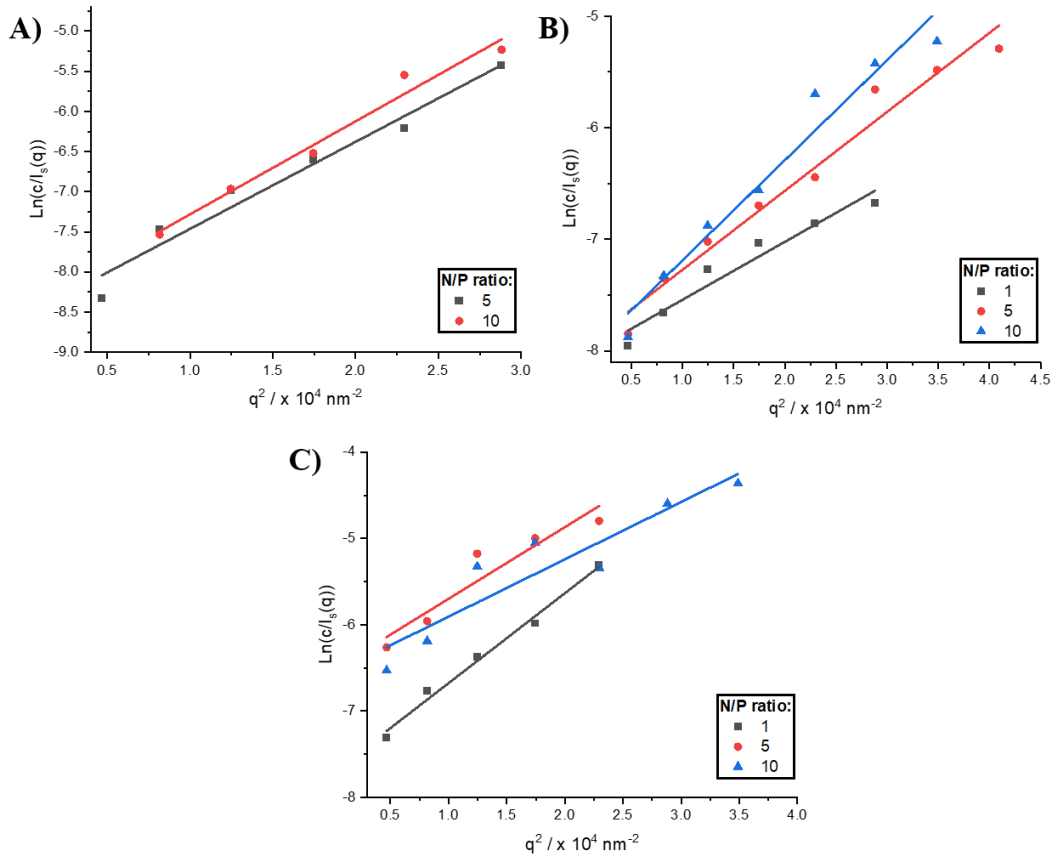

Figure A9. Guinier plots for (A) Q-*b*-B_{25}-*b*-D_{55}, (B) Q-*b*-B_{44}-*b*-D_{99} and (C) Q-*b*-B_{17}-*b*-D_{212} polyplexes with dsRNA, at N/P ratios 1, 5 and 10, with their respective linear fits.

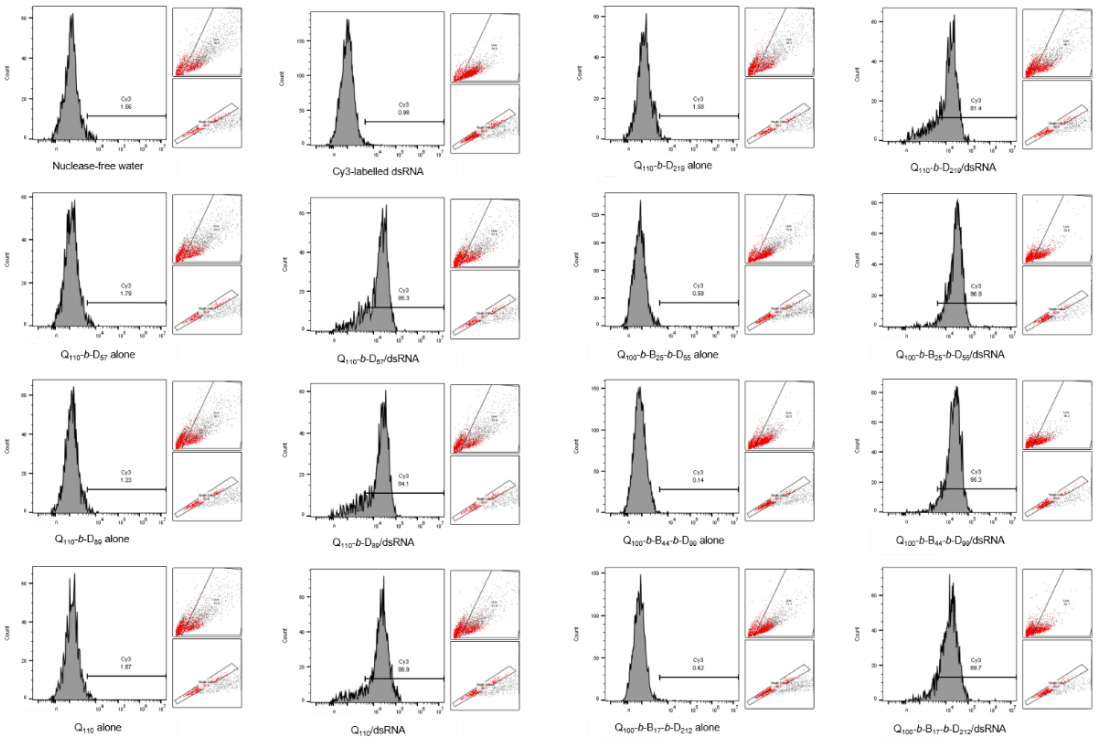

Figure A10. Flow cytometry data, with histogram plots of the relative fluorescence intensity (Cy3) of single, live HEK-293T cells (gating shown). Alongside are dot plots showing the live/dead gating on all cells measured in the sample (top) and the single cell gating of the cells determined as 'live' (bottom, with the red dots highlighting the single cells in both instances). Samples are labelled according to the incubation conditions.

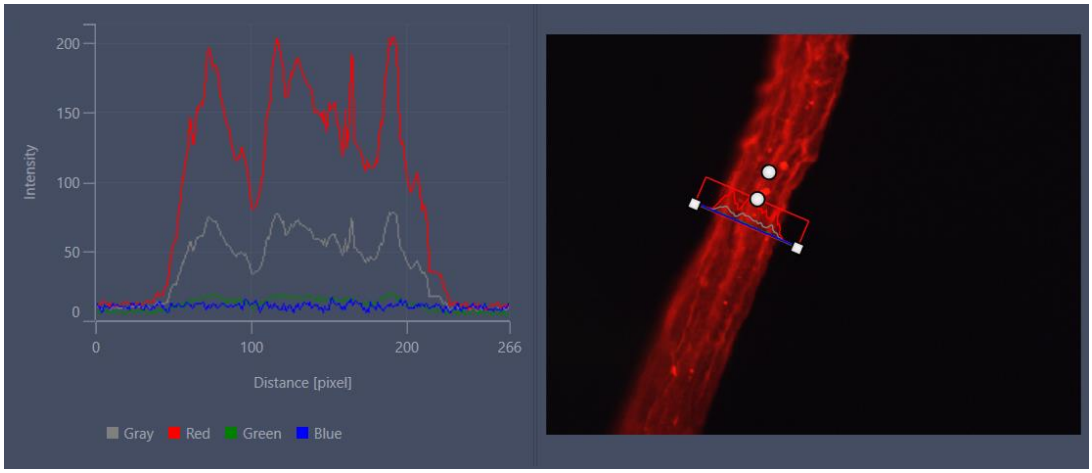

Figure A11. Example of the measurement of Cy3 fluorescence intensity from fluorescence microscopy images of the gut section of *D. suzukii* L3 larvae. Lines were drawn perpendicular to the gut, in the middle of the gut in the micrograph (right). The intensity of the red signal was extracted from the Zeiss ZEN Blue software (left), and an average of the intensity calculated. The average intensity across all gut images for each sample was taken, as well as a standard deviation calculated.